



HAL
open science

Plats pays et mornes plaines ? : dynamique du transfert sédimentaire au sein de grands drainages continentaux

Jean-Louis Grimaud

► **To cite this version:**

Jean-Louis Grimaud. Plats pays et mornes plaines ? : dynamique du transfert sédimentaire au sein de grands drainages continentaux. Sciences de la Terre. Sorbone Université, 2023. tel-04317879

HAL Id: tel-04317879

<https://hal.science/tel-04317879>

Submitted on 20 Dec 2023

HAL is a multi-disciplinary open access archive for the deposit and dissemination of scientific research documents, whether they are published or not. The documents may come from teaching and research institutions in France or abroad, or from public or private research centers.

L'archive ouverte pluridisciplinaire **HAL**, est destinée au dépôt et à la diffusion de documents scientifiques de niveau recherche, publiés ou non, émanant des établissements d'enseignement et de recherche français ou étrangers, des laboratoires publics ou privés.



Distributed under a Creative Commons Attribution - NoDerivatives 4.0 International License

Plats pays et mornes plaines ? : dynamique du transfert sédimentaire au sein de grands drainages continentaux

Jean-Louis Grimaud, chargé d'enseignement et de recherche à Mines Paris, Université PSL

Soutenu le 20 septembre 2023 devant le jury suivant :

CASTELLTORT Sébastien, Professeur Université de Genève (rapporteur)

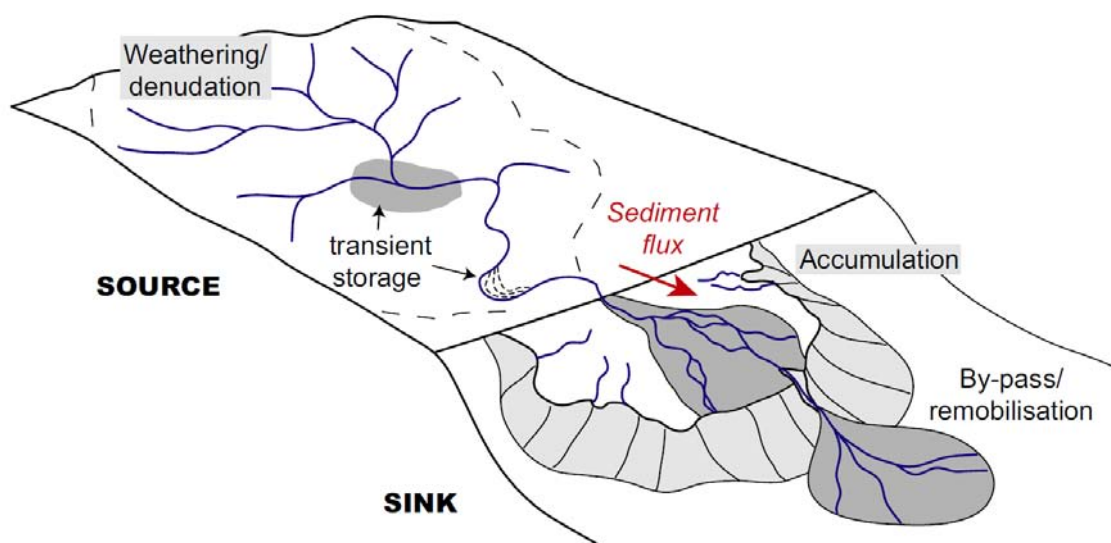
CARRETIER Sébastien, Directeur de Recherche IRD, Université Paul SABATIER Toulouse (examineur)

GAUTHERON Cécile, Maître de Conférences HDR IS Terre Grenoble (rapporteuse)

GORINI Christian, Professeur Sorbonne Université – IStEP (président du jury)

LESPEZ Laurent, Professeur Université de Paris Est Créteil-LGP (rapporteur)

Plats pays et mornes plaines ? : dynamique du transfert sédimentaire au sein de grands drainages continentaux



Jean-Louis Grimaud, *Chargé d'Enseignement et de recherche* Mines Paris

Résumé des activités de recherches : 9 ans après la thèse (2014), 1 thèse encadrée soutenue, 1 thèse en co-encadrement soutenue, 2 thèses en cours, 4 M1/M2 encadrés, 14 articles publiés (dont 7 en premier auteur et 6 en second auteur), deux articles acceptés et un soumis.

<https://cv.archives-ouvertes.fr/jean-louis-grimaud>

<https://www.researchgate.net/profile/Jean-Louis-Grimaud>

Métriques (au 04/04/2023) : H-index : 10 (Google Scholar), 8 (Scopus) / Citations : 315 (Google Scholar), 203 (Scopus)

RESUME

Le transfert des sédiments vers les océans s'organise en différents compartiments : la zone source en érosion, la zone de transfert (les corridors fluviaux) et la zone de sédimentation. Ce système est influencé par des forçages externes -tels que la tectonique ou le climat- mais il possède également une dynamique interne, qui peut absorber ou modifier le signal des forçages externes. De plus, les différents compartiments du système de routage ne sont pas déconnectés : des communications s'effectuent d'amont en aval ou d'aval en amont. Comprendre au mieux ce système, c'est donc intégrer au maximum l'ensemble de ses compartiments. Cette habilitation présente les résultats d'études menés dans les zones « plates » du système de routage des sédiments : les zones anorogéniques, les plaines alluviales et les deltas. L'originalité de ce travail réside dans la variété de ses approches : études de terrain, grandes synthèses, expériences analogiques et modélisation numérique.

Le manuscrit est organisé en trois grandes parties, reprenant les trois zones du système de routage des sédiments. La première partie est donc consacrée à la dynamique d'érosion des sources sédimentaires, principalement en milieu tropical latéritique. Plusieurs échelles sont abordées, depuis la dynamique des versants jusqu'à la quantification de la dynamique de surface à l'échelle sous-continentale. Ces résultats illustrent la redistribution des ressources minérales dans les paysages et permettent de proposer un bilan « source-to-sink » intégré sur l'ensemble du Cénozoïque en Afrique de l'Ouest. La seconde partie s'intéresse à la zone de transfert. J'y intègre différentes approches, depuis la reconstruction des profils en long des rivières à l'échelle de plusieurs millions d'années à la dynamique du stockage temporaire de sédiments à l'échelle millénaire dans les plaines alluviales. Ces résultats contraignent l'incision des paysages, illustrant notamment l'effet de la lithologie du substrat. La troisième partie concerne la zone d'accumulation et les bilans sédimentaires. J'y étudie la mobilité des chenaux depuis les environnements deltaïques jusqu'aux systèmes turbiditiques sous-marins pour proposer des clés de distinction entre dynamique interne et forçages externes de la redistribution sédimentaire.

A la fin du manuscrit est détaillé le projet scientifique que je souhaite mener au cours des prochaines années à Mines Paris. Ce projet s'inscrit dans la continuité de mes thématiques et outils de recherche actuels : la géomorphologie des zones stables, la modélisation analogique de la dynamique des systèmes chenalés mais aussi les interactions entre climat et flux sédimentaires. Je souhaite enfin donner une dimension plus sociétale à mon profil de recherche en étudiant les interactions entre l'Homme et son milieu naturel, notamment sur l'exemple des plaines alluviales telles que la Seine.

« Quand la plaine est fumante
Et tremble sous juillet
Quand le vent est au rire
Quand le vent est au blé
Quand le vent est au sud
Écoutez-le chanter
Le plat pays
...»

Jacques Brel

Contexte

La rédaction de ce manuscrit d'HDR intervient à la suite de 7 années passées au Centre de Géosciences de Fontainebleau et bientôt 10 ans après la thèse de doctorat. Elle est pour moi l'occasion de tirer un premier bilan sur mon parcours scientifique à Rennes, Toulouse, Minneapolis puis Fontainebleau.

De Rennes, je garderai d'incroyables souvenirs associés à des profs charismatiques, l'amour du terrain et ce bon « gros premier ordre » si cher à l'école rennaise, qui fait encore parler de lui lorsque je discute avec des collègues sur le terrain. De Toulouse, je garderai une thèse ambitieuse et incroyable, portée par un encadrant ultra-disponible et rigoureux. De Minneapolis, je garderai la crainte puis le plaisir de la prise d'autonomie mais surtout le côté sans-limite des projets expérimentaux et les formidables équipes de chercheurs, ingénieurs et techniciens au laboratoire St Anthony Falls. L'histoire n'est pas finie à Fontainebleau, où j'ai pu développer des compétences sur les systèmes fluviaux méandriques et les plaines alluviales au sein de l'équipe de modélisation numérique FLUMY, monter un laboratoire de géomorphologie et initier des collaborations avec des collègues d'horizons variés, en particulier au sein de l'équipe de géostatistique. De nombreux autres projets verront j'espère le jour avec mes collègues géophysiciens, géomécaniciens et hydrologues.

La géomorphologie -l'étude des paysages et de leur évolution- est la discipline centrale dans mes recherches, plus particulièrement les zones « plates », anorogéniques et alluviales. Une autre spécificité de mon profil est son approche intégrée. Ceci m'a donné l'opportunité d'avoir des collaborations avec des spécialistes divers et m'a permis de mener des travaux à différentes échelles spatiales et temporelles dans de nombreux compartiments du système de routage des sédiments depuis leurs sources continentales jusqu'aux bassins sédimentaires. J'ai grâce à cela pu aborder certaines questions à la fois sous l'angle du géologue de terrain en complément de synthèses régionales mais aussi sous celui du modélisateur (physique et parfois numérique). Cet exercice de modélisation présente de nombreuses difficultés et limites mais il reste selon moi un incontournable pour l'étude des processus physiques et leur expression dans les milieux naturels. C'est donc tout naturellement que cette approche sera abordée dans le présent manuscrit.

Introduction générale

Évolution des paysages et transferts sédimentaires sont deux notions intimement liées. L'érosion des paysages va en effet contrôler la quantité de sédiments exportés vers les bassins sédimentaires (Allen, 2008) tandis que la dynamique d'incision des rivières et le façonnement des versants vont être modulés par la charge sédimentaire (Paola et al., 1992 ; Sklar et Dietrich, 2004). La question des flux sédimentaires, et des forçages permanents ou transitoires qui les contrôlent, est donc centrale pour mieux comprendre l'enregistrement dans les bassins sédimentaires en lien avec la paléogéographie (Bishop, 1995 ; Castellort et van den Driessche, 2003 ; Tofelde et al., 2021). Au sein du système de routage des sédiments, on distingue trois compartiments : la zone source en érosion, la zone de transfert qui peut être assimilée aux corridors fluviaux et la zone de sédimentation (Fig. 1). Si l'impact des forçages externes -dits allogéniques- (principalement climatiques ou tectoniques) sur ces compartiments est avéré, il convient de prendre en compte la dynamique intrinsèque à ces systèmes (Scheingross, et al., 2020). Les rivières en particulier sont des entités mobiles latéralement de façon autogénique, c'est à dire sans aucune autre action que les interactions entre fluide et sédiments transportés. Il n'est donc pas toujours aisé de distinguer la part autogénique de la part allogénique dans les enregistrements sédimentaires (Sadler et Jerolmack, 2015 ; Straub et al., 2020). De plus, l'enregistrement sédimentaire est par nature parcellaire, la probabilité de préservation diminuant avec l'âge des sédiments (Sadler, 1981) (Fig. 2). Intégrer au maximum les différents compartiments du système de routage des sédiments apparaît donc fondamental pour mieux comprendre la dynamique des flux sédimentaires sur l'ensemble du réseau.

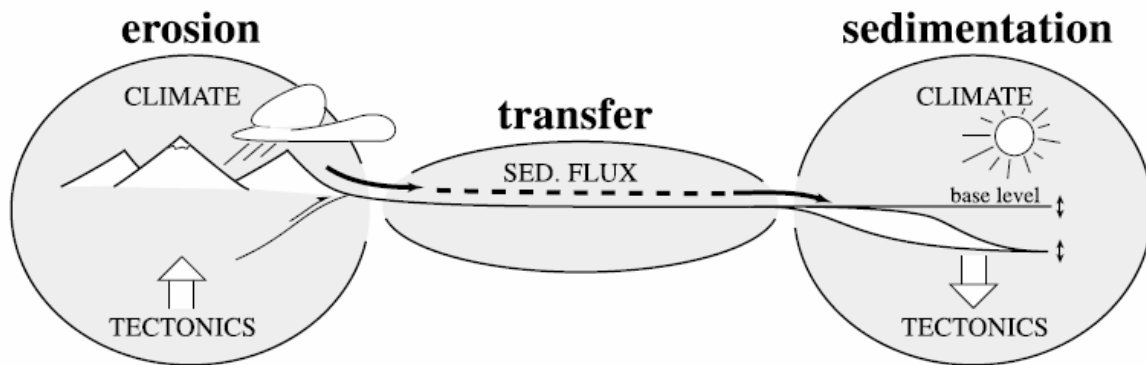


Fig. 1 : Schéma simplifié du « sediment routing system » matérialisant la zone en érosion, la zone de transfert et la zone de sédimentation (Castellort et van den Driessche, 2003).

Sur Terre, on peut opposer zones orogéniques et zones anorogéniques par leur dynamique de surface. Les premières ont des taux de production sédimentaire supérieurs à 100 t/km²/an allant jusqu'à 150 à 1400 t/km²/an pour l'Amazonie et les grands systèmes de drainage de l'Asie respectivement. Les secondes ont des taux de production plus faibles d'un à deux ordres de grandeur comme en Afrique de l'Ouest ou en Europe avec des valeurs de 16,5 et 12 t/km²/an respectivement (Milliman et Meade, 1983). Le relief au sein des grands systèmes de drainage continentaux a un contrôle de premier ordre sur les taux de dénudation (Summerfield et Hulton, 1994). Du point de l'export vers les océans, le signal des zones « planes » n'est donc qu'un bruit de fond comparé aux zones montagneuses aux reliefs plus vigoureux, même si l'obtention

d'estimations précises de l'export des zones anorogéniques reste un sujet de débat (Warrick et al., 2014). Cependant, ces zones peuvent tout de même engendrer un export fort à l'exutoire des bassins-versants d'aires drainées élevées. C'est le cas pour le fleuve Niger, avec un delta ayant accumulé une épaisseur de 9 km de sédiments au cours du Cénozoïque (Haack et al., 2000). De fait, la quantification de l'évolution de la géométrie et de la taille des grands drainages continentaux revêt une importance forte dans ces zones tectoniquement calmes où il a été suggéré que les réorganisations des bassins-versants peuvent être rapides (Willet et al., 2014).

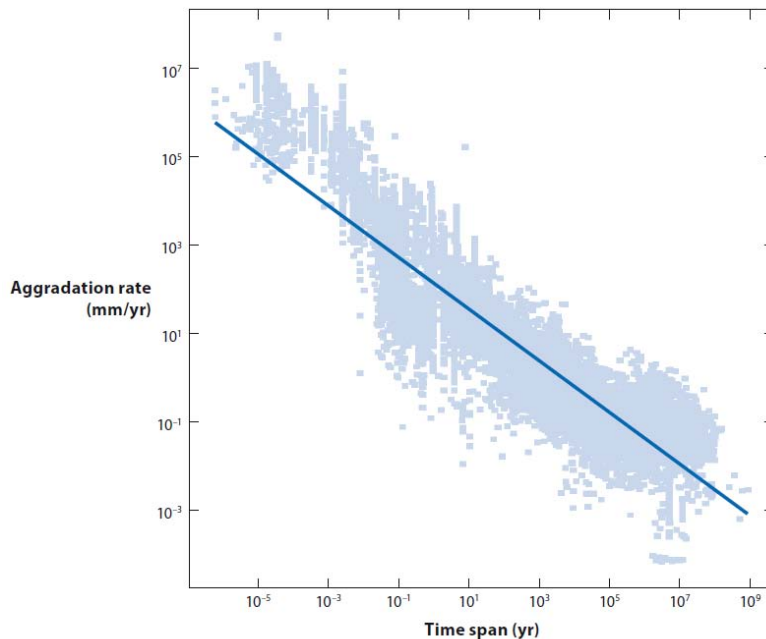


Fig. 2 : Taux d'aggradation locaux en fonction de l'intervalle de temps de mesure considéré, d'après une compilation de données dans les systèmes alluviaux (Paola et al., 2018 ; d'après Sadler et Jerolmack, 2015). L'exposant de la loi de puissance utilisée en bleu est de -0,585.

Les plaines alluviales constituent une autre catégorie de domaines « plats ». Elles représentent une zone de transfert et de stockage temporaire de sédiment qui peut tamponner les flux sédimentaires (Métivier et Gaudemer, 1999 ; Castelltort et van den Driesche, 2003 ; Jerolmack et Paola, 2010 ; Romans et al., 2016). Leur rôle sur les flux solides vers les océans est donc majeur. Il l'est également sur les flux chimiques et donc sur les grands cycles biogéochimiques (Meybeck, 1976 ; Lupker et al., 2012). Comprendre leur fonctionnement passé permet également de prendre du recul sur leur fonctionnement présent, en lien avec les usages anthropiques de plus en plus intenses des corridors fluviaux (Best et Darby, 2020).

Dans ce manuscrit, les résultats de mes recherches portant sur le système de routage des sédiments sont présentés. La question générale ayant motivé ce travail est : quel enregistrement reste-t-il de la dynamique de surface de la Terre dans les paysages et les roches sédimentaires ? En particulier, je me suis intéressé (1) à la dynamique de surface des zones anorogéniques ainsi qu'à l'export sédimentaire résultant (par unité de surface et par bassin -versant en tentant de prendre en compte les réorganisations de drainage), (2) à l'évolution de la zone de transfert par reconstitution des profils en long des rivières, des volumes stockés dans les plaines alluviales et de la dynamique de remobilisation sédimentaire, et enfin (3) à l'enregistrement dans les

bassins sédimentaires par quantification des volumes de sédiments stockés et par analyse des redistributions sédimentaires.

Le présent manuscrit est organisé en trois grandes parties, reprenant les trois zones du système de routage des sédiments (Fig. 1). La Partie 1 sera donc consacrée à la dynamique d'érosion des sources sédimentaires, principalement en milieu tropical. La Partie 2 s'intéressera à la zone de transfert, en particulier la dynamique des rivières dans les plaines et vallées alluviales. La Partie 3 s'intéressera enfin à la zone d'accumulation et aux bilans sédimentaires. Ce manuscrit s'appuie sur cinq de mes articles, qui sont présentés en annexe. Leur contenu est résumé dans les différentes parties du manuscrit.

À la fin du manuscrit est détaillé le projet scientifique envisagé pour les prochaines années, au sein du Centre de Géosciences de Fontainebleau à Mines Paris. Je souhaite continuer à travailler sur la thématique de la géomorphologie des zones stables, en insistant sur les rétroactions entre paléo paysages et altérations. Mon activité de modélisation analogique se poursuivra : en étudiant d'une part les relations entre tectonique et dynamique des systèmes chenalisés et d'autre part l'impact d'événements pluvieux extrêmes sur l'érosion des sols. Je voudrais donner une dimension plus sociétale à mon profil de recherche en étudiant les interactions entre l'Homme et son milieu naturel, notamment sur l'exemple des plaines alluviales telles que la Seine. Enfin, je souhaite m'appuyer sur les compétences nouvelles au sein de l'équipe géologie du Centre de Géosciences pour aborder les questions de l'enregistrement des signaux climatiques sur la (paléo)dynamique des rivières.

1- Dynamique des sources sédimentaires en milieu tropical

L'étude de l'évolution long-terme des paysages offre l'opportunité de quantifier les mouvements verticaux et estimer les flux sédimentaires vers les océans. Deux domaines s'opposent par leur dynamique lithosphérique : les zones orogéniques, où s'effectue la déformation continentale sous l'effet de la convergence des plaques tectoniques, et les zones anorogéniques -ou cratons- situées loin des limites des plaques. Étant les plus éloignées de l'influence de contraintes tectoniques, ces dernières sont les plus propices à l'enregistrement de la déformation épirogénique de la lithosphère, par exemple sous influence mantellique (i.e., topodynamique ; [Braun, 2010](#)). Dans ces domaines, il est difficile de contraindre la dénudation par les méthodes thermochronologiques classiques car on atteint les limites de leur résolution, lorsque les taux de dénudations sont très faibles ([Bierman et Caffee, 2001](#) ; [Beauvais et Chardon, 2013](#)). Par exemple, les très nombreuses données en Afrique australe montrent principalement des pics de dénudation au Mésozoïque (e.g., [Brown et al., 2002](#)), même si des données plus récentes ont une meilleure résolution pour le Cénozoïque (e.g., [Flowers et Schoene, 2010](#) ; [Margirier et al., 2019](#)). Il est en revanche possible de contraindre la dénudation cénozoïque dans des zones où les mouvements verticaux sont plus vifs (exemple du Hoggar en Afrique de l'Ouest ; [Rougier et al., 2013](#) ; [English et al., 2017](#)).

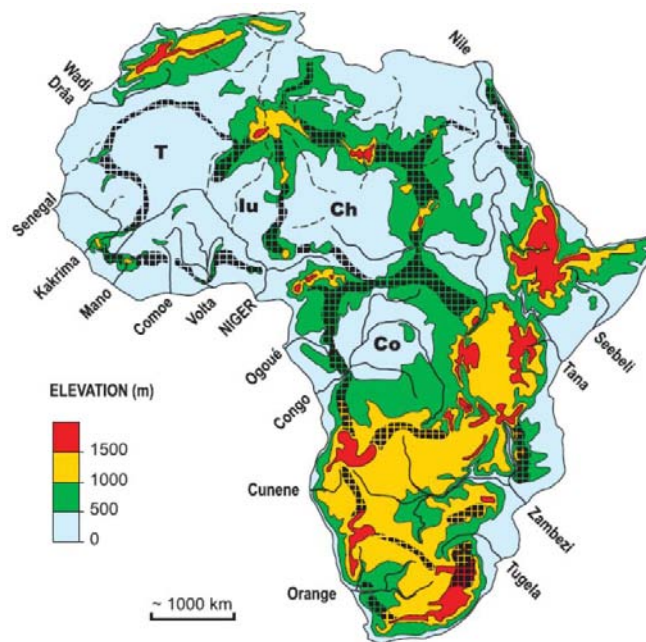


Fig. 3 : Topographie en bassins et dômes de l'Afrique interprétée comme étant liée à la dynamique mantellique ([Chardon et al., 2016](#)), en particulier l'Afrique méridionale et sa topographie élevée.

Les zones anorogéniques sont également propices à l'enregistrement de la dynamique passée des surfaces continentales et du climat grâce à la préservation d'altérations intenses datant du méso-cénozoïque ([Grandin et Thiry, 1983](#) ; [Tardy et Roquin, 1998](#)). Lorsqu'elles sont correctement caractérisées et/ou datées, les reliques d'altération peuvent être de puissants outils pour suivre l'évolution des domaines cratoniques, particulièrement dans la zone intertropicale. Elles permettent de calibrer les taux d'incision et de dénudation ([Beauvais and Chardon, 2013](#) ; [Grimaud, 2014](#) ; [Grimaud et al., 2014](#)) à l'échelle du sous-continent (100-1000 km) et de

proposer des modèles d'évolution des grands drainages continentaux sous l'influence de forçages extérieurs (Chardon et al., 2018). À l'échelle locale (1-10 km), les surfaces d'altération permettent de suivre les progressions et les rétroactions entre l'incision des rivières, le colluvionnement sur les versants et l'altération du substrat par écoulement des eaux souterraines. Le suivi de ces redistributions de matière peut avoir des implications industrielles lorsque les matériaux concernés sont d'intérêt économique, comme c'est le cas pour l'or et le nickel.

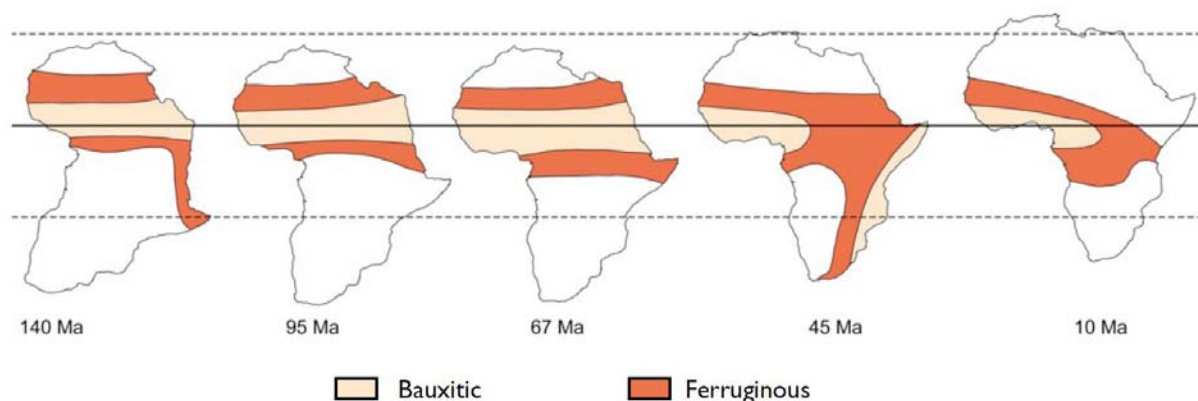


Fig. 4 : Dérive du continent africain depuis le Crétacé montrant la variation de l'extension latitudinale des zones d'altération ferrugineuse et bauxitique (adapté de Vrielynck et Bouysse, 2003 et Tardy et Soler, 1993 par D. Chardon).

La présente partie reprend de nombreux résultats de ma thèse -réalisée sous la direction de Dominique Chardon- et intègre des éléments nouveaux, issus de mon travail en cours sur la Nouvelle-Calédonie (Projet Transnum ; porté par Michel Cathelineau, Géoressources Nancy).

1.1. Fonctionnement des paysages tropicaux

1.1.1 Modelés tropicaux et séquences morphoclimatiques

L'étude des paléo-altérations latéritiques fut un sujet majeur au sein de l'ORSTOM (aujourd'hui l'IRD) des années 50 aux années 80. Malheureusement, les nombreuses publications faites par les chercheurs de l'ORSTOM le furent principalement en français, ce qui freina leur dissémination à l'international. Cependant, certains ouvrages de synthèse (Tardy et Roquin, 1998 ; Burke et Gunnell, 2008) et contribution récentes -auxquelles j'ai eu l'opportunité de participer- ont permis de remettre au goût du jour certaines idées et concepts.

a) Fonctionnement actuel

Dans de nombreuses régions -et notamment en Afrique de l'Ouest- on distingue différents modelés du paysage qui sont symptomatiques de climats différents (Fig. 5). Sous climat équatorial, le modelé est de type « demi-orange » (voir références dans Grimaud, 2014). Ce type de paysage est caractéristique de la prédominance des processus géochimiques et conduit à la formation de profils d'altération latéritiques. Une lente mise en solution et un export des éléments contenus se met en place dans les roches par la percolation des eaux météoritiques dans le sous-sol. Elle est facilitée par les températures élevées, l'activité biologique et les précipitations importantes. Cette transformation est d'abord isovolumétrique lors du lessivage des éléments les plus solubles. Elle conserve la structure originale de la roche et crée de la

porosité. Lorsque les éléments plus immobiles sont mis en solution, les tranches altérées changent de volume et leur structure évolue. C'est la « fonte géochimique » qui permet l'abaissement de la topographie (Nahon, 1976 ; Büdel, 1982) à mesure que progresse la base du front d'altération. Les bilans géochimiques proposés par Tardy et Roquin (1998) pour l'Afrique de l'Ouest et Trescases (1975) et aussi S. Favier (thèse en cours, projet Transnum) pour la Nouvelle Calédonie permettent d'estimer des échelles de temps de l'ordre de plusieurs millions d'années pour la formation de ces manteaux d'altération.

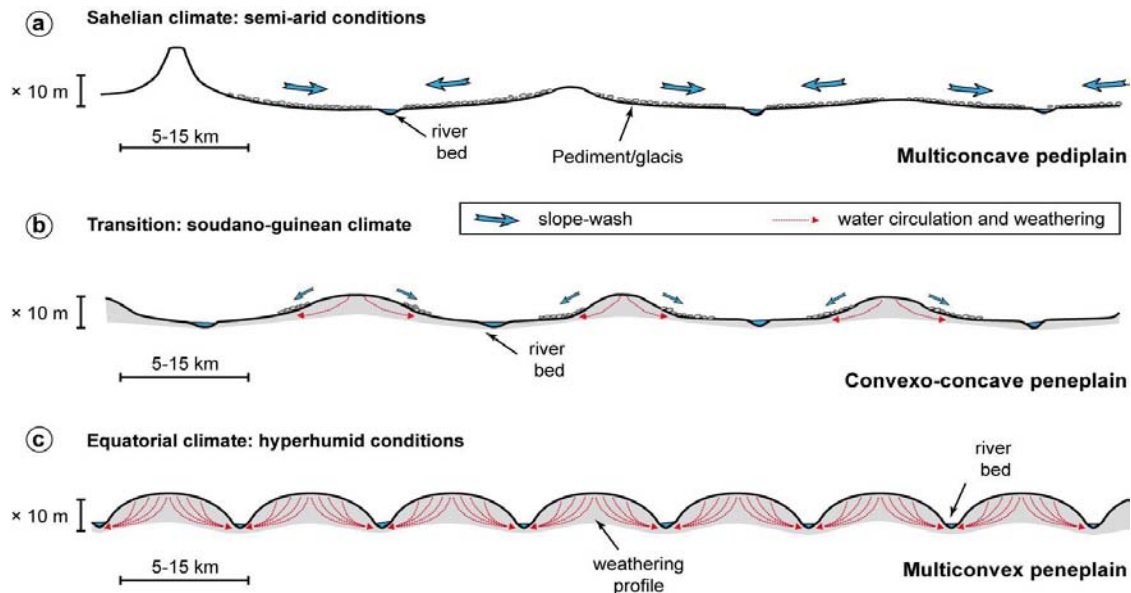


Fig. 5 Paysages types et mode d'altération/érosion tropicaux en fonction du climat (Grimaud, 2014). (a) Sous climat sahélien les précipitations se font sous un régime de mousson durant lequel l'érosion s'effectue via le développement de pédiments ou « glacis ». (b) Sous climat soudano-guinéen, les vallées se creusent légèrement alors que l'altération fonctionne. (c) Sous climat équatorial, l'altération intense en contexte de drainage efficace provoque la formation de morphologie en « demi-orange ».

Sous climat sahélien, le modelé est très différent. La végétation est clairsemée du fait de la sécheresse une grande partie de l'année. Dans ces conditions, les sols sont vulnérables aux événements pluvieux intenses lors des périodes de mousson (Michel, 1973). On assiste alors au développement de grands glacis ou pédiments – surfaces d'érosion et de transit de colluvions de forme légèrement concave (Grandin, 1976). Ces surfaces sont caractéristiques des milieux semi-arides et sont décrites par exemple en Australie et au Sud des USA (Nevada) (Twidale, 1981 ; Pelletier, 2010).

b) Modelés passés et séquences morphoclimatiques

Principe

En appliquant le principe d'actualisme à certaines formes du relief, on peut en déduire qu'elles sont héritées de périodes climatiques passées différentes. Par exemple, on retrouve des formes cuirassées et parfois des collines en forme de demi-orange dans des zones sahéliennes en Afrique sub-saharienne alors que le modelé dominant est de type pédimentaire (Watson, 1887). La répétition de ces séquences topographiques dans les différents paysages et leurs similitudes

ont mené différents auteurs à proposer une séquence type, qui serait synchrone à l'échelle de zones géographiques (Michel, 1973 ; Grandin, 1976) (Figs. 6 et 7). Elle répondrait à des cillations du climat qui alterneraient entre des phases dominées par l'érosion (périodes plus froides) -durant lesquelles les rivières inciseraient- et des phases plus propices à l'altération (périodes plus chaudes) – durant lesquelles les manteaux latéritiques se formeraient.

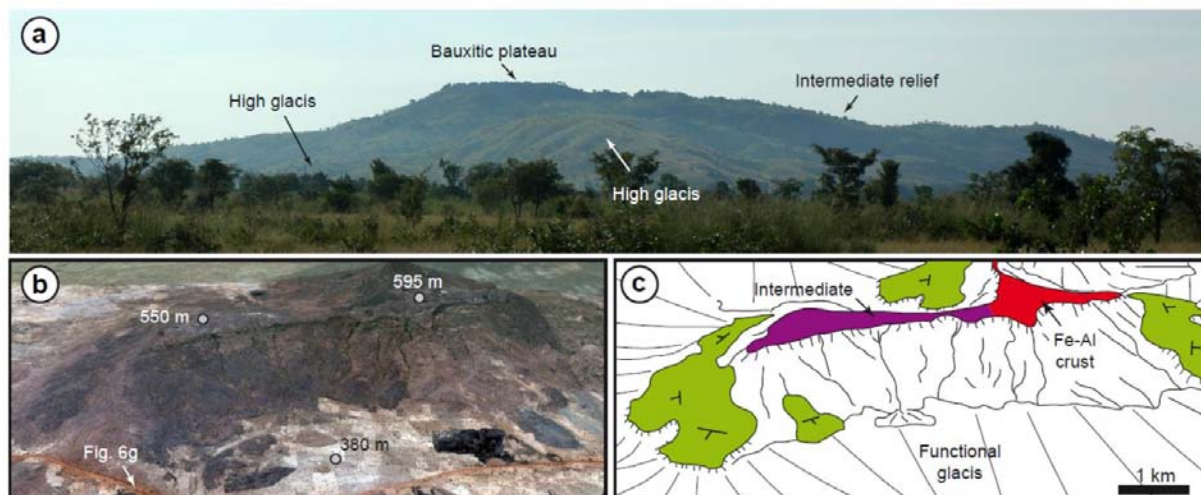


Fig. 6 Exemples de paysages où sont préservés des éléments de la morphoséquence climatique de Michel (1973) (Grimaud et al., 2015). (a) plateau bauxitique surmontant une zone de ceinture de roches vertes à Iridiaka. (b)–(c) Vue Google Earth et son interprétation sur dolérite d'un massif près de Kokoro, bassin de Taoudéni.

Des séquences comparables sont décrites dans différentes zones du globe (Tardy et Roquin, 1998). L'exemple le plus documenté reste à ce jour celui de l'Afrique de l'Ouest. Il tient aux travaux récents sur la zone mais surtout aux nombreuses descriptions de terrain qui ont aidé à généraliser cette séquence à l'échelle sous-continentale (voir une synthèse dans Grimaud, 2014). La séquence africaine est composée de cinq surfaces identifiables en se basant sur l'analyse morphologique et la pétrologie des cuirasses (i.e., le sommet préservé des profils d'altération associés) (Fig. 7). Cette séquence témoigne du refroidissement terrestre observé au Cénozoïque, tout du moins de la contraction de la zone équatoriale, dont la limite nord a migré vers le sud depuis la fin du Crétacé (Tardy et Roquin, 1998 ; Zachos et al., 2001 ; Scotese et al., 2021). En effet, les surfaces les plus anciennes (bauxitique et intermédiaire) sont caractéristiques de périodes d'altération chimique intense, notamment la surface bauxitique éocène qui possède des éléments résiduels alumineux. Les trois surfaces postérieures (les glacis) sont surmontées de cuirasses ferrugineuses- tout comme l'Intermédiaire- mais avec une épaisseur de ces ferruginisations qui décroît entre le Haut, le Moyen puis le Bas Glacis. Le passage d'un modelé seulement chimique à un modelé plus érosif -de même que la décroissance de l'épaisseur d'altération au cours du temps- est également cohérent avec le refroidissement global.

L'approche selon la séquence morphoclimatique -que j'ai employée durant ma thèse- a de nombreuses similitudes avec la stratigraphie séquentielle (van Wagoner et al., 1988). Il s'agit de retrouver tout ou partie d'un « pattern » non pas empilé dans une succession sédimentaire mais étagé dans les reliefs. Il peut être guidé par la pétrographie des cuirasses mais également par les datations lorsque celles-ci sont possibles. Le modèle sur lequel nous sommes appuyés dans ma thèse est celui développé par Grandin (1976) par suite des travaux de Michel

(1973). Il souffre des mêmes limites que la stratigraphie séquentielle : il peut localement y avoir des soucis de corrélation si toutes les formes ne sont pas bien préservées. Cependant, il s'appuie sur une étude fine des formes du paysage et pas seulement sur l'interprétation de variations de la topographie à grande échelle (e.g., King, 1955 ; Guillocheau et al., 2014) qui peuvent souffrir d'imprécisions (voir section 2.1.1).

Datations

Les âges radiométriques sur oxydes de manganèse les mieux calibrés en Afrique de l'Ouest sont à Tambao (Nord Burkina Faso) (Hénocque et al., 1998 ; Colin et al., 2005 ; Beauvais et al., 2008). Ils ont permis de donner des contraintes sur les périodes d'altération cénozoïques dans la région –qui précèdent l'abandon des profils d'altération et des surfaces associées. Sont également mises en évidence : (1) des périodes d'arrêt de l'altération -probablement lors d'épisodes plus érosifs- et (2) une corrélation entre âges des oxydes et altitudes -marquant l'enfoncement du paysage. En combinant ces données avec celles de Syama (sur alunite et jarosite ; Sud Mali) (Vasconcelos et al., 1994), j'ai pu montrer une corrélation temporelle entre les deux localités (Grimaud et al., 2015, 2018) (Fig. 7). On observe néanmoins un certain diachronisme avec par exemple l'occurrence à Syama d'oxydes supergènes durant la période 40-30 Ma qui ne sont pas représentés à Tambao. On peut proposer comme explication (1) la variabilité d'enregistrement qui peut exister d'un lieu à un autre, en lien avec son évolution morphologique locale, mais aussi (2) le décalage qui peut exister en lien avec l'évolution de la distribution des zones climatiques dans le temps (Syama, plus au Sud, a pu subir plus longtemps un climat propice à l'altération que Tambao). Ces résultats montrent l'intérêt de dater régionalement les profils d'altération – en combinant différentes méthodes- afin de mieux appréhender la dynamique d'évolution des gradients de température et de précipitations lors de changements climatiques.

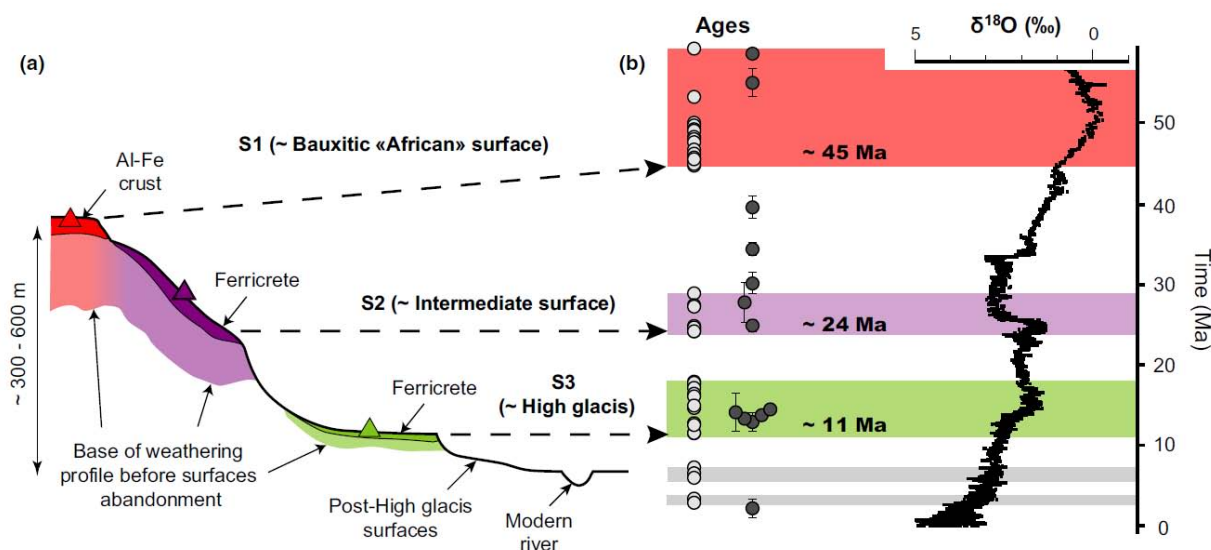


Fig. 7 : Séquence morphoclimatique ouest-africaine (Grimaud et al., 2018). (a) Schéma de la distribution des surfaces et des altérations associées dans le paysage. (b) Comparaison entre les âges des localités de Tambao and Syama (Beauvais et al. (2008) (points gris clair) et Vasconcelos et al. (1994) (points gris foncé)). La courbe de variation du $\delta^{18}\text{O}$ océanique sur foraminifères benthiques est celle de (Zachos et al., 2001).

Actuellement, de nombreux travaux sont menés pour encore améliorer la datation des latérites. On peut citer les travaux récents au Brésil (Riffel et al., 2015 ; Vasconcelos et Conroy, 2003) ou en Inde (Beauvais et al., 2016 ; Jean et al., 2020) se basant principalement sur les oxydes de manganèse. À cela s'ajoute de nombreux développements sur oxydes de fer comme la méthode (U-Th)/He sur goethite, qui montrent des héritages complexes et du polyphasage sur les profils d'altération (e.g., Heller et al., 2022). Dernièrement, une nouvelle méthode basée sur l'ESR (Electron Spin Résonance) dans les kaolinites a été présentée (Matthian, 2018 ; Allard et al., 2018). Ces deux dernières méthodes présentent l'avantage de se baser sur des minéraux plus ubiquistes que les oxydes de manganèse.

En Nouvelle-Calédonie, il existe une séquence cuirassée qui a été proposée par Chevillotte et al. (2006) sur la base des travaux de Trescases (1975). Cette séquence est composée de huit surfaces. Contrairement à l'Afrique de l'Ouest, il n'y a pas de surface bauxitique et il est plus difficile de distinguer pétrologiquement les profils d'altération. Cette homogénéité est due à au substrat dépourvu d'aluminium sur lequel on trouve les altérites en Nouvelle-Calédonie (péridotites-serpentinites). Chevillotte et al. (2006) proposent également une chronologie pour cette séquence avec peu de contraintes. Cette séquence s'appuie principalement sur les relations géométriques entre ces surfaces et les dépôts de la région de Népoui. Depuis, une série d'études a apporté des contraintes nouvelles, notamment dans le cadre de la thèse de Brice Sévin (Sévin et al., 2013 ; Sévin, 2014) et les datations sur oxydes des manganèses menées par Florence Quesnel, Johan Yans et Gilles Ruffet (reprises dans Bailly et al. (2014) et Sévin et al. (2020)). Ces derniers auteurs n'ont à ce jour pas mis en évidence les relations entre les âges obtenus et les surfaces paléo-surfaces latéritiques étagées. Il serait donc pertinent de pouvoir croiser les deux approches (géochronologique et morphologique) pour mieux contraindre la chronologie de la dynamique de surface cénozoïque en Nouvelle Calédonie.

1.1.2 Cartographie des altérites : intérêts académiques et industriels

Les reliques latéritiques sont de précieux témoins de l'évolution topographique en domaine anorogénique. Leur cartographie permet de restituer l'évolution des paysages et de calculer des taux de dénudation. Cela constitue également un premier pas pour aborder des facteurs qui contrôlent cette évolution et suivre les processus de redistribution des matériaux d'intérêt économique sur les versants.

a) Dynamique d'érosion et réorganisation des réseaux de drainage

Le Burkina Faso

Le premier des cinq articles représentatifs que j'ai sélectionnés est celui paru dans *Geomorphology* en 2015 (voir Annexe 2). Il illustre la démarche de cartographie du régolithe utilisée pendant ma thèse avec le cas du sud-ouest du Burkina Faso. L'approche combine reconnaissances de terrain recoupées avec des données topographiques et radiométriques (données de spectrométrie gamma ray obtenues par WAXI) pour proposer une cartographie complète des reliques de Haut-Glaciais dans la région. Elle a permis de reconstituer la topographie de la zone à 11 Ma afin d'estimer la taille des glaciais de l'époque (~ 20 km de long) et d'identifier des réorganisations du réseau de drainage, montrant une réorientation d'affluents du fleuve Mouhoun vers le Sud-Est. L'impact de la lithologie du substrat est démontré par les

modèles de préservation des surfaces différents sur granitoïdes ou ceintures de roches vertes : ils sont plus mous sur les premiers et plus entaillés sur les seconds (Fig. 8).

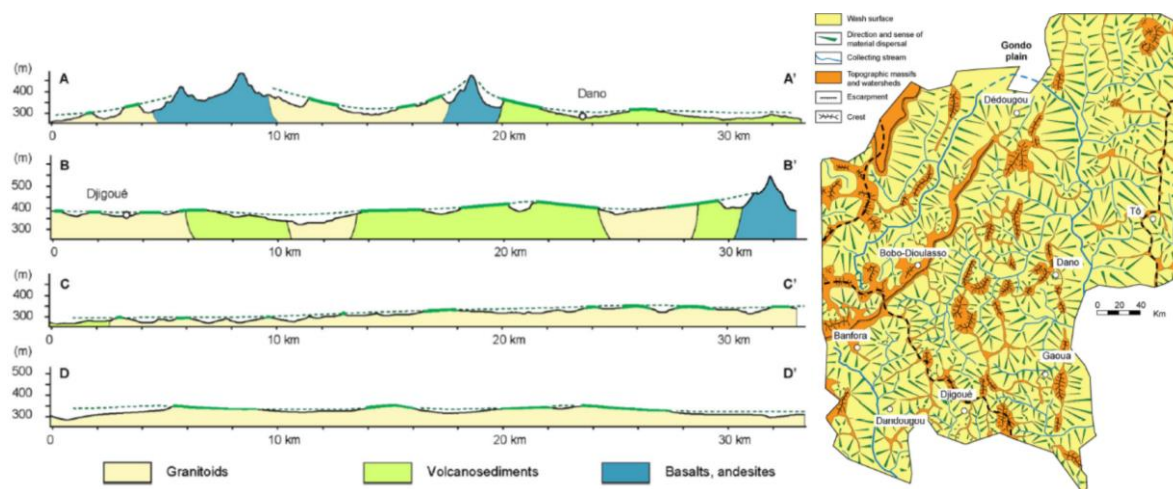


Fig.8 : (gauche) Coupes morpho-géologiques montrant le modèle des paysages et les relations entre le substrat géologique et la surface de Haut glaciaire. La morphologie évolue de haut en bas d'un paysage très incisé sur substrat basique à un paysage « mou » sur substrat acide. (droite) Restitution du drainage et des surfaces de glaciaire à 11 Ma d'après la cartographie du Haut glaciaire (Grimaud et al., 2015).

Avec cette étude, j'ai pu calibrer le « bruit de fond » de dénudation cratonique (2m /Ma) dans une zone loin de l'influence des mouvements épirogéniques. Les résultats sont cohérents avec les études de Brown et al. (1994) et Braucher et al. (1998) au Burkina Faso qui suggèrent respectivement des taux de dénudation de 3-8 et 2 m /Ma sur la base de données cosmogéniques locales sur des veines des quartz. Notre étude propose une estimation du temps pour rééquilibrage d'une surface cratonique de l'ordre de grandeur de 20 Ma au minimum : on ne peut donc pas considérer les zones cratoniques comme étant à l'équilibre (Bishop, 2007). Enfin, si de nombreuses captures potentielles sont identifiées, elles concernent des aires drainées modestes et représentent principalement des auto-captures au sein du réseau Mouhoun. Elles ont donc peu d'influence sur le flux sédimentaire exporté par le fleuve. Nous y reviendrons plus longuement dans les parties 2 et 3.

La Nouvelle Calédonie

J'ai récemment travaillé en Nouvelle-Calédonie, à proximité du site minier de Goro (anciennement Vale, maintenant Prony), en complément des précédentes études cartographiques effectuées sur la zone (Trescases, 1975 ; Chevillotte, 2005 ; Sévin, 2014). Contrairement à ce que proposent ces études, j'identifie plusieurs générations de surfaces dans la zone, ce qui permet de mieux contraindre la dynamique d'incision. En particulier, on observe une dynamique différente entre les zones côtières du sud et les bassins à l'intérieur des terres comme le Goro pit (Fig. 9). Les premières sont dominées par des surfaces jeunes (S4-S5) tandis que les seconds préservent plus largement des surfaces plus vieilles (S2-S3). Par corrélation entre les deux zones, on peut en déduire (1) que le bassin de Goro est exoréique et connecté vers le sud depuis la surface S3 (soit depuis le début du Néogène ; Cathelineau et al., sous presse) et (2) qu'une incision post S3 importante existe au sud et se propage vers le Nord et le Goro pit.

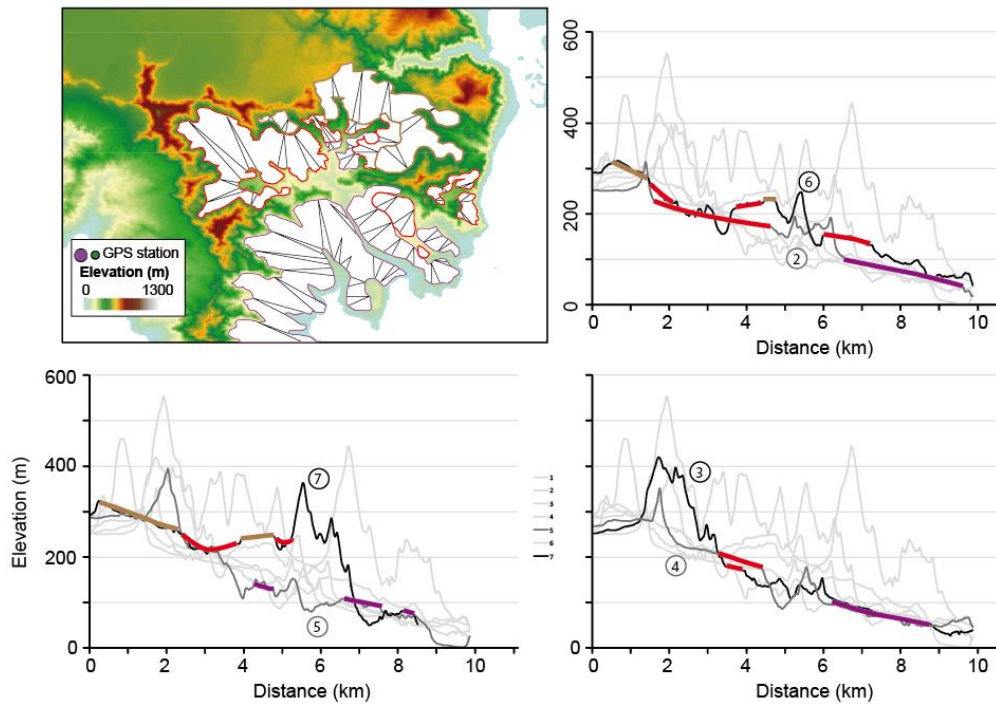


Fig. 9 : Distribution des reliques de paléosurfaces latéritiques en carte et en coupes dans le sud-est de la Nouvelle Calédonie à proximité du Goro Pit (Grimaud et al., in prep (a))

En accord avec une incision post-S3 plus agressive, on observe des évidences de captures post-S2-S3 dans le sud-est de l'île, dont le moteur pourrait être un basculement général de l'île vers le Sud-Ouest (Chardon et Chevillotte, 2006). Ces observations sont en accord avec la carte de χ (Perron et Royden, 2013 ; Willet et al., 2014 ; Grimaud et al., in prep(a)) de la zone (Fig. 9). Cette dynamique de capture fut pressentie dès les années 1970 par Trescases (1969, 1975) qui propose un modèle d'évolution néo-calédonien avec comme départ des morphologies similaires à celles de la zone de Goro. Le fonctionnement initial de ces bassins, endoréiques, est supposé « karstique » : les matériaux érodés et dissous sur les versants sont évacués via des dolines dans des réseaux souterrains jusqu'à des résurgences ou par connexion directe à la mer (Bailly et al., 2014). Les systèmes karstiques entraînent -en synergie avec la dynamique d'incision- une redistribution de la silice et du nickel (Cathelineau et al., sous presse). Puis, les bassins endoréiques se font progressivement inciser et inverser, amenant à des systèmes de plateau puis de pente. Ce modèle est aujourd'hui largement repris dans l'industrie minière car il intègre, dans cette évolution morphologique, la dimension géochimique et la redistribution du nickel dans les profils d'altération. Or, les premiers résultats de mon travail en Nouvelle Calédonie semblent indiquer que les bassins du sud-ouest près de Goro peuvent être exoréiques depuis longtemps, questionnant le modèle initial.

b) Dynamique des versants et impact sur les ressources minérales

Les pièges de l'exploration en milieu latéritique

Mes travaux de thèse ont été effectués dans le cadre de l'initiative d'exploration ouest africaine (projet WAXI). Un volet de la thèse concernait la dynamique du régolithe et particulièrement la redistribution des matériaux par colluvionnement. De manière générale, les couvertures latéritiques sont un frein à la prospection : la roche saine -porteuse de minéralisation- est

masquée par le régolithe (Perseil et Grandin, 1978 ; Metelka et al., 2018). Le colluvionnement et la redistribution de matière peuvent également conduire à tomber dans des pièges lors des phases d'exploration géochimiques si la géomorphologie des sites n'est pas bien appréhendée (Chardon et al., 2018). En particulier, les cuirasses peuvent (1) masquer la géochimie réelle du substrat et le colluvionnement peut générer des « nuages » de dispersion des anomalies chimiques (C. Ginest, communication personnelle 2010), en particulier l'or qui est peu facilement altérable chimiquement. Lors de ma thèse, nous avons donc proposé des démarches à suivre à destination des explorateurs miniers ouest africains. En particulier, j'ai développé sous logiciel SIG des procédures d'intersections entre shapefiles du sous-sol et de cuirasses latéritiques, et indices de minéralisation pour identifier de potentielles zones minéralisées masquées par la couverture latéritique.

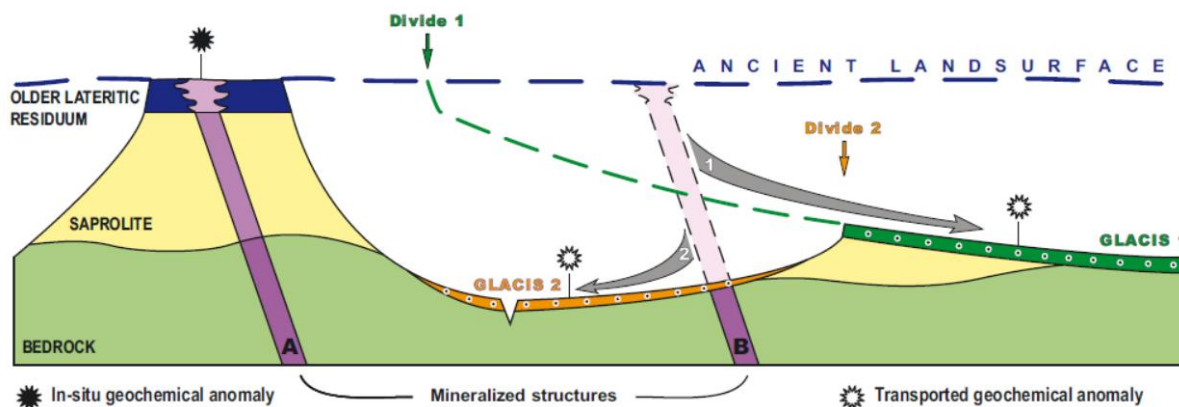


Fig. 10 : Coupe schématique montrant les liens entre minéralisations associées au régolithe et minéralisations endogènes. Dans le cas des minéralisations transportées associées à des surfaces type glacis, il est primordial d'analyser finement la dissection du paysage et les pentes de colluvionnement pour ne pas rater les minéralisations endogènes (Chardon et al., 2018).

Dynamique de l'altération vs incision

Mes collaborations dans le cadre du projet CNRT Transnum m'ont permis de pouvoir accéder au site minier de Goro à plusieurs échelles. Nous avons ainsi pu nous rendre sur le site pour y faire des observations et accéder à une base de données de sondages très dense (~3000 sondages). La combinaison de ces observations a permis de voir le site sous un jour nouveau (Grimaud et al., in prep (a)). On identifie des indices de polygénisme de la surface principale, c'est-à-dire que celle-ci ne résulte pas d'un cycle de phase d'érosion suivi d'une phase d'altération mais de la répétition d'au moins deux de ces cycles. Ce phénomène est notamment observable sur la bordure sud du Goro pit. On y voit deux niveaux de cuirasse séparés par un rebord d'environ quelques mètres (Fig. 11). Dans le niveau cuirassé le plus bas, on observe des blocs de la cuirasse du dessus remobilisés et recuirassés. Cette transition est visible dans la topographie et permet de compléter la cartographie de plusieurs générations de paléo-surfaces cuirassées dans la zone (Fig. 9). Elle correspond en outre à une transition dans la carte interpolée de l'épaisseur des profils d'altération (S. Favier PhD ; Grimaud et al., in prep (a)).

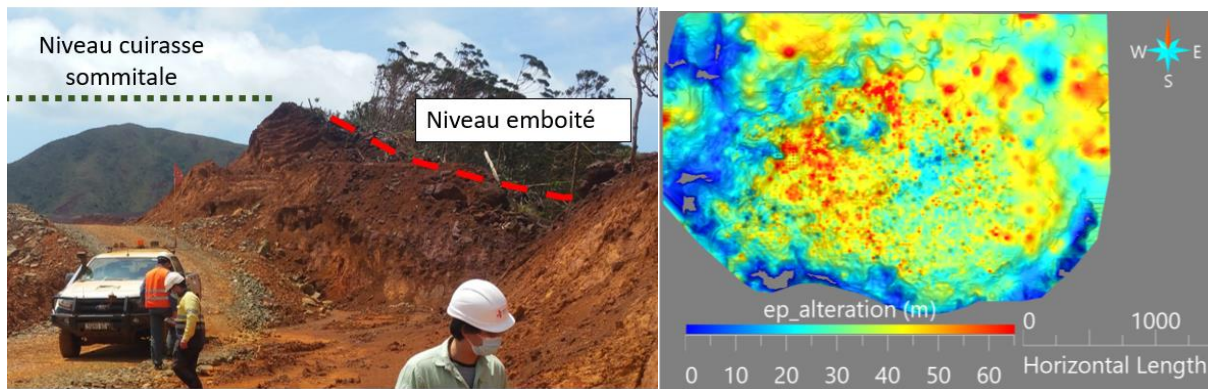


Fig. 11 : (gauche) Rebord sud du site d'exploitation de Goro montrant une cuirasse préservée avec des évidences d'emboîtement d'un niveau sous un autre. Cette géométrie suggère de faibles gammes d'incision entre les deux stades (surfaces 2 et 3 ici). (droite) Carte interpolée sous gocad, montrant une augmentation de l'épaisseur de l'altération -dont la limite coïncide avec la limite cuirasse montrée à gauche (figure S. Favier) (Grimaud et al., in prep (a))

On peut donc proposer qu'il y ait eu faible incision entre les deux surfaces décrites à la transition entre les deux cuirasses (nous proposons que ce soit S2 et S3), ce qui a permis de reprendre l'altération du profil S2 pendant la phase S3 et de le rendre plus épais. C'est un modèle nouveau pour une zone « type » de bassin : le sur-épaississement du profil d'altération est dû non pas à l'aggradation dans une zone de bas-fond (Trescases, 1975) mais à un mécanisme d'incision faible qui permet un polygénisme des surfaces et des profils d'altération associés. Ainsi, la cartographie fine des étagements des cuirasses permet une meilleure connaissance de la géométrie des gisements de nickel, associés dans cette zone à l'horizon latéritique (i.e., lithomarge ou saprolite fine, d'après Tardy et al., 1993) du profil d'altération.

1.2 Taux de dénudation cratoniques et export vers les océans

Le principal travail de ma thèse fut de compiler une base de données recensant la position et l'altitude de reliques de paléo surfaces latéritiques et de les identifier (S1 : bauxite 45 Ma, S2 : intermédiaire 24 Ma et S3 : Haut Glacis 11 Ma). Le second des cinq articles sélectionnés est celui paru à *Basin Research* en 2018 (voir Annexe 2). Pour ce travail, environ 2900 stations sont compilées, dans la zone en érosion, mais aussi dans les bassins sédimentaires intracontinentaux ou côtiers de la zone (Iuellemmeden, Sénégal, côte d'Ivoire et Togo-Bénin) (liste complète des références dans Grimaud et al., 2018). Nous avons pu ainsi développer une technique d'interpolation entre ces stations qui prend en compte le stockage intracontinental en utilisant le logiciel Gocad. En guidant ou non cette interpolation avec la topographie (Fig. 12), nous avons enfin pu calculer des incertitudes sur la géométrie de ces surfaces. Cette phase de ma thèse, qui a permis de proposer la restitution de la paléogéographie et des flux sédimentaires cénozoïques, a été effectuée en collaboration avec Delphine Rouby au GET Toulouse.

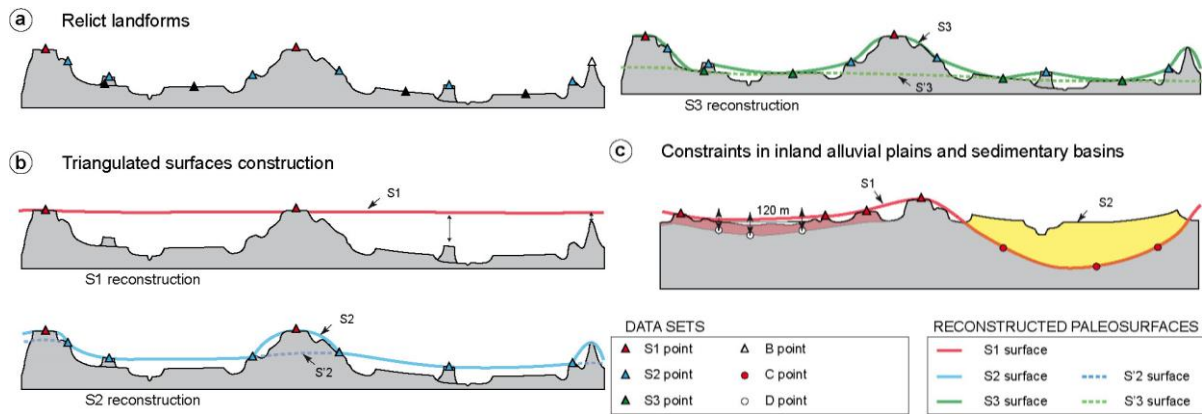


Fig. 12 : Représentation schématique en coupe de paysages ouest africains et construction de surfaces d'après les reliques de paléo surfaces préservées (Grimaud et al., 2018, supporting information). (a) Distribution des reliques dans le paysage actuel. (b) Géométrie des surfaces S1, S2, S2', S3 et S3' reconstruites d'après les reliques bauxitiques, intermédiaires et de Haut glacis, respectivement. (c) Connection de la surface S1 aux dépôts éocènes (top Yprésien / base Lutétien) dans les bassins sédimentaires continentaux et côtiers.

1.2.1 Dynamique et réorganisation des bassins-versants

Dans un premier temps, les interpolations des reliques de paléo-surfaces ont permis de proposer une reconstruction de la paléogéographie de la zone et de l'évolution de la géométrie des bassins de drainage (Chardon et al., 2016). Il faut noter que les données morphologiques sur lesquelles nous nous basons sont issues de la topographie actuelle et ne correspondent pas aux paléo-altitudes absolues de leur époque de formation. Nous utilisons donc à la fois les données des bassins sédimentaires compilées pendant ma thèse et un modèle d'isostasie calculant la déformation post-abandon des paléo-surfaces pour restituer au mieux la paléogéographie.

Les résultats de l'étude montrent que le drainage ouest africain est vieux, les principaux bassins-versants étant similaires à ceux d'aujourd'hui depuis au moins 24 Ma. Nous proposons en outre un drainage différent à l'Éocène, guidé par un bourrelet marginal longeant la côte à l'ouest et au sud. Ce bourrelet fut traversé par les grands drainages (Niger, Mouhoun), permettant l'afflux de sédiments. Cette interprétation contraste avec celle de Séranne (1999) qui propose que l'augmentation des flux observés sur la marge ouest africaine plus au sud soit liée à des variations climatiques. Nous proposons en outre que le moteur de cette réorganisation soit la dynamique mantellique de la zone, en lien avec l'accélération de la dénudation dans le Hoggar (Burke, 1996 ; Rougier et al., 2013). Ainsi, nous montrons en Afrique de l'Ouest une certaine stabilité des drainages, contrairement au postulat de Willett (2014) selon lequel les drainages des zones anorogéniques sont sujets à des dynamiques de capture intenses. On peut tenter de réconcilier ces faits en s'interrogeant sur la vitesse des captures -probablement plus lente en domaine cratonique- et l'implication d'aires drainées modestes dont l'impact sur les flux de bassins de taille subcontinentale est faible (section 1.1.2a).

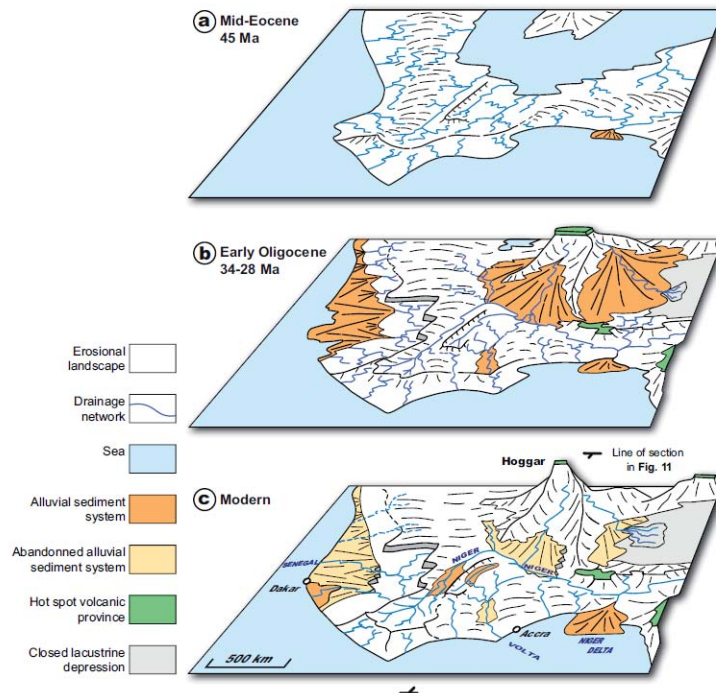


Fig. 13 : Reconstitution de l'évolution paléogéographique cénozoïque de l'Afrique de l'Ouest (Chardon *et al.*, 2016). (a) Stade éocène (~ 45 Ma) montrant un bourrelet marginal séparant un drainage sud vers l'Atlantique et un drainage nord (b) Stade oligocène (~34–29 Ma) montrant la connexion des grands systèmes (Mouhoun, Niger) vers l'Atlantique au gré du basculement de l'Afrique en lien avec le soulèvement du Hoggar qui se prolonge à l'actuel (c).

1.2.2 Taux d'érosion et export des zones anorogénique

Dans un second temps, les interpolations des reliques de paléo-surfaces ont permis d'effectuer des estimations de taux de dénudation et d'export de matière vers l'océan. Ces estimations sont proposées par simple soustraction des surfaces, prenant en compte les variations de porosité des profils d'altération et le stockage de sédiments dans les bassins sédimentaires continentaux et côtiers (Grimaud, 2014 ; Grimaud *et al.*, 2018).

À l'échelle ouest africaine, les résultats obtenus montrent un taux de dénudation moyen de 6 m/Ma qui est converti en charge sédimentaire exportée de ~ 20 t/km²/an au total. Considérant que la porosité est obtenue par lessivage chimique, on peut estimer une charge soluble de ~ 5 t/km²/an au minimum. Ces résultats sont proches des mesures modernes de particules en suspension (19 t/km²/an à l'exutoire du Niger ; Summerfield et Hulton, 1994). Considérant une charge de fond faible dans les rivières tropicales (Wirthmann, 2000 ; Allen et Allen, 2005), le flux solide actuel du Niger pourrait donc être équivalent à son flux long-terme depuis 24 Ma. Cette stabilité est comparable à celle montrée pour les grands fleuves asiatiques au Cénozoïque (Métivier et Gaudemer, 1999). Ils ont permis (voir papier Grimaud *et al.*, 2018 Basin Research en Annexe 2) de calculer l'export sédimentaire des grands bassins-versants ouest africains depuis 45 Ma, en particulier vers le delta du Niger. La comparaison avec l'enregistrement sédimentaire sera détaillée en section 3.1.1. Nous proposons également d'utiliser les taux ouest africains pour extrapoler le flux sédimentaire exporté des zones anorogéniques (Fig. 14) vers les océans (2 ± 0.6 Gt/an). L'estimation faite est supérieure au bruit de fond calculé plus tôt

(section 1.1.2a), suggérant une contribution non-négligeable des mouvements verticaux (flexure, topodynamique) sur les bilans sédimentaires des zones anorogéniques.

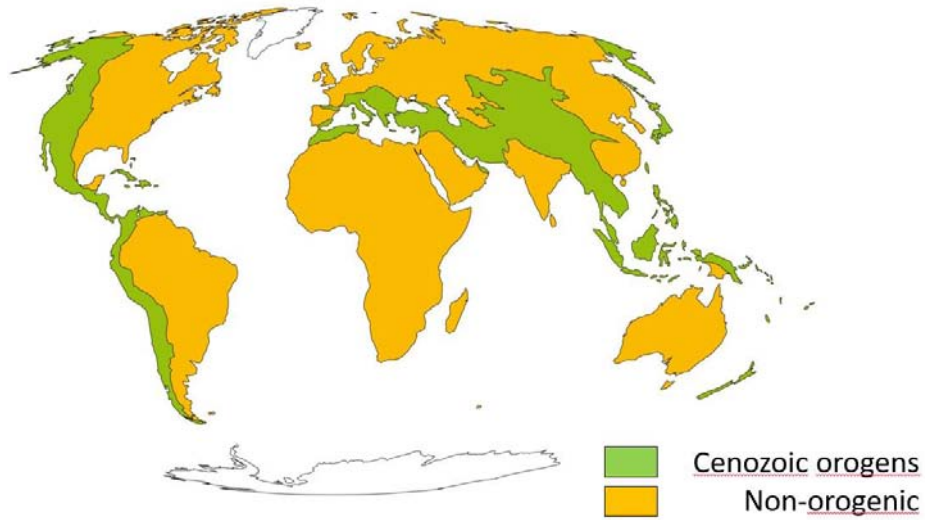


Fig. 14 : Carte de la distribution des zones orogéniques et anorogéniques (Grimaud, inédit 2014). Utilisant les valeurs ouest africaines pour une extrapolation mondiale résulterait en un export cénozoïque de 2 ± 0.6 Gt/an.

2- Dynamique de la zone de transfert : creusement du substrat et (re)mobilisation sédimentaire

La zone de transfert occupe une place centrale dans les systèmes de routage des sédiments (Fig. 1). Assurant la continuité entre source et bassins sédimentaires, elle peut transmettre les changements environnementaux (niveau de base, débit, flux sédimentaire...) depuis l'un de ces compartiments vers l'autre. Cependant, ce transfert n'est pas toujours correctement effectué : le signal peut être tamponné, atténué ou modifié au fur et à mesure qu'il se propage (e.g., [Jerolmack and Paola, 2011](#) ; [Romans et al., 2016](#) ; [Straub et al., 2020](#) ; [Tofelde et al., 2021](#)). Comprendre dans quelle mesure les signaux sont transmis -et quels sont les facteurs qui impactent la zone de transfert- est capital pour pouvoir mieux interpréter les enregistrements sédimentaires dans les bassins.

La zone de transfert constitue la partie sur laquelle je travaille le plus activement actuellement. Je m'intéresse principalement aux corridors fluviaux et à leurs plaines alluviales. Cette seconde partie aborde donc (1) la géométrie à plus grande échelle des corridors fluviaux, et les facteurs qui la contrôlent, et (2) la dynamique des remplissages alluviaux et de l'enregistrement sédimentaire dans ces zones.

2.1 Géométrie des corridors alluviaux et impact de la lithologie du substrat

2.1.1 Exemple ouest africain

Une approche classique d'étude et de modélisation des paysages consiste à regarder comment la dynamique des profils en long des rivières influence l'évolution des domaines continentaux ([Whipple, 2004](#)). En réponse à des sollicitations extérieures, les rivières vont inciser pour se rééquilibrer, entraînant des ajustements qui vont se propager et affecter l'ensemble du paysage. L'exemple le plus connu est le retrait vers l'amont d'un knickpoint -le locus d'un changement de pente- en réponse à un changement du niveau de base (provoqué par une baisse eustatique ou un soulèvement tectonique). Lors de ma thèse, j'ai proposé une restitution de la dynamique d'incision néogène le long des grandes rivières ouest africaines ([Grimaud et al., 2014](#)). Grâce à l'extrapolation de l'altitude des reliques de paléosurfaces latéritiques au niveau des talwegs de ces rivières, j'ai pu reconstruire -là encore basé sur leurs altitudes modernes- les paléo-profil en long de ces rivières (Fig. 15). Les résultats obtenus alors continuent d'alimenter mes projets de recherche actuels (voir ci-dessous).

En cohérence avec les reconstitutions paléogéographiques ([Chardon et al., 2016](#)), les profils en long montrent une géométrie différente à 45 Ma, alors qu'un bourrelet marginal côtier est en place, et à 24 Ma, au moment où le drainage est similaire à l'actuel. Les taux d'incision ainsi calibrés sont inférieurs à 10 m/Ma et de 5 m/Ma en moyenne ([Grimaud et al., 2014](#)). Enfin et surtout, les restitutions montrent qu'une grande partie des grandes knickzones majeures de ces profils sont localisées à des transitions lithologiques et sont stationnaires depuis 11 Ma. Ainsi, on peut difficilement interpréter ces knickzones comme étant activement en recul ; alors même que certains auteurs le supposent pour réaliser une inversion des profils en long des rivières et en déduire la distribution et la chronologie de l'uplift des zones anorogéniques (e.g., [Paul et al., 2014](#)). Les résultats sont cohérents avec d'autres études en Australie ou le long du Grand

Canyon (Goldrick and Bishop, 1998 ; Pederson et Tressler, 2012 ; Beauvais et al., 2016), suggérant qu'ils s'appliquent globalement. Enfin, on montre que certains escarpements sont stables depuis l'Éocène, ce qui contredit le modèle d'évolution par retrait d'escarpement (King, 1955 ; Guillocheau et al., 2014).

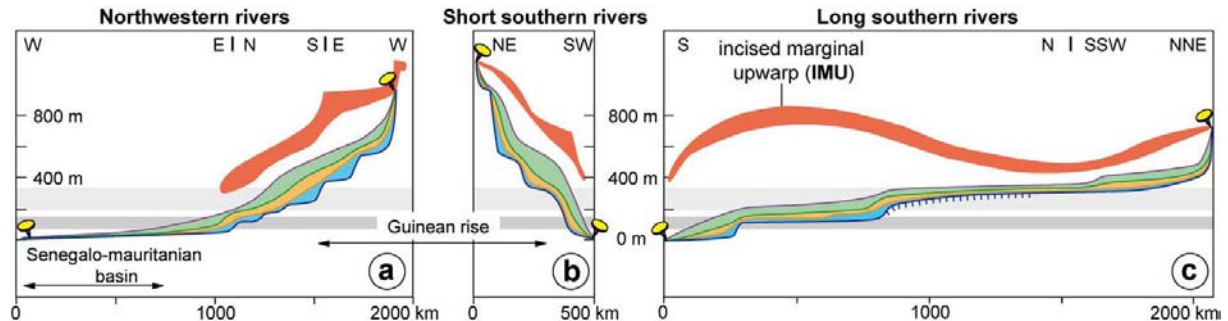


Fig. 15 : Restitutions schématiques des profils successifs d'Afrique de l'Ouest (Grimaud et al., 2014). (a) Groupe Nord-Ouest (Sénégal, Gambie). (b) Drains sud courts (Kakrima, Mano). (c) Drains sud longs (Volta, Comoé).

2.1.2 Apport de la modélisation analogique

a) Modèles mono-substrat

Le troisième des cinq articles sélectionnés est celui paru à *Earth Surface Dynamics* en 2016 (voir Annexe 2). Il s'agit d'une série d'expériences très simples conçues dans la continuité des résultats de l'étude ouest africaine (Grimaud et al., 2014) afin de tester les influences respectives de la lithologie du substrat et de la vitesse d'abaissement du niveau de base sur la vitesse de retrait et la géométrie de knickpoints (que nous appellerons « unitaires » par la suite). Le dispositif -un mini-chenal 1D de 2cm de large et moins d'un mètre de long- fut conçu en quelques semaines et les expériences réalisées au tout début de mon postdoctorat à Minneapolis sous l'influence de mon encadrant (C. Paola) qui m'encouragea à développer mes propres thématiques de recherche. Je lui en suis encore très reconnaissant.

Dans cette série d'expériences, je montre que les knickpoints ont une taille unitaire dépendante des propriétés du substrat (Fig. 16) et qu'ils se développent et reculent le long du profil après érosion d'une couche alluviale laissée par le retrait du knickpoint précédent. Des phénomènes similaires d'ajustement interne du système ont récemment été observés dans des expériences 2D puis 3D (Baynes et al., 2018 ; de Lavaissière et al., 2022). Ainsi, lorsqu'on augmente la vitesse d'abaissement du niveau de base, le retrait de plusieurs knickpoints successifs est observé. Le taux d'abaissement du niveau de base ne montre d'influence claire ni sur la vitesse de retrait des knickpoints ni sur leurs propriétés géométriques. Une série d'expériences complémentaires (Benett et al., 2000) montre en revanche que le débit appliqué (qui est maintenu constant dans ma série d'expériences) peut exercer une influence sur les propriétés du knickpoint (profondeur du surcreusement notamment).

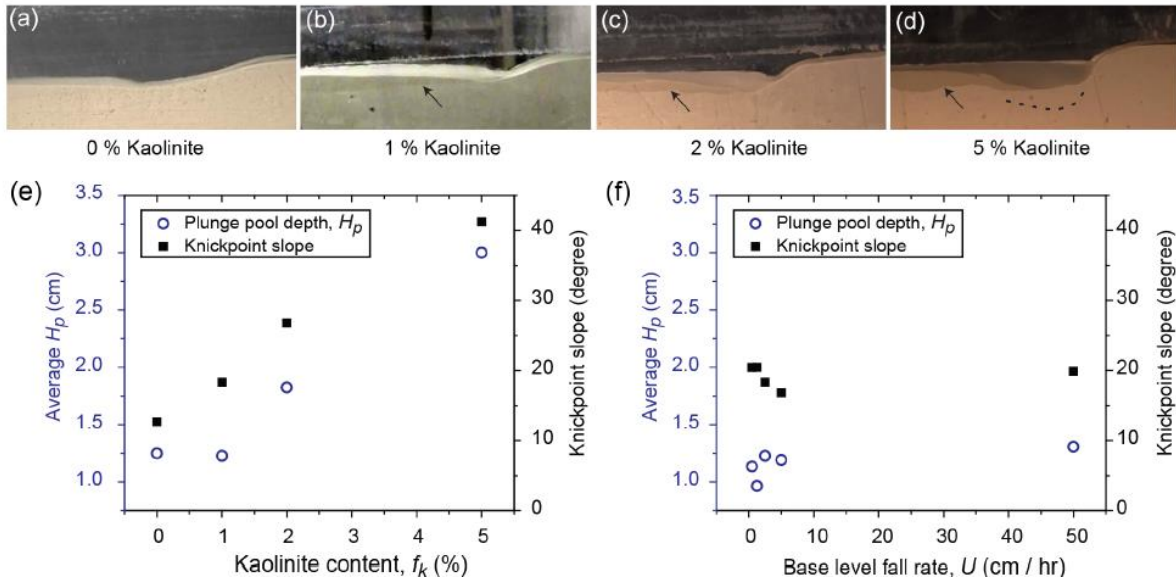


Fig. 16 : Influence de la lithologie du substrat sur les propriétés (ici la profondeur du surcreusement en amont) de knickpoints (Grimaud et al., 2016). Photographies de knickpoints développés sur des substrats lithologiques avec 0% (a), 1% (b), 2% (c) et 5% (d) de kaolinite mélangée à du sable fin. La profondeur du surcreusement montre une relation avec le % de kaolinite, ce qui n'est pas le cas avec le taux d'abaissement du niveau de base appliqué.

b) Modèle à 2 substrats

Si les résultats décrits en début de section sont cohérents (i.e., ils démontrent l'influence de la lithologie sur la dynamique d'incision le long des profils en long des rivières), le lien entre la dynamique des knickpoints unitaires et celle des grandes knickzones reste à faire. Dans ce but, j'ai encadré le stage de recherche de Morgane Goulain (alors en 2ème année à l'École des Mines), où un dispositif similaire au précédent (Grimaud et al., 2016) a été mis en place ; mais avec deux substrats différents. La limite entre les deux substrats est verticale : on distingue en aval un substrat avec 5% de kaolinite et en amont un substrat avec 8% de kaolinite (Fig. 17).

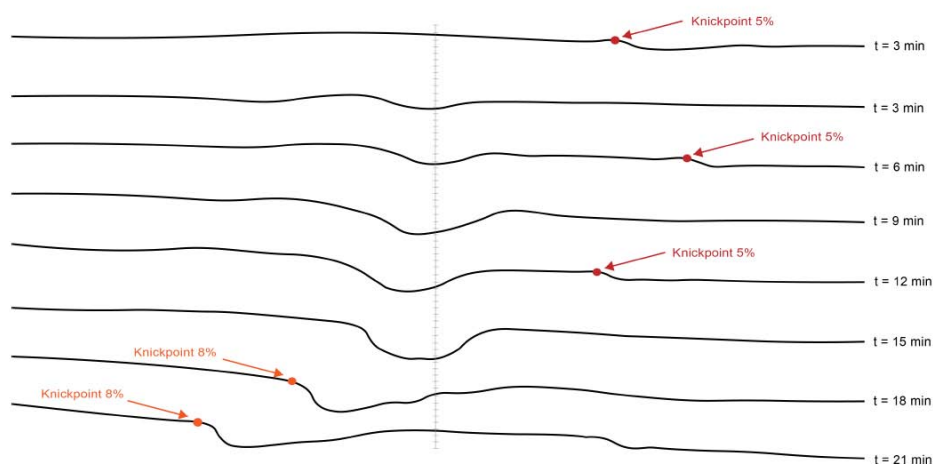


Fig. 17 : Résultats de l'expérience d'érosion à deux substrats en mini-canal (Stage M. Goulain 2019). Les géométries successives du fond de la lame d'eau sont dessinées d'après les photographies de suivi

de l'expérience prises de côté. L'eau s'écoule de la gauche vers la droite où le niveau de base est abaissé. La ligne en pointillés correspond à la transition entre substrat à 5% et 8% de kaolinite.

La simulation réalisée montre qu'il faut attendre la propagation de trois petits knickpoints dans le substrat à 5% de kaolinite avant qu'un grand knickpoint ne commence à reculer dans le substrat à 8% de kaolinite. Entre temps, on observe l'apparition d'une zone de surcreusement qui se fixe à l'interface entre les deux substrats et s'approfondit progressivement. Ces premiers résultats montrent que les contrastes lithologiques ont la faculté de fixer la propagation des knickpoint et donc d'être directement responsables de la formation de knickzones. Ils permettraient de considérer différemment la dynamique de retrait de knickpoints, notamment dans les modèles d'évolution des paysages à long-terme.

2.1.3 Géométrie et remplissage sédimentaire des fonds de vallées alluviales

Les résultats présentés dans les sections 2.1.1 et 2.1.2 montrent toute la difficulté d'interpréter la dynamique passée des paysages et d'en déduire l'impact de forçages extérieurs -comme les changements climatiques ou tectoniques- si l'on ne considère pas également l'impact des variations lithologiques du substrat. Pour aller plus loin dans l'analyse de la dynamique des corridors fluviaux, il convient de regarder à une échelle temporelle plus fine (< 1 Ma). À cette échelle de temps, on se situe plus proche des temps de remise à l'équilibre des profils de rivière par diffusion (Castelltort et van den Driesche, 2003 ; Tofelde et al., 2021) mais aussi à la limite théorique de l'expression de « l'effet Sadler » (1981) selon Schumer et Jerolmack, (2011). C'est également l'échelle de temps des variations climatiques du Quaternaire.

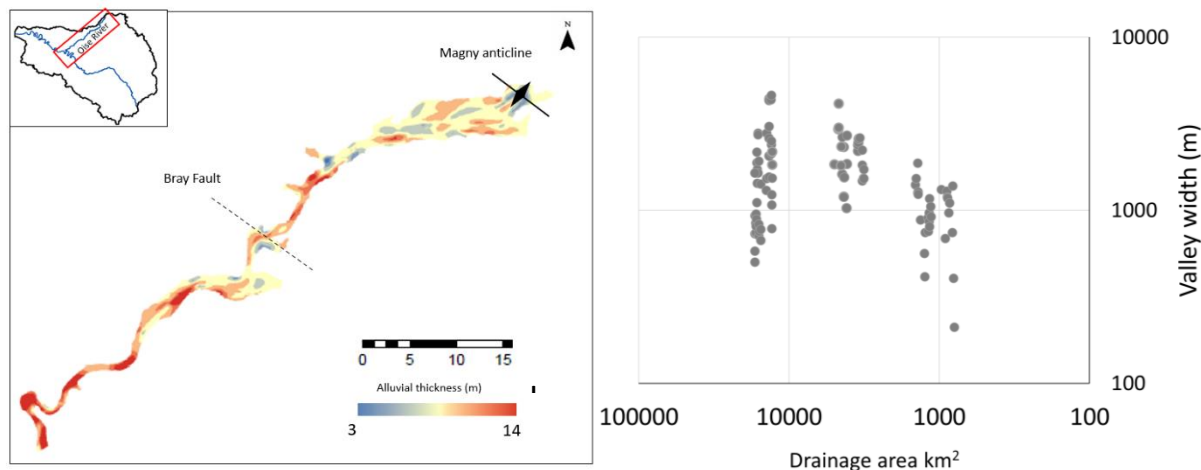


Fig. 18 : (gauche) Carte de restitution par krigeage directionnel de l'épaisseur des alluvions dans le fond de vallée de l'Oise d'après ~ 900 sondages (Grimaud et al., in prep (c) ; données D. Chourio Camacho). (droite) Exemple d'analyse de la géométrie des alluvions, ici la largeur du remplissage alluvial de fond de la vallée de l'Oise (Thèse Diana Chourio Camacho).

Afin de poursuivre l'étude des relations entre forçages extérieurs, lithologie du substrat et dynamique des corridors alluviaux dans les zones anorogéniques, j'ai proposé le projet Alluv3D dans le cadre du RGF- Bassin de Paris et co-financé par l'Agence de l'Eau Seine-Normandie. Le projet s'articule autour de la thèse de Diana Chourio Camacho (soutenance prévue fin 2023). Il s'agit de contraindre la géométrie du remplissage alluvionnaire de fond des vallées principales du bassin-versant de la Seine.

Pour atteindre les objectifs scientifiques de la thèse de Diana, j'ai adapté la méthode de krigeage directionnelle développée au Centre de Géosciences (Pererira et al., 2022) aux environnements alluviaux (Grimaud et al., in prep (c)). On utilise pour cela le tracé géologique de la limite des alluvions du fond de vallée pour générer un champ de vecteurs qui contraint les directions d'interpolation des points de données d'intérêt (il s'agit dans ce cas de la profondeur de l'interface substrat-alluvions). Des résultats préliminaires sont présentés sur la vallée de l'Oise (Fig. 18 (gauche)). On distingue des changements dans la géométrie de l'interface substrat-alluvions qui peuvent s'apparenter à un changement de style fluvial : passant de tresse (en amont) à méandre (en aval). Cette nouvelle méthode produit des résultats réalistes. Nous travaillons actuellement à trouver un moyen optimal pour inférer les petites et grandes portées utilisées pour l'interpolation selon le champ de vecteurs (le « nous » désignant principalement mes collègues N. Desassis, D. Renard et F. Ors).

Le travail de Diana consiste donc à élaborer une base de données de forages répertoriant le toit du substrat sous les alluvions, d'après la base de données du sol et sous-sol du BRGM. Cela concerne des milliers de puits de forage dans les vallées de la Seine, l'Aube, l'Yonne, le Loing, la Marne, L'Eure et l'Oise (~6000). Diana appliquera donc la méthode de krigeage que nous finissons de mettre au point pour restituer la géométrie du fond des vallées étudiées. Afin de mieux quantifier l'impact de la lithologie et de la (paléo-)hydrologie sur la géométrie, elle a mis au point une série de méthodes d'analyse automatisées des largeurs, profondeurs et aires des sections transversales du remplissage de fond de vallée (Fig. 18 (droite)) en se basant sur les outils existants (e.g., TAK ; Forte et Whipple, 2019). Dans un second temps, ces données seront utilisées pour estimer les capacités de stockage (volume) des rivières alluviales cratoniques de manière similaire à Blöthe et Korup (2013) pour l'Himalaya.

Enfin, un volet complet de la thèse de Diana concerne la datation des alluvions, à la fois dans les fonds des vallées et sur les terrasses basses, par méthodes OSL (collaboration E. Vartanian) et ESR (collaborations P. Voinchet, H. Tissoux et J.-J. Bahain). Un article est notamment en cours de rédaction sur le site d'extraction CEMEX de Manoir-Brésil (Chourio Camacho et al., in prep). Il sera peu abordé dans ce manuscrit. Il viendra pourtant compléter mes travaux en cours sur la dynamique du remplissage alluvionnaire, présentés dans la section suivante.

2.2 Dynamique alluviale : stockage et remobilisation sédimentaire

Si les temps théoriques d'ajustement des systèmes alluviaux peuvent être estimés à grande échelle, les bilans des processus de remobilisation sédimentaire et leurs liens avec les enregistrements sédimentaires restent à compléter. Dans les plaines alluviales, ces connaissances touchent à la fois la compréhension et la restauration des milieux naturels, ainsi que la restitution des paléoenvironnements archéologiques.

2.2.1 Dynamique d'abandon et géométrie du remplissage dans les chenaux abandonnés

La dynamique d'abandon des chenaux et le processus de déconnexion au niveau des bifurcations sont des processus fondamentaux dans la dynamique des plaines alluviales et dans le stockage et la redistribution des sédiments (Jordan et Pryor, 1992 ; Constantine et al., 2010). Les événements de type cutoff relâchent des quantités importantes de sédiment qui vont créer des accélérations de l'érosion en cascade en aval des cutoffs (Constantine et al., 2014 ; Ahmed

et al., 2019). De même, en complément du processus de construction des levées (Han et Kim, 2022), la dynamique de construction des bouchons sableux est à l'initiation des avulsions.

Dans ce cadre, la thèse de Léo Szewczyk m'offrit de nombreuses opportunités : celle donnée par Mines Paris aux jeunes chercheurs de prendre en main l'encadrement très tôt, celle offerte par Isabelle Cojan de m'impliquer dans le projet FLUMY et enfin celle de monter un (petit) laboratoire de modélisation analogique sur le site de Fontainebleau. L'objectif initial était de développer -au sein de l'équipe FLUMY- une meilleure compréhension de la géométrie des corps sableux au sein des chenaux abandonnés afin d'améliorer le réalisme des simulations de réservoir. La thèse de Léo s'est organisée en deux volets : une partie de simulations en laboratoire et une partie d'analyses de données de terrain. La première partie fut menée grâce à un dispositif permettant de forcer les abandons en variant la géométrie de bifurcation (Fig. 19). Pour la seconde, nous sommes allés dans la rivière Ain, suivre des abandons de type chute cutoff puis dans la plaine alluviale de la Bassée (Seine-et-Marne).

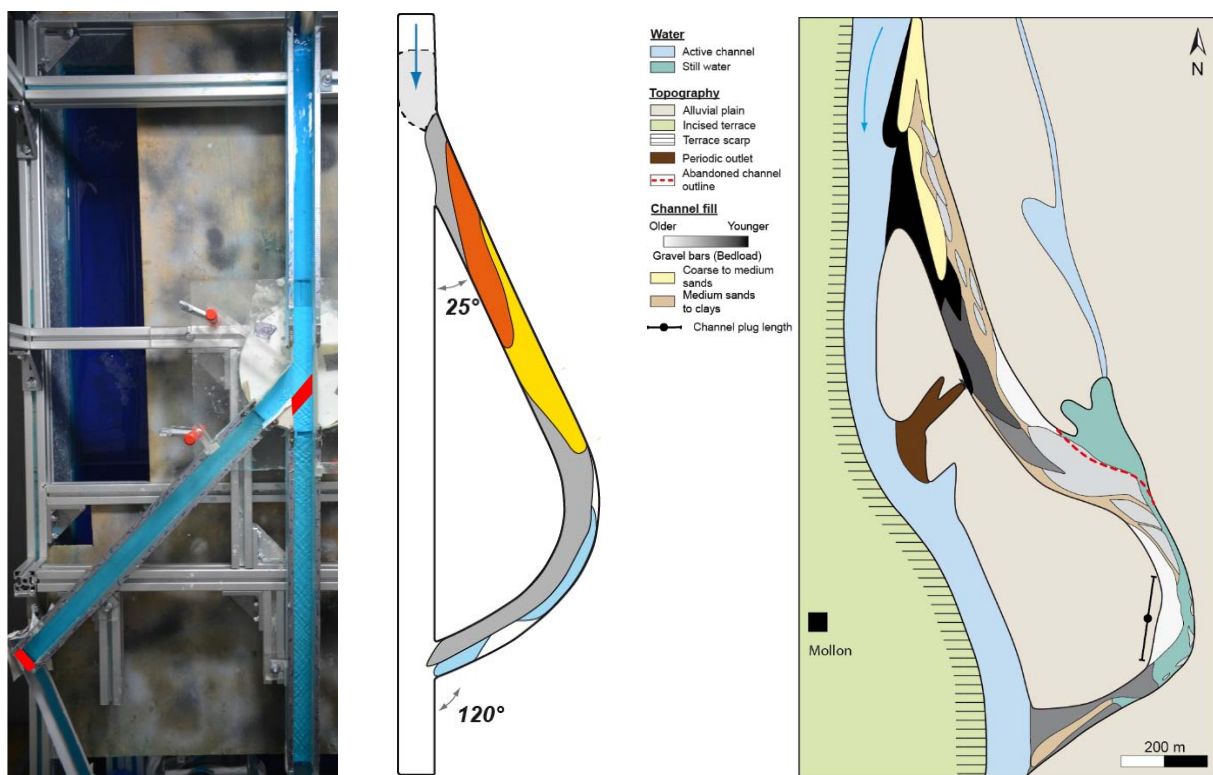


Fig. 19 : Illustrations des différentes approches menées dans la thèse sur l'étude des chenaux abandonnés (gauche) Exemple de simulation de bifurcation avec l'aval libre (Szewczyk et al., 2020). (centre) Visualisation des différentes générations de barres sableuses déposées dans un chenal reconnecté à l'aval. (Szewczyk et al., in prep ; Stage Maria-Crouzet 2019) (droite) Comparaison des résultats expérimentaux avec la cartographie du remplissage d'un chenal abandonné à Mollon, Ain (Szewczyk et al., 2022)

Les données de laboratoires ont montré : (1) une relation entre la longueur des bouchons sableux et l'angle de diversion entre chenal abandonné et chenal principal (Szewczyk et al., 2020), (2) une relation entre longueur des bouchons sableux et ratio des pentes (ou des longueurs) de ces deux chenaux (3) une meilleure compréhension de l'amalgamation des barres sableuses avant et pendant la formation du bouchon dans le chenal en abandon (Szewczyk, 2020). Cette dynamique a été étudiée de près dans l'Ain, système dominé par la charge de fond, composée de galets et graviers. On a ainsi pu distinguer les barres associées à la phase

d'initiation des bouchons -durant laquelle une partie du chenal peut ajuster sa largeur- des barres amalgamées formant le bouchon. Ces dernières se déposent durant une phase de progradation suivie d'une phase d'aggradation -tout dernier stade de déconnexion. Les observations faites ont donc pu renseigner un nouveau modèle d'évolution morpho-sédimentaire des chenaux et des changements granulométriques associés (Szewczyk et al., 2022).

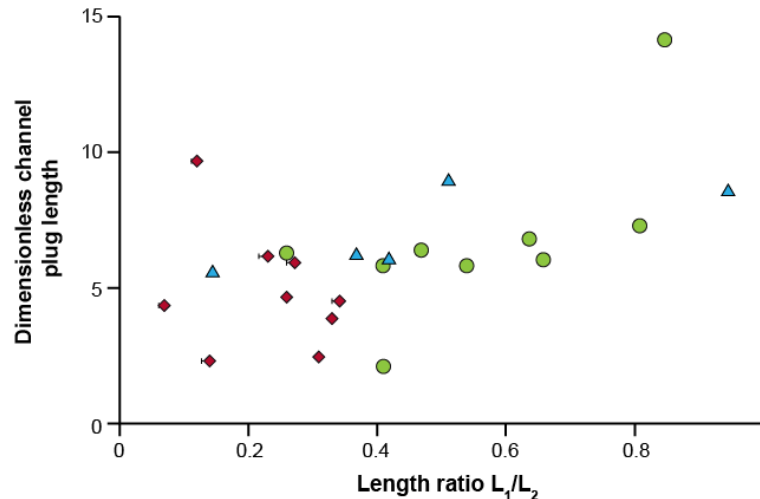


Fig. 20 : Synthèse des données de longueur de bouchon sableux dans les chenaux dans des systèmes récents comparés à la régression d'après les données expérimentales (Szewczyk et al., in prep).

La synthèse des données de la thèse de Léo (Fig. 20) suggère des similitudes entre les résultats de terrain et ceux des expériences en considérant le rapport de longueur entre chenaux. Ce rapport semble le plus pertinent pour estimer les longueurs des bouchons sableux sur le terrain. La relation à l'angle reste utile en revanche pour mieux caractériser la dynamique de comblement au niveau de la bifurcation même. Ainsi, ces données sont un premier pas pour estimer les volumes de sédiment grossier stockés au début des phases de déconnexion des chenaux (durée de 5-10 ans maximum) et qui participent au tamponnement des flux sédimentaires vers les océans (Métivier et Gaudemer, 1999).

Les données de terrain dans les systèmes quaternaires ou plus anciens montrent que le remplissage des chenaux, s'il est principalement argileux, peut être plus complexe. Dans ces cas, il peut être une source de renseignements supplémentaires pour mieux comprendre l'évolution paléogéographique des milieux alluviaux. Nous avons pu, dans le cadre de la thèse de Léo, nous intéresser à la géométrie d'un chenal abandonné : la « Vieille Seine » à Vimpelles. Le paléochenal forme une dépression constituant cinq boucles de méandres sur 3 km (Fig. 21b). On peut observer sur sa partie amont des dépôts sableux -que nous interprétons comme appartenant au bouchon sableux en accord avec la topographie- tandis que la partie aval est constituée de remplissage argileux. Les restitutions de débit de plein bord calculées d'après la morphologie du chenal (Williams, 1986 ; Deleplancque, 2016) permettent d'identifier un débit bien inférieur de ce chenal de la Seine de l'époque. Les âges radiocarbone, dont l'un dans un niveau argileux intercalé dans une barre de méandre sur une section amont, suggèrent que le chenal réoccupe un tracé plus ancien après une phase de quiescence. Il y a donc deux périodes d'abandon, l'une datant du Néolithique et l'autre du haut Moyen Âge. Ces résultats suggèrent également que la Seine appartenait alors à un système anabranché. L'existence de ce style fluvial par le passé -différent de l'actuelle Seine au tracé unique et domestiqué depuis 1850-

est confirmée par des études récentes sur d'autres chenaux en Bassée par des élèves de l'École des Mines de Paris que j'ai pu encadrer (Grimaud et al., rapport-PIREN 2021 ; Rapport stage Catry, 2021 ; Grimaud et al, rapport-PIREN 2022 ; Rapport stage Imperor et Quaisse, 2022). Enfin, il n'est pas possible d'estimer avec certitude la longueur totale du bouchon sableux amont de la Vieille Seine à Vimpelles, car il a été érodé par migration de la Seine après son dernier abandon vers 450 après J.C. Ceci illustre la difficulté de préservation dans les plaines alluviales, qui sera abordée dans la section suivante.

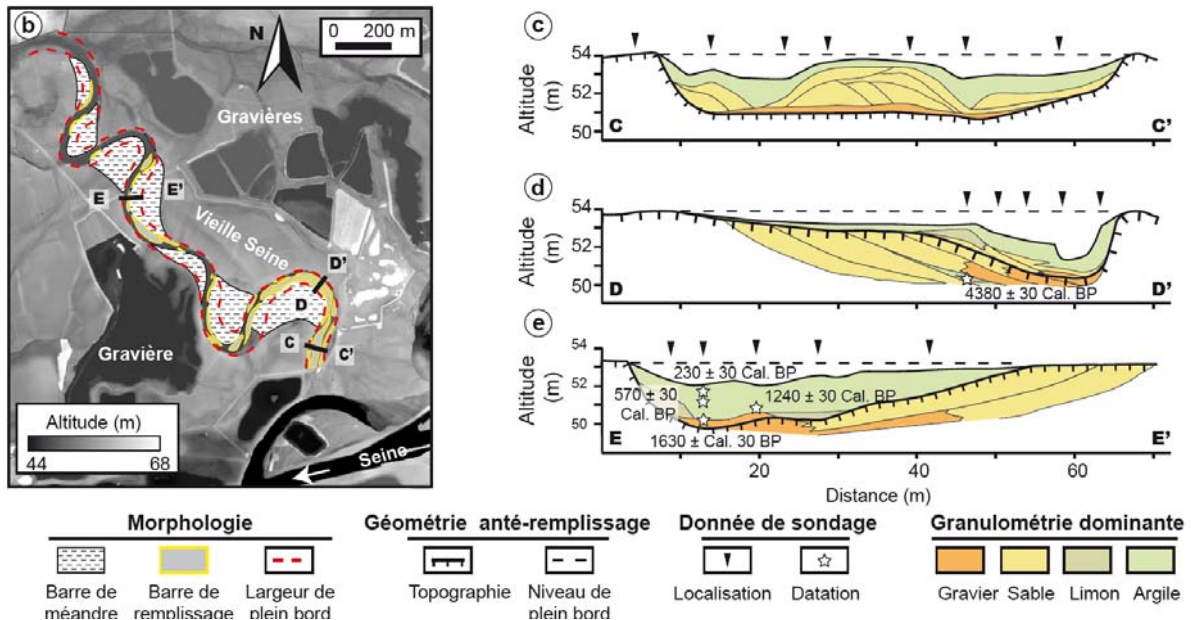


Fig. 21 : (b) Topographie de la Vieille Seine au sud de Vimpelles et localisation des coupes du chenal. (c, d, e) Coupes réalisées à travers le chenal de la Vieille Seine (Petit et al., 2021).

2.4 Intégrité du signal sédimentaire en milieu alluvial

2.4.1 Apports de la modélisation numérique

Le quatrième des cinq articles sélectionnés est celui paru à *Journal of Geophysical Research: Earth Surface* en 2022 (voir Annexe 2). Il s'agit d'une étude basée sur des simulations effectuées avec le logiciel FLUMY. Ce papier est une tentative de combler en partie le fossé existant entre les considérations théoriques et les données de terrain sur l'estimation de l'intégrité stratigraphique - mesure de la quantité de temps enregistré le long d'un sondage (Sadler, 1981 ; Sadler and Strauss, 1990 ; voir Fig. 2). En particulier, on utilise FLUMY, modèle numérique pragmatique et réaliste de simulation de dépôts fluviaux méandri-formes, pour étudier la mesure de l'intégrité stratigraphique C en fonction de différents paramètres. Je propose ainsi de faire le lien entre les paramètres physiques (migration, aggradation et avulsion) et la mesure de C . Ces résultats ont permis de réévaluer les prédicteurs théoriques de C proposés par Sadler (1981) ainsi que de préciser un peu plus le lien entre les processus physiques et leur assimilation à des modèles mathématiques de type mouvement brownien fractionnaire (Schumer et al., 2009 ; Paola et al., 2018). La nouveauté principale de cette étude (Grimaud, et al., 2022) est de proposer une nouvelle formulation de C , dépendant de grandeurs caractérisant la dynamique de dépôt à un certain intervalle de temps : la fraction de surface non affectée par les dépôts S (ou stasis) et le ratio remobilisation / sédimentation R . Enfin, je propose que des

mesures des paramètres géométriques des chenaux permettraient d'obtenir des valeurs de R et S , et donc d'estimer C . Cette approche pourrait être testée sur le terrain dans le futur.

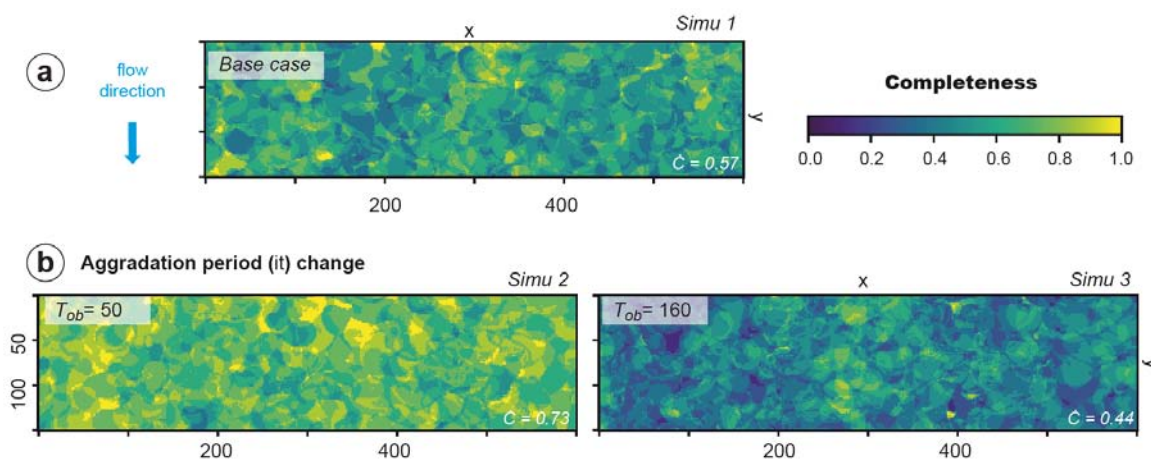


Fig. 22 : Exemples de cartes montrant la distribution de l'intégrité stratigraphique C dans une plaine alluviale (Grimaud et al., 2022). La simulation 3 possède le plus fort taux d'aggradation ; elle va donc enregistrer plus de temps et avoir les plus fortes valeurs de C .

2.4.2 Dynamique alluviale à proximité de sites archéologiques : exemple de Noyen-sur-Seine

La section précédente a souligné la complexité de la préservation des séries fluviales : les plaines alluviales forment des mosaïques avec des degrés d'intégrité variés, même localement (Fig. 22) (voir aussi Huffman et al., 2022). La remobilisation sédimentaire constante a donc un impact sur la façon dont l'enregistrement paléoenvironnemental nous parvient. C'est aussi vrai pour appréhender le contexte géo-archéologique.

Dans cette dernière section, je présente une étude en cours (Grimaud et al., in prep (c)) en collaboration avec des archéologues (principalement P. Gouge et C. Petit). Cette collaboration est mutuellement bénéfique : l'étude de la morphodynamique donne de précieux renseignements sur l'évolution des paysages – à mettre en lien avec les occupations humaines – tandis que les vastes opérations de diagnostics et fouilles archéologiques donnent accès à des surfaces d'affleurement considérables avec de nombreux éléments de paléoenvironnement et de datation. L'étude porte sur le site alluvial de Noyen-sur-Seine qui fut le lieu de découvertes archéologiques exceptionnelles en Europe : des vestiges du mésolithique (bois dont une barque monoxyle et des nasses à poisson) et du néolithique (céramique et silex), une enceinte du néolithique et une barque monoxyle carolingienne, dont une grande partie est aujourd'hui conservée au musée de la Préhistoire de Nemours (Seine-et-Marne). L'analyse fine de la topographie, complétée par des travaux de terrain que j'ai coordonnés avec des étudiants de Mines Paris (Grimaud et al., rapport-PIREN 2021 ; Rapport stage Catry, 2021 ; Grimaud et al., rapport-PIREN 2022 ; Rapport stage Imperor et Quaisse, 2022) et une synthèse bibliographique contenant par exemple des rapports inédits (Mordant et al., 1993 ; source P. Gouge) ont permis une réévaluation de l'évolution paléogéographique du site (Fig. 23).

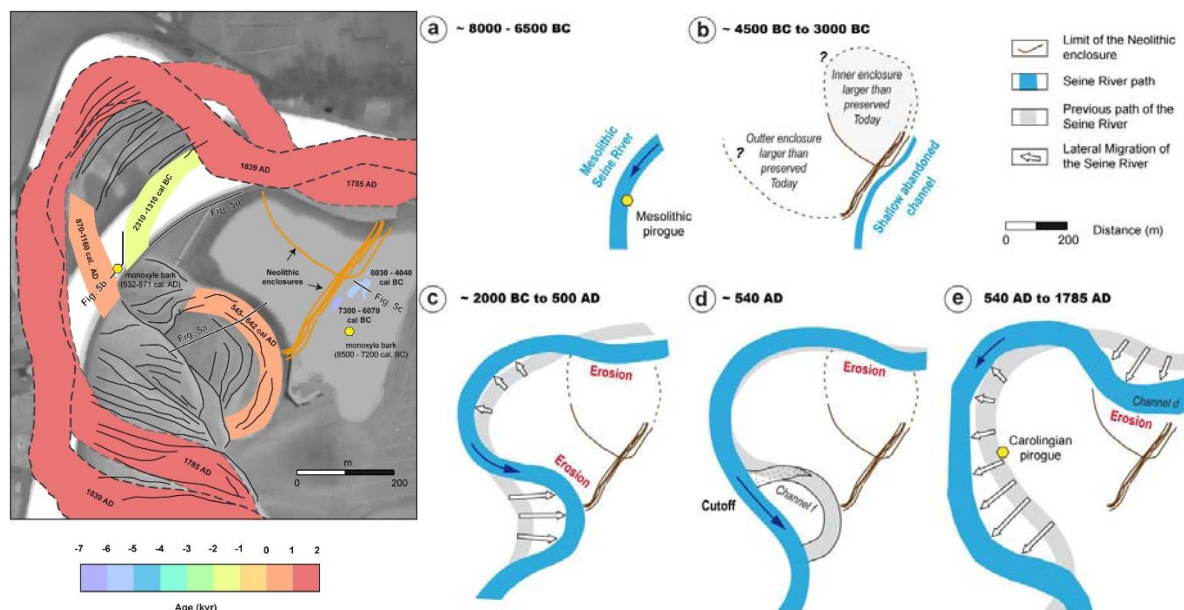


Fig. 23 : (gauche) Synthèse des éléments de datation des paléochenaux retrouvés sur le site de Noyen-sur-Seine (lieux-dits « le Pré aux Bœufs et le « Haut des Nachères »). (droite) Proposition de reconstitution de l'évolution du paysage depuis le Mésolithique (Grimaud *et al.*, in prep (c)). Nos résultats suggèrent que les restes de l'enceinte néolithique sont intersectés et donc érodés par des chenaux d'âge carolingien au sud et modernes au nord. Il n'y avait donc pas une enceinte appuyée sur la Seine au néolithique. L'enceinte était alors plus vaste et très probablement fermée.

Le résultat majeur de cette étude est de montrer que la reconstruction paléogéographique communément utilisée pour la période néolithique est erronée : l'enceinte d'alors ne s'appuyait pas sur la Seine, comme cela a été suggéré dans les premières reconstitutions (Mordant et Mordant, 1992), qui sont encore largement reprises aujourd'hui (Deseine et al., 2019). La migration de la Seine a donc engendré l'érosion d'une partie de l'enceinte après le Néolithique. Une conséquence est qu'il faut réévaluer la perception géométrique que l'on peut avoir des portions d'enceintes protohistoriques retrouvées en milieu alluvial (Brenot et al., 2021) et se méfier des mesures (aires, périmètres, etc.) que l'on peut effectuer pour proposer des interprétations (Lietar, 2016). Ces mesures sont faites sur des objets seulement, qui ne sont pas préservés dans leur intégralité.

Enfin, on note que le chenal carolingien de Noyen-sur-Seine est de taille similaire à celui de Vimpelles, ce qui suggère d'autant plus l'existence d'un réseau de drainage avec des tailles plus petites qu'à l'actuel dans la Bassée pour cette période de temps (section 2.2.1 ; voir aussi Deleplancque, 2016).

3- Dynamique des systèmes chenalisés dans les zones d'accumulation

Une partie plus modeste de mon travail porte sur les bassins sédimentaires. Dans cette dernière partie sont présentés les bilans sédimentaires sur le temps long par comparaison entre volumes déposés sur la marge ouest africaine et les résultats présentés en section 1.2.2 – de même que les questions qui en résultent. Je me focalise ensuite sur les systèmes chenalisés comme moteur de remobilisation sédimentaire dans les deltas et plaines abyssales. La dynamique deltaïque est d'abord montrée sous son angle autogénique, puis sous influence de forçages externes. Certains résultats pourraient s'appliquer à la zone de transfert, mais j'ai choisi de les considérer comme représentatifs de la partie la plus proximale (fluviale) des deltas pour mieux les intégrer à mes travaux sur le système Gange-Brahmapoutre-Meghna. Enfin, la dernière section rassemble mes contributions à la comparaison de la dynamique des systèmes chenalisés turbiditiques avec leurs équivalents fluviaux, dans le cadre de la transposition du modèle FLUMY (initialement fluviale), vers un mode turbiditique plus réaliste.

3.1 Bilans sédimentaires cénozoïques ouest africains

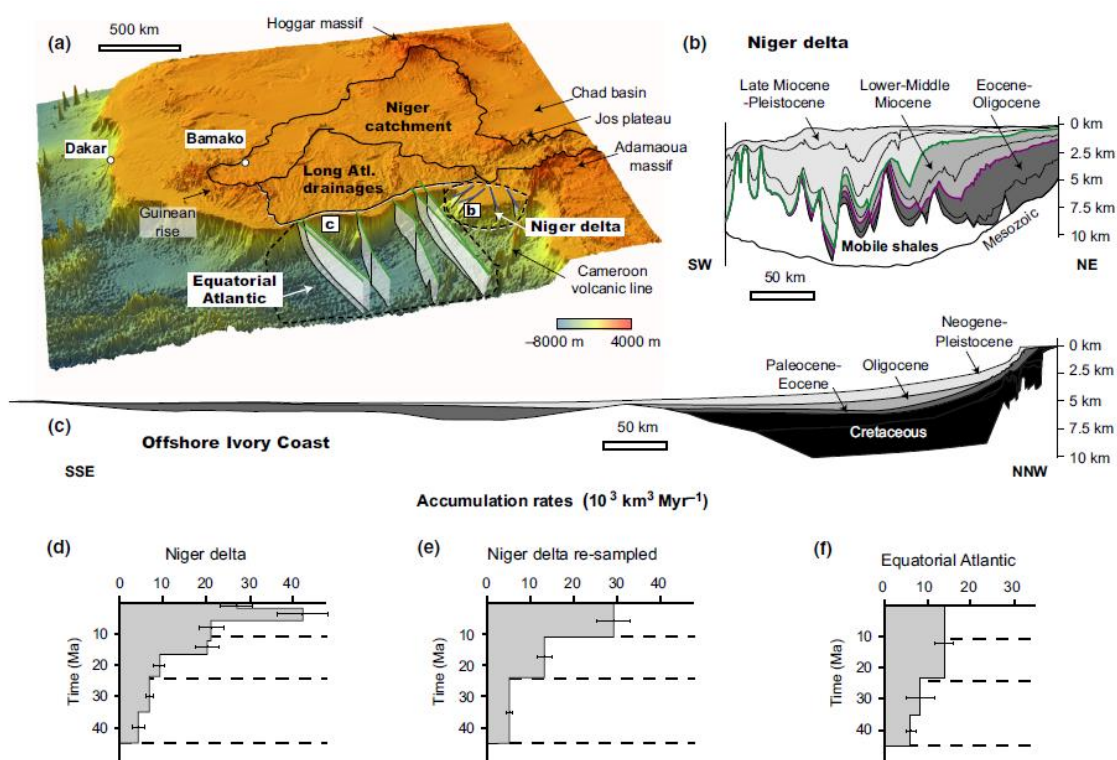


Fig. 24 : Accumulations sédimentaires cénozoïques sur la marge ouest africaine (Grimaud et al., 2018).

L'utilisation de la méthode d'interpolation présentée par Guillocheau et al. (2012) sur un ensemble de coupes sédimentaires issues de la littérature (compilation en partie dans Helm, 2009) ont permis d'estimer les volumes déposés depuis 45 Ma sur la marge ouest africaine, notamment au niveau du delta du Niger (Grimaud et al., 2018 ; Fig. 24). Les résultats montrent

une bonne cohérence volumétrique au premier ordre avec les estimations reposant sur la cartographie des paléosurfaces latéritiques.

On note une différence entre les volumes exportés (qui restent constants autour de 10 milliers de km³ par million d'années, avec probablement une légère augmentation entre l'Oligocène et le Miocène ; Fig. 24) et les volumes préservés dans le delta du Niger (qui suggèrent une augmentation de 5 à 30 milliers de km³ par million d'années depuis 45 Ma). Cette différence entre enregistrements peut s'expliquer par un problème de préservation : plus les dépôts sont anciens, moins ils ont de chance d'être préservés (Sadler, 1981). On est en revanche à une échelle de temps bien supérieure à celle de « saturation » théorique de l'effet Sadler (Schumer, 2011). De plus, les plaines alluviales sont prises en compte dans nos reconstitutions géométriques, il ne peut donc pas y avoir un volume stocké non pris en compte dans la partie continentale. Il se passe probablement quelque chose dans le delta similaire à la dynamique de remobilisation (cannibalisme) décrite dans la section précédente. Je propose deux moteurs potentiels pour cette remobilisation (Grimaud et al., 2018) : les variations du niveau relatif de la mer -qui sont marquées en Afrique par le développement de canyons à la transition éocène-oligocène- et la dynamique fluviale associée à la forte progradation du delta au Miocène.

3.2 Dynamique d'occupation des systèmes deltaïques

Depuis mon postdoctorat à Minneapolis, je m'intéresse tout particulièrement à la dynamique fluviale au sein des bassins sédimentaires. Le dernier article sélectionné est celui paru à *Basin Research* en 2020 (voir Annexe 2) sur la zone du Garo-Rajmahal-Gap en amont du delta Brahmapoutre-Gange-Meghna (BGM). Il s'agit d'une étude combinant (i) analyse sédimentologique à partir de 75 sondages réalisés dans les sédiments meubles du delta, (ii) analyse de la provenance à partir de la géochimie de ces sédiments, (iii) analyse géomorphologique et enfin (iv) modélisation géophysique. Cette dernière partie s'est largement appuyée sur les compétences de mes co-auteurs (C. Grall et M. Steckler).

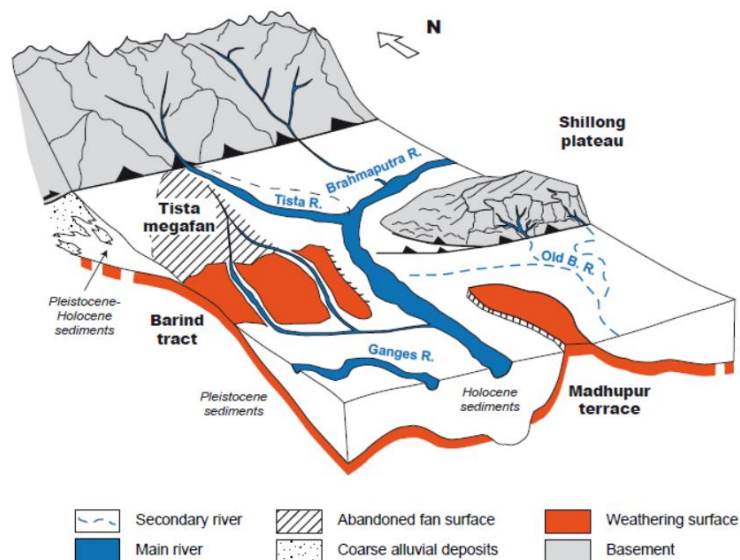


Fig. 25 : Représentation schématique de la zone du Garo-Rajmahal Gap, au Bengal, montrant l'influence de la flexure de la plaque indienne sous l'effet du poids de l'Himalaya (Grimaud et al., 2020).

Dans cette étude, je montre un partitionnement des sédiments influencé par la déformation lithosphérique -probablement flexurale- et les interactions entre deux systèmes alluviaux : la rivière Brahmapoutre et le méga-cône alluvial de la rivière Tista (Grimaud et al., 2018). On retrouve également une distribution des sols à la surface de la zone cohérente avec ces forçages : des sols très développés dans la zone du bourrelet flexural et une différence pédologique entre les lobes ouest et est du cône alluvial.

En parallèle de ces travaux, j'ai réalisé en 2015 une expérience dans le Jurassic tank -bassin de 18 m² de surface où la subsidence peut être contrôlée. L'expérience a généré un système deltaïque dans plusieurs configurations mimant certains processus à l'œuvre dans le delta BGM : soulèvement tectonique et sédimentation transverse (Fig. 26).

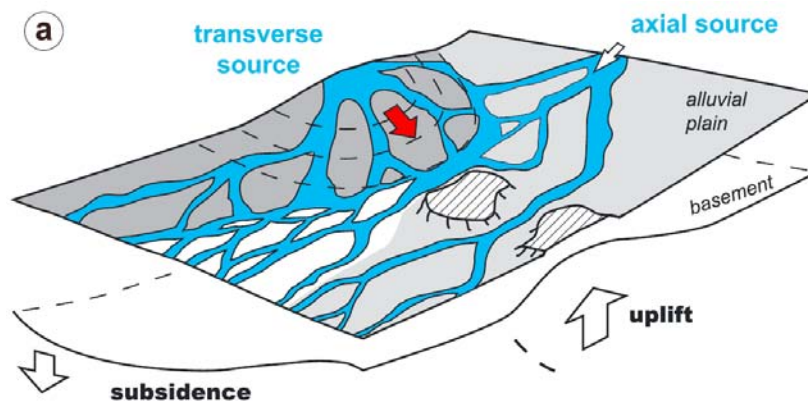


Fig. 26 : Représentation schématique de l'expérience XES-2015 et des processus simulés, individuellement puis en compétition (Grimaud et al., 2017).

Dans un premier temps, j'ai pu analyser la dynamique alluviale dans trois configurations (Fig. 27) : autogénique, tectonique et avec sédimentation transverse. J'identifie une géométrie d'occupation de la surface deltaïque propre à chaque configuration (Fig. 27). La phase autogénique est caractérisée par une occupation plutôt homogène de la surface, même si des chemins préférentiels de réoccupation sont observés (voir Ashworth et al., 2007), notamment en amont. La phase tectonique génère une zone d'exclusion du flow au niveau de la zone soulevée, où l'écoulement ne persiste qu'au niveau de vallées incisant l'anticlinal. La configuration avec interaction de sources alluviales génère une zone de concentration des écoulements dans une zone de convergence que nous appelons zone de mélange ('mixing zone' ; Kim et al. 2011). Ces configurations ont donc des dynamiques différentes au niveau spatiales mais également au niveau temporel (Fig. 28). Repartant des approches théoriques (Cazanacli & al., 2002 ; Reitz et al., 2015 ; Chadwick et al., 2020), j'ai adapté la formule pour estimer le temps nécessaire au système fluvial pour visiter l'ensemble de la surface du delta T_{ch} :

$$\frac{T_{ch}}{f_d} = H q_s^{-1} \quad (1)$$

où f_d est la moyenne de la fraction sèche (non-occupée par les rivières), H la profondeur moyenne des chenaux et q_s le flux sédimentaire par unité de longueur du bassin sédimentaire. Cette formule adaptée permet d'expliquer la dynamique d'occupation des données du Jurassique tank, considérant une profondeur moyenne de chenaux de 1 cm. De manière intéressante, l'expérience avec deux sources sédimentaires peut également être expliquée par

l'équation (1) mais en utilisant une profondeur de 2 cm, en cohérence avec l'augmentation de la profondeur de la zone de mélange observée dans l'expérience XES 2015. Ce surcreusement est typiquement observé expérimentalement mais aussi sur le terrain (Ashmore et Parker, 1983 ; Best et Ashworth, 1997). Le soulèvement de l'anticlinal en revanche va augmenter le temps d'occupation par rapport au régime autogénique (Fig. 27). L'équation (1) atteint alors ses limites car au fur et à mesure que des terrasses se développent dans l'anticlinal, une partie de la surface alluviale n'est plus visitable. Ce type d'équation a pu être appliqué au delta GBM (Grimaud et al., 2020). Les calculs de mobilité montrent des différences entre Tista et Brahmapoutre, ce qui peut expliquer pourquoi le cône alluvial repose sur le bourrelet observé en profondeur quand le fleuve a la capacité pour l'éroder (Fig. 25) (voir aussi Bufe et al., 2016).

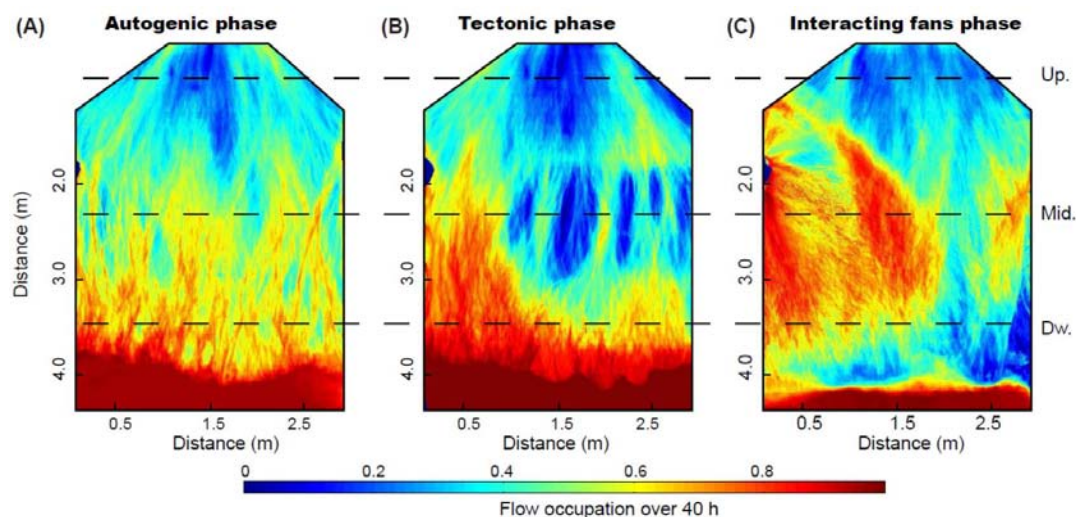


Fig. 27 : Calcul de l'occupation relative de la surface alluviale par le système fluviatile grâce à l'analyse d'image (voir Tal et al., 2012) dans l'expérience XES-2015 (Grimaud, inédit 2016).

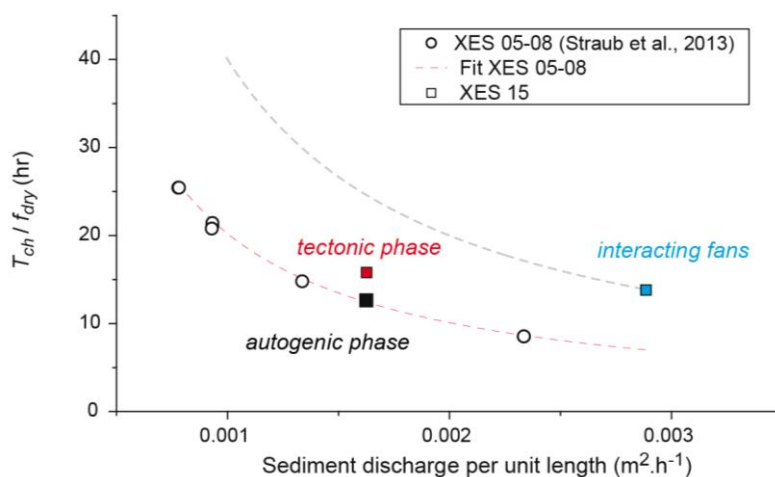


Fig. 28 : Estimation du temps nécessaire pour occuper la surface du Jurassic tank en fonction du flux sédimentaire, calculé par unité de longueur et pas par unité de largeur comme classiquement admis. L'équation (1) est représentée par les courbes en pointillées : rouge pour une profondeur moyenne de chenal de 1cm et grise pour une profondeur moyenne de chenal de 2 cm (Grimaud, inédit 2016).

Une fois les dynamiques unitaires mieux comprises, j'ai regardé comment les deux forçages respectifs (tectonique et sédimentation transverse) entraînent en compétition (Grimaud et al., 2017). Je montre que la présence du cône alluvial alors que la zone de soulèvement est active

pousse la zone de mélange vers l'anticlinal, participant à son érosion. Cependant, on n'arrive pas à éroder complètement l'anticlinal, malgré une forte augmentation du flux sédimentaire dans le cône transverse. Ce phénomène s'explique par la dynamique de la zone de mélange qui absorbe le surplus sédimentaire tout en limitant la mobilité latérale du système fluviatile (justification théorique en Fig. 28). Les zones de mélange sont donc des objets importants des zones deltaïques. En amont du delta BGM, elles participent à la stabilisation du tracé du Brahmapoutre (Grimaud et al., 2017).

3.3 Géométrie et dynamique de migration des systèmes turbiditiques

Le transport sédimentaire vers les abysses génère de la redistribution sédimentaire. Dans de nombreux cas, c'est même cette redistribution, gravitaire, qui est le moteur des écoulements chenalisés (Mulder et Alexander, 2001). Comme suggéré par l'étude comparative source-to-sink ouest africaine (Grimaud et al., 2018), la prise en compte de la dynamique de cet ultime sursaut sédimentaire est nécessaire pour faire le bilan calmement (Jacky et Ben-J, 2000). Mes travaux sur les systèmes turbiditiques sont surtout des collaborations : avec des collègues de Minneapolis durant mon postdoctorat puis en soutien de l'encadrement de Martin Lemay à Mines Paris. Ces travaux ont porté sur la comparaison entre systèmes fluviatiles et turbiditiques, faisant écho à mes travaux sur les systèmes alluviaux.

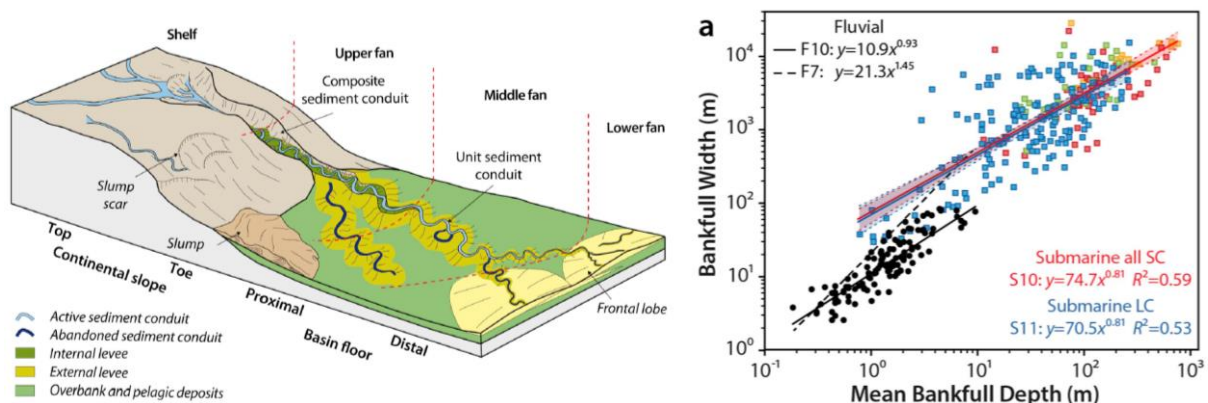


Fig. 29 : (gauche) Schéma d'un système chenalisé sous-marin. (droite) Exemple de relation géométrique comparant systèmes fluviatile et turbiditique (Lemay et al., 2020).

Nous avons, avec Ajay Limaye, alors également en postdoctorat à Minneapolis, conçu en 2015 un dispositif de simulation d'écoulements denses en injectant une saumure dans un bassin d'eau douce. Ce type d'expérience reste le plus compliqué que j'ai eu à réaliser à ce jour. L'idée était de continuer les travaux initiés à SAFL sur les turbidites en tresse (Foreman et al., 2015). Nous avons ainsi pu documenter plus précisément les propriétés de ces dépôts subaquatiques du point de vue géométrique et dynamique (Lai et al., 2017 ; Limaye et al., 2018). Nous montrons notamment que les systèmes sous-marins sont caractérisés par un réseau de chenaux moins nombreux mais plus profonds et plus pentus que leurs équivalents fluviatiles avec les autres paramètres constants. Ces résultats sont cohérents avec une estimation théorique de ces propriétés en prenant en compte la différence des densités du fluide d'écoulement et du fluide ambiant (Imran et al., 1999). C'est ce type de raisonnement qui a été mené par Martin Lemay lors de sa thèse pour proposer une transposition de FLUMY depuis le fluviatile vers le turbiditique.

Le logiciel FLUMY qui génère des dépôts sédimentaires engendrés par la migration de chenaux méandriiformes fut à l'origine développé en milieu fluvial (Lopez, 2003 ; Cojan et al., 2005 ; Rivoirard et al., 2008 ; Lopez et al., 2009). Afin de calibrer la transposition vers les environnements sous-marins, Martin a tout d'abord réalisé une comparaison géométrique des chenaux fluviaux et turbiditiques, en parallèle d'une classification des différents types de conduits sous-marins (Lemay et al., 2020). Il en ressort que : (i) la distribution des types de conduits n'est pas aléatoire (on retrouve des conduits incisifs sur les pentes continentales et des conduits aggradants vers la plaine abyssale), (ii) les chenaux sous-marins avec levées sont les plus analogues aux rivières alluviales méandriiformes, ce sont donc ceux-ci qu'il sera pertinent de transposer au sein du logiciel FLUMY (Lemay, 2018 ; Lemay et al., 2020). Enfin, (iii) l'aire des sections des chenaux sous-marins augmente vers l'aval – principalement parce qu'ils deviennent proportionnellement plus larges. On interprète ces comportements comme une perte de confinement de l'écoulement, qui peut éventuellement être synonyme d'une évolution vers des turbidites en tresse comme suggéré par Foreman et al. (2015).

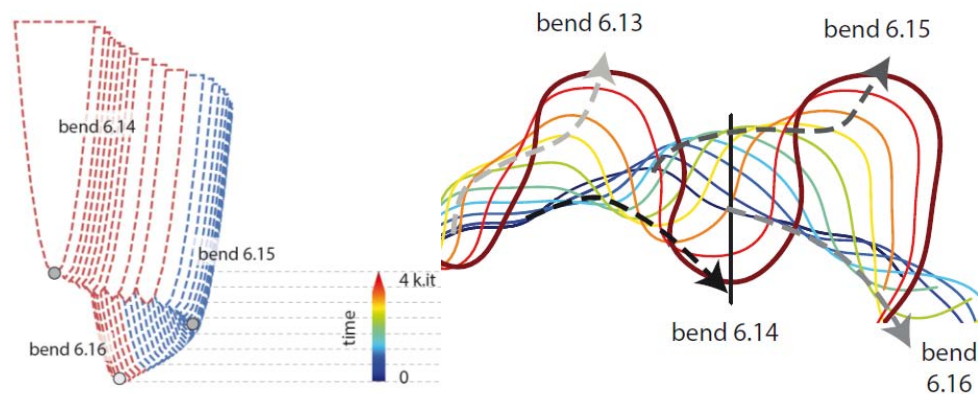


Fig. 30 : Enregistrement de la migration du chenal généré dans FLUMY sur une coupe géologique synthétique (gauche) comparée avec sa trajectoire en carte (Lemay et al., accepté). On note que la coupe géologique enregistre en fait le passage de plusieurs boucles et non une seule.

Tout dernièrement, nous avons utilisé FLUMY dans son nouveau mode turbiditique (Lemay, 2018) pour analyser plus finement la trajectoire des chenaux sous l'effet de la compétition entre aggradation et migration latérale (Lemay et al., sous presse). Comme indiqué en section 2.4.1, cette compétition contrôle l'intégrité de l'enregistrement stratigraphique. C'est vrai aussi en milieu turbiditique (Grimaud et al., 2022). Malgré des similitudes avec le fluvial, les turbidites ont des trajectoires propres à leur milieu : elles sont dominées par l'accrétion verticale alors que les environnements fluviaux sont dominés par la mobilité latérale (Jobe et al., 2016). Les taux d'aggradation sont en effet plus forts en milieu turbiditique, particulièrement au niveau des levées, et les temps d'avulsion y sont ralentis (Straub et al., 2008). Si cette particularité fait consensus, il y a encore débat pour savoir s'il faut interpréter les changements de direction au sein des « stacking patterns » comme étant autogéniques (Sylvester et al., 2011) ou comme résultants de forçages extérieurs (McHargue et al., 2011).

Dans cette étude (Lemay et al., sous presse), nous analysons les trajectoires de plusieurs centaines de boucles de méandre générées dans une simulation avec des paramètres constants. Nous générons des coupes stratigraphiques synthétiques le long des sections transverses à ces méandres, que nous comparons avec les trajectoires en carte (Fig. 30). Les résultats montrent (i) que l'on peut générer de nombreux « stacking patterns » à partir de ce seul jeu de paramètres

-donc sans changement de forçage extérieur- et (ii) que chaque coupe géologique enregistre en fait le passage de plusieurs boucles de méandre et non une seule. Les changements de trajectoire sont donc apparents (*Fig. 30*). Le passage d'une boucle à une autre donne l'impression d'une migration latérale forte. En revanche, la migration au sein d'une boucle est maximale vers l'aval. On a alors l'impression -à tort- qu'il n'y a pas ou peu de migration latérale lorsque l'on regarde l'enregistrement en coupe transversale. Cette dynamique autogénique engendre la formation de géométries proches de celles dites en crosse de hockey : enregistrement d'abord migration latérale puis -en apparence- une augmentation du taux d'aggradation. On conclut donc, comme Sylvester et al. (2011), que les stackings patterns ne peuvent pas être simplement interprétés en termes de changements de forçage extérieurs.

4- Synthèse des recherches et projet scientifique

Mon profil de recherche est tourné vers la géomorphologie : l'étude des paysages et de leur évolution, avec pour implications les flux de matière vers les bassins et les enregistrements sédimentaires. Je me suis spécialisé dans les paysages « plats » : j'ai travaillé en géomorphologie tropicale en contexte anorogéniques et sur des systèmes alluviaux. Enfin, j'ai pu développer des compétences en modélisation analogique. Les projets dans lesquels j'ai été impliqués concernaient aussi bien la recherche fondamentale qu'appliquée. Cette spécificité – souhaitée aux Mines - était déjà présente dans mon parcours. Je souhaite lui donner une dimension plus sociétale à terme, comme le soulignent mes participations à des projets comme le PIREN, ou plus récemment des implications avec l'ANDRA.

Pour la suite de ma carrière, j'entends continuer sur la thématique de la géomorphologie des zones stables, en insistant sur les rétroactions entre paléo paysages et altérations. De même, je continuerai de mettre à profit mes connaissances en modélisation analogique. Mes recherches porteront sur l'impact des forçages externes (qu'ils soient climatiques ou tectoniques) sur la dynamique du transfert sédimentaire. Deux projets de modélisation analogique sont en préparation : l'étude des interactions entre tectonique et dynamique des systèmes chenalisés - pour une application au modèle numérique FLUMY développé à Mines Paris - et l'étude d'événements extrêmes pluvieux sur l'érosion des sols (thèse G. Portzer WSP-ANDRA).

J'aimerais à moyen terme intégrer de nouvelles approches. Tout d'abord, il semble pertinent de monter en compétence sur l'étude de la dynamique de l'altération et les bilans minéralogiques et géochimiques associés pour mieux appréhender les flux dissouts dans les rivières. Ensuite, je souhaite donner la part belle à l'étude des interactions entre l'Homme et son milieu naturel, notamment sur l'exemple des plaines alluviales telles que la Seine qui sont aujourd'hui largement domestiquées en France. Enfin, je souhaite m'appuyer sur les compétences nouvelles au sein de l'équipe géologie du Centre de Géosciences pour aborder les questions de l'enregistrement des signaux climatiques dans le passé afin de mieux percevoir l'impact de ces signaux sur la dynamique des rivières (Collaborations D. Huyghe).

Évolution des paysages tropicaux : signal climatique et bilans d'altération

Je veux continuer de travailler sur la dynamique d'altération à plusieurs échelles. Premièrement, je souhaite m'appuyer sur mon expérience dans l'évolution morphologique des paysages tropicaux pour aller plus loin dans la compréhension des profils d'altération et leur impact sur les bilans géochimiques. Il paraît important de continuer de progresser dans la datation des profils et des surfaces d'altérations associées. Une étude multi-proxy en Nouvelle-Calédonie pourrait par exemple être bénéfique pour améliorer les techniques de datations et pour mieux comprendre l'évolution de la Grande Terre. De nombreuses tentatives de datation ont été menées, certaines ont permis des avancées sur la connaissance de la chronologie globale des paléosurfaces quand d'autres restent mitigés (Sévin et al., 2020). Les nouvelles méthodes de datation ESR sur kaolinite pourraient par exemple apporter des données complémentaires (Mathian, 2018), mais il faut trouver le matériel datable. À terme, il faudrait mener des

approches similaires dans de multiples zones du globe et les comparer pour mieux distinguer les effets climatiques globaux des effets locaux sur les processus de dénudation chimiques et physiques. C'est probablement plus que le projet d'une carrière de chercheur mais restons ambitieux. On pourrait tenter de prolonger le transect Africain vers le sud (travaux initiés à Rennes ; communication personnelle F. Guillocheaux 2020) puis intégrer les travaux australiens (e.g., Danišik et al., 2019) à ceux de la Nouvelle Calédonie une fois que ceux-ci auront été améliorés.

En parallèle, les premiers modèles numériques menés par l'équipe de Nancy dans le cadre du projet Transnum (Thèse S. Favier, 2023) ont amené des résultats prometteurs sur l'évolution de la géométrie des profils et des minéralisations en Nickel. Ce type d'approche pourrait être appliqué dans d'autres contextes (prenant des pas de temps plus larges et/ou des types de substrats différents, et surtout intégrant de manière plus fine l'évolution topographique associés à l'enfoncement des profils d'altération) pour mieux contraindre les bilans géochimiques associés (voir Goddérus et al., 2019). Avec le logiciel Hytec de transport réactif développé à Mines Paris, il y a également une opportunité à Fontainebleau.

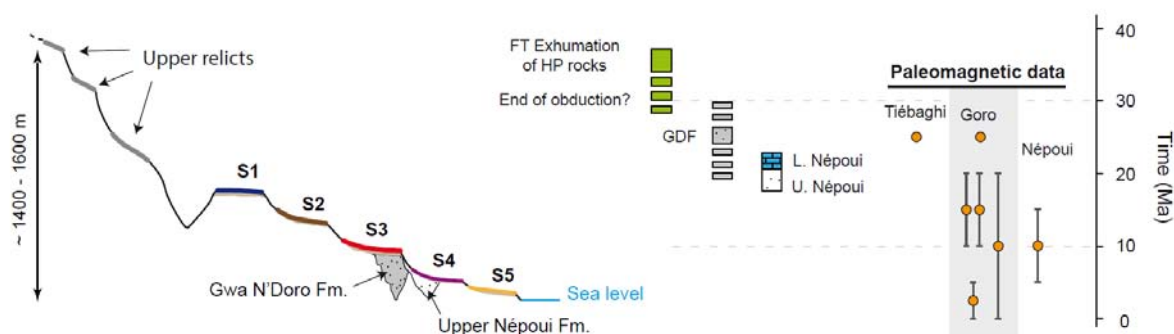


Fig. 31 : Figure synthétiques de contraintes chronologiques existantes en Nouvelle-Calédonie d'après les données de la littérature (Grimaud et al. (in prep (a)) ; synthèse complète dans Sévin et al., 2020).

En complément, je m'intéresse également au fonctionnement géochimique des plaines alluviales en lien avec leur évolution géomorphologique. Le cône alluvial de la Tista (Fig. 25) apparaît comme un laboratoire de choix car son évolution de surface a été bien contrainte récemment (Abrahami et al., 2018 ; Grimaud et al., 2020). Le projet DACA, que j'ai soumis à l'ANR JCJC, propose de regarder en détail les liens entre les âges des terrasses alluviales et les bilans géochimiques d'altération en contexte alluvial, en s'appuyant sur la minéralogie des profils d'altération, la géochimie des flux des rivières en parallèle de modélisation de transport réactif (logiciel Hytec développé au Centre de Géosciences ; collaboration N. Seigneur).

Modélisation des systèmes chenalisés : forçages naturels et relations à l'anthropique

Dans le cadre du projet FLUMY, qui a été renouvelé pour un programme de recherche avec deux partenaires (ENI et Total Energie) jusqu'en fin 2024, je suis amené à travailler sur les systèmes méandriformes dans les environnements fluvial et turbiditique. Ce travail sur FLUMY me tient à cœur, il n'est pourtant pas récompensé par un nombre élevé de publications du fait de sa forte dimension appliquée. Le projet reste cependant un formidable incubateur de projets variés, en collaboration avec géologues de réservoir et géostatisticiens. La thèse de Léo Szewczyk a par exemple eu pour origine le projet FLUMY, malgré le fait qu'elle n'utilise pas

directement le logiciel. En revanche, les résultats de la thèse de Léo ont permis de repenser récemment la géométrie du remplissage des chenaux dans FLUMY, en contexte fluvial.

FLUMY est actuellement utilisé par des partenaires principalement intéressés par les systèmes turbiditiques. Dans ce cadre, un projet de postdoctorat (Louison Mercier, début 1^{er} juin 2023) est en cours pour améliorer plusieurs aspects du logiciel. Deux aspects semblent particulièrement intéressants, tant du point de vue académique que du point de vue appliqué. Premièrement, il faudrait mieux intégrer les rétroactions entre déformation du substrat et processus chenalisés. En collaboration avec Fabien Ors, nous avons inclus un module de déformation du substrat FLUMY (Fig. 32). Si ce module donne des géométries réalistes pour des scénarios de faible subsidence, il reste beaucoup de travail à faire dans le cas de taux de subsidence plus forts, mais surtout dans le cas de soulèvements comme pour les plis anticlinaux. Une piste en cours de réflexion repose sur la meilleure intégration dans FLUMY de la charge sédimentaire locale, qui peut moduler incision et dépôt, ce qui n'est pas pris en compte à l'heure actuelle.

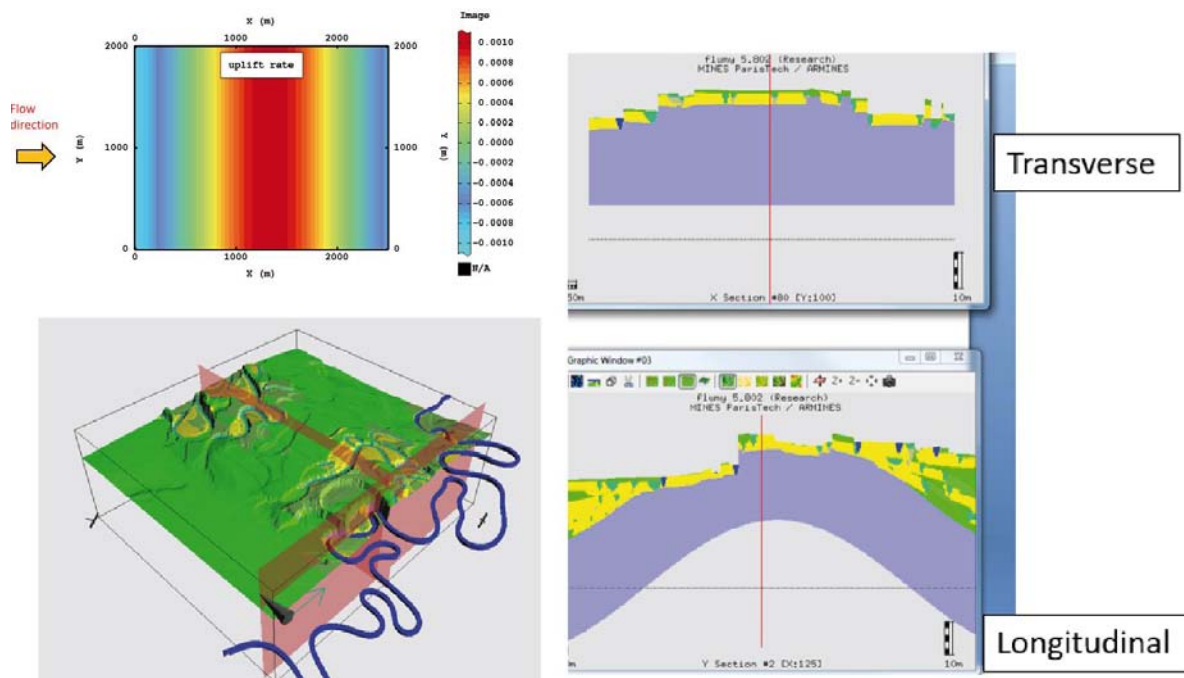


Fig. 32 : Exemple de test de modèle de déformation de la topographie dans FLUMY. La carte de soulèvement /subsidence est en mètre par itération. On peut observer une vue 3D de la topographie aussi qu'une coupe transverse et une vue longitudinale des dépôts.

Deuxièmement, il serait novateur d'intégrer la génération de lobes terminaux aux systèmes turbiditiques dans FLUMY. Il est envisagé de le faire à la manière de la modélisation basé-objet dans un premier temps. L'objet lobe existe en effet déjà dans FLUMY pour les lobes de crevasse (Lopez, 2003), il faut cependant le calibrer finement en mode turbiditique. Je souhaite proposer à Louison de réaliser une synthèse des géométries de lobes en fonction notamment des tailles de chenaux d'alimentation pour effectuer cette transposition.

Dans le futur, je souhaiterais concilier les besoins du projet FLUMY avec l'expertise de mon collègue Damien Huyghe sur le domaine sud-pyrénéen. Plusieurs formations cénozoïques le permettraient. Par exemple, la formation de Sariñena près de Huesca présente des géométries de chenaux fluviaux déjà bien étudiées (Donselar et Overeen, 2008). On pourrait tenter une

application sur le terrain de la mesure de la remobilisation (voir [Grimaud et al., 2022](#)) en utilisant la géométrie des levées et des barres d'accrétion latérale des chenaux. Il serait pertinent de mener des approches similaires sur des formations ayant enregistré des événements hyperthermaux comme le PETM ou le MECO (e.g., [Chen et al., 2018](#)). Enfin, d'autres formations seraient de bons analogues à étudier en comparaison des simulations de FLUMY, plus particulièrement les lobes turbiditiques profonds du bassin d'Hecho.

Enfin, je pense continuer de travailler sur les effets de la lithologie du substrat sur les processus d'érosion, afin de mieux calibrer les modèles d'incision des rivières. Dans cette optique, je pourrais développer d'ici quelques années des modèles analogiques d'érosion incluant des variations du substrat lithologique (la suite de la section 2.1.2). Je ne perds cependant pas de vue la comparaison avec le terrain : cette thématique est déjà présente dans les travaux de Diana Chourio Camacho sur le Bassin parisien. J'espère ainsi pouvoir aller plus loin sur le sujet.

Dynamique de surface du Nord de la France : passé, présent et futur

Le Bassin parisien et sa périphérie constituent une entité géologique intéressante à plusieurs égards. Tout d'abord, la crise sanitaire récente a démontré toute la pertinence d'avoir des chantiers locaux pour des raisons logistiques. De plus, cette région concentre des activités anthropiques avec des besoins en ressources et des problématiques environnementales concrètes, comme le montrent plusieurs chantiers scientifiques en cours (RGF, PEPR sous-sol, PIREN-Seine, ZA-Seine, etc.). Il y a là un objet d'étude sur lequel je souhaite passer du temps, en cohérence avec mes travaux sur les zones anorogéniques. Il faut noter que les taux d'incision des rivières y sont environ cinq fois plus élevés (55 m/Ma ; [Antoine et al., 2007](#)) qu'en Afrique de l'Ouest (10 m/Ma ; [Grimaud et al., 2014](#)). Savoir s'il s'agit d'un biais de mesure ou d'un vrai forçage -climatique ou tectonique- est au cœur de mon questionnement actuel.

Tout d'abord, la thèse de Diana Chourio Camacho a permis d'initier des travaux de datation sur les systèmes de terrasses de la Seine et de ses affluents. Il paraît opportun de continuer ce travail de longue haleine pour préciser la chronologie et la distribution spatiale de l'incision en lien avec les forçages externes (tectonique et/ou climatiques) sur le système. Des premiers résultats en cours de rédaction par Diana sur le site de Manoir Brésil en Normandie montrent de plus des chronologies et interactions fortes entre dynamique d'incision des rivières et colluvionnement, notamment au niveau de transitions climatiques sous l'effet de la fonte du pergélisol ([Chourio Camacho et al., in prep](#)). Je souhaite continuer les collaborations dans cette voie avec l'équipe d'encadrement de la thèse de Diana (P. Bessin, H. Tissoux et P. Voinchet notamment).



Fig. 33 : Exemple de concrétions carbonatées observées en association avec des terrasses alluviales quaternaires dans le Bassin parisien en Bassée (à gauche) et en Basse Seine (à droite).

Pour aller plus loin dans les relations entre dynamique d'incision et dynamique des versants, il paraît fondamental de regarder comment la géométrie de corps supergènes (ex : grésifications comme dans les sables de Fontainebleau et surtout meulière) s'intègrent dans cette évolution. Sur le site de Manoir-Brésil étudié par Diana, j'ai pu trouver lors d'une reconnaissance de terrain des figures de concrétions carbonatées montrant des circulations après des dépôts tidaux vieux de 200-250 milliers d'année. D'autres concrétions similaires sont observées en Bassée en base d'un niveau de terrasse quaternaire au contact de la craie (Fig. 33). Avec mon collègue Damien Huyghe et des chercheurs d'Orsay, nous projetons d'étudier ces concrétions en lame mince et par analyse géochimique pour contraindre leur âge et leur cinétique de cristallisation. Pour les fractions siliceuses, nous projetons par exemple d'analyser l'isotopie de l'oxygène, de façon similaire à l'étude à laquelle je suis associé sur la Nouvelle-Calédonie ([Cathelineau et al., sous presse](#)).

L'étude des fonds de vallées de la Seine a constitué une partie importante de mes travaux des dernières années qui sont en cours de valorisation. Je souhaite pérenniser cette activité et renforcer mes collaborations en archéologie environnementale (avec P. Gouge ou C. Petit notamment et de nombreux contacts plus occasionnels avec des collègues de l'INRAP ou d'autres sociétés comme Evéha). Je suis impliqué dans plusieurs PCR dans ce cadre. La Bassée constitue un site d'étude que je privilégie pour sa proximité géographique et également pour son intérêt archéologique : d'un point de vue surfacique, c'est un des territoires les plus fouillés par l'archéologie préventive. Il y a là matière à avancer de front sur plusieurs thématiques : (i) la quantification de l'évolution du débit et du modelé fluvial de la Seine au cours de l'Holocène en comparaison avec les travaux pionniers de Pastre et al. (1997) dans la Marne et l'Oise, (ii) l'étude des relations entre l'Homme et son environnement et enfin (iii) l'utilisation de proxy pour quantifier le paléoclimat à plus haute fréquence ([Grimaud et al., Rapports PIREN 2020, 2021](#)). La calibration de mesures isotopiques sur les coquilles de mollusques en particulier pourrait mener à des applications à d'autres échelles, comme celle du Cénozoïque (HDR Huyghe, 2022).

Finalement, j'ai récemment obtenu un projet de thèse CIFRE pour explorer la réponse des sols de couverture d'un site de stockage de déchets radioactifs (CSM : Centre de Stockage de la Manche, à la Hague) en réponse au changement climatique. Il est proposé d'utiliser un système

expérimental d'érosion en laboratoire pour tester l'effet d'évènements pluvieux caractéristiques de climats conformes avec les projections. Plusieurs scénarios critiques -envisagés pour les 300 prochaines années- seront testés. Une partie d'entre eux inclura un arrêt de la pluie jusqu'à la dessiccation du matériau afin de tester l'impact de cycles sécheresse/pluie sur l'érosion. Le doctorant (Gabriel Portzer) a été recruté en décembre 2022, il réalisera ses expériences sur des échantillons de sol du CSM en partenariat avec Samuel Abiven directeur de l'Ecotron, structure expérimentale de l'Université PSL basée à Saint-Pierre les Nemours en Seine-et-Marne.

Références bibliographiques

- Abrahami, R., P. Huyghe, P. van der Beek, S. Lowick, J. Carcaillet, and T. Chakraborty (2018), Late Pleistocene-Holocene development of the Tista megafan (West Bengal, India): ^{10}Be cosmogenic and IRSL age constraints, *Quaternary Science Reviews*, 185, 69-90.
- Ahmed, J., J. A. Constantine, and T. Dunne (2019), The role of sediment supply in the adjustment of channel sinuosity across the Amazon Basin, *Geology*, 47(9), 807-810.
- Allard, T., C. Gautheron, S. B. Riffel, E. Balan, B. F. Soares, R. Pinna-Jamme, A. Derycke, G. Morin, G. T. Bueno, and N. Do Nascimento (2018), Combined dating of goethites and kaolinites from ferruginous duricrusts. Deciphering the Late Neogene erosion history of Central Amazonia, *Chemical Geology*, 479, 136-150.
- Allen, P. A. (2008), From landscapes into geological history, *Nature*, 451(7176), 274-276.
- Allen, P., and J. Allen (2005), *Basin analysis: principles and applications*: Malden, Massachusetts, edited, Blackwell Publishing.
- Antoine, P., N. L. Lozouet, C. Chaussé, J.-P. Lautridou, J.-F. Pastre, P. Auguste, J.-J. Bahain, C. Falguères, and B. Galehb (2007), Pleistocene fluvial terraces from northern France (Seine, Yonne, Somme): synthesis, and new results from interglacial deposits, *Quaternary Science Reviews*, 26(22-24), 2701-2723.
- Ashmore, P., and G. Parker (1983), Confluence scour in coarse braided streams, *Water Resources Research*, 19(2), 392-402.
- Ashworth, P. J., J. L. Best, and M. A. Jones (2007), The relationship between channel avulsion, flow occupancy and aggradation in braided rivers: insights from an experimental model, *Sedimentology*, 54(3), 497-513.
- Bailly, L., J.-P. Ambrosi, J. Barbarand, A. Beauvais, D. Cluzel, C. Lerouge, F. Prognon, F. Quesnel, E. Ramanaidou, and C. Ricordel-Prognon (2014), *Nickal-Typologie des minerais latéritiques de Nouvelle-Calédonie et facteurs de concentration de Co et Ni. Rapport scientifique final. Les gisements de nickel latéritique de Nouvelle-Calédonie, volume II, CNRT Nickel et son environnement.*
- Baynes, E. R., D. Lague, M. Attal, A. Gangloff, L. A. Kirstein, and A. J. Dugmore (2018), River self-organisation inhibits discharge control on waterfall migration, *Scientific reports*, 8(1), 1-8.
- Beauvais, A., and D. Chardon (2013), Modes, tempo, and spatial variability of Cenozoic cratonic denudation: The West African example, *Geochemistry, Geophysics, Geosystems*, 14(5), 1590-1608.
- Beauvais, A., G. Ruffet, O. Hénocque, and F. Colin (2008), Chemical and physical erosion rhythms of the West African Cenozoic morphogenesis: the ^{39}Ar - ^{40}Ar dating of supergene K-Mn oxides, *Journal of Geophysical Research: Earth Surface*, 113(F4).
- Beauvais, A., N. J. Bonnet, D. Chardon, N. Arnaud, and M. Jayananda (2016), Very long-term stability of passive margin escarpment constrained by $^{40}\text{Ar}/^{39}\text{Ar}$ dating of K-Mn oxides, *Geology*, 44(4), 299-302.
- Bennett, S. J., C. V. Alonso, S. N. Prasad, and M. J. Römkens (2000), Experiments on headcut growth and migration in concentrated flows typical of upland areas, *Water Resources Research*, 36(7), 1911-1922.

- Best, J. L., and P. J. Ashworth (1997), Scour in large braided rivers and the recognition of sequence stratigraphic boundaries, *Nature*, 387(6630), 275-277.
- Best, J., and S. E. Darby (2020), The pace of human-induced change in large rivers: Stresses, resilience, and vulnerability to extreme events, *One Earth*, 2(6), 510-514.
- Bierman, P. R., and M. Caffee (2001), Slow rates of rock surface erosion and sediment production across the Namib Desert and escarpment, southern Africa, *American Journal of Science*, 301(4-5), 326-358.
- Bishop, P. (1995), Drainage rearrangement by river capture, beheading and diversion, *Progress in physical geography*, 19(4), 449-473.
- Bishop, P. (2007), Long-term landscape evolution: linking tectonics and surface processes, *Earth Surface Processes and Landforms: the Journal of the British Geomorphological Research Group*, 32(3), 329-365.
- Blöthe, J. H., and O. Korup (2013), Millennial lag times in the Himalayan sediment routing system, *Earth and Planetary Science Letters*, 382, 38-46.
- Braucher, R., F. Colin, E. Brown, D. Bourles, O. Bamba, G. Raisbeck, F. Yiou, and J. Koud (1998), African laterite dynamics using in situ-produced ^{10}Be , *Geochimica et Cosmochimica Acta*, 62(9), 1501-1507.
- Braun, J. (2010), The many surface expressions of mantle dynamics, *Nature Geoscience*, 3(12), 825-833.
- Brenot, J., S. Poirier, D. Ravry, J. Kovacik, and C. Petit (2021), L'implantation de l'enceinte monumentale de La Villeneuve-au-Châtelot (Aube) du Néolithique récent à la confluence Seine-Aube: premiers résultats géoarchéologiques, *Bulletin de la Société Préhistorique Française*, 118(3), 576-579.
- Brown, R. W., M. A. Summerfield, and A. J. Gleadow (2002), Denudational history along a transect across the Drakensberg Escarpment of southern Africa derived from apatite fission track thermochronology, *Journal of Geophysical Research: Solid Earth*, 107(B12), ETG 10-11-ETG 10-18.
- Brown, E. T., D. L. Bourlès, F. Colin, Z. Sanfo, G. M. Raisbeck, and F. Yiou (1994), The development of iron crust lateritic systems in Burkina Faso, West Africa examined with in-situ-produced cosmogenic nuclides, *Earth and Planetary Science Letters*, 124(1-4), 19-33.
- Büdel, J., L. Fischer, and D. Busche (1982), *Climatic geomorphology*, Princeton University Press Princeton, NJ.
- Bufe, A., C. Paola, and D. W. Burbank (2016), Fluvial bevelling of topography controlled by lateral channel mobility and uplift rate, *Nature Geoscience*, 9(9), 706-710.
- Burke, K. (1996), The african plate, *South african journal of geology*, 99(4), 341-409.
- Burke, K., and Y. Gunnell (2008), The African erosion surface: a continental-scale synthesis of geomorphology, tectonics, and environmental change over the past 180 million years, *Geological Society of America*.
- Castelltort, S., and J. Van Den Driessche (2003), How plausible are high-frequency sediment supply-driven cycles in the stratigraphic record?, *Sedimentary geology*, 157(1-2), 3-13.

- Cathelineau, M., Boiron, M.-C., Grimaud, J.-L., S. Favier, Teitler, Y. and Golfier, F. (sous presse) Silcrete formation in karsts, evidence of late Ni reworking in New Caledonia. Minerals. Special issue Nickel.
- Cazanacli, D., C. Paola, and G. Parker (2002), Experimental steep, braided flow: application to flooding risk on fans, *Journal of Hydraulic Engineering*, 128(3), 322-330.
- Chadwick, A. J., M. P. Lamb, and V. Ganti (2020), Accelerated river avulsion frequency on lowland deltas due to sea-level rise, *Proceedings of the National Academy of Sciences*, 117(30), 17584-17590.
- Chardon, D., and V. Chevillotte (2006), Morphotectonic evolution of the New Caledonia ridge (Pacific Southwest) from post-obduction tectonosedimentary record, *Tectonophysics*, 420(3-4), 473-491.
- Chardon, D., J.-L. Grimaud, A. Beauvais, and O. Bamba (2018), West African lateritic pediments: Landform-regolith evolution processes and mineral exploration pitfalls, *Earth-Science Reviews*, 179, 124-146.
- Chardon, D., J. L. Grimaud, D. Rouby, A. Beauvais, and F. Christophoul (2016), Stabilization of large drainage basins over geological time scales: Cenozoic West Africa, hot spot swell growth, and the Niger River, *Geochemistry, Geophysics, Geosystems*, 17(3), 1164-1181.
- Chen, C., L. Guerit, B. Z. Foreman, H. J. Hassenruck-Gudipati, T. Adatte, L. Honegger, M. Perret, A. Sluijs, and S. Castelltort (2018), Estimating regional flood discharge during Palaeocene-Eocene global warming, *Scientific Reports*, 8(1), 13391.
- Chevillotte, V., D. Chardon, A. Beauvais, P. Maurizot, and F. Colin (2006), Long-term tropical morphogenesis of New Caledonia (Southwest Pacific): Importance of positive epeirogeny and climate change, *Geomorphology*, 81(3-4), 361-375.
- Chourio Camacho, D. N., Grimaud, J. -L., Tissoux, H., Bessin, P., Voinchet, P., Noble, M. and P. Bertran (in prep). The stepped alluvial terrace of Manoir-Brésil, Lower Seine: a conundrum of fluvial, alluvial and slope deposits. prévu pour *Quaternaire*.
- Cojan, I., O. Fouché, S. Lopéz, and J. Rivoirard (2005), Process-based reservoir modelling in the example of meandering channel, in *Geostatistics Banff 2004*, edited, pp. 611-619, Springer.
- Colin, F., A. Beauvais, G. Ruffet, and O. Hénocque (2005), First $^{40}\text{Ar}/^{39}\text{Ar}$ geochronology of lateritic manganese pisolites: implications for the Palaeogene history of a West African landscape, *Earth and Planetary Science Letters*, 238(1-2), 172-188.
- Constantine, J. A., T. Dunne, H. Piégay, and G. Mathias Kondolf (2010), Controls on the alluviation of oxbow lakes by bed-material load along the Sacramento River, California, *Sedimentology*, 57(2), 389-407.
- Constantine, J. A., T. Dunne, J. Ahmed, C. Legleiter, and E. D. Lazarus (2014), Sediment supply as a driver of river meandering and floodplain evolution in the Amazon Basin, *Nature Geoscience*, 7(12), 899-903.
- Danišik, M., N. J. Evans, E. R. Ramanaidou, B. J. McDonald, C. Mayers, and B. I. McInnes (2013), (U-Th)/He chronology of the Robe River channel iron deposits, Hamersley Province, Western Australia, *Chemical Geology*, 354, 150-162.

- de Lavaissière, L., S. Bonnet, A. Guyez, and P. Davy (2022), Autogenic knickpoints in laboratory landscape experiments, *Earth Surface Dynamics*, 10(2), 229-246.
- Deleplancque, B. (2016), Caractérisation des hétérogénéités sédimentaires d'une plaine alluviale: Exemple de l'évolution de la Seine supérieure depuis le dernier maximum glaciaire, Paris Sciences et Lettres (ComUE).
- Deseine, A., C. Gueret, J.-D. Vigne, D. Mordant, and B. Valentin (2019), Nouveau regard sur les occupations du second Mésolithique du «Haut des Nachères» à Noyen-sur-Seine (Seine et Marne), edited.
- Donselaar, M. E., and I. Overeem (2008), Connectivity of fluvial point-bar deposits: An example from the Miocene Huesca fluvial fan, Ebro Basin, Spain, *AAPG bulletin*, 92(9), 1109-1129.
- English, K. L., J. Redfern, G. Bertotti, J. M. English, and R. Y. Cherif (2017), Intraplate uplift: new constraints on the Hoggar dome from the Illizi basin (Algeria), *Basin research*, 29(3), 377-393.
- Flowers, R. M., and B. Schoene (2010), (U-Th)/He thermochronometry constraints on unroofing of the eastern Kaapvaal craton and significance for uplift of the southern African Plateau, *Geology*, 38(9), 827-830.
- Foreman, B. Z., S. Y. Lai, Y. Komatsu, and C. Paola (2015), Braiding of submarine channels controlled by aspect ratio similar to rivers, *Nature Geoscience*, 8(9), 700-703.
- Forte, A. M., and K. X. Whipple (2019), The topographic analysis kit (TAK) for TopoToolbox, *Earth Surface Dynamics*, 7(1), 87-95.
- Goldrick, G., and P. Bishop (1995), Differentiating the roles of lithology and uplift in the steepening of bedrock river long profiles: an example from southeastern Australia, *The Journal of Geology*, 103(2), 227-231.
- Grandin, G. (1976), Aplatissements cuirassés et enrichissement des gisements de manganèse dans quelques régions d'Afrique de l'Ouest.
- Grandin, G., and M. Thiry (1983), Les grandes surfaces continentales tertiaires des régions chaudes. Succession des types d'altération, *Cah. ORSTOM, Sér. Géol*, 13(1), 3-18.
- Grimaud, J.-L., D. Chardon, and A. Beauvais (2014), Very long-term incision dynamics of big rivers, *Earth and Planetary Science Letters*, 405, 74-84.
- Grimaud, J.-L., C. Paola, and V. Voller (2016), Experimental migration of knickpoints: influence of style of base-level fall and bed lithology, *Earth Surface Dynamics*, 4(1), 11-23.
- Grimaud, J. L., C. Paola, and C. Ellis (2017), Competition between uplift and transverse sedimentation in an experimental delta, *Journal of Geophysical Research: Earth Surface*, 122(7), 1339-1354.
- Grimaud, J. L., D. Rouby, D. Chardon, and A. Beauvais (2018), Cenozoic sediment budget of West Africa and the Niger delta, *Basin research*, 30(2), 169-186.
- Grimaud, J.-L., D. Chardon, V. Metelka, A. Beauvais, and O. Bamba (2015), Neogene cratonic erosion fluxes and landform evolution processes from regional regolith mapping (Burkina Faso, West Africa), *Geomorphology*, 241, 315-330.

- Grimaud, J. L., F. Ors, M. Lemay, I. Cojan, and J. Rivoirard (2022), Preservation and completeness of fluvial meandering deposits influenced by channel motions and overbank sedimentation, *Journal of Geophysical Research: Earth Surface*, e2021JF006435.
- Grimaud, J.-L., A. Huguet, P. Gouge, D. Huyghe, C. Petit, and L. Lestel (2021), Évolution des paysages dans la plaine alluviale de la Petite-Seine depuis le Néolithique, restitution des tracés fluviaux et contexte paléoenvironnemental, PIREN Seine phase 8.
- Grimaud, J. L., C. Grall, S. Goodbred, M. S. Steckler, R. Sincavage, J. L. Pickering, C. Paola, L. Seeber, and M. S. Hossain (2020), Flexural deformation controls on Late Quaternary sediment dispersal in the Garo-Rajmahal Gap, NW Bengal Basin, *Basin research*, 32(5), 1242-1260.
- Grimaud, J.-L., L. Szewczyk, P. Gouge, I. Cojan, L. Lestel, D. Eschbach, C. Petit, P. Charrondière-Lewis, D. Huyghe, and A. Huguet (2020), Dynamique d'abandon de chenaux dans le territoire de la Petite-Seine, PIREN Seine.
- Grimaud, J.-L., Favier, S., Teitler, Y., Guiomar, Y. and Cathelineau, M. (in prep (a)) – Slow adjustment of river network and incision dynamics in a moderately uplifting area, SE New Caledonia. prévu pour *Geomorphology*.
- Grimaud, J.-L., Desassis, N., Chourio-Camacho, D. N., Ors, F., Renard, D., Tissoux, H. Paul Bessin, P., Noble, M. (in prep (b)). Restituting valley bottom geometry at the alluvium-substrate interface using directional kriging. prévu pour *Mathematical Geology*.
- Grimaud, J.-L., Gouge, P., Huyghe, D., Petit, C., Lestel, L., Eschbach, D., Catry, J., Quaisse, I. Imperor, A. (in prep (c)) Reconsidering the size and function of Neolithic enclosures: a river dynamic point of view. prévu pour *Scientific Reports*
- Guillocheau, F., D. Rouby, C. Robin, C. Helm, N. Rolland, C. L. C. De Veslud, and J. Braun (2012), Quantification and causes of the terrigenous sediment budget at the scale of a continental margin: a new method applied to the Namibia–South Africa margin, *Basin research*, 24(1), 3-30.
- Haack, R. C., P. Sundararaman, J. O. Diedjomahor, H. Xiao, N. J. Gant, E. D. May, and K. Kelsch (2000), AAPG Memoir 73, Chapter 16: Niger Delta Petroleum Systems, Nigeria.
- Han, J., and W. Kim (2022), Linking levee-building processes with channel avulsion: geomorphic analysis for assessing avulsion frequency and channel reoccupation, *Earth Surface Dynamics*, 10(4), 743-759.
- Heller, B. M., S. B. Riffel, T. Allard, G. Morin, J.-Y. Roig, R. Couëffé, G. Aertgeerts, A. Derycke, C. Ansart, and R. Pinna-Jamme (2022), Reading the climate signals hidden in bauxite, *Geochimica et Cosmochimica Acta*, 323, 40-73.
- Helm, C. (2009), Quantification des flux sédimentaires anciens à l'échelle d'un continent: le cas de l'Afrique au Méso-Cénozoïque, Rennes 1.
- Hénocque, O., G. Ruffet, F. Colin, and G. Féraud (1998), $^{40}\text{Ar}/^{39}\text{Ar}$ dating of West African lateritic cryptomelanes, *Geochimica et Cosmochimica Acta*, 62(16), 2739-2756.
- Imran, J., G. Parker, and C. Pirmez (1999), A nonlinear model of flow in meandering submarine and subaerial channels, *Journal of Fluid Mechanics*, 400, 295-331.

- Jean, A., A. Beauvais, D. Chardon, N. Arnaud, M. Jayananda, and P. Mathe (2020), Weathering history and landscape evolution of Western Ghats (India) from $40\text{Ar}/39\text{Ar}$ dating of supergene K–Mn oxides, *Journal of the Geological Society*, 177(3), 523-536.
- Jerolmack, D. J., and C. Paola (2010), Shredding of environmental signals by sediment transport, *Geophysical Research Letters*, 37(19).
- Jobe, Z. R., N. C. Howes, and N. C. Aughter (2016), Comparing submarine and fluvial channel kinematics: Implications for stratigraphic architecture, *Geology*, 44(11), 931-934.
- Jordan, D. W., and W. A. Pryor (1992), Hierarchical levels of heterogeneity in a Mississippi River meander belt and application to reservoir systems, *AAPG bulletin*, 76(10), 1601-1624.
- Kim, W., S. D. Connell, E. Steel, G. A. Smith, and C. Paola (2011), Mass-balance control on the interaction of axial and transverse channel systems, *Geology*, 39(7), 611-614.
- King, L. C. (1948), On the ages of African land-surfaces, *Quarterly Journal of the Geological Society*, 104(1-4), 439-459.
- Lai, S. Y., S. S. Hung, B. Z. Foreman, A. B. Limaye, J. L. Grimaud, and C. Paola (2017), Stream power controls the braiding intensity of submarine channels similarly to rivers, *Geophysical Research Letters*, 44(10), 5062-5070.
- Lemay, M. (2018), *Transposition à l'environnement turbiditique chenalisé d'un modèle de systèmes fluviaux méandriformes pour la modélisation de réservoirs*, Paris Sciences et Lettres (ComUE).
- Lemay, M., J.-L. Grimaud, I. Cojan, J. Rivoirard, and F. Ors (2020), Geomorphic variability of submarine channelized systems along continental margins: Comparison with fluvial meandering channels, *Marine and Petroleum Geology*, 115, 104295.
- Lemay, M., Grimaud, J. -L., Cojan, I., Rivoirard, J., and F. Ors, (sous presse). Submarine channels stacking patterns controlled by the 3D kinematics of meander bends. *Journal of Geological Society of London. Special Issue on meandering flow.*
- Lietar, C. (2016), The role of enclosures in territorial organization in the Paris Basin between 4500 and 3800 BC, *Giants in the Landscape: monumentality and Territories in the European Neolithic*, 31.
- Limaye, A. B., J. L. Grimaud, S. Y. Lai, B. Z. Foreman, Y. Komatsu, and C. Paola (2018), Geometry and dynamics of braided channels and bars under experimental density currents, *Sedimentology*, 65(6), 1947-1972.
- Lopez, S. (2003), *Modélisation de réservoirs chenalisés méandriformes: une approche génétique et stochastique*, École Nationale Supérieure des Mines de Paris.
- Lopez, S., I. Cojan, J. Rivoirard, and A. Galli (2009), Process-based stochastic modelling: meandering channelized reservoirs, *Analogue and Numerical Modelling of Sedimentary Systems: From Understanding to Prediction*, Wiley, Oxford, UK, 139-144.
- Lupker, M., C. France-Lanord, V. Galy, J. Lavé, J. Gaillardet, A. P. Gajurel, C. Guilmette, M. Rahman, S. K. Singh, and R. Sinha (2012), Predominant floodplain over mountain weathering of Himalayan sediments (Ganga basin), *Geochimica et Cosmochimica Acta*, 84, 410-432.

- Margirier, A., J. Braun, C. Gautheron, J. Carcaillet, S. Schwartz, R. P. Jamme, and J. Stanley (2019), Climate control on Early Cenozoic denudation of the Namibian margin as deduced from new thermochronological constraints, *Earth and Planetary Science Letters*, 527, 115779.
- Mathian, M. (2018), Étude de l'enregistrement minéralogique des événements paléoclimatiques dans les sols tropicaux: nouveaux apports de la datation de kaolinites par irradiations expérimentales, Sorbonne université.
- McHargue, T., M. J. Pyrcz, M. D. Sullivan, J. Clark, A. Fildani, B. Romans, J. Covault, M. Levy, H. Posamentier, and N. Drinkwater (2011), Architecture of turbidite channel systems on the continental slope: patterns and predictions, *Marine and Petroleum Geology*, 28(3), 728-743.
- Metelka, V., L. Baratoux, M. W. Jessell, A. Barth, J. Ježek, and S. Naba (2018), Automated regolith landform mapping using airborne geophysics and remote sensing data, Burkina Faso, West Africa, *Remote Sensing of Environment*, 204, 964-978.
- Métivier, and Gaudemer (1999), Stability of output fluxes of large rivers in South and East Asia during the last 2 million years: implications on floodplain processes, *Basin Research*, 11(4), 293-303.
- Meybeck, M. (1976), Total mineral dissolved transport by world major rivers/Transport en sels dissous des plus grands fleuves mondiaux, *Hydrological Sciences Journal*, 21(2), 265-284.
- Michel, P. (1973), Les bassins des fleuves Sénégal et Gambie: étude géomorphologique.
- Milliman, J. D., and R. H. Meade (1983), World-wide delivery of river sediment to the oceans, *The Journal of Geology*, 91(1), 1-21.
- Mordant, D., and C. Mordant (1992), Noyen-sur-Seine: a Mesolithic waterside settlement, paper presented at The wetland revolution in prehistory (Exeter, April 1991).
- Mordant, D., Evin, J., Galoyer, A., Giffault, M., Koeniguer, J.-C., Lambert, G. and C. Lavier (1993), Programme d'intervention archéologique dans les extractions de granulats de la Bassée (Seine-et-Marne). Comptes-rendus d'opération et d'analyse. (3). Noyen-sur-Seine. « Le pré-aux-Bœufs ». 77-341-004 OH. 99 pp.
- Mulder, T., and J. Alexander (2001), The physical character of subaqueous sedimentary density flows and their deposits, *Sedimentology*, 48(2), 269-299.
- Nahon, D. (1976), Cuirasses ferrugineuses et encroûtements calcaires au Sénégal occidental et en Mauritanie. Systèmes évolutifs: géochimie, structure, relais et coexistence, *Persée-Portail des revues scientifiques en SHS*.
- Paola, C., P. L. Heller, and C. L. Angevine (1992), The large-scale dynamics of grain-size variation in alluvial basins, 1: Theory, *Basin research*, 4(2), 73-90.
- Paola, C., V. Ganti, D. Mohrig, A. C. Runkel, and K. M. Straub (2018), Time not our time: physical controls on the preservation and measurement of geologic time, *Annual Review of Earth and Planetary Sciences*, 46(1), 409-438.
- Paul, J. D., G. G. Roberts, and N. White (2014), The African landscape through space and time, *Tectonics*, 33(6), 898-935.

- Pederson, J. L., and C. Tressler (2012), Colorado River long-profile metrics, knickzones and their meaning, *Earth and Planetary Science Letters*, 345, 171-179.
- Pelletier, J. D. (2010), How do pediments form?: A numerical modeling investigation with comparison to pediments in southern Arizona, USA, *Bulletin*, 122(11-12), 1815-1829.
- Pereira, M., N. Desassis, and D. Allard (2022), Geostatistics for large datasets on Riemannian manifolds: a matrix-free approach, arXiv preprint arXiv:2208.12501.
- Perron, J. T., and L. Royden (2013), An integral approach to bedrock river profile analysis, *Earth Surface Processes and Landforms*, 38(6), 570-576.
- Perseil, E., and G. Grandin (1978), Evolution minéralogique du manganèse dans trois gisements d'Afrique de l'Ouest: Mokta, Tambao, Nsuta, *Mineralium Deposita*, 13(3), 295-311.
- Riffel, S. B., P. M. Vasconcelos, I. O. Carmo, and K. A. Farley (2015), Combined $^{40}\text{Ar}/^{39}\text{Ar}$ and (U–Th)/He geochronological constraints on long-term landscape evolution of the Second Paraná Plateau and its ruiniform surface features, *Paraná, Brazil, Geomorphology*, 233, 52-63.
- Rivoirard, J., I. Cojan, D. Renard, and F. Geffroy (2008), Advances in quantification of processbased models for meandering channelized reservoirs, paper presented at VIII international geostatistics congress, GEOSTATS.
- Romans, B. W., S. Castelltort, J. A. Covault, A. Fildani, and J. Walsh (2016), Environmental signal propagation in sedimentary systems across timescales, *Earth-Science Reviews*, 153, 7-29.
- Rougier, S., Y. Missenard, C. Gautheron, J. Barbarand, H. Zeyen, R. Pinna, J.-P. Liégeois, B. Bonin, A. Ouabadi, and M. E.-M. Derder (2013), Eocene exhumation of the Tuareg Shield (Sahara Desert, Africa), *Geology*, 41(5), 615-618.
- Sadler, P. M. (1981), Sediment accumulation rates and the completeness of stratigraphic sections, *The Journal of Geology*, 89(5), 569-584.
- Sadler, P. M., and D. J. Strauss (1990), Estimation of completeness of stratigraphical sections using empirical data and theoretical models, *Journal of the Geological Society*, 147(3), 471-485.
- Sadler, P. M., and D. J. Jerolmack (2015), Scaling laws for aggradation, denudation and progradation rates: the case for time-scale invariance at sediment sources and sinks, *Geological Society, London, Special Publications*, 404(1), 69-88.
- Scheingross, J. S., A. B. Limaye, S. W. McCoy, and A. C. Whittaker (2021), Author Correction: The shaping of erosional landscapes by internal dynamics, *Nature Reviews Earth & Environment*, 2(5), 375-375.
- Schumer, R., and D. J. Jerolmack (2009), Real and apparent changes in sediment deposition rates through time, *Journal of Geophysical Research: Earth Surface*, 114(F3).
- Schumer, R., D. Jerolmack, and B. McElroy (2011), The stratigraphic filter and bias in measurement of geologic rates, *Geophysical Research Letters*, 38(11).
- Scotese, C. R., H. Song, B. J. Mills, and D. G. van der Meer (2021), Phanerozoic paleotemperatures: The earth's changing climate during the last 540 million years, *Earth-Science Reviews*, 215, 103503.

- Séranne, M. (1999), Early Oligocene stratigraphic turnover on the west Africa continental margin: a signature of the Tertiary greenhouse-to-icehouse transition?, *Terra Nova-Oxford*, 11(4), 135-140.
- Sevin, B. (2014), Cartographie du régolithe sur formation ultrabasique de Nouvelle-Calédonie: Localisation dans l'espace et le temps des gisements nickélicifères, Nouvelle Calédonie.
- Sevin, B., C. Ricordel-Prognon, F. Quesnel, D. Cluzel, S. Lesimple, and P. Maurizot (2012), First palaeomagnetic dating of ferricrete in New Caledonia: new insight on the morphogenesis and palaeoweathering of 'Grande Terre', *Terra Nova*, 24(1), 77-85.
- Sevin, B., P. Maurizot, D. Cluzel, E. Tournadour, S. Etienne, N. Folcher, J. Jeanpert, J. Collot, M. Iseppi, and S. Meffre (2020), Post-obduction evolution of New Caledonia, *Geological Society, London, Memoirs*, 51(1), 147-188.
- Sklar, L. S., and W. E. Dietrich (2004), A mechanistic model for river incision into bedrock by saltating bed load, *Water Resources Research*, 40(6).
- Straub, K. M., R. A. Duller, B. Z. Foreman, and E. A. Hajek (2020), Buffered, incomplete, and shredded: The challenges of reading an imperfect stratigraphic record, *Journal of Geophysical Research: Earth Surface*, 125(3), e2019JF005079.
- Straub, K. M., D. Mohrig, B. McElroy, J. Buttles, and C. Pirmez (2008), Interactions between turbidity currents and topography in aggrading sinuous submarine channels: A laboratory study, *Geological Society of America Bulletin*, 120(3-4), 368-385.
- Strauss, D., and P. M. Sadler (1989), Stochastic models for the completeness of stratigraphic sections, *Mathematical Geology*, 21(1), 37-59.
- Summerfield, M., and N. Hulton (1994), Natural controls of fluvial denudation rates in major world drainage basins, *Journal of Geophysical Research: Solid Earth*, 99(B7), 13871-13883.
- Sylvester, Z., C. Pirmez, and A. Cantelli (2011), A model of submarine channel-levee evolution based on channel trajectories: Implications for stratigraphic architecture, *Marine and Petroleum Geology*, 28(3), 716-727.
- Szewczyk, L. (2020), Bedload fill of abandoned channels, *Université Paris sciences et lettres*.
- Szewczyk, L., J.-L. Grimaud, and I. Cojan (2020), Experimental evidence for bifurcation angles control on abandoned channel fill geometry, *Earth Surface Dynamics*, 8(2), 275-288.
- Szewczyk, L., J. L. Grimaud, I. Cojan, and H. Piegay (2022), Bedload infilling and depositional patterns in chute cutoffs channels of a gravel-bed river: The Ain River, France, *Earth Surface Processes and Landforms*, 47(2), 459-476.
- Szewczyk, L., J. L. Grimaud, I. Cojan, and H. Piegay (in prep). Sand plug length in abandoned channels as a function of the slope ratio of distributaries. prévu pour *Earth Surface Processes and Landforms*
- Tal, M., P. Frey, K. Wonsuck, E. Lajeunesse, A. Limare, and F. ois Metivier (2012), 13 The Use of Imagery in Laboratory Experiments, *Fluvial remote sensing for science and management*, 299.
- Tardy, Y., and J. M. Soler (1993), *Pétrologie des latérites et des sols tropicaux*, Masson Paris.

- Tardy, Y., and C. Roquin (1998), *Derive des continents paleoclimats et altérations tropicales*, éd. BRGM.
- Tofelde, S., A. Bernhardt, L. Guerit, and B. W. Romans (2021), Times associated with source-to-sink propagation of environmental signals during landscape transience, *Frontiers in Earth Science*, 9, 227.
- Trescases, J. (1969), Premières observations sur l'altération des péridotites de Nouvelle-Calédonie, *Pédologie, Géochimie, Géomorphologie*, cahier. ORSTOM, Série. Géologie, Paris, 1, 27-57.
- Trescases, J.-J. (1975), L'évolution géochimique supergène des roches ultrabasiques en zone tropicale: formation des gisements nickélicifères de Nouvelle-Calédonie, Orstom France.
- Twidale, C. (1981), Origins and environments of pediments, *Journal of the Geological Society of Australia*, 28(3-4), 423-434.
- Van Wagoner, J. C., H. Posamentier, R. Mitchum, P. Vail, J. Sarg, T. Loutit, and J. Hardenbol (1988), An overview of the fundamentals of sequence stratigraphy and key definitions.
- Vasconcelos, P. M., and M. Conroy (2003), Geochronology of weathering and landscape evolution, Dugald River valley, NW Queensland, Australia, *Geochimica et Cosmochimica Acta*, 67(16), 2913-2930.
- Vasconcelos, P. M., G. H. Brimhall, T. A. Becker, and P. R. Renne (1994), $^{40}\text{Ar}/^{39}\text{Ar}$ analysis of supergene jarosite and alunite: Implications to the paleoweathering history of the western USA and West Africa, *Geochimica et Cosmochimica Acta*, 58(1), 401-420.
- Vrielynck, B., and P. Bouysse (2003), *The changing Face of the Earth*, Commission for the Geological Map of the World.
- Warrick, J., J. D. Milliman, D. Walling, R. Wasson, J. Syvitski, and R. Aalto (2014), Earth is (mostly) flat: Apportionment of the flux of continental sediment over millennial time scales: Comment, *Geology*, 42(1), e316-e316.
- Whipple, K. X. (2004), Bedrock rivers and the geomorphology of active orogens, *Annu. Rev. Earth Planet. Sci.*, 32, 151-185.
- Willett, S. D., S. W. McCoy, J. T. Perron, L. Goren, and C.-Y. Chen (2014), Dynamic reorganization of river basins, *Science*, 343(6175), 1248765.
- Williams, G. P. (1986), River meanders and channel size, *Journal of hydrology*, 88(1-2), 147-164.
- Wirthmann, A. (2000), *Geomorphology of the Tropics*, Springer Science & Business Media.
- Zachos, J., M. Pagani, L. Sloan, E. Thomas, and K. Billups (2001), Trends, rhythms, and aberrations in global climate 65 Ma to present, *Science*, 292(5517), 686-693.

Annexe 1 : CV étendu

Jean-Louis GRIMAUD

né le 30 mai 1987 à Ancenis (44)
Français

**Chargé d'Enseignement et de recherche,
MINES ParisTech**

Centre de Géosciences – Equipe Géologie
35 rue Saint-Honoré
77305 Fontainebleau Cedex

jean-louis.grimaud@mines-paristech.fr

Tél.: +33(0)1-64-69-49-58

PRINCIPALES THEMATIQUES SCIENTIFIQUES

- ✓ Etude des processus d'érosion / sédimentation en relation avec le climat et la déformation de la lithosphère
- ✓ Modélisation expérimentale des processus d'érosion et de sédimentation
- ✓ Dynamique de surface des domaines cratoniques et bilans sédimentaires à l'échelle continentale
- ✓ Compréhension des processus d'altération tropicale et d'érosion des pédiments (glacis)
- ✓ Stratigraphie et dynamique des milieux alluviaux

FORMATION ET EXPERIENCE PROFESSIONNELLE

Depuis 2016	Chargé Enseignement-Recherche	<i>Centre de Géosciences FONTAINEBLEAU</i>	MINES ParisTech
2014-2016	Post-doctorant	<i>St Anthony Falls Laboratory - Sediment dynamics group</i>	University of Minnesota
2010-2014	Doctorant en Géosciences	<i>GET Toulouse - Groupe LOA</i>	Université de Toulouse, Paul Sabatier
2009-2010	Master Européen BASIN MASTER	<i>Géosciences Rennes Département Sciences de la Terre</i>	Université de Rennes 1 VU Amsterdam
2005-2008	Licence Sciences de la Terre	<i>Géosciences Rennes</i>	Université de Rennes 1

DETAILS DES ACTIVITES DE RECHERCHE

- 2014-2016 **Projets de post-doctorat** (superviseur : Chris Paola [Univ. Minnesota])
- (1) Etude expérimentale de la migration de knickpoints en fonction des variations du niveau de base et de la lithologie et réutilisation des résultats dans un modèle numérique très simple (*expériences réalisées en aout-septembre 2014 ; collaboration Vaughan Voller [Univ. Minnesota]*)
 - (2) Etude de la dynamique des cônes alluviaux et de leurs interactions avec la déformation du substrat dans un bassin expérimental de 18 m², le Jurassic tank (*expérience réalisée en continu de février à mai 2015, analyse des dépôts en aout-septembre 2015*)
 - (3) Analyse stratigraphique des dépôts alluviaux quaternaires du méga-cône du Tista et du fleuve Brahmapoutre, delta du Bengale à partir de sondages carottés (30-60 m): datation, étude des provenances des chenaux (géochimie des éléments majeurs des sédiments (Sr,...)) et classification de l'altération des plaines d'inondation (*campagne de terrain en préparation pour mars 2016 ; collaborations : BenglaPIRE project, Steve Goodbred [Univ. Vanderbilt], Nano Seeber, Michael Steckler [Univ. Columbia], Saddam Hossain [Univ. Dakhar Bangladesh]*)
 - (4) Construction d'un modèle expérimental de dépôts turbiditiques en tresse comme base d'un modèle de réservoir (*expériences en cours depuis janvier 2015 ; collaborations : Ajay Limaye [Univ. Minnesota], Steven Lai [NCKU Taiwan], Brady Foreman [Univ. Washington State], Komatsu Yuhei [JOGMEC Japan]*)
- 2010-2014 **Doctorat en Géosciences** (encadrant : Dominique Chardon [GET Toulouse] ; financement WAXI (PI : Mark Jessell, CET Australia) et ANR TopoAFRICA (PI : François Guillocheau, Géosciences Rennes))

Dynamique de surface cénozoïque de l'Afrique de l'ouest à partir des surfaces latéritiques (terrain au Burkina Faso, Mali et Sénégal)

(1) Reconstruction des profils longitudinaux des principales rivières (Niger, Sénégal, Voltas,..): influence de la lithologie sur leur stabilité depuis 11 Ma et déformation des profils par des mouvements verticaux

(2) Reconstructions paléogéographiques et étude de l'évolution du drainage en réponse aux mouvements verticaux (*collaborations : Delphine Rouby [GET Toulouse], Anicet Beauvais [CEREGE]*)

(3) Production de cartes de dénudation à l'échelle régionale (à partir de la cartographie des latérites ouest africaines) et étude des bilans d'érosion en comparaison avec les dépôts cénozoïque dans le golfe de Guinée (*delta du Niger ; collaborations : Delphine Rouby [GET Toulouse], Anicet Beauvais [CEREGE]*)

(4) Etude de la dissection du paysage à partir de cartographie des glacis d'érosion au Burkina Faso; liens avec la dynamique des régolithes et implications pour l'exploration minière (*collaborations : Ousmane Bamba [Univ. Ouagadougou], Vacláv Metelka [CET, Australia], Anicet Beauvais [CEREGE]*)

2010 **Stage de recherche de Master 2** (encadrant : Stéphane Bonnet [Géosciences Rennes, GET Toulouse])

(6 mois) Dynamique des réseaux de drainage dans les chaînes de montagne

(1) Etude de terrain en Argentine de la géomorphologie de bassins-versants intra-montagneux, cartographie GPS et analyse des terrasses fluviales, et échantillonnage OSL et ¹⁰Be pour datation (*collaboration : Sébastien Moyano [Univ. Tucumán]*)

(2) Modélisation expérimentale de la migration de la ligne de partage des eaux sous influence de gradient pluviométriques (*Laboratoire de modélisation Géosciences Rennes*)

2009 **Projet de recherche de Master 2** (encadrants : Thierry Nalpas [Géosciences Rennes], John Reijmer [VU Amsterdam])

(1) Analyse stratigraphique et échantillonnage de conglomérats sud pyrénéens (séries de Sant Llorrenç de Morunys, Espagne) et analyse des provenances d'après la lithologie des clastes (galets) et de la matrice (lame mince) : relation avec les unités de l'intérieur de la chaîne et de l'avant-pays

(2) Analyse pétro-physique des matrices des conglomérats (porosité, perméabilité, vitesse des ondes sismiques): liens entre les propriétés réservoir, enfouissement potentiel et degré d'altération.

Stage professionnel de Master 1 (équipe structurale Total, Pau ; encadrants : Jean-François Ballard [CSTJF Pau], Thierry Nalpas [Géosciences Rennes])

Analyse de modèles analogiques compressifs avec sédimentation syn-cinématique ; aide à l'interprétation de la géométrie de données sismiques dans l'avant-pays andin

2008 **Stage de Licence 3 en Ecosse** (encadrant : Rob Butler [Univ. Aberdeen])

(2 mois) Interprétation de données sismiques et mise en ligne sur le site 'Virtual Seismic Atlas'

LANGUES

Français : langue maternelle ; Anglais : excellent niveau (niveau C2 CECRL + CLES2 en 2008) ; Espagnol : bases (niveau B1 CECRL)

1) ENCADREMENT

Thèses :

Martin Lemay (co-encadrement / soutenue en 2018) : *Transposition à l'environnement turbiditique chenalisé d'un modèle de systèmes fluviaux méandriformes pour la modélisation de réservoirs* (contrat doctoral Mines Paris)

Léo Szewczyk (soutenue en 2020) : *Bedload fill of abandoned channels* (contrat doctoral Mines Paris)

Diana Chourio Camacho (en cours, début nov. 2020) : *Restitution de la géométrie 3D du mur des alluvions de fond des vallées de la Seine* (thèse RGF-BRGM-Agence de l'Eau Seine Normandie)

Gabriel Portzer (en cours, début décembre 2022) : *Quantification de l'érosion des couvertures du Centre de Stockage de la Manche en fonction de leurs caractéristiques géotechniques et de la pluviométrie* (thèse Cifre avec l'ANDRA et la société WSP).

Masters / stages recherche 2A Ecole des Mines :

Alexandre Leveque (M2 RGF-BRGM ; 2020) : *Géométrie des alluvions de fond de vallée de l'Oise*

Morgane Goulain (Stage recherche 2A Mines Paris ; 2019) : *Influence of lithology on knickpoint migration in homogeneous and heterogeneous substrates*

Jean Catry (Stage recherche 2A Mines Paris ; 2021) : *Relation between abandoned channels morphology and clay fill thickness: insight from the Bassée, upper Seine River France*

Amélie Imperor / Ibtissem Quaisse (Stage recherche 2A Mines Paris ; 2022) : *Evolution of the Seine River before the industrial revolution: a geo-archaeological and geomorphological approach*

2) LISTE DE PUBLICATION

*Le bilan de mes publications est le suivant : 14 Articles rang A et 1 chapitre d'ouvrage publiés, ainsi que 38 résumés dans des congrès/workshops. Un article est actuellement sous presse à un numéro spécial du *Journal of the Geological Society of London* et un autre dans un numéro spécial de *Minerals*. Un article est en révision à *Nature Communication*. Quatre autres articles sont actuellement en préparation.*

*Mes cinq derniers articles sont avec des étudiants que j'ai encadrés. Mon nom est en **Gras** et les étudiants avec qui j'ai pu publier sont [en bleu](#).*

Articles:

[Lemay, M.](#), **Grimaud, J. L.**, Cojan, I., Rivoirard, J., & Ors, F. (accepté). Submarine channels stacking patterns controlled by the 3D kinematics of meander bends. *Journal of Geological Society of London*. Special Issue on meandering flow.

Grimaud, J.-L., Ors, F., [Lemay, M.](#), Cojan, I., & Rivoirard, J. (2022). Preservation and completeness of fluvial meandering deposits influenced by channel motions and overbank sedimentation. *Journal of Geophysical Research: Earth Surface*, 127, e2021JF006435.

[Szewczyk, L.](#), **Grimaud, J. L.**, Cojan, I., & Piegay, H. (2022). Bedload infilling and depositional patterns in chute cutoffs channels of a gravel-bed river: The Ain River, France. *Earth Surface Processes and Landforms*, 47(2), 459-476.

[Szewczyk, L.](#), **Grimaud, J. L.**, & Cojan, I. (2020). Experimental evidence for bifurcation angles control on abandoned channel fill geometry. *Earth Surface Dynamics*, 8(2), 275-288.

[Lemay, M.](#), **Grimaud, J. L.**, Cojan, I., Rivoirard, J., & Ors, F. (2020). Geomorphic variability of submarine channelized systems along continental margins: Comparison with fluvial meandering channels. *Marine and Petroleum Geology*, 115, 104295.

Grimaud J-L, Grall C, Goodbred S, et al. (2020), Flexural deformation controls on Late Quaternary sediment dispersal in the Garo-Rajmahal Gap, NW Bengal Basin, *Basin Research*, <https://doi.org/10.1111/bre.12425>

Limaye, A. B., **J. L. Grimaud**, S. Y. Lai, B. Z. Foreman, Y. Komatsu, and C. Paola (2018), Geometry and dynamics of braided channels and bars under experimental density currents, *Sedimentology*.

Chardon, D., **J.-L. Grimaud**, A. Beauvais, and O. Bamba (2018), West African lateritic pediments: Landform-regolith evolution processes and mineral exploration pitfalls, *Earth-Science Reviews*.

Grimaud, J. L., D. Rouby, D. Chardon, and A. Beauvais (2018), Cenozoic sediment budget of West Africa and the Niger delta, *Basin Research*.

Lai, S. Y., S. S. Hung, B. Z. Foreman, A. B. Limaye, **J. L. Grimaud**, and C. Paola (2017), Stream power controls the braiding intensity of submarine channels similarly to rivers, *Geophysical Research Letters*.

Grimaud, J. L., C. Paola, and C. Ellis (2017), Competition between uplift and transverse sedimentation in an experimental delta, *Journal of Geophysical Research: Earth Surface*.

Chardon, D., **J. L. Grimaud**, D. Rouby, A. Beauvais, and F. Christophoul (2016), Stabilization of large drainage basins over geological time scales: Cenozoic West Africa, hot spot swell growth, and the Niger River, *Geochemistry, Geophysics, Geosystems*, 17(3), 1164-1181.

Grimaud, J.-L., C. Paola, and V. Voller (2016), Experimental migration of knickpoints: influence of style of base-level fall and bed lithology, *Earth Surface Dynamics*, 4(1), 11.

Grimaud, J.-L., D. Chardon, V. Metelka, A. Beauvais, and O. Bamba (2015), Neogene cratonic erosion fluxes and landform evolution processes from regional regolith mapping (Burkina Faso, West Africa), *Geomorphology*, 241, 315-330.

Grimaud, J.-L., D. Chardon, and A. Beauvais (2014), Very long-term incision dynamics of big rivers, *Earth and Planetary Science Letters*, 405, 74-84.

Chapitre d'ouvrage :

Petit, C., Charrondière-Lewis, P., Cojan, I. Cruz, F. Deborde, G., Deleplancque, B., Durost, R., Fechner, K., Fontana, L., Frouin, M., Gouge, P., Granai, S., **Grimaud, J. L.**, Lenda, S., Peltier, V., Riquier, V., [Szewczyk, L.](#), Tegel, W. et Vanmoerkerke, J. (2021). Relations entre sociétés et environnement en Petite Seine du Mésolithique à la fin du Moyen Âge: nouvelles problématiques et résultats récents d'archéologie environnementale. In *L'Aube, un espace clé sur le cours de la Seine, Actes du colloque ArkéAube 2019, Troyes* (pp. 17-19).

Thèse :

Grimaud, J.-L. (2014). Dynamique long-terme de l'érosion en contexte cratonique : l'Afrique de l'Ouest depuis l'Eocène. PhD Thesis, Toulouse University, Toulouse, France, 300 pp.

Master 2 :

Grimaud, J.-L. (2010). Impact de la dynamique de la ligne de crête sur l'organisation des bassins versants dans la Sierra Aconquija, argentine. *Rapport master 2 Géosciences Rennes, 24 pp.*

Conférences :

Grimaud, J. L., [L. Szewczyk](#), P. Gouge, I. Cojan, A. Huguet, C. Petit, E. Doyen, D. Huyghe and J. Catry (2022) An evolving landscape in the Bassée alluvial plain since the Neolithic, river path changes and paleo-environments. *Q13 Strasbourg*

[Chourio-Camacho D.](#), **J.-L. Grimaud**, F. Ors, N. Desassis, D. Renard, H. Tissoux, P. Bessin, M. Noble and P. Voinchet (2022) Adjustment of alluvial fill geometry to regressive erosion and bedrock lithology in the Oise valley, Seine River catchment. *Q13 Strasbourg*

[Szewczyk, L.](#), **J.-L. Grimaud**, I. Cojan, H. Piégay. (2021) Infill dynamics and depositional patterns in gravel-bed chute cutoffs channels: the Ain River, France. *IMS 2021*, Jun 2021, Prague, France.

Grimaud, J.-L., F. Ors, [M. Lemay](#), I. Cojan and Rivoirard, J. (2021). Preservation and completeness of meandering rivers deposits: insights from numerical simulations. *IMS 2021*, Jun 2021, Prague, France.

[Chourio-Camacho D.](#), **J.-L. Grimaud**, H. Tissoux, P. Bessin, and M. Noble. Late Quaternary in the Paris Basin: 3D restitution of alluvium geometry in the bottom of major valleys in the Seine catchment. *RST*, Nov 2021, Lyon, France.

Grimaud, J.-L., C. Petit, D. Eschbach, L. Lestel, P. Gouge, [L. Szewczyk](#) et al. (2020) Dynamique sociétale et évolutions des paysages fluviaux de la Seine : exemples de paléo-chenaux sur le territoire de la Petite-Seine. *5eme colloque des Zones Ateliers-CNRS, May 2020, Blois, France.*

Grimaud, J.-L., C., Homberg, F., Bergerat, C., Mehl, D., Bruel (2019) Champs de déformation et fracturation des séries méso-cénozoïques sur le pourtour sud-est du plateau ardéchois. *17ème Congrès Français de Sédimentologie*

[Szewczyk, L.](#), **J.-L. Grimaud**, and I. Cojan (2019), Controls of bifurcation geometry on bed deposition patterns during experimental channel abandonments, *Geophysical Research Abstracts (21)*.

[Lemay, M.](#), F. Ors, **J.-L. Grimaud**, J. Rivoirard and I. Cojan. (2019) Forward model applied to channelized turbidite systems: a case study of the Benin major valley fill. *Petroleum Geostatistics 2019 (1)*, 1-5

Grimaud, J.-L., C. Grall, C. Paola, S. Goodbred, S. Hossain, R. Sincavage, J. Pickering, M. Steckler, and N. Seeber (2018) **Sediment partitioning related to a deep structure in Northwestern Bengal during the Late Quaternary** *EGU* 2018

Steckler, M. S., C. Grall, **J.-L. Grimaud**, L. Seeber, P. M. Betka, S. H. Akhter et al. (2018) Sinuous track of the flexural bulge in the eastern Himalayas and Bengal Basin from multiple loads on a variable rigidity plate, an explanation for the Barind and Madhupur Pleistocene uplands. AGU 2018

[Lemay, M.](#), I. Cojan, J. Rivoirard, **J.-L. Grimaud** and F. Ors (2017). Transposition of a Process-Based Model, Flumy: from Meandering Fluvial Systems to Channelized Turbidite Systems. *AGU Fall Meeting Abstracts 2017, EP13C-1644*

Singh A., A. Tejedor, **J.-L. Grimaud**, I. V Zaliapin and E Foufoula-Georgiou. (2016) Quantifying the scale- and process- dependent reorganization of landscape under climatic change: inferences from an experimental landscape, *AGU Fall Meeting 2016*

Grimaud J.-L., C. Grall, C. Paola, S. L. Goodbred, S. Hossain, R. Sincavage, J. L. Pickering, M. S. Steckler, L. Seeber, I. Cojan and C. Franke (2016) Geomorphic evolution and sediment partitioning in the Tista Fan and Barind Tract areas, NW Bangladesh, during the Late Quaternary, *AGU Fall Meeting 2016*

Grimaud, J.-L., A. Limaye, and C. Paola. (2016), Submarine deposition and braiding under experimental density current. *25e Réunion des Sciences de la Terre*, Oct 2016, Caen, France.

Rouby, D., D. Chardon, D. Huyghe, J. Ye, F. Guillocheau, C. Robin, M. Dall'Asta, R. Brown, M. Wildman, D. Webster, **J.-L. Grimaud** (2016) Meso-Cenozoic Source-to-Sink analysis of the African margin of the Equatorial Atlantic, *Rift III meeting, Geol. Society, London*.

Limaye, A. B., **J.-L. Grimaud**, and C. Paola (2015) Formation of braided channels and associated deposits by experimental turbidity currents, *AGU Fall Meeting 2015*

Chardon, D., **J.-L. Grimaud**, D. Rouby, and A. Beauvais (2015) Sediment budget of cratons: insights from West Africa over the Cenozoic, *AGU Fall Meeting 2015*.

Grimaud, J.-L., C. Paola, and V. Voller (2015) River path selection in response to uplift and interaction with alluvial fans, *AGU Fall Meeting 2015*.

Sincavage, R., S. Goodbred, J. Pickering, C. Wilson, Meagan Patrick, S. Hossain, S. H. Akhter, M. Steckler, L. Seeber, C. Grall, C. Paola, and **J.-L. Grimaud** (2015) Holocene construction and evolution of the Ganges-Brahmaputra-Meghna delta: the influence of climate, eustasy, and tectonics on stratigraphic architecture and fluvial dynamics, *AGU Fall Meeting 2015*.

Grimaud, J.-L., D. Chardon, A. Beauvais, and V. Metelka (2014), Lateritic Landform-Regolith Mapping of Southwestern Burkina Faso (West Africa): Implications for Long-term Landscape Evolution Processes and Mineral Exploration, *AGU Fall Meeting Abstracts #EP13B-3524*

Grimaud, J.-L., D. Chardon, A. Beauvais, and C. Paola (2014) Incision dynamics along river profiles: the influence of uplift and lithology. *AGU Fall Meeting Abstracts #EP31D-3592*

Huyghe, D., D. Chardon, D. Rouby, J. Ye, **J.-L. Grimaud**, O. Broucke, F. Guillocheau, and C. Robin (2014) Cenozoic evolution of the Ivory Coast-Ghana transform margin : implication for a source-to-sink analysis of the Volta drainagesystem. *RST 2014, Pau, France, 76-77*

Grimaud, J.-L., D. Chardon, D. Rouby, and A. Beauvais (2014) Evolution and incision dynamics of big rivers over the Cenozoic in West Africa, *RST 2014, Pau, France*

Grimaud, J.-L., D. Chardon, D. Rouby, and A. Beauvais (2014) 45 my of denudation in West Africa: implications for cratonic erosion budgets and the Cenozoic evolution of the Niger catchment-delta system, *RST 2014*, Pau, France

Grimaud, J.-L., D. Chardon, D. Rouby, and A. Beauvais (2014), Quantifying denudation of the West African passive-transform margin: implications for Cenozoic erosion budget of cratons and source-to-sink systems, *Vol. 16, EGU2014-9913, 2014 EGU General Assembly 2014*

Grimaud, J.-L., D. Chardon, D. Rouby, and A. Beauvais (2013), Long-term evolution of West African drainage, denudation and paleo-river long profiles using the lateritic record from the Cenozoic, *IAG Abstract Number: 629*

Grimaud, J.-L., D. Chardon, A. Beauvais, and D. Rouby (2013) Cenozoic drainage evolution of the West African transform marginal Upwarp, *Geophysical Research Abstracts Vol. 15, EGU2013-4888-2, 2013 EGU General Assembly 2013*

Chardon, D., D. Rouby, C. Robin, G. Calves, **J.-L. Grimaud**, F. Guillocheau, A. Beauvais, and J. Braun, (2013), Source to sink study of non-cylindrical rifted passive margins: the case of the Gulf of Guinea, *EGU2013-5223, 2011 EGU General Assembly 2013*

Rouby, D., J. Braun, D. Chardon, O. Dauteuil, F. Guillocheau, C. Robin, **J.-L. Grimaud**, G. Calves, and G. Baby, (2012), Source to sink study of non-cylindrical rifted passive margins: insights from a numerical model incorporating variable elastic thickness, surface processes and 3d thermal subsidence, *EP41B-0793, 2012 AGU Fall Meeting*

Chardon, D., **J.-L. Grimaud**, A. Beauvais, D. Rouby, and M. Jessell (2012), Constraints on long-term evolution of West African topography through reconstruction of paleo-river long profiles and drainages, *CAG 24, Adis Abeba*

Grimaud, J.-L., D. Chardon, A. Beauvais, and F. Christophoul (2011), Cenozoic drainage evolution of West Africa: Spatial and temporal constraints from the lateritic record, *Geophysical Research Abstracts Vol. 13, EGU2011-4308-3, 2011 EGU General Assembly 2011*

Grimaud, J.-L., Bonnet, S. Shrinking and splitting of drainage basins along the Aconquija Range (Argentina) from the migration of its main drainage divide. *American Geophysical Union, Fall Meeting 2010, abstract #EP52A-04*

Workshops :

Chardon, D., **J.-L. Grimaud**, A. Beauvais, and D. Rouby (2013), Long-term erosion dynamics of cratonic lithospheres: 45 my long record of climate variability and long-wavelength deformation at the scale of West Africa, *TopoEurope 2013, Roma*

Chardon, D., **J.-L. Grimaud**, A. Beauvais, and D. Rouby (2012), Cenozoic dynamics of the West African transform margin: Drainage evolution, denudation patterns, sediment budget and vertical mobility, *TopoAfrica Meeting - 20-25 January 2013 NNMU, Port Elizabeth and George (Saasveld)*

Grimaud, J.-L., D. Chardon, and A. Beauvais (2012), Evolution of river long profiles in West Africa since the Eocene, *TopoAfrica Meeting - 20-25 January 2013 NNMU, Port Elizabeth and George (Saasveld)*

Grimaud, J.-L., D. Chardon, A. Beauvais, and D. Rouby (2012), Cenozoic erosion budget and sediment routing systems at the scale of West Africa, *TopoAfrica Meeting - 20-25 January 2013 NNMU, Port Elizabeth and George (Saasveld)*

Grimaud, J.-L., D. Chardon, A. Beauvais, D. Rouby, and F. Christophoul (2012), Paleogene drainage reorganization in West Africa, *TopoAfrica Meeting - 20-25 January 2013 NNMU, Port Elizabeth and George (Saasveld)*

Rapports :

Cathelineau, M., S. Favier, **J.-L. Grimaud**, J. Jeanpert, S. Etienne, Y. Teitler, F. Golfier, M. Ulrich, M. Munoz, E. Ramanaidou, and S. Grangeon. (2021) TRANSNUM Facteurs d'enrichissements et transferts de Ni, Co-Sc dans les saprolites de Nouvelle Calédonie : approche géométrique, minéralo-géochimique et numérique Rapport intermédiaire

Grimaud, J.-L., A. Huguet, P. Gouge, D. Huyghe, C. Petit, and L. Lestel. (2021) Évolution des paysages dans la plaine alluviale de la Petite-Seine depuis le Néolithique, restitution des tracés fluviaux et contexte paléoenvironnemental. [Rapport de recherche] PIREN Seine phase 8.

Cathelineau, M., S. Favier, **J.-L. Grimaud**, J. Jeanpert, S. Etienne, Y. Teitler, F. Golfier, M. Ulrich, M. Munoz, E. Ramanaidou, and S. Grangeon. (2020) TRANSNUM Facteurs d'enrichissements et transferts de Ni, Co-Sc dans les saprolites de Nouvelle Calédonie : approche géométrique, minéralo-géochimique et numérique Rapport intermédiaire

Grimaud, J.-L., [L. Szewczyk](#), P. Gouge, I. Cojan, L. Lestel, D. Eschbach, P. Charrondière-Lewis, D. Huyghe and A. Huguet. (2020) Dynamique d'abandon de chenaux dans le territoire de la Petite-Seine. [Rapport de recherche] PIREN Seine phase 8.

Limaye, A. B., **Grimaud, J.-L.**, Lai, S. Y. J., Foreman, B. Z., Komatsu, Y. and Paola, C. (2018). Topography, image, and flow model data for experimental density currents, St. Anthony Falls Laboratory, 2015-2017. Retrieved from the Data Repository for the University of Minnesota, <https://doi.org/10.13020/D6R088>.

Grimaud, J.-L. (2017) SD2S : Simulation Dynamique des Dépôts Sédimentaires CARNOT 2017 : 1700557

3) ACTIVITE D'ENSEIGNEMENT AUX MINES

Mon contrat aux Mines stipule que je dois faire de l'enseignement mais pas le nombre d'heures. Les UE / stage de terrain dont j'ai la responsabilité sont en [bleu](#).

2016-2017 (~ 110 heures) -> Géologie terrain 1A Mines (Castellane), Géologie terrain 3AST-VS Mines (Digne-les-Bains), Géologie terrain Corps des Mines (Castellane)

2017-2018 (~ 110 heures) -> Géologie terrain 1A Mines (Castellane), Géologie terrain 3AST-VS Mines (Digne-les-Bains), Géologie terrain Corps des Mines (Laragne)

2018-2019 (~ 90 heures) -> [Géologie terrain 1A Mines](#), Géologie terrain 2AST Mines (Laragne)

2019-2020 (~ 70 heures) -> [Géologie terrain 1A Mines](#) (Castellane), [Géologie terrain 3AST-VS Mines](#) (Castellane)

2020-2021 (~ 70 heures) -> [Géologie terrain 3AST-VS](#) (Montage d'un camp de terrain Bassin de Paris-Morvan), annulation terrain 1A pour cause Covid, Grand ensembles géologiques (M2 PSL), Semestre recherche Denatura (2A Mines)

2021-2022 (~ 100 heures) -> [Géologie terrain 3AST-VS](#) (Bassin de Paris-Morvan), Géologie terrain 1A Mines (Pyrénées), Grand ensembles géologiques (M2 PSL), Semestre recherche Denatura (2A Mines)

2022-2023 (~ 110 heures) -> [Géologie terrain 3AST-VS](#) (Bassin de Paris-Morvan), [Géologie terrain 1A Mines \(Bassin de Paris\)](#), Grand ensembles géologiques (M2 PSL), Semestre recherche Denatura (2A Mines), Géologie terrain M1 PSL (Castellane-Digne)

4) IMPLICATION DANS DES PROJETS DE RECHERCHE

Depuis mon arrivée à Fontainebleau, j'ai été impliqué dans la rédaction de plusieurs appels d'offre et ai pris la direction de projets scientifiques. Je suis membre de l'équipe FLUMY et participe aux décisions concernant les directions à suivre et la promotion du logiciel auprès de partenaires industriels. Depuis le départ en retraite d'Isabelle Cojan, mes responsabilités dans la partie processus et analogues naturels ont augmentées. J'ai la responsabilité de l'axe « chenaux abandonnés », dans lequel sont impliqués une demi-douzaine de chercheurs au sein du PIREN-Seine depuis 2020. J'ai obtenu en 2018 un financement à l'INSU pour le projet GéoFrac. J'ai surtout rédigé et coordonne le projet Alluv3D (thèse Diana Chourio-Camacho), qui a fait l'objet d'un financement après un montage complexe entre le RGF (BRGM) et l'agence de l'eau Seine-Normandie. Récemment, l'ANDRA a répondu favorablement à un appel d'offre que j'ai rédigé pour l'étude de la dynamique d'érosion de la couverture du site de stockage de la Manche (thèse Aminata Yabre). Enfin, je coordonne actuellement la rédaction d'un ANR JCJC ; il a été accepté en phase 2 en 2022 mais n'a finalement pas été sélectionné. Il a été resoumis à l'appel de 2023.

Nombre de mois/homme	Organisme financeur, montant	Titre du projet	Coordinateur	Début - Fin
3	PIREN-Seine - 45k€	Action chenaux abandonnés	Jean-Louis Grimaud	2020-2023
6	CNRT -33 k€	TransNUM	Michel Cathelineau (Géoressources- Nancy)	2020-2023
3	Mines Paris (ENI) -225 k€ RGF-Bassin de Paris - 112 k€	FLUMY Consortium	Steering comity (Including JLG)	2022-2024
9	Agence de l'Eau Seine Normandie - 39 k€	Alluv3D	Jean-Louis Grimaud	2020-2023
9	CIFRE ANDRA-WSP - 145k€	Couverture CSM	Jean-Louis Grimaud	2022-2025
3	INSU TelluS -6k€	Geofrac	Jean-Louis Grimaud	2018-2019
4	Carnot Mines - 40 k€	SD2S	Jean-Louis Grimaud	2017-2020

5) TACHES ADMINISTRATIVES

Je me suis engagé dans l'association des élèves en géologie, Géocontact, pendant 2 ans à Rennes. A Toulouse, j'ai été représentant des doctorants au conseil de laboratoire. Je participe activement

à la vie du Centre de Recherche en coordonnant des ateliers thématiques lors du séminaire du Centre. J'ai récemment été élu représentant du personnel au Conseil de laboratoire.

Pour le reste, mes tâches administratives sont principalement liées aux enseignements et à la recherche. Ainsi, les tâches de coordination de projets scientifiques, notamment les parties financières, me mobilisent activement. Il en est de même pour la préparation de nombreux camps de terrain qui sont à ma charge, avec la logistique de transport, hébergement et la préparation du matériel. Ces responsabilités impliquent également de nombreuses interactions avec la direction des enseignements.

Annexe 2 : Sélection de publications

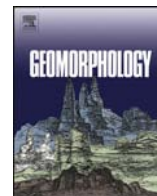
Grimaud, J.-L., Ors, F., [Lemay, M.](#), Cojan, I., & Rivoirard, J. (2022). Preservation and completeness of fluvial meandering deposits influenced by channel motions and overbank sedimentation. *Journal of Geophysical Research: Earth Surface*, 127, e2021JF006435.

Grimaud J-L, Grall C, Goodbred S, et al. (2020), Flexural deformation controls on Late Quaternary sediment dispersal in the Garo-Rajmahal Gap, NW Bengal Basin, *Basin Research*, <https://doi.org/10.1111/bre.12425>

Grimaud, J. L., D. Rouby, D. Chardon, and A. Beauvais (2018), Cenozoic sediment budget of West Africa and the Niger delta, *Basin Research*.

Grimaud, J.-L., C. Paola, and V. Voller (2016), Experimental migration of knickpoints: influence of style of base-level fall and bed lithology, *Earth Surface Dynamics*, 4(1), 11.

Grimaud, J.-L., D. Chardon, V. Metelka, A. Beauvais, and O. Bamba (2015), Neogene cratonic erosion fluxes and landform evolution processes from regional regolith mapping (Burkina Faso, West Africa), *Geomorphology*, 241, 315-330.



Neogene cratonic erosion fluxes and landform evolution processes from regional regolith mapping (Burkina Faso, West Africa)



Jean-Louis Grimaud^{a,b,c,d,*}, Dominique Chardon^{a,b,c}, Václav Metelka^{a,b,c,e}, Anicet Beauvais^f, Ousmane Bamba^g

^a Université de Toulouse, UPS (OMP), GET, 14 avenue Edouard Belin, 31400 Toulouse, France

^b CNRS, GET, 31400 Toulouse, France

^c IRD, UR 234, GET, 31400 Toulouse, France

^d St Anthony Falls Laboratory, University of Minnesota, 2 Third Avenue SE, Minneapolis, MN 55414, USA

^e Center for Exploration Targeting, School of Earth and Environment, The University of Western Australia, (M006) 35 Stirling Highway, Crawley, WA 6009, Australia

^f Aix Marseille Université, IRD, CNRS, CEREGE UM34, BP 80, 13545 Aix en Provence Cedex 4, France

^g Université de Ouagadougou, Laboratoire des géoressources et de l'Environnement, B.P. 7021, Ouagadougou, Burkina Faso

ARTICLE INFO

Article history:

Received 7 November 2014

Received in revised form 1 April 2015

Accepted 6 April 2015

Available online 15 April 2015

Keywords:

Regolith

Pediment

Landform evolution processes

Sediment routing system

Source to sink

ABSTRACT

The regionally correlated and dated regolith–paleolandform sequence of Sub-Saharan West Africa offers a unique opportunity to constrain continental-scale regolith dynamics as the key part of the sediment routing system. In this study, a regolith mapping protocol is developed and applied at the scale of Southwestern Burkina Faso. Mapping combines field survey and remote sensing data to reconstruct the topography of the last pediplain that formed over West Africa in the Early and Mid-Miocene (24–11 Ma). The nature and preservation pattern of the pediplain are controlled by the spatial variation of bedrock lithology and are partitioned among large drainage basins. Quantification of pediplain dissection and drainage growth allows definition of a cratonic background denudation rate of 2 m/My and a minimum characteristic timescale of 20 Ma for shield resurfacing. These results may be used to simulate minimum export fluxes of drainage basins of constrained size over geological timescales. Background cratonic denudation results in a clastic export flux of ~4 t/km²/year, which is limited by low denudation efficiency of slope processes and correlatively high regolith storage capacity of tropical shields. These salient characteristics of shields' surface dynamics would tend to smooth the riverine export fluxes of shields through geological time.

© 2015 Published by Elsevier B.V.

1. Introduction

Interactions between landform evolution and regolith production and mobility over shields exert first-order controls on the source, pathways and fluxes of sediments and solutes over very large emerged surfaces on geological timescales (e.g., Fairbridge and Finkl, 1980; Millot, 1983). Constraining these interactions on continental scales is therefore relevant to quantifying the contribution of shields, as opposed to that of orogens, to global sediment budgets and biogeochemical cycles in the context of long-term Cenozoic climate cooling (Ollier and Pain, 1996a; Molnar, 2004; Willenbring and von Blanckenburg, 2010; Goudie and Viles, 2012; Willenbring et al., 2013; Larsen et al., 2014). Large-scale studies of regolith transfers are also necessary for “source to sink” analyses of coupled drainage areas and sedimentary basins. The present contribution aims to quantify long-term landform evolution, regolith mobility and erosional export fluxes over a large region representative of shields' sediment routing systems.

Tropical shields are mantled by lateritic regoliths derived from intense rock weathering. Such lateritic covers are subject to remobilization by slope and fluvial processes, and the reworked regoliths are commonly re-weathered after transport (Ollier and Pain, 1996b). Renewed periods of regolith production by weathering and remobilization by pedimentation lead to the formation of composite landscapes consisting in a mosaic of lateritic paleo-landsurface remnants of various generations. Such landscapes are spectacularly preserved throughout Sub-Saharan West Africa, a region of more than 4.5 million km² over which a long-recognized Cenozoic regolith–paleo-landsurface sequence has been dated (Beauvais et al., 2008) and correlated (Beauvais and Chardon, 2013).

Here we develop a field- and remote sensing-based regolith–landform mapping protocol applied over Southwestern Burkina Faso (Fig. 1). The investigated area is large (ca. 300 × 300 km) and exposes the most widespread, type geologic and morphoclimatic configuration of the West African surface (granite–greenstone terrains and flat sandstones in the Guinean and Soudanian climatic zones i.e., between 10 and 13°N; Fig. 1). Given the constrained chronological framework of regolith–landform production over the sub-region, the selected area is therefore suitable for the characterization of landscape and regolith

* Corresponding author at: St Anthony Falls Laboratory, University of Minnesota, 2 Third Avenue SE, Minneapolis, MN 55414, USA.

E-mail address: jgrimaud@umn.edu (J.-L. Grimaud).

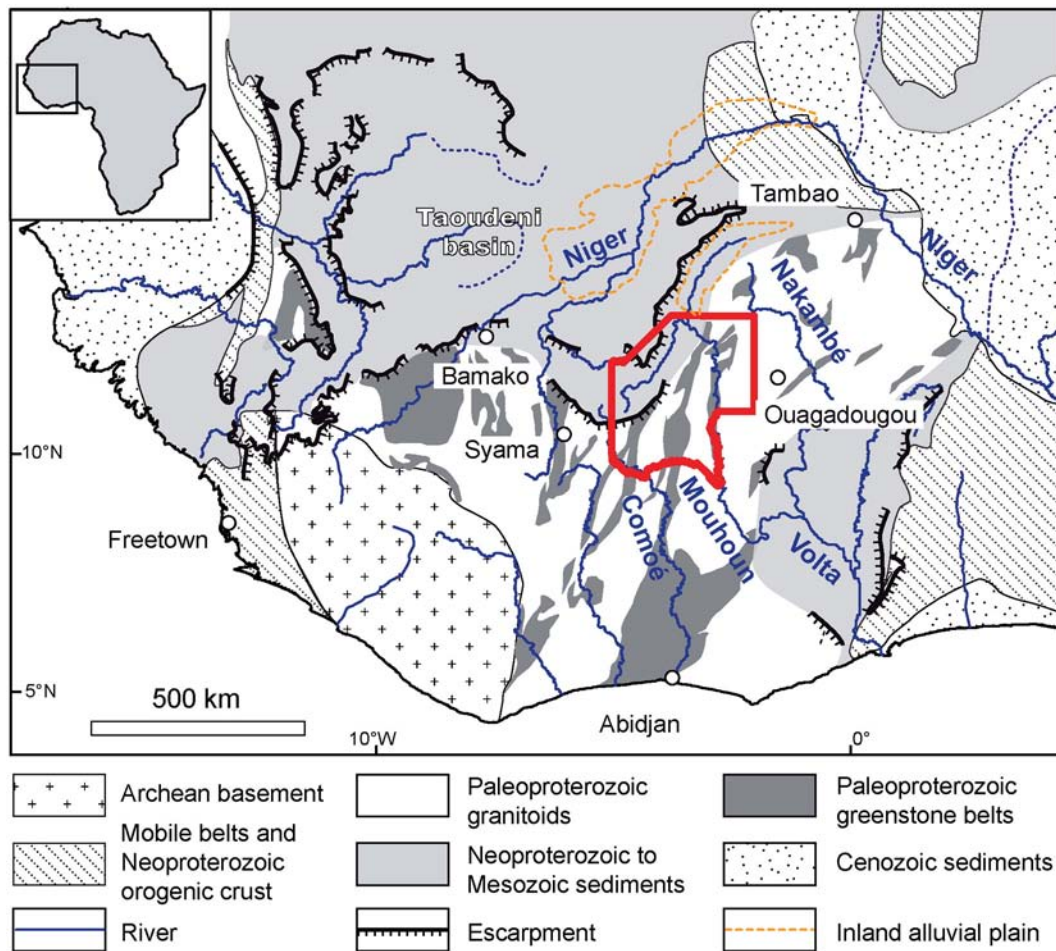


Fig. 1. Simplified geology of sub-Saharan West Africa. The study area is shown by a red frame (map modified from Feybesse et al., 2006). (For interpretation of the references to color in this figure legend, the reader is referred to the web version of this article.)

dynamics and the quantification of long-term (10^6 – 10^7 years) erosion representative of shields surfaces. Regoliths are studied here both as in-situ produced or transported sediments and as paleo-landscape remnants. The obtained regolith–landform map allows evaluation of the nature, distribution and preservation of regolith mantles derived from a pediplain elaborated during the Early and Middle Miocene (ca. 24–11 Ma) over the sub-region. Based on this map, a topographic reconstruction of the pediplain is used to visualize regolith redistribution on slopes during pedimentation and to evaluate landscape and drainage evolution after its abandonment 11 Ma ago. Quantification of post-11 Ma dissection of the pediplain leads to estimate a type-erosion flux for shields, emphasizing the low capacity of slope and alluvial processes to remove and export regolith mantles.

2. Geomorphological and geological background

2.1. The West African geomorphic sequence and its regoliths

The following summary of the West African sequence of stepped lateritic paleo-landsurfaces (Fig. 2a) is based mostly on the works of Michel (1959, 1973, 1974), Eschenbrenner and Grandin (1970), Boulangé et al. (1973), Grandin (1976), and Boulangé and Millot (1988) (see Chardon et al., 2006; Beauvais and Chardon, 2013).

Each member in the sequence has a distinct regolith cover and geomorphic character. The first two members of the sequence are the bauxitic and so-called Intermediate surfaces, which bear thick in-situ formed regoliths capped by bauxites and ferricretes, respectively. Bauxites are the end-product of a period of enhanced chemical

weathering that started in the Late Cretaceous and culminated in the Mid-Eocene. Bauxites seal a topography called the African Surface, which makes the present-day envelope of the West African relief. The Intermediate surface corresponds to a differentiated landscape carved in the African bauxitic surface. The following three stepped paleo-landsurfaces of the sequence are glacis (French term for pediments) called the High, Middle and Low glacis. Glacis surfaces are commonly covered by a detrital layer issued from degradation of earlier landforms. Each glacis has undergone weathering after pedimentation, indicating repeated transitions from arid or semi-arid pedimentation to seasonally contrasted or wet tropical weathering. Weathering periods generally ended with the formation of a ferricrete cementing the glacis surfaces and their detrital cover. Today, glacis occupy an overwhelming part of the West African landsurface (Beauvais and Chardon, 2013; Grimaud, 2014). The sequence is best preserved in the Sahelian and Soudanian climatic zones. The glacis, having undergone relief inversion, show evidence of degradation further south under the humid climate of the forest zone (Grandin, 1976). Though originally defined in the French-speaking countries, the sequence or elements of the sequence have been formally or implicitly identified and mapped in other countries of the sub-region (e.g., Fölster, 1969; Grandin and Hayward, 1975; Bowden, 1987; Durotoye, 1989; Thomas, 1980, 1994; Teeuw, 2002; see Beauvais and Chardon, 2013; Grimaud, 2014).

The Lower to Mid-Eocene age of peak weathering and abandonment of the bauxitic surface had long been stratigraphically bracketed (e.g., Millot, 1970). In absence of any stratigraphic constraints or radiometric data, the three glacis were thought to reflect Quaternary glacial–interglacial climatic cycles having led to the dissection of the

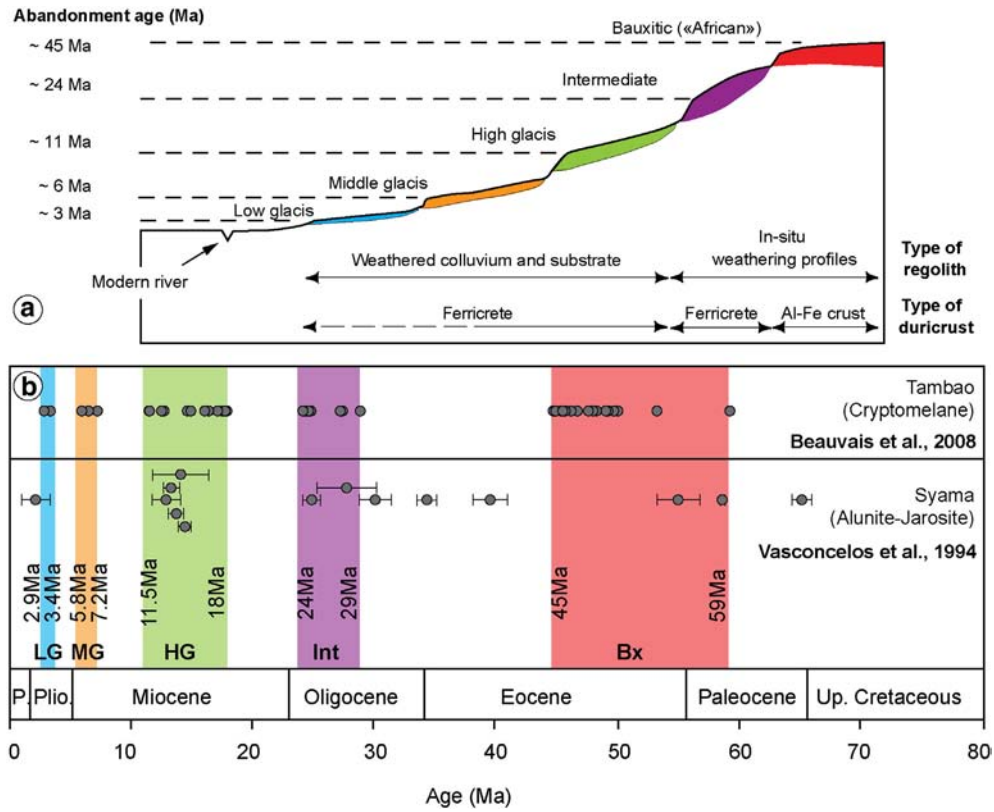


Fig. 2. (a) Lateritic paleo-landscape sequence and incision chronology of West Africa (compiled after Michel, 1973; Beauvais et al., 2008; Beauvais and Chardon, 2013 and modified after Grimaud et al., 2014). (b) Synthesis of Ar–Ar age data obtained on supergene Mn oxides. Colored time slices represent the main periods of weathering correlated with the successive paleo-landsurfaces, based on dating of cryptomelane in Tambao (after Beauvais et al., 2008; Beauvais and Chardon, 2013). Ages reported from Syama were obtained on alunite and jarosite (after Vasconcelos et al., 1994). Note that only alunite and jarosite ages with error of less than 5 Ma are reported. Terminology of the paleo-landsurfaces: Bx – Bauxite; Int – Intermediate; HG – High glaciais; MG – Middle glaciais; and LG – Low glaciais. Syama and Tambao are located in Fig. 1. (For interpretation of the references to color in this figure legend, the reader is referred to the web version of this article.)

Intermediate landscape of supposedly Latest Pliocene age (Michel, 1959). Absolute age constraints on the paleo-landscape sequence were provided by radiometric ^{40}Ar – ^{39}Ar dating of supergene cryptomelane ($\text{K}_1 - 2(\text{Mn}^{3+} + \text{Mn}^{4+})_8\text{O}_{16} \cdot n\text{H}_2\text{O}$) around Tambao in Northeastern Burkina Faso (Hénoque et al., 1998; Colin et al., 2005; Beauvais et al., 2008; summarized in Beauvais and Chardon, 2013; Fig. 1). Data retrieved from the weathering profiles of each surface relict define five Ar–Ar age groups (ca. 59–45, 29–24, 18–11, 7–6, and 3 Ma; Fig. 2b) bracketing periods of chemical weathering of the paleosurfaces. The lower limit of these age groups corresponds to the abandonment age of each paleosurface, i.e., the stabilization of the weathering front by the end of the weathering period preceding duricrusting and subsequent incision of each paleosurface (Fig. 2b). Abandonment ages are ca. 45 Ma for the African bauxitic surface and 24 Ma for the Intermediate surface. The High glaciais surface developed between ca. 24 and 11 Ma with a predominance of weathering between 18 and 11 Ma. In Syama (Southern Mali; Fig. 1), Ar–Ar ages on supergene alunite and jarosite (Vasconcelos et al., 1994) confirm predominance of weathering conditions during elaboration of the Intermediate surface until the end of the Oligocene and weathering of the High glaciais during the Mid-Miocene (Fig. 2b). Weathering and later abandonment of the Middle and Low glaciais have occurred around 7–6 and 3 Ma, respectively (Fig. 2).

2.2. Geological context

The study area belongs to the Paleoproterozoic portion of the West African craton exposed south of the Sahara (e.g., Feybesse et al., 2006; Fig. 1). This area comprises Birimian (2.2–2.1 Ga) granite–greenstone terrains over two-thirds of its surface and the Neoproterozoic

sandstones of the Taoudeni basin, which were intruded by dolerite sills (Fig. 3). The basement comprises the Banfora, Houndé and Boromo greenstone belts and intervening granitoids (Baratoux et al., 2011; Metelka et al., 2011; Fig. 3b). Greenstones consist mainly of mafic volcanics (basalts and andesites) and volcanosediments, whereas granitoids comprise TTG (tonalite–trondhjemite–granodiorite) and granitic plutons. The escarpment delimiting the Banfora plateau marks the southeastern boundary of the Taoudeni basin (Fig. 3a). The southern part of the plateau bears the highest summits of the region and the height of the escarpment decreases towards the NE. The study area mostly belongs to the Mouhoun drainage system (the main stream of the Volta drainage system, i.e., the Black Volta) and is fringed by the catchments of the Upper Niger River to the west, the Comoé River to the southwest and the Nazinon River to the east (part of the Nakambé drainage system i.e., the White Volta; Figs. 1 and 3).

2.3. Earlier works on the study area

The pioneering study of Daveau et al. (1962) around Houndé and Gaoua (Fig. 3) led to the identification of stepped lateritic landscapes and to the description of what will be recognized later as the High glaciais. Later on, the southern part of the study area and its extension in the Ivory Coast became one of the first regions where the entire West African regolith–landform sequence was thoroughly documented (Eschenbrenner and Grandin, 1970). Boeglin and Mazaltarim (1989) and Boeglin (1990) later focused on an area of ca. 50×30 km around Gaoua (Fig. 3), where they mapped the High glaciais relicts and performed a detailed geochemical study of their ferricretes. More recently, Bamba (1996) and Bamba et al. (2002) have refined detailed mapping of the three glaciais around the Poura mine (left bank of the Mouhoun

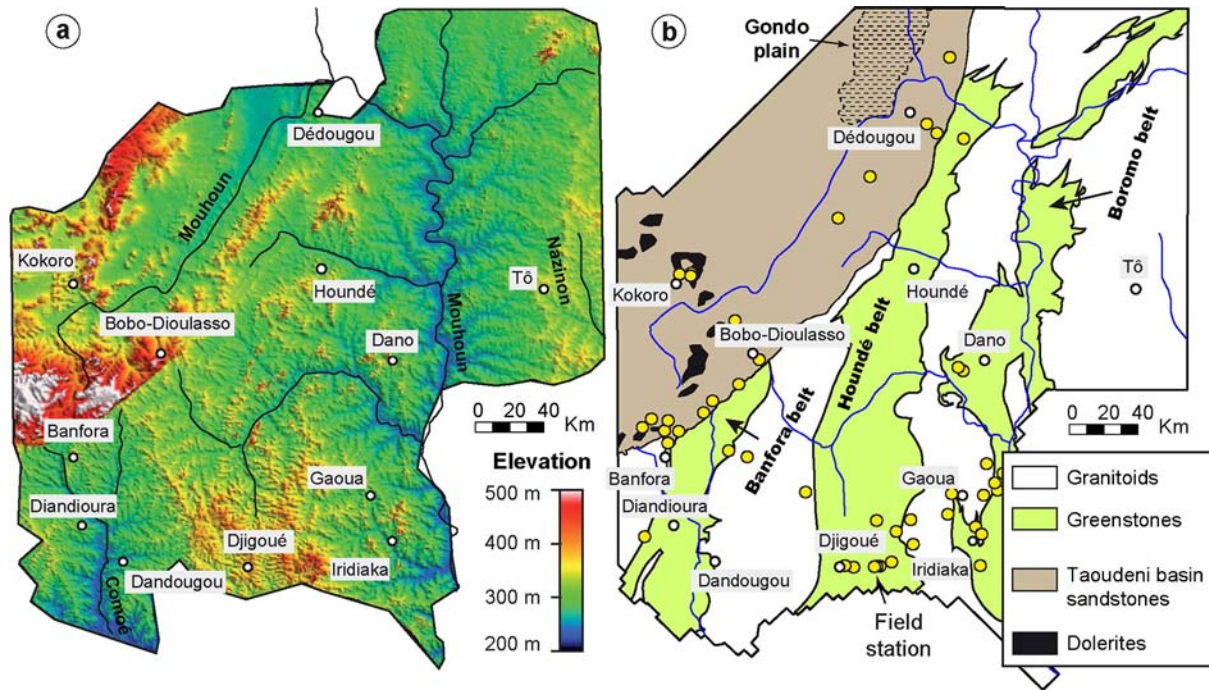


Fig. 3. Topography and simplified geology of the study area (see Fig. 1 for location). Shaded topography (a) based on SRTM digital elevation model smoothed to 500 m resolution. Simplified geology (b) is adapted from Baratoux et al. (2011). Field stations are shown by yellow dots. (For interpretation of the references to color in this figure legend, the reader is referred to the web version of this article.)

River, West of Tô; Fig. 3) to study surface remobilization of gold. Lately, Butt and Bristow (2013), reporting on gold prospects of the area, argued for the stepped character of the glacia and the detrital nature of their ferricretes, which had been documented by geomorphologists since the late 1950's (e.g., Michel, 1959; Daveau et al., 1962) but largely ignored since then.

3. Field relationships and regional-scale regolith–landform mapping

3.1. Rationale

As opposed to the other regolith–landform associations of the lateritic paleo-landscapes sequence, High glacia remnants have both distinctive field and remotely-sensed mappable properties at the resolution of the digital data and given the size of the map area (see below). Our work therefore focused on the High glacia regolith–landform associations, which were characterized and mapped for evaluation of the pedimentation and weathering processes controlling the development of the High glacia paleo-landsurface. The topography of this paleo-landsurface was then reconstructed as a datum for the quantification of regional erosion after its abandonment. Higher paleo-landsurface relicts of the sequence (i.e., bauxitic and Intermediate) were already inherited landforms incorporated to the High glacia landscape and are still preserved in the current landscape. As seen below, their duricrusts are also found as reworked elements in the High glacia regoliths. Field characteristics of the higher landsurfaces are therefore described and their occurrences reported in the regolith–landform map. Relicts of the Middle and Low glacia (i.e., lower landsurfaces) occupy lower parts of today's landscape that have been excavated in the High glacia surface. Their field characteristics are briefly described below.

3.2. Field typology of landforms and associated regoliths

3.2.1. Field survey

Our field observations were carried out at stations (Fig. 3b), which consist of areas of several km², where landscape analysis was

undertaken by interpreting sceneries using 1/50 000 and 1/200 000 scale topographic maps. Mapping of regolith–landform units was undertaken at key stations. Landscape interpretations/chronologies and identification of paleo-landsurface relicts were complemented by in-situ examination of the regolith along tracks through the landscape and at road cuts. This work included the identification of the textures of the exposed lateritic weathering profile horizons and the description of the sedimentary facies of the transported regoliths.

3.2.2. Higher landsurfaces

Bauxite relicts form mesas on the highest summits. On the basement, those mesas are restricted to mafic substrates and their size is generally limited (i.e., less than 100 m wide) (Fig. 4a). In the Taoudeni basin, bauxitic plateaus are larger and mostly restricted to dolerites (Fig. 4b, c). The bauxites have typical pink-whitish pisolithic textures (Fig. 4d) or less evolved, nodular-mottled textures (Fig. 4e). In the Taoudeni basin, particularly on dolerites, the Intermediate ferricrete caps gently dipping convex–concave surfaces forming the downslope extension of the bauxitic plateaus (Fig. 4b, c). These ferricretes (Fig. 4f, g) show gradational variation in composition and texture with the bauxites. This is interpreted to result from iron leaching that leads to relative aluminum enrichment of the bauxites and net concomitant iron accumulation in the ferricretes (Boulangé, 1986). Intermediate ferricretes on sandstones display typical nodular textures (Fig. 4g). On the basement, the Intermediate ferricrete is rarely found in-situ but rather as pebbles or cobbles reworked in the High glacia ferricrete (see below). Instead, a residual “Intermediate relief” surrounds bauxitic duricrusts (Fig. 4a) and may be locally paved with a cemented scribe of bauxite cobbles. Bauxites are underlain by weathering profiles that are at least 80 m thick, as estimated on the stripped slopes of mesas, whereas Intermediate weathering profiles exceed 20 m in thickness.

3.2.3. High glacia

The best visible High glacia relicts are kilometer-scale plateaus (the largest ones being concave) shallowly dipping away from the topographic massifs made of mafic volcanics, which may carry higher relict paleo-landscapes (Fig. 5a). Such High glacia relicts are often separated

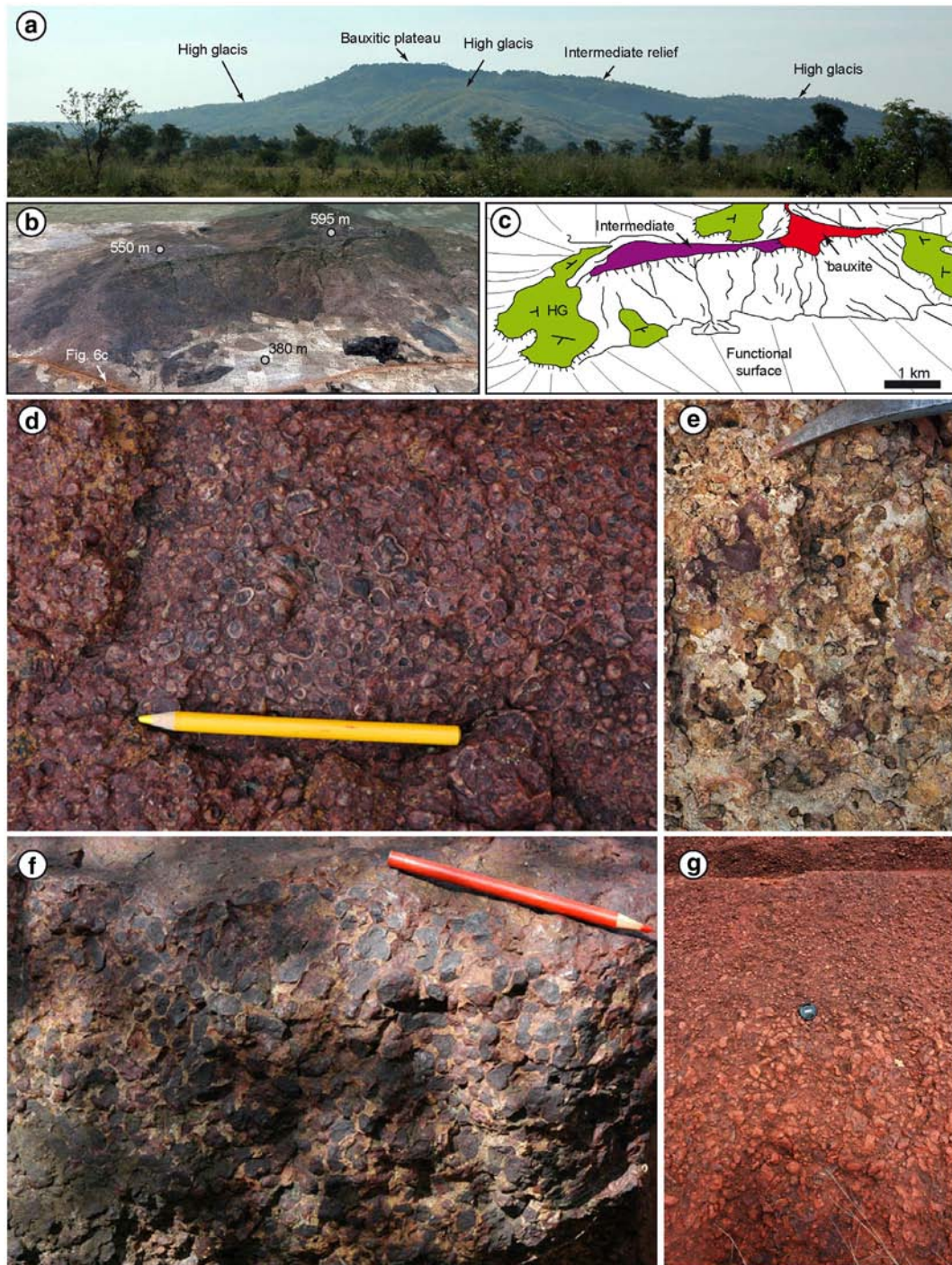


Fig. 4. Illustrations of field characteristics of the higher lateritic paleo-landsurfaces in Southwestern Burkina Faso. (a) Bauxite-capped greenstone massif, 15 km SE of Iridiaka (location in Fig. 3; see also Fig. 9b). The bauxitic plateau is ca. 300 m long. (b)–(c) South-looking Google Earth view and interpretation of a dolerite topographic massif near Kokoro, Taoudeni basin (location in Fig. 3; Vertical exaggeration $\times 3$). HG – High glaxis. (d) Close-packed pisolitic texture of the Iridiaka bauxite shown in (a). (e) Nodular-mottled texture of the Kokoro bauxite shown in (b) and (c). (f) Massive nodular facies of the Intermediate ferricrete shown in (b)–(c). (g) Iron nodulation at the root of the Intermediate ferricrete over sandstones, Taoudeni basin north of Banfora (location in Fig. 3).

from the massifs by a peripheral hollow due to incision of their upslope parts (see also Beauvais et al., 1999). This configuration indicates that the High glaxis has occupied large piedmonts that have been dissected. Dissection of the High glaxis ferricrete has carved 1 to 20 m-high scarps dominating slopes cut into soft regoliths and covered by ferricrete debris (Figs. 5 and 6a, b).

Most High glaxis plateau ferricretes consist of a conglomerate ranging from gravel to cobble, with a predominance of gravels mostly

made of ferruginous nodules (Fig. 6). Matrix silts and sands may bear quartz, particularly on volcano-sediments and granitoids. Coarse gravels and cobbles are made of Intermediate-type ferricretes, vein quartz and bauxites (Fig. 6a–e). Conglomerates are commonly matrix- or block-supported, suggesting emplacement by mudflow or debris flow process. Channels are observed at the base of the ferricrete and decimeter- to meter-scale oblique stratifications are recognized in the downslope parts of some large High glaxis relicts (Fig. 6d). The

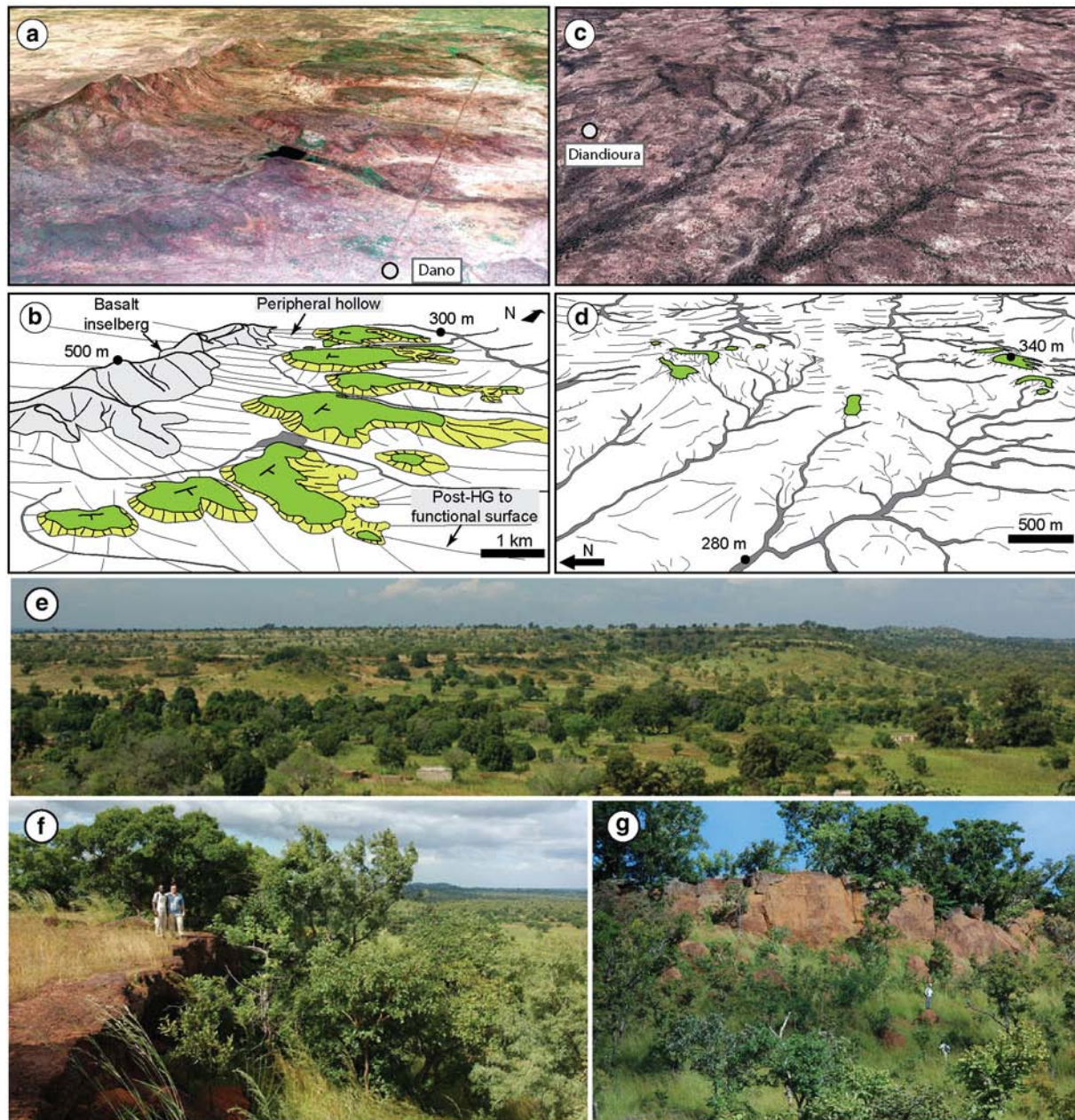


Fig. 5. Illustrations of the High glacial relict landforms. (a)–(b) Google Earth view and interpretation of the eastern piedmont of a volcanic inselberg near Dano (Fig. 3). (c)–(d) Google Earth view and interpretation of parse High glacial relict hills resulting from dissection by a dendritic river network on granitic substrate, Dandougou area (Fig. 3). High glacial relicts are shown in green. Dip symbols indicate High glacial paleolandsurface direction and sense of slope. (e) Gently west-dipping plateau bounded by a 10–15 m high scarp (5 km West of Gaoua, view looking SW). (f) Closer view of the plateau edge shown in (e). (g) Scarp carved in > 10 m thick ferricrete cementing glacial cover material (in between Djigoué and Gaoua). (For interpretation of the references to color in this figure legend, the reader is referred to the web version of this article.)

coexistence of mud or debris flow and alluvial facies in the High glacial cover is indicative of interplay of slope and fluvial processes during pedimentation (Dohrenwend and Parsons, 2009).

The noticeable absence of a mottled horizon under the glacial conglomerate or exposure of deep portions of weathering profiles right under that cover (Fig. 6a–c) indicates that these weathering profiles have been truncated before deposition of the conglomerate. Duricrusting (i.e., iron impregnation or cementation) is mostly restricted to the conglomerate cover (Fig. 6a, b). Still, soft ferricretes, i.e., pedogenic impregnations of mottled clay lateritic horizons (Tardy, 1997), are common under the cemented conglomerate. This suggests renewed weathering along the upper fringe of the truncated lateritic profiles under the conglomerates. At certain locations, the ferricrete made of cemented debris flows may even be underlain by a type-

succession of weathering profile horizons (i.e., soft ferricrete, mottled layer, fine saprolite, coarse saprolite; Fig. 6e, f), suggesting the full development of a weathering profile after pedimentation.

On granitoids located away from topographic massifs (e.g., west of Djigoué and south of Bobo Dioulasso, Tô region), the High glacial ferricretes are generally thinner (0.5–2 m) and mantle smooth interfluvial (Fig. 5c, d). Such ferricretes have vermicular and nodular textures and are devoid of clasts. They appear less ferruginous and less indurated than their plateau counterparts. These ferricretes show gradational contacts with underlying soft ferricretes and are part of in-situ weathering profiles.

3.2.4. Lower landsurfaces

The restricted size of higher paleo-landsurfaces remnants is primarily due to the development of the High glacial. But rejuvenation of the

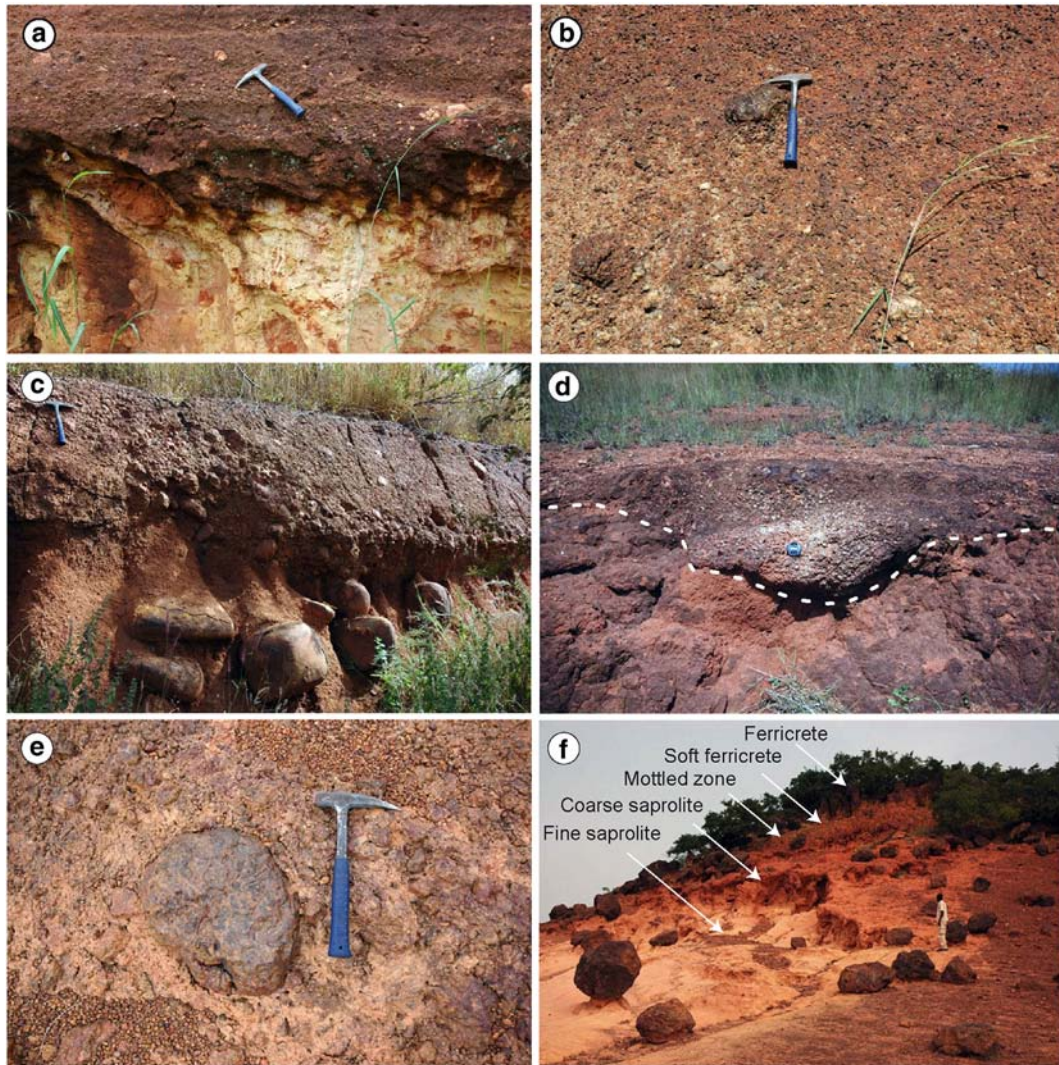


Fig. 6. Illustrations of High glacia regoliths. (a) Base of a High glacia ferricrete truncating a granitic weathering profile (Djigoué area). Light-colored cobbles in the ferricrete are quartz clasts. (b) Details of a High glacia ferricrete showing cobbles of Intermediate ferricrete and quartz in a finer grained conglomerate, base of the cliff shown in Fig. 5g. (c) Cemented debris flow on dolerites near Kokoro (site of Fig. 4b, c). Light-colored debris consists of bauxite clasts. The flow rests upon a truncated weathering profile developed from dolerites that remain as core stones in the saprolite. (d) Alluvial channel at the base of High glacia ferricrete carved into weathered sandstones of the Taoudeni basin (South of Bobo-Dioulasso). (e) Cobble of Intermediate ferricrete cemented in a High glacia ferricrete. (f) Weathering profile underlying that same ferricrete (northeast of Dédougou). See Fig. 3 for locations. (For interpretation of the references to color in this figure legend, the reader is referred to the web version of this article.)

slopes of the residual reliefs carrying those remnants and the formation of peripheral hollows (Fig. 5) is attributed to the following periods of glacia formation. The landsurface between High glacia relicts and the modern alluvia is almost exclusively occupied by the Middle and Low glacia. These glacia may be stepped or may combine to form a single polygenic landsurface. The regolith of the Middle and Low glacia is comparable to that of the High glacia, but their ferricrete is generally thinner to absent and may be covered over large areas by loose material made of reworked saprolite, sand and ferruginous gravels.

3.3. Regional-scale regolith–landform mapping protocol

On basement terrains, High glacia units were manually mapped in GIS on the basis of their airborne gamma ray spectrometry and their photo-interpretation signature (Google Earth), both validated by the field survey/maps (Figs. 3 and 7). Airborne gamma ray spectrometry was acquired during the 1998–1999 SYSMIN (System for Mineral Products) project (Metelka et al., 2011). Those data display uranium (U), potassium (K) and thorium (Th) contents of the upper 30 cm of the Earth surface (Dickson and Scott, 1997). The spatial resolution of the data on the basement is 125 m (with an original line spacing of

500 m). Spatial resolution of 250 m (line spacing of 1000 m) over the Taoudeni basin has required resampling to 125 m in the area to obtain a harmonized image. Both the raw and enhanced (Th/K ratio) gamma ray spectrometry data were used (Fig. 7) during the analysis and combined with the shaded relief maps of the SRTM (Shuttle Radar Topographic Mission) data (90 m spatial resolution). The High glacia ferricretes have a distinctive photo-interpretation texture that spatially matches blue–green colors in raw gamma ray data. This attests of a strong depletion in potassium, and a relative enrichment in thorium and uranium as a result of weathering processes (Dickson and Scott, 1997; Wilford et al., 1997; Metelka et al., 2011). However, uranium has a complex behavior during weathering and regolith formation (Dickson and Scott, 1997; Wilford et al., 1997; Dequincey et al., 2002). Therefore, the Th/K ratio was preferred to further enhance the signature of the High glacia ferricretes (in yellow–red) and remove any regional gradients in the data (Fig. 7b–d).

The spatially homogeneous radiometric signature of the High glacia relicts suggests that their ferricretes have been geochemically homogenized by weathering despite the variability of their substrate. Indeed, trace element concentrations systematically converge as a function of the Fe_2O_3 content of the ferricrete taken as an index of

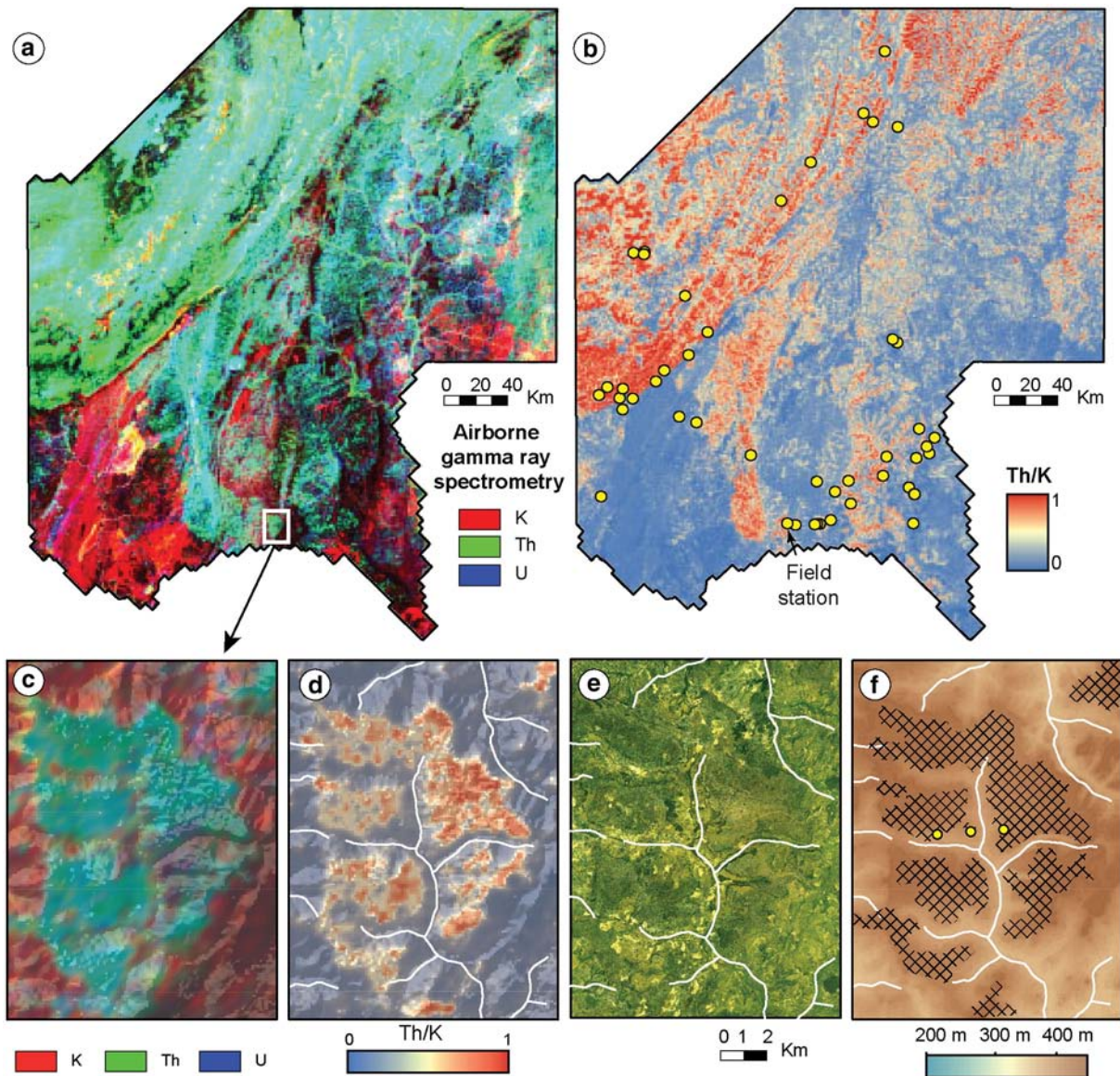


Fig. 7. Ternary image of the airborne gamma ray spectrometry survey (a) and the enhanced Th/K ratio image of the survey (b) over the study area. (c)–(f) Details of the datasets that were combined for the identification and mapping of High glacia relicts on the example of the Djigoué area. (c) Airborne gamma ray spectrometry 100–250 m (resampled to 100 m) resolution ternary image. The area corresponding to the High glacia ferricrete has a strong thorium signature in green and a medium uranium signature in blue. In this area, the substrate has a strong potassium signature in red. (d) Ratio image of thorium over potassium (100 m resampled resolution). The High glacia ferricrete, enriched in thorium and depleted in potassium, is highlighted in white to red colors. (e) 15-m resolution LANDSAT image. (f) Mapping by construction of the polygons (crossed frame) corresponding to the High glacia ferricrete, superimposed on the SRTM topography. Field stations are shown as yellow dots. Rivers are shown in white. (For interpretation of the references to color in this figure legend, the reader is referred to the web version of this article).

their geochemical maturity (Boeglin and Mazaltarim, 1989; Boeglin, 1990). Conversely, the ambiguous radiometric signature of the Middle and Low glacia may be interpreted as a lower maturity of their ferricrete and a mixed signature of the material covering their ferricrete.

The strong Th and exceptionally low K signatures of the Taoudeni basin (Fig. 7a, b) are explained by the mineralogy of the sandstones that are originally quartz rich and correlatively poor in clays. The larger pixel size (250 m) of the gamma ray spectrometry may have further modified the Th signature of High glacia ferricretes by sampling other surface material with high Th content (e.g., Bauxite and Intermediate duricrusts). Therefore, the high values (red colors) of Th/K ratio image (Fig. 7b) may not only be due to High glacia ferricretes. Hence, regolith–landform mapping over the Taoudeni basin was mainly based on photo-interpretation in Google Earth and field observations.

Bauxite and Intermediate surface relict occurrences were mapped by photo-interpretation, field observations and after Petit (1994). River plain sediments were mapped mainly on the basis of their negligible relief and the characteristic geometries of stream networks in the gamma-ray imagery. Because of the higher mobility of U compared to Th, river plain sediments raw gamma-ray signature may indeed vary, i.e. color of the source material (variable content of radioelements), very light to white color (high U/Th/K signal), or very dark color (low U/Th/K signal). It might reflect the composition of the source material, sediment mixing, or strong attenuation by vegetation or water (Fig. 7a).

3.4. Interpretation of the High glacia regolith–landform map

For the purpose of the interpretation, the mapped regolith–landform units were superimposed on the topography in Fig. 8 and on the

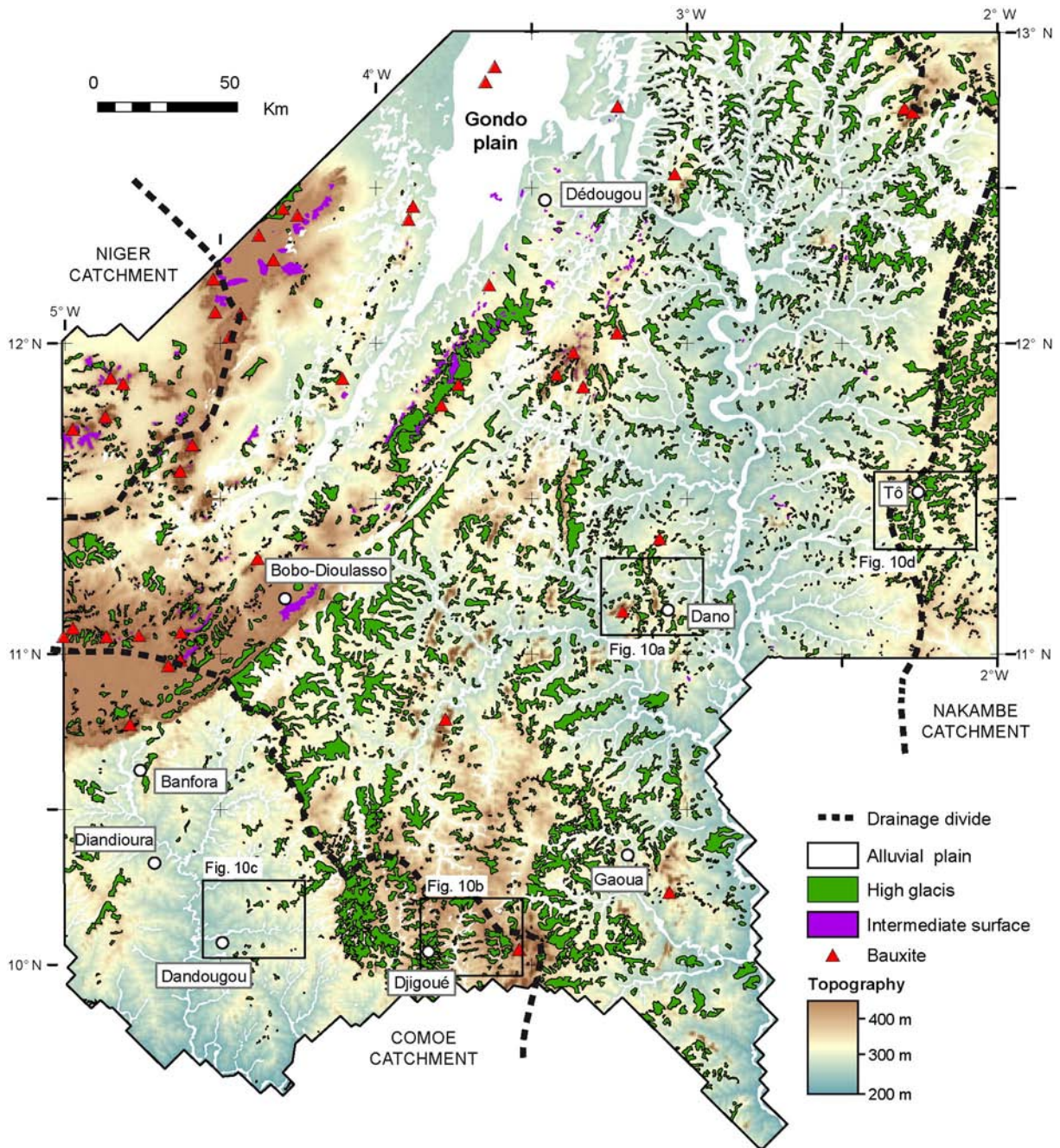


Fig. 8. Regolith–landform map superimposed on the STRM digital elevation model (90 m resolution). Black boxes correspond to the frame of the maps shown in Fig. 10.

geological map from Metelka et al. (2011) in Fig. 9. Comparison of these two maps highlights major contrasts in the pattern of High glacia relicts' distribution on either side of the main watersheds, even on the same geological substrate. This is particularly exemplified on TTG across the southwestern and eastern Mouhoun watersheds (Figs. 8 and 9a). Density of High glacia relicts generally decreases when approaching the main streams (Fig. 8). Relicts are best preserved on TTG and granite (45 and 20% of the total surface of the relicts, respectively). Greenstones underlay less than 25% of the total area of the preserved High glacia ferricrete (Figs. 3b and 9c). Fifteen percent of the map area of the TTG and more than 20% of the granitoids are covered by High glacia ferricretes, whereas only 10% of the greenstones are covered (Fig. 9d).

Type-patterns of High glacia regolith–landforms may be distinguished in the study area (Figs. 5, 9 and 10). In high relief volcanic

terrains, High glacia relicts are well preserved on piedmonts (Fig. 10a), equally on greenstones and granitoids. Volcano–sedimentary–granitic terrains of moderate relief (e.g., Djigoué area) display High glacia relicts that once coated wide N–S trending valleys, which were in turn dissected by second-order narrower E–W oriented valleys (Fig. 10b). Over TTG terrains of the Comoé catchment (e.g., Dandougou–Bobodioulasso area), a very low relief and very low slope High glacia surface is preserved on sparse residual hills where the ferricrete may be dismembered into boulders resting on the soft ferricrete (Fig. 10c). The resulting landscape is a convex–concave plain of low amplitude that is gently dipping towards the main stream (Fig. 10c). Equivalent TTG terrains in the Nakambe catchment reveal a better-preserved High glacia paleo-landsurface (see above), with planar to weakly concave relicts delineating a plain of very low-relief surface envelope (Fig. 10d).

The occurrence of strong and thick plateau ferricretes upon granitoids on the piedmonts of volcanic reliefs contrasts with the weak and thin ferricretes preserved on the same granitoids of the low land (Fig. 5a–d). This reflects the high iron content and thickness of the piedmont conglomerates made of reworked bauxitic and Intermediate duricrusts that formed on iron-rich mafic rocks. On the contrary, low land ferricretes are solely issued from in-situ weathering of iron-poor granitoids. The limited lateritic cover of mafic volcanic massifs further argues for the transfer of upland iron-rich duricrusts as colluviums to the High glaciais piedmonts. This transfer has resulted in net iron accumulation on glaciais surfaces

further down in the landscape (Michel, 1973, 1974; Beauvais et al., 1999).

The above analysis indicates that the High glaciais landsurface was a pediplain, defined as a surface of coalescent pediments (Maxson and Anderson, 1935). The spatial distribution of these pediments and their regolith as well as the preservation pattern of the High glaciais pediplain is spatially controlled at various scales. A first, local control of this distribution is exerted by the lithology of the bedrock. This sets the relief and therefore the pedimentation process, as well as the weathering mode of the pediplain. On a regional scale, pediplain dissection and erosion mode appear to have been compartmentalized among drainage basins.

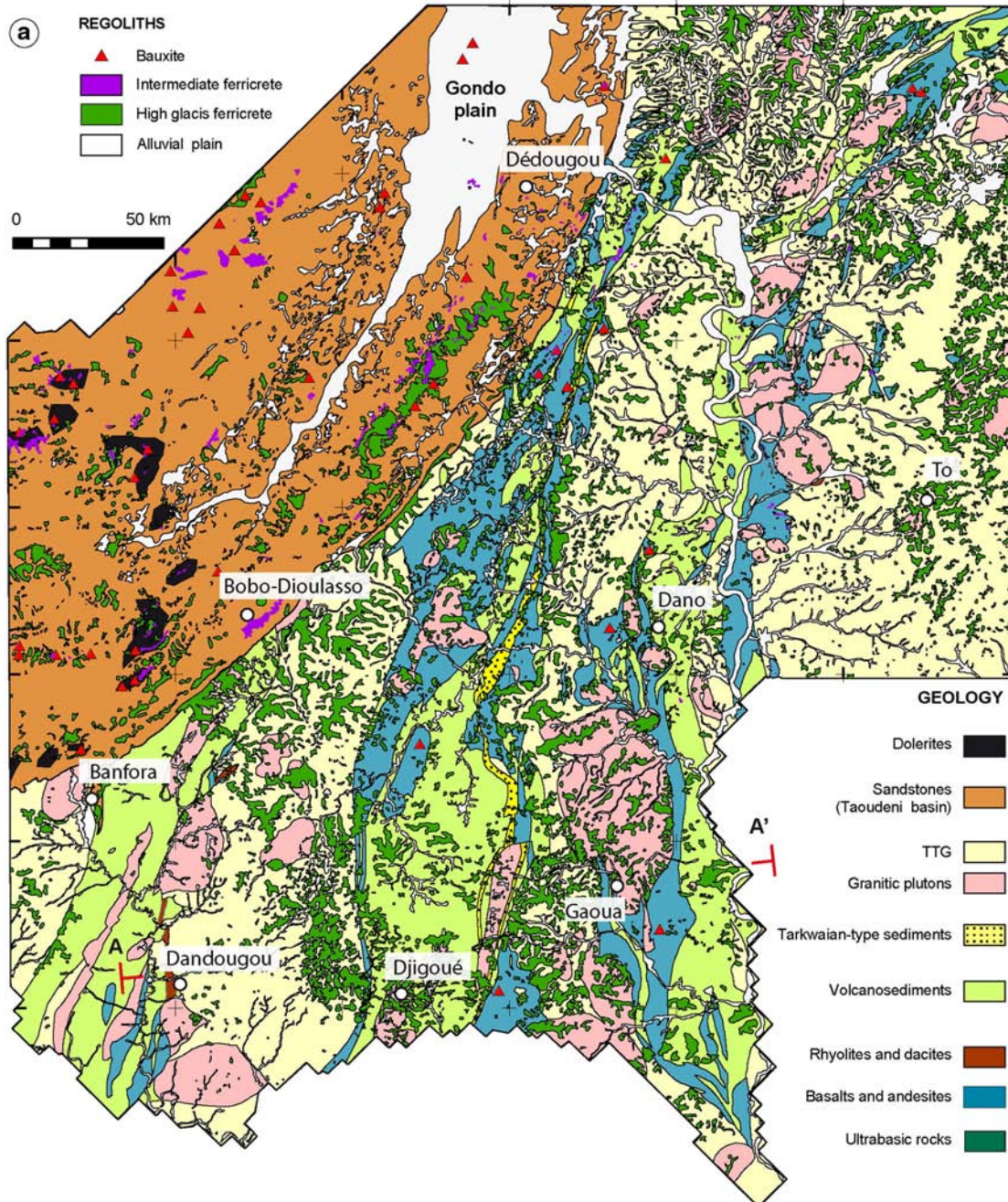


Fig. 9. (a) Regolith–landform map superimposed on the geology that is simplified from Metelka et al. (2011). (b) Synthetic regional cross-section of the study area. The line of section is located in (a). Trace of the HG surface is shown in dark green (dashed where eroded). (c) Histogram of the High glaciais ferricrete total area partitioned on each substrate. (d) Proportion of the High glaciais surface on each lithology covered by ferricrete. For the whole Birimian basement, this percentage is of about 11%. Dolerites and sandstones were not distinguished in the Taoudeni basin. (For interpretation of the references to color in this figure legend, the reader is referred to the web version of this article.)

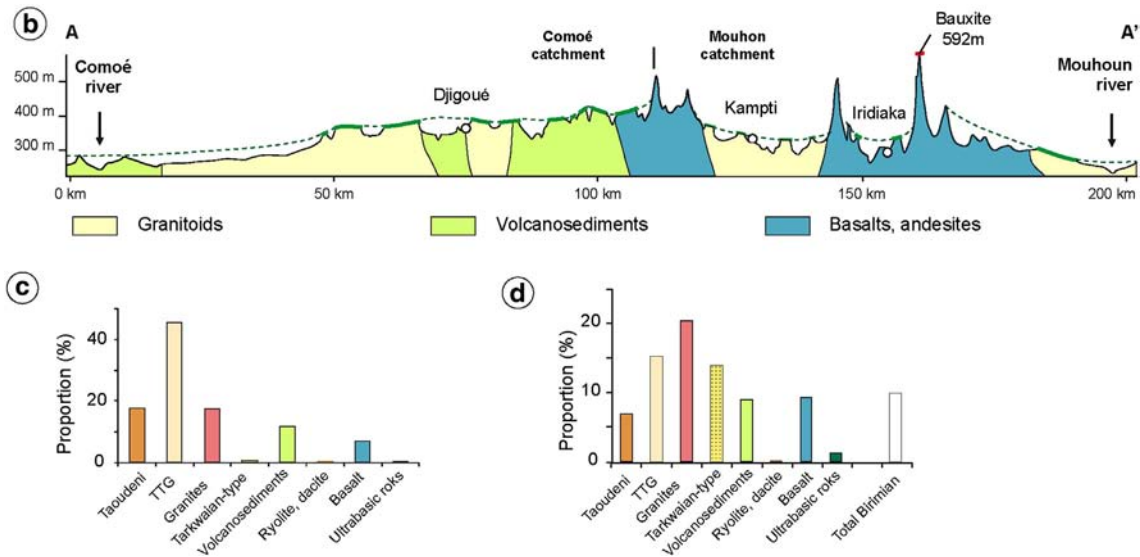


Fig. 9 (continued).

4. Reconstruction of the Late Mid-Miocene pediplain and quantification of its erosion

4.1. Methodology

The high density of High glaciais relicts warrants reconstruction of the pediplain they were part of. The reconstructed topography is a triangulated surface interpolated from a set of geo-referenced points generated from the polygons of the High glaciais relicts using the DSI method (Gocad software; Mallet, 1992). Each High glaciais polygon was converted to a grid of 500 m-spaced points inside its limits. The elevation of the SRTM digital elevation model, degraded to 500 m resolution, was then sampled for each point to form the High glaciais relicts' elevation dataset. The interpolated surface was created from this dataset through a series of iterations. The number of surface's triangles, which reflected the distribution of the dataset for the first incremental surface, was increased at each iteration step, while the High glaciais surface was forced to remain above the modern topography. This allowed for the inclusion of the reliefs dominating the pediplain and preserved the composite nature of the High glaciais landscape. The resulting topography is shown in Fig. 11. Erosion post-dating the abandonment of the pediplain was obtained by subtracting the modern topography from that of the reconstructed pediplain (Fig. 11a–c). The drainage network and a slope map were then automatically extracted from both the modern and pediplain digital elevation models for comparison (Fig. 11d–h).

4.2. Late Mid-Miocene topography and landscape dynamics

The pediplain displays the same first-order relief pattern as the current topography. The main divides such as the inselbergs and the main escarpment already existed at the time the pediplain was functional and did not migrate since then (Fig. 11a–b). The main river network was therefore already established since the Late Mid-Miocene with the exception of a few local river rearrangements (Fig. 11d–h). Our reconstruction does not allow for testing whether the Upper Mouhoun (flowing on the Taoudeni basin) was connected to the lower Mouhoun at the time of the High glaciais (Fig. 11h). This rearrangement (Hubert, 1912; Palausi, 1959) occurred after the upper Mouhoun River, which used to flow northeastward into the Niger River since the Eocene, formed the Gondo Plain internal delta (Beauvais and Chardon, 2013; Grimaud et al., 2014; Fig. 1).

The spatial variability of the pediplain relief on the basement is representative of the type-landscapes shown in Fig. 10 (comparisons with Figs. 9a and 12). One distinguishes (i) an inselberg-studded pediplain around volcanic terrains, (ii) almost flat lands over TTG, and (iii) a mix of the first two landscape types over volcanosediments and associated granite plutons. In the Taoudeni basin, the pediplain consists of wide and shallowly dipping piedmonts connecting sandstone or higher landsurface plateaus to the main streams.

4.3. Interpretation of the pediplain dissection pattern

The pediplain has a low drainage density compared to that of the modern landscape, with typical pediment widths of 10–20 km (up to 30 km over the sandstones; Figs. 11 and 12). Dissection of the High glaciais landscape accompanied an increase in the drainage density. The modern valley sides rarely exceed 5 km in width (Figs. 3 and 8). Dissection of the pediplain also resulted in an increase in slopes (Fig. 11g), which is in agreement with the evolution from a pediplain towards narrower/deeper valleys. In other words, the Middle and Low glaciais, which contributed to the dissection of the pediplain, never attained the width of the High glaciais.

Post-11 Ma dissection of the pediplain is non-uniformly distributed, with denudation depths ranging from 0 to 100 m and corresponding denudation from 0 to 10 m/My (Fig. 11c). Extreme denudations (>60 m, >5 m/My) over basement terrains are concentrated on the steep slopes of residual reliefs (Figs. 6, 10 and 11). Along the two main streams, denudation is moderate to high (30–60 m; 2.5–5 m/My). The denudation is rather uniformly distributed in the Comoé drainage, meanders being delineated by denudation patterns in the vicinity of the Mouhoun River (Fig. 11c). The lowest erosion range (<10 m, <1 m/My) is recorded east of Tô, southeast of Bobo-Dioulasso and around Gaoua and Djigoué (Fig. 11c), in agreement with the high degree of preservation of the pediplain relicts (Fig. 8). The volume eroded from the pediplain over the map area represents a spatially averaged denudation of ca. 20 m, corresponding to a denudation rate of about 2 m/My.

Dissection of the Late Miocene pediplain affected the whole region and did not propagate upstream by scarp or knickzone retreat as advocated by King (1962) and as implicitly included in river profile inversion works based on stream power incision models (e.g., Paul et al., 2014). As an illustration, the bounding escarpment

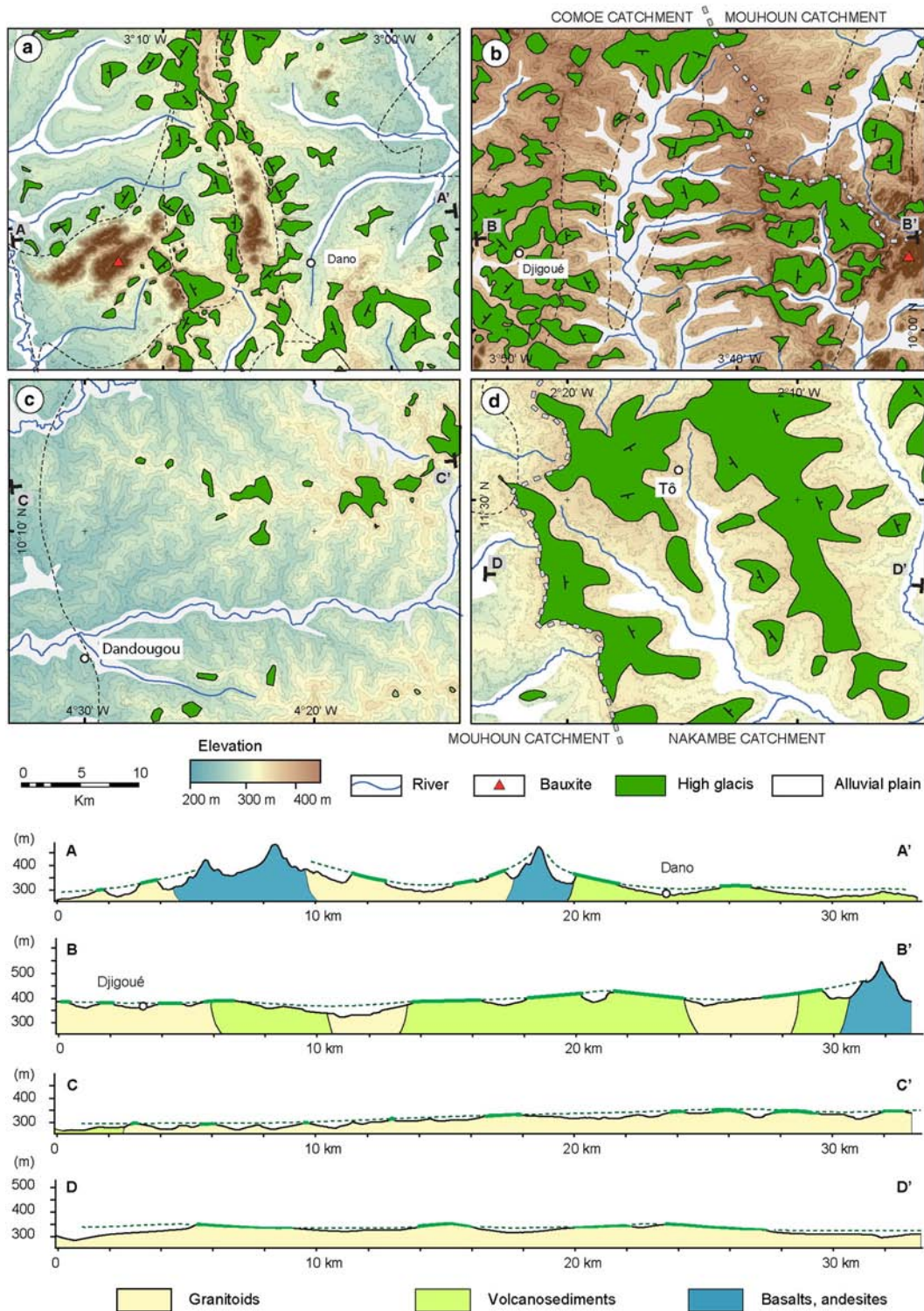


Fig. 10. Maps and cross-sections of type-landscapes on basement terrains. Frames of the maps are located in Fig. 8. Dip symbols represent the direction and sense of slope of the High glacial relicts (in green). Dashed lines on the maps are lithological boundaries (see Fig. 9a). (For interpretation of the references to color in this figure legend, the reader is referred to the web version of this article.)

of the Taoudeni basin is stable since at least 11 Ma (Fig. 11) and most probably 45 Ma (see Grimaud et al., 2014). Higher erosion rates coincide with the main drains outside the High Mouhoun, suggesting a control of the stream power (e.g., Whipple and Tucker, 1999) on pediplain dissection. Moderate stream power in the rest of the river network would have preserved the pediplain from complete stripping. Scarps bounding High glacial relicts often coincide with second-order divides of the modern topography, indicating a component of slope retreat in

the dissection of the pediplain. Meandering patterns of the Mouhoun River (Figs. 8 and 11c) further suggest that channel migrations may have contributed to slope retreat. The typical retreat distance of the High glacial relicts' edges over the study area (1–10 km) suggests a retreat rate of 100–1000 m/My. Therefore, under the erosion dynamics at play since ca. 10 Ma and assuming an initial valley side width of 20 km (Fig. 12), a minimum of 20 My would be required to entirely re-surface the High glacial pediplain.

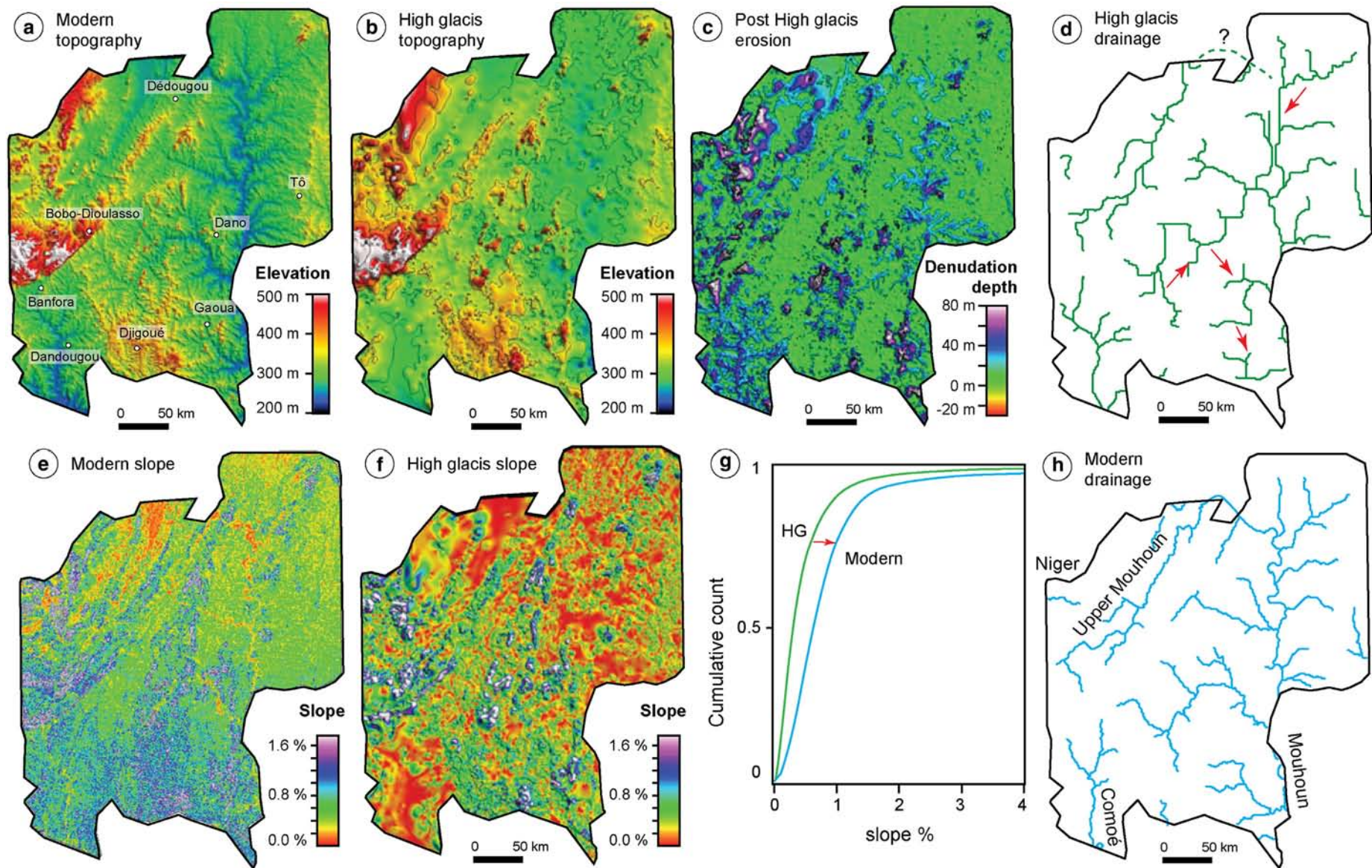


Fig. 11. (a) Modern topography based on SRTM digital elevation model smoothed to 500 m resolution. (b) Reconstructed topography of the High glacial pediplain. (c) Denudation map obtained by subtracting present-day topography from that of the High glacial stage. (d) River network automatically extracted from the digital elevation model of the High glacial stage. Red arrows represent drainage rearrangements in between the High glacial stage (d) and the present-day landscape (a). (e) Slope map of the current topography derived from (a). (f) Slope map of the High glacial pediplain derived from (b). (g) Comparative slope distribution for the High glacial and modern topographies. (h) River network automatically extracted from the present-day topography in (a). (For interpretation of the references to color in this figure legend, the reader is referred to the web version of this article.)

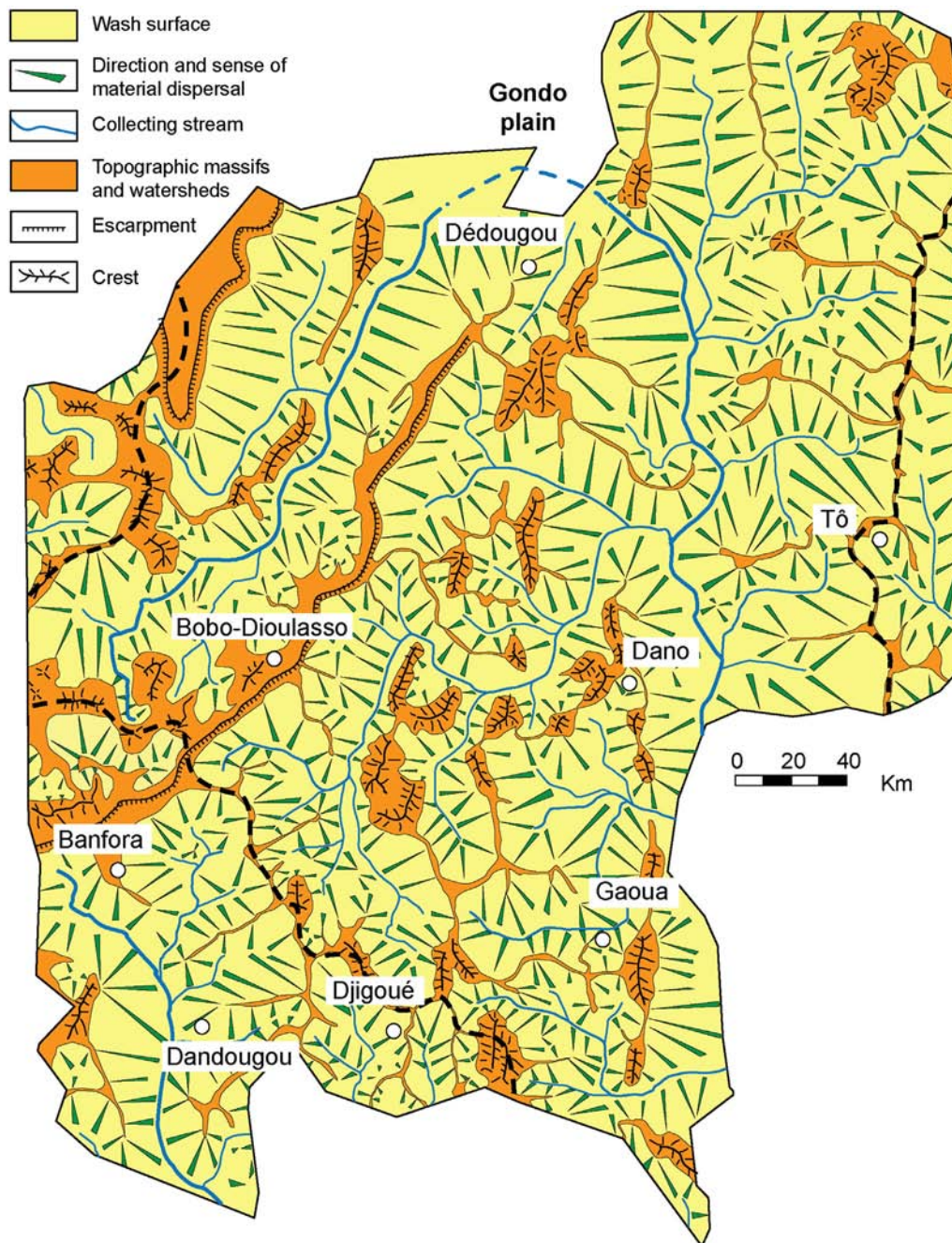


Fig. 12. Geomorphological map of the High glaciais pediplain before its abandonment in the Earliest Late-Miocene (ca. 11 Ma). The thick black dashed line represents the boundary of the Mouhoun catchment.

5. Discussion

Our results complement denudation and incision rates estimated from differential elevation of sparse High glaciais remnants and local base levels that have mean values of 5–7 m/My but non-uniform distributions over the sub-region from 2 to 15 m/My (Beauvais and Chardon, 2013; Grimaud et al., 2014). This suggests a partitioning of erosion among geomorphic provinces, with implications on the spatial variability of the sediment routing system. This variability may be a function of the regional topographic relief and/or positive epeirogeny, which seem to focus higher denudation (Beauvais and Chardon, 2013; Grimaud et al., 2014). Importantly, this variability is also and primarily due to contrasted river network evolution among sub-drainage basins separated by stationary knickzones (Grimaud et al., 2014; this work).

Our approach has consisted in a regional scale, volumetric quantification of denudation from a dated paleo-landscape datum, which enhances accuracy of denudation measurement over a West African province of lowest Neogene erosion. The obtained averaged denudation rate of 2 m/My is close to the lower limit of Cenozoic cratonic denudation rates measured worldwide (Beauvais and Chardon, 2013). Given the relevance of the size and morpho-geological context of the study area, we propose that this rate determines the background denudation ‘noise’ of shields. The Late Neogene increase in clastic sedimentation documented worldwide and particularly in African deltas such as that of the Niger (Séranne, 1999; Jermannaud et al., 2010; Fig. 1) should however be somehow included in the 2 m/My of background denudation averaged since the Early Late Miocene. This issue constitutes a sizable research challenge.

The material derived from dissection of the pediplain and removed since the Late Mid-Miocene was made of regolith, i.e. the High glacia cover and its underlying laterites. Indeed, no outcrop of significant surface/height has been exhumed since the abandonment of the pediplain. The fact that only the main stream channels locally flow atop the bedrock and that an averaged denudation of less than 20 m since abandonment of the pediplain is estimated further argues for denudation being restricted to the regolith. Denudation is however not strictly weathering-limited because if glacia typically cut preexisting and potentially old regoliths (i.e., Late Cretaceous to Eocene and Oligocene for the bauxitic and Intermediate weathering episodes, respectively, Fig. 2), they rarely attained the bedrock. Therefore, although weathering is instrumental in producing regolith mantles available to future stripping (Fairbridge and Finkl, 1980), low abrasion power of the pedimentation process combined with a probably limited transport capacity of the river network should be regarded as the limiting factor of tropical shields denudation.

The minimum characteristic timescale of 20 My for shield resurfacing indicated by post-Mid-Miocene drainage growth reinforces the view that shields are non-equilibrium landscapes, which increase their relief through geological time by preserving old landforms (Thomas, 1989; Twidale, 1991; Bishop, 2007; Beauvais and Chardon, 2013). A long resurfacing timescale also implies the high sediment retention capacity of shields as those sediments stem from weathering mantles dating back from at least the Early Paleogene and have been slowly recycled through the landscape since then. This suggests that weathering and slope processes play a major role, comparable to or greater than sediment transport by rivers (Métivier and Gaudemer, 1999; Jerolmack and Paola, 2010) in “shredding” and particularly smoothing or buffering climatic signals in the sedimentary record. Still, the ubiquitous character of the West African lateritic paleo-landsurfaces sequence and its chronology would suggest that Cenozoic landscape rejuvenation and sediment fluxes were punctuated by major climatic periods. Subdued clastic exports are indeed expected for time intervals of enhanced weathering during the Lower and Mid-Eocene, Late Oligocene, Mid Miocene, Latest Miocene and Latest Pliocene (e.g., Fig. 2b).

The background denudation rate of 2 m/My may be converted into a volumetric export rate of $2 \times 10^{-3} \text{ km}^3/\text{km}^2/\text{My}$ and a clastic yield of 4 t/km²/year, considering an effective grain density of 2500 kg/m³ (estimated from a bulk density of 2000 kg/m³ and a 20% porosity) for the stripped regolith. This value corresponds to the lower limit of modern West African solid river loads (3.5–300 t/km²/year) and to the 4 t/km²/year measured at the outlet of the Volta catchment (Milliman and Farnsworth, 2013). Therefore, cratonic erosion fluxes derived from a 2 m/My denudation rate appear to be realistic for low-capacity shield drainage systems on geological timescale. Conversely, this could suggest that the lower limit of large tropical shields catchments yields is governed by a cratonic background denudation noise. Importantly, background cratonic denudation of 2 m/My may be used to simulate the minimum export fluxes of drainage basins of constrained size over geological timescales.

6. Conclusions

Regional regolith–landform mapping allows characterizing surface dynamics, weathering patterns, paleotopography and dissection mechanisms of the last pediplain formed over West Africa from Early to Mid-Miocene. The nature and preservation/dissection patterns of the pediplain are controlled by the spatial distribution of bedrock lithologies and are partitioned between large drainage basins. Quantification of the post Mid-Miocene dissection of the pediplain determines a cratonic background denudation noise of 2 m/My and a minimum shield resurfacing characteristic timescale of 20 My. The minimum clastic yield of the major African catchments seems to be currently dominated by such a cratonic noise. Our results, once combined with landscape/weathering

chronologies, point to the shields' high storage capacity of sediments, consisting exclusively of regoliths that have been mainly recycled in the landscapes since the Late Cretaceous. Such a slow regolith turnover is due to the low efficiency of slope denudation processes by pedimentation and would tend to smooth riverine export fluxes of shields over geological timescales.

Acknowledgments

This work was funded by WAXI, the CNRS and the ANR TopoAfrica (ANR-08-BLAN-572 0247–02). The manuscript benefited from the comments of R. Teeuw and an anonymous referee as well as from editorial suggestions by A. Plater. We thank M. Jessell, D. Rouby, L. Baratoux and D. Huyghe for discussions and support and A. Fofana for participation in the fieldwork. We acknowledge AMIRA International and the industry sponsors, including AusAid and the ARC Linkage Project LP110100667, for their support of the WAXI project (P934A) as well as the Geological Surveys/Departments of Mines in West Africa as sponsors in kind of WAXI.

References

- Bamba, O., 1996. L'or disséminé dans les Albitites de Larafella (Burkina Faso), évolution dans les altérites et les cuirasses ferrugineuses: Métallogénie - Pétrologie - Géomorphologie. PhD Thesis, Aix-Marseille III University, Marseille, France.
- Bamba, O., Parisot, J.-C., Grandin, G., Beauvais, A., 2002. Ferricrete genesis and supergene gold behaviour in Burkina Faso, West Africa. *Geochem. Explor. Environ. Anal.* 2 (1), 3–13.
- Baratoux, L., Metelka, V., Naba, S., Jessell, M.W., Grégoire, M., Ganne, J., 2011. Juvenile Paleoproterozoic crust evolution during the Eburnean orogeny (~2.2–2.0 Ga), Western Burkina Faso. *Precambrian Res.* 191 (1–2), 18–45.
- Beauvais, A., Chardon, D., 2013. Modes, tempo and spatial variability of Cenozoic cratonic denudation: the West African example. *Geochem. Geophys. Geosyst.* 14, 1590–1608.
- Beauvais, A., Ritz, M., Parisot, J.-C., Dukhan, M., Bantsimba, C., 1999. Analysis of poorly stratified lateritic terrains overlying a granitic bedrock in West Africa, using 2-D electrical resistivity tomography. *Earth Planet. Sci. Lett.* 173 (4), 413–424.
- Beauvais, A., Ruffet, G., Hénocque, O., Colin, F., 2008. Chemical and physical erosion rhythms of the West African Cenozoic morphogenesis: the ³⁹Ar–⁴⁰Ar dating of supergene K–Mn oxides. *J. Geophys. Res.* 113, F04007.
- Bishop, P., 2007. Long-term landscape evolution: linking tectonics and surface processes. *Earth Surf. Process. Landf.* 32 (3), 329–365.
- Boeglin, J.-L., 1990. Évolution minéralogique et géochimie des cuirasses ferrugineuses de la région de Gaoua (Burkina Faso). PhD Thesis, Louis Pasteur University, Strasbourg.
- Boeglin, J.-L., Mazaltarim, D., 1989. Géochimie, degré d'évolution et lithodépendance des cuirasses ferrugineuses de Gaoua au Burkina Faso. *Sci. Géol. Bull.* 42 (1), 27–44.
- Boulangé, B., 1986. Relation Between Lateritic Bauxitization and Evolution of Landscape. *Trav. Int. Com. Stud. Bauxite, Alumina & Aluminum (ICSOBA)* 16–17 pp. 155–162.
- Boulangé, B., Millot, G., 1988. La distribution des bauxites sur le craton ouest-africain. *Sci. Géol. Bull.* 41 (1), 113–123.
- Boulangé, B., Sigolo, J.B., Delvigne, J., 1973. Descriptions morphoscopiques, géochimiques et minéralogiques des faciès cuirassés des principaux niveaux géomorphologiques de Côte d'Ivoire. *Cah. ORSTOM, sér. Géol.* 5(1) pp. 59–81.
- Bowden, D.J., 1987. On the composition and fabric of the footslop laterites (duricrusts) of the Sierra Leone, West Africa, and their geomorphological significance. *Z. Geomorphol. Suppl.* 64, 39–53.
- Butt, C.R.M., Bristow, A.P.J., 2013. Relief inversion in the geomorphological evolution of sub-Saharan West Africa. *Geomorphology* 185, 16–26.
- Chardon, D., Chevillotte, V., Beauvais, A., Grandin, G., Boulangé, B., 2006. Planation, bauxites and epeirogeny: one or two paleosurfaces on the West African margin? *Geomorphology* 32, 273–282.
- Colin, F., Beauvais, A., Ruffet, G., Hénocque, O., 2005. First ⁴⁰Ar/³⁹Ar geochronology of lateritic manganese pisolites; implications for the Palaeogene history of a West African landscape. *Earth Planet. Sci. Lett.* 238 (1–2), 172–188.
- Daveau, S., Lamotte, M., Rougerie, G., 1962. Cuirasses et chaînes birrimiennes en Haute-Volta. *Ann. Géogr. Fr.* 387, 260–282.
- Dequincey, O., Chabaux, F., Clauer, N., Sigmarsson, O., Liewig, N., Leprun, J.C., 2002. Chemical mobilizations in laterites: evidence from trace elements and ²³⁸U–²³⁴U–²³⁰Th disequilibria. *Geochim. Cosmochim. Acta* 66, 1197–1210.
- Dickson, B.L., Scott, K.M., 1997. Interpretation of aerial gamma-ray surveys – adding the geochemical factors. *AGSO J. Aust. Geol. Geophys.* 17 (2), 187–200.
- Dohrenwend, J.C., Parsons, A.J., 2009. Pediments in arid environments. In: Parsons, A., Abrahams, A. (Eds.), *Geomorphology of Desert Environments*. Springer Netherlands, The Netherlands, pp. 377–411.
- Durotoye, B., 1989. Quaternary sediments in Nigeria. In: Kogbe, C.A. (Ed.), *Geology of Nigeria, second edition Rock View International, Paris*, pp. 431–444.
- Eschenbrenner, R., Grandin, G., 1970. La séquence de cuirasses et ses différenciations entre Agnibiléfrou et Diébougou (Haute-Volta). *Cah. ORSTOM, Sér. Géol.* 2(2) pp. 205–246.

- Fairbridge, R.W., Finkl, C.W., 1980. Cratonic erosional unconformities and peneplains. *J. Geol.* 88, 69–86.
- Feybesse, J.-L., Billa, M., Guerrot, C., Duguey, E., Lescuyer, J.-L., Milesi, J.-P., Bouchot, V., 2006. The Paleoproterozoic Ghanaian province: geodynamic model and ore controls, including regional stress modeling. *Precambrian Res.* 149 (3–4), 149–196.
- Fölster, H., 1969. Late Quaternary erosion phases in SW Nigeria. *Bull. Ass. SÉNÉG. Quatern. Ouest Afr.* 21, 29–35.
- Goudie, A.S., Viles, H.A., 2012. Weathering and the global carbon cycle: geomorphological perspectives. *Earth-Sci. Rev.* 113 (1–2), 59–71.
- Grandin, G., 1976. Aplanissements cuirassés et enrichissement des gisements de manganeuse dans quelques régions d'Afrique de l'Ouest. *Mém. ORSTOM* 82 pp. 1–276.
- Grandin, G., Hayward, D.F., 1975. Aplanissements cuirassés de la péninsule de Freetown (Sierra Leone). *Cah. ORSTOM, sér. Géol.* 7(1) pp. 11–16.
- Grimaud, J.-L., 2014. Dynamique long-terme de l'érosion en contexte cratonique: l'Afrique de l'Ouest depuis l'Eocène. PhD Thesis, Toulouse University, Toulouse, France.
- Grimaud, J.-L., Chardon, D., Beauvais, A., 2014. Very long-term incision dynamics of big rivers. *Earth Planet. Sci. Lett.* 405, 74–84.
- Hénoque, O., Ruffet, G., Colin, F., Féraud, G., 1998. $^{40}\text{Ar}/^{39}\text{Ar}$ dating of West African lateritic cryptomelanes. *Geochim. Cosmochim. Acta* 62 (16), 2739–2756.
- Hubert, H., 1912. Sur un important phénomène de capture dans l'Afrique occidentale. *Ann. Géogr. Fr.* 21 (117), 251–262.
- Jermannaud, P., Rouby, D., Robin, C., Nalpas, T., Guillocheau, F., Raillard, S., 2010. Plio-Pleistocene sequence stratigraphic architecture of the Eastern Niger Delta: a record of eustasy and aridification of Africa. *Mar. Pet. Geol.* 27, 810–821.
- Jerolmack, D.J., Paola, C., 2010. Shredding of environmental signals by sediment transport. *Geophys. Res. Lett.* 37 (19), L19401.
- King, L.C., 1962. *The Morphology of the Earth*. Oliver and Boyd, Edinburgh (799 pp.).
- Larsen, I.J., Montgomery, D.R., Greenberg, H.M., 2014. The contribution of mountains to global denudation. *Geology* 42 (6), 527–530.
- Mallet, J.-L., 1992. Discrete smooth interpolation in geometric modelling. *Comput. Aided Des.* 24 (4), 178–191.
- Maxson, J.H., Anderson, G.H., 1935. Terminology of surface forms of the erosion cycle. *J. Geol.* 43, 88–96.
- Metelka, V., Baratoux, L., Naba, S., Jessell, M.W., 2011. A geophysically constrained litho-structural analysis of the Eburnean greenstone belts and associated granitoid domains, Burkina Faso, West Africa. *Precambrian Res.* 190 (1–4), 48–69.
- Métivier, F., Gaudemer, Y., 1999. Stability of output fluxes of large rivers in South and East Asia during the last 2 million years: implications on floodplain processes. *Basin Res.* 11 (4), 293–303.
- Michel, P., 1959. L'évolution géomorphologique des bassins du Sénégal et de la Haute-Gambie, ses rapports avec la prospection minière. *Rev. Géomorphol. Dynam.* 10, 117–143.
- Michel, P., 1973. Les bassins des fleuves Sénégal et Gambie: étude géomorphologique. *Mém. ORSTOM* 63 pp. 1–752.
- Michel, P., 1974. Les glacis cuirassés d'Afrique occidentale et centrale. *Géomorphologie des glacis. Colloques scientifiques de l'Université de Tours, Tours, France* (1974), pp. 70–80.
- Milliman, J.D., Farnsworth, K.L., 2013. *River Discharge to the Coastal Ocean: A Global Synthesis*. Cambridge University Press, Cambridge (392 pp.).
- Millot, G., 1970. *Geology of Clays*. Springer Verlag, Berlin (429 pp.).
- Millot, G., 1983. Planation of continents by intertropical weathering and pedogenetic processes. In: Melfi, A.J., Carvalho, A. (Eds.), *Lateritisation Processes. Proceedings of the 11nd international Seminar on Lateritisation Processes, Sao Paulo, Brazil* (1982), pp. 53–63.
- Molnar, P., 2004. Late Cenozoic increase in accumulation rates of terrestrial sediment: how might climate change have affected erosion rates? *Ann. Rev. Earth Planet. Sci.* 32 (1), 67–89.
- Ollier, C.D., Pain, C.F., 1996a. *Regolith, Soils and Landforms*. John Wiley & Sons, Chichester (316 pp.).
- Ollier, C.D., Pain, C.F., 1996b. *Regolith stratigraphy: principles and problems*. *AGSO J. Aust. Geol. Geophys.* 16, 197–202.
- Palauti, G., 1959. Contribution à l'étude géologique et hydrogéologique des formations primaires au Soudan et en Haute-Volta. *Bull. Serv. Géol. Prosp. Min.* 33, 1–209.
- Paul, J.D., Roberts, G.G., White, N., 2014. The African landscape through space and time. *Tectonics* 33, 898–935.
- Petit, M., 1994. Carte Géomorphologique du Burkina Faso au 1/1 000 000. ORSTOM – University of Ouagadougou, Ouagadougou, Burkina Faso (unpublished).
- Séranne, M., 1999. Early Oligocene stratigraphic turnover on the West Africa continental margin: a signature of the tertiary greenhouse-to-icehouse transition? *Terra Nova* 11 (4), 135–140.
- Tardy, Y., 1997. *Petrology of Laterites and Tropical Soils*. Balkema, Rotterdam (408 pp.).
- Teeuw, R.M., 2002. Regolith and diamond deposits around Tortiya, Ivory Coast, West Africa. *Catena* 49 (1–2), 111–127.
- Thomas, M.F., 1980. Timescales of landform development on tropical shields—a study from Sierra Leone. In: Cullingford, R.A., Davidson, D.A., Lewin, J. (Eds.), *Timescales in Geomorphology*. Wiley, Chichester, pp. 333–354.
- Thomas, M.F., 1989. The role of etch processes in landform development II. Etching and the formation of relief. *Z. Geomorphol.* 33 (3), 257–274.
- Thomas, M.F., 1994. *Geomorphology in the Tropics: A Study of Weathering and Denudation in Low Latitudes*. Wiley & Sons, New York (482 pp.).
- Twidale, C.R., 1991. A model of landscape evolution involving increased and increasing relief amplitude. *Z. Geomorphol.* 35 (1), 85–109.
- Vasconcelos, P.M., Brimhall, G.H., Becker, T.A., Renne, P.R., 1994. $^{40}\text{Ar}/^{39}\text{Ar}$ analysis of supergene jarosite and alunite: implications to the paleoweathering history of the western USA and West Africa. *Geochim. Cosmochim. Acta* 58 (1), 401–420.
- Whipple, K.X., Tucker, G.E., 1999. Dynamics of the stream-power river incision model; implications for height limits of mountain ranges, landscape response timescales, and research needs. *J. Geophys. Res.* 104 (B8), 17661–17674.
- Willford, J.R., Bierwirth, P.N., Craig, M.A., 1997. Application of airborne gamma-ray spectrometry in soil/regolith mapping and applied geomorphology. *AGSO J. Aust. Geol. Geophys.* 17, 201–216.
- Willenbring, J.K., von Blanckenburg, F., 2010. Long-term stability of global erosion rates and weathering during late-Cenozoic cooling. *Nature* 465, 211–214.
- Willenbring, J.K., Codilean, A.T., McElroy, B., 2013. Earth is (mostly) flat: apportionment of the flux of continental sediment over millennial time scales. *Geology* 41, 343–346.



Experimental migration of knickpoints: influence of style of base-level fall and bed lithology

J.-L. Grimaud^{1,2}, C. Paola^{1,2}, and V. Voller^{1,3}

¹St. Anthony Falls Laboratory, University of Minnesota, 2 Third Avenue SE, Minneapolis, MN 55414, USA

²Department of Earth Sciences, University of Minnesota, Minneapolis, MN 55414, USA

³Department of Civil, Environmental, and Geo- Engineering, University of Minnesota, Minneapolis, USA

Correspondence to: J.-L. Grimaud (jgrimaud@umn.edu)

Received: 4 August 2015 – Published in Earth Surf. Dynam. Discuss.: 25 August 2015

Revised: 4 December 2015 – Accepted: 10 December 2015 – Published: 15 January 2016

Abstract. Knickpoints are fascinating and common geomorphic features whose dynamics influence the development of landscapes and source-to-sink systems – in particular the upstream propagation of erosion. Here, we study river profiles and associated knickpoints experimentally in a microflume filled with a cohesive substrate made of silica, water and kaolinite. We focus on the effect on knickpoint dynamics of varying the distribution of base-level fall (rate, increment, and period) and substrate strength, i.e., kaolinite content. Such simple cases are directly comparable to both bedrock and alluvial river systems. Under a constant rate of base-level fall, knickpoints of similar shape are periodically generated, highlighting self-organized dynamics in which steady forcing leads to multiple knickpoint events. Temporary shielding of the bed by alluvium controls the spacing between these *unit knickpoints*. Shielding is, however, not effective when base-level drops exceed alluvium thickness. While the base-level fall rate controls the overall slope of experiments, it is not instrumental in dictating the major characteristics of unit knickpoints. Instead the velocity, face slope and associated plunge pool depth of these knickpoints are all strongly influenced by lithology. The period between knickpoints is set by both alluvium thickness and base-level fall rate, allowing use of knickpoint spacing along rivers as an indicator of base-level fall rate.

1 Introduction

The retreat of knickpoints, i.e., localized steps in the river profile, is a common process in erosion systems. Knickpoints are created in response to an erosional perturbation and propagate information upstream into the landscape as opposed to the downstream transport of sediments fed from hillslopes (Whipple, 2004; Bishop, 2007; Allen, 2008). They are usually triggered by relative fall of the river base level, whether by uplift of the river bed or drop of the base level to which the river profile adjusts (e.g., a lake, a dam, a fault offset or the sea level). Knickpoints distributed within a landscape can thus be thought of as key signal carriers of external forcing at play in the sediment routing system.

Through use of physical experiments, base-level falls can successfully produce knickpoints over both alluvial/non-cohesive or bedrock/cohesive substrates (for example: Brush

and Wolman, 1960; Holland and Pickup, 1976; Begin et al., 1981; Gardner, 1983; Bennett et al., 2000; Frankel et al., 2007; Cantelli and Muto, 2014). Under supercritical flow conditions, the shape of the knickpoints is well preserved (Bennett et al., 2000; Cantelli and Muto, 2014). In some cases, upstream-migrating steps occur as a train of closely spaced knickpoints bounded by hydraulic jumps, termed “cyclic steps” by Parker (1996; Fig. 1). One might directly associate the presence of single knickpoints or trains of cyclic steps along a river with an ongoing or past external change, e.g., a relative base-level fall triggered by climate change or tectonics. However, knickpoints may also form in response to the reduction of sediment discharge along the river or can even be autogenic, arising from natural variability within a drainage basin (Hasbergen and Paola, 2000). Furthermore, dissipation is commonly observed as knickpoint retreat, and so the height of a knickpoint face does not neces-

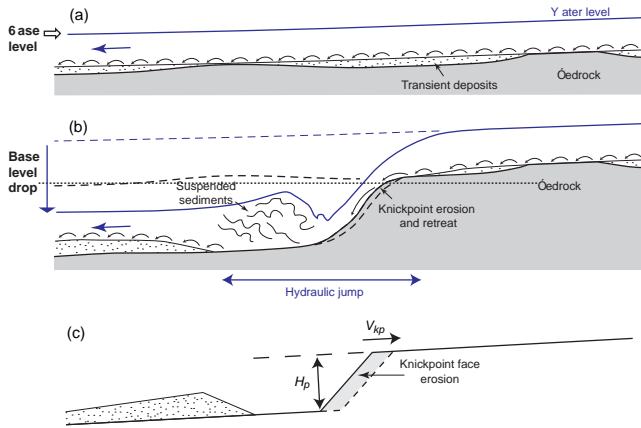


Figure 1. Schematic longitudinal section of a river bed before (a) and during (b) the propagation of a knickpoint triggered by relative base-level fall. Blue arrows represent flow direction and black arrows the motion of the bedload. The black and blue dashed lines respectively represent the bedrock and water levels before knickpoint propagation. (c) Idealized representation of a knickpoint characterized by its velocity, V_{kp} , and the depth of associated plunge pool, H_p .

sarily reflect the initial base-level fall (Parker, 1977; Gardner, 1983; Crosby and Whipple, 2006; Whipple, 2004; Bishop et al., 2005). Overall, there is still much to be worked out about the specifics of how knickpoints encode and carry erosional information.

Additionally, lithologic controls over river profiles and their knickpoints have long been recognized (Hack, 1957; Bishop et al., 1985; Miller, 1991; Pederson and Tressler, 2012). In recent field examples, Cook et al. (2013) measured lower rates of knickpoint retreat above more resistant rock, while Grimaud et al. (2014) documented the persistence of lithogenic knickzones (e.g., > 30 km long steeper reaches) at continental scale. Finally, Sklar and Dietrich (2001, 2004) highlighted bed lithology, i.e., variations in bedrock strength or alluvium thickness, as a major limiting factor of river abrasion capacity, through, for example, boulder armoring (Seidl et al., 1994), and therefore a control over the response timescale of the sediment routing system (see also Gasparini et al., 2006).

In this study, we investigate experimentally the effect of bed lithology and uplift style on knickpoint evolution. The experiments provide simple cases of 1-D evolution that are relevant for comparison with individual river segments. The results highlight the strong effect of bedrock lithology on knickpoint characteristics and show how incision and knickpoint propagation are influenced by transient deposits along streams. They also show a form of self-organization in which multiple small base-level steps may be required to produce a single knickpoint. This points to a new form of knickpoint self-organization that controls the relative rate at which knickpoints are generated as a function of the rate and mag-

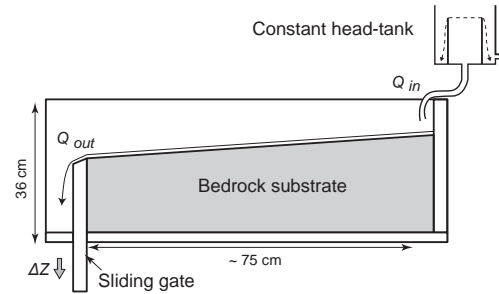


Figure 2. Experimental setup. Base-level fall, of rate U , is produced by lowering the sliding gate. Q_{in} is the water discharge introduced the flume using a constant head tank. Q_{out} is the water discharge measured at the outlet of the flume. Because of absorption by the substrate, Q_{in} (1250 mL min^{-1}) is superior to Q_{out} in every experiment (see Table 1).

nitude of base-level fall. The results suggest that knickpoint spacing, though not vertical magnitude alone, is an indicator of base-level fall rate.

2 Experimental setup

2.1 Flume design and experiment sets

We carried out experiments on river incision at the St. Anthony Falls Laboratory, University of Minnesota, Minneapolis. To minimize planform complications such as bars, we constructed a small, narrow flume to test the impact of base-level fall style and bed lithology on stream erosion. The flume is 1.9 cm wide, about 100 cm long and 36 cm high (Fig. 2). We supplied a constant water discharge ($Q_{in} = 1250 \text{ mL h}^{-1}$) over a cohesive substrate, which eroded and formed a profile. The substrate is very similar to the one used by Hasbargen and Paola (2000). It is composed of silica sand (density = 2.65; $d_{50} = 90 \mu\text{m}$), kaolinite (density = 2.63; $d_{50} < 4 \mu\text{m}$) and water. The composition of the substrate controls its erodibility, one of the key variables we wished to study. This substrate is placed wet into the flume and its top surface flattened as much as possible. The experiment starts immediately. Water introduction causes the slow erosion of the first upstream 10 cm of the flume that provides a constant minimum bedload ($q_s \sim 3 \text{ g min}^{-1}$). This bedload acts as an abrasion tool throughout the experiments (Sklar and Dietrich, 2004; Fig. 1). The stream is perturbed by lowering the downstream end of the flume using a sliding gate (Fig. 2). In response to this perturbation, knickpoints develop and retreat upstream (Figs. 3 and 4).

We carried out several experimental sets. Experiment 1 is the base case to which other experiments can be compared (rate of base-level fall, $U = 2.5 \text{ cm h}^{-1}$; incremental base-level drops, $\Delta Z = 0.25 \text{ cm}$ and kaolinite fraction $f_k = 1\%$ by weight when dry; see Table 1). First, we tested base-level fall scenarios. During experiments 2, 3, 5 and 6, U was set

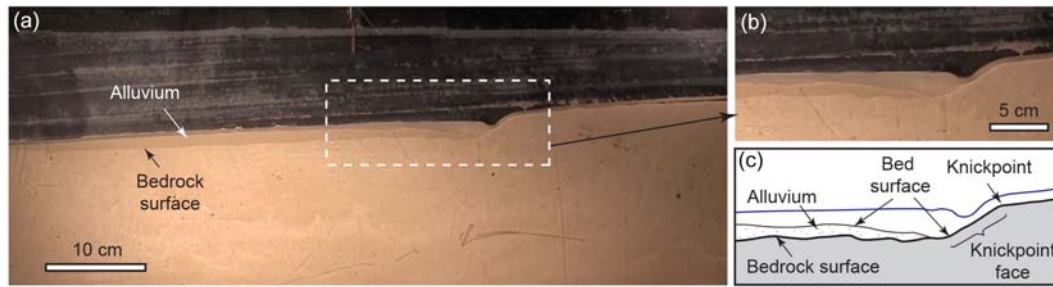


Figure 3. Illustration of a knickpoint observed along the flume during experiment 10. (a) Overall view of the profile and (b, c) details of the knickpoint. Note the white color of the water due to suspended sediments.

Table 1. Summary of the main characteristics for each experiments. τ_{eq} represents the equilibrium shear stress. NA stands for no acquisition.

Experiment	1	2	3	5	6	7	8	9	10	11
Base-level fall rate, U (cm h ⁻¹)	2.5	5	1.25	0.5	50	2.5	5	2.5	2.5	2.5
Base-level drop, ΔZ (cm)	0.25	0.25	0.25	0.25	0.25	2.5	2.5	0.25	0.25	0.25
Kaolinite fraction, f_k (%)	1	1	1	1	1	1	1	0	2	5
Discharge, Q_{out} (mL min ⁻¹)	800	770	730	900	820	895	890	970	900	755
Flow depth, h (mm)	2.5	2	2.75	3.25	1.1	2	2.5	2.5	1.75	2
Flow velocity, V_f (m s ⁻¹)	0.28	0.34	0.23	0.24	0.65	0.39	0.31	0.34	0.45	0.33
Froude number	2.10	2.41	1.31	1.22	3.95	2.8	1.99	2.82	3.82	2.36
Reynolds number	2222	2232	1986	2353	2579	2594	2472	2694	2667	2188
Equilibrium slope	0.061	0.077	0.051	0.037	0.15	NA	NA	0.054	0.066	NA
τ_{eq} (Pa)	1.18 ± 0.14	1.28 ± 0.17	1.11 ± 0.11	0.88 ± 0.08	1.9 ± 0.33	NA	NA	0.91 ± 0.12	NA	NA
KP velocity, V_{kp} (cm min ⁻¹)	8.2	8.1	6.8	8.8	11.6	9.8	11.8	17	7	0.7
KP frequency (Hz)	0.0006	0.0008	0.0003	0.0001	0.0046	0.0003	0.0006	0.0009	0.0004	0.0003
Period between KP, Δt (min)	28.8	20.0	48.0	118.0	3.6	60.0	30.0	18.4	43.6	48.6
Plunge pool depth, H_p (cm)	1.23	1.19	0.97	1.13	1.31	NA	NA	1.25	1.82	3
	Base case		Base-level fall variations			Base-level drop variations		Substrate variations		

to 5, 1.25, 0.5 and 50 cm h⁻¹, respectively, while ΔZ and f_k were kept similar to experiment 1. In other words, the base level was dropped 0.25 cm every 30 min to get a 0.5 cm h⁻¹ rate and every 3 min to get a 5 cm h⁻¹ rate. During experiment 7, U and f_k were similar to experiment 1 (2.5 cm h⁻¹ and 1 %) but ΔZ was changed to 2.5 cm (Table 1). To keep the same base-level fall rate, the base level was then dropped 2.5 cm every 60 min. Similarly, the base level was dropped 2.5 cm every 30 min in experiment 8 so that it could be compared to experiment 2. Finally, different substrate lithologies were tested. The kaolinite fraction, f_k , was changed to 0, 2 and 5 % during experiments 9, 10 and 11, respectively, while U and ΔZ were kept similar to experiment 1 (Table 1).

2.2 Measurements and uncertainties

We define the *knickpoint* as the point where a river steepens, whereas the *knickpoint face* corresponds to the steep reach starting at this knickpoint and ending at the bottom of the plunge pool (e.g., Gardner, 1983; Figs. 1c and 3c). We measured geometries of the profile and knickpoints using a camera placed along the flume. Pictures were extracted every 24–30 s and corrected for lens distortion and vertical stretching in order to measure the overall experimental slope, knickpoint face slope, and knickpoint face length. Water depth

was measured using a point gauge, while water discharge (e.g., Q_{out} ; Fig. 2) was measured throughout experiments using a graduated cylinder. The hydraulic parameters of each experiment were calculated using these measures (Table 1). Reynolds numbers fall between 1900 and 2700, while Froude numbers are all above 1, indicating that the flow regime is respectively transitional to turbulent and supercritical (Table 1).

On the extracted pictures, no vertical or horizontal position could be accurately measured below a two-pixel resolution, i.e., 1.33 mm. These vertical and horizontal errors were combined in a simple propagation formula based on variance (Ku, 1966) to assess uncertainties in the metrics used in this study. A test evaluation calculated for experiment 3 showed that variance of the overall experiment’s slope was around 0.0017 (i.e., ~ 5 % equilibrium slope of experiment 3) and knickpoint velocity variance was about 2 mm h⁻¹ (i.e., ~ 3 % of average knickpoint velocity for experiment 3). Therefore, both overall slope and knickpoint velocity do not vary significantly due to measurement. On the other hand, measures of the variance of knickpoint face length and slope have greater uncertainties. For instance, when the overall experiment is steep (e.g., experiment 6; Table 1), the transition to the knickpoint face along the profile is not sharp and a horizontal measurement error up to 15 mm is possible, es-

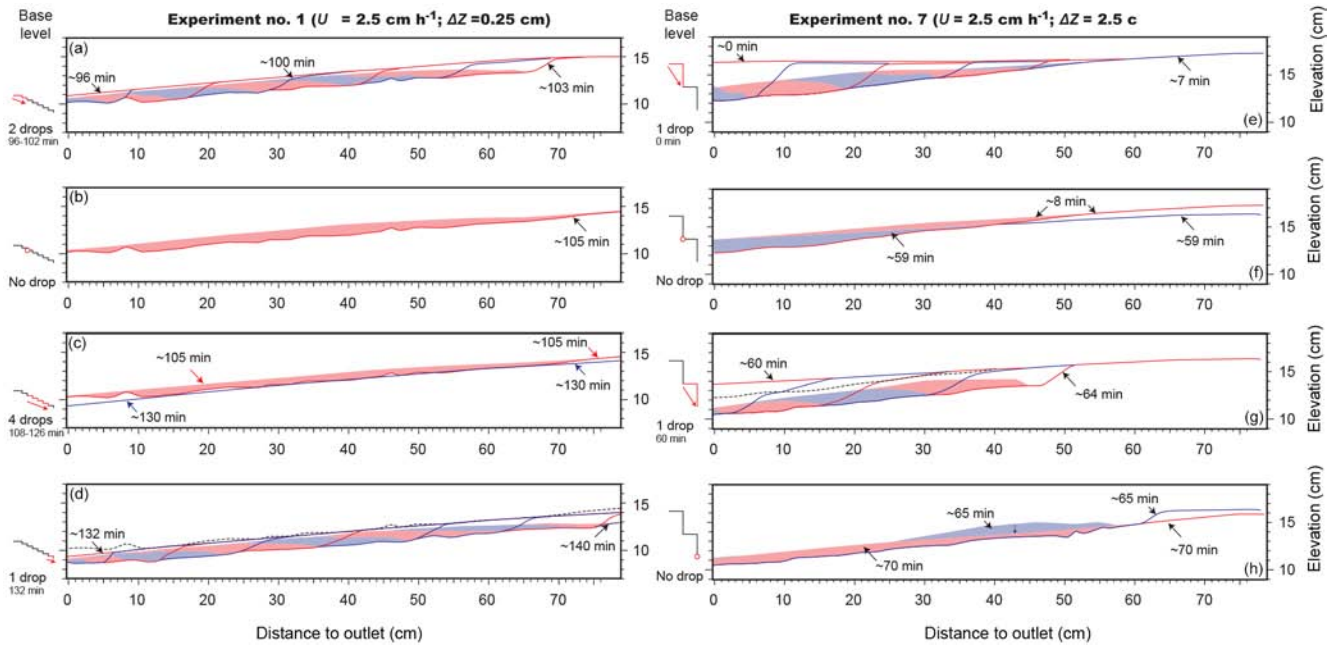


Figure 4. Evolution of two experiments with the same average rate of base-level fall ($U = 2.5 \text{ cm h}^{-1}$), but different incremental base-level drops, ΔZ . (a)–(d) For experiment 1 ($\Delta Z = 0.25 \text{ cm}$), a knickpoint is propagating in between 96 and 103 min (a), leaving a alluvial layer (b) that will be progressively removed as the base level of the experiment is lowered between 105 and 130 min (c). A new knickpoint starts retreating in between 132 and 140 min once the alluvium has disappeared (d). (e)–(h) For experiment 7 ($\Delta Z = 2.5 \text{ cm}$), a new knickpoint is generated each time the base level is dropped (i.e., in between 0 and 8 min (e) and in between 60 and 69 min (g)). In between these drops, the profile's slope is lowered by overall diffusion ((f) and (h); see also Fig. 7b). Blue and red colored lines correspond to the successive elevation of the bedrock surface, while the light-blue and red area corresponds to the alluvium. The position of the base level is tracked on the left side of each frame. Vertical exaggeration is 1.375.

pecially approaching the plunge pool (Figs. 1 and 3). The resulting knickpoint face slope variance, calculated for experiment 6 assuming a vertical error of 1.33 mm, is about 3° . Therefore, two knickpoint face slopes would be significantly different only if their difference is greater than 3° . Plunge pool depth was calculated from knickpoint face slope and knickpoint face length and corrected for the overall slope of experiments (e.g., Fig. 1c). Error on flow depth, h , is approximately 0.25 mm. This together with uncertainty in slope allowed us to estimate the uncertainty in the shear stress, τ_{eq} , shown in Table 1.

3 Results

3.1 Knickpoint generation and periodicity

We observe threshold behavior in the total base-level drop needed to generate a knickpoint. In the case of $\Delta Z = 0.25 \text{ cm}$, two to eight drops are needed to generate the first knickpoint. A small initial knickpoint retreats about 30 average stream depths (7 cm) upstream and then remains stationary for 1–2 min. During this period, the plunge pool at the foot of the knickpoint face deepens and a hydraulic jump forms. This phase is characterized by over-erosion, i.e., the bottom of the plunge pool becomes lower than the

newly imposed base level. After the plunge pool reaches a depth of 1–3 cm (Fig. 4), the knickpoint begins to retreat at constant speed. In the case of $\Delta Z = 2.5 \text{ cm}$, a knickpoint is generated for each base-level drop and retreats uniformly (Fig. 4e). During knickpoint retreat, the sand–kaolinite substrate is eroded and the kaolinite and sand separate. The kaolinite is transported out of the system in suspension, while the sand is deposited downstream of the knickpoint to form a layer (*alluvium*; Figs. 3, 4a and e). Once a knickpoint reaches the upstream end of the flume, the alluvium remains along the profile (Fig. 4b and f). This layer is slowly removed as the river profile is smoothly lowered by overall diffusion over both the alluvium and the bedrock substrate (Fig. 4b, c and f). This indicates that the sediment layer acts as a shield that prevents erosion of the bedrock substrate (Sklar and Dietrich, 2004): no significant knickpoint–hydraulic jump couple is observed during the diffusion phase. Only close observation of the bed indicates that smaller knickpoints (i.e., shallower than the stream depth) develop and propagate while the bed is shielded by sediment.

Depending on the magnitude of base-level drop, ΔZ , the period between knickpoints is not constant. In the case of $\Delta Z = 2.5 \text{ cm}$, and after the alluvium is in place, the base-level drop is greater than the alluvium thickness, allowing

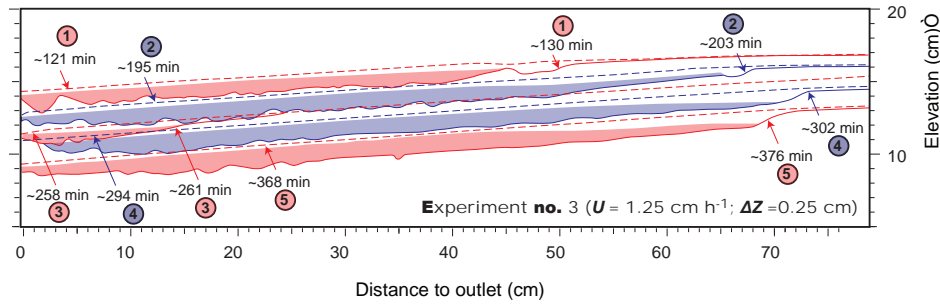


Figure 5. Evolution of the entire experiment 3 ($U = 1.25 \text{ cm h}^{-1}$; $\Delta Z = 0.25 \text{ cm}$) showing alluvium thickness deposited in response to the retreat of knickpoints (enumerated from 1 to 5). Blue and red colored lines correspond to the elevation of the bedrock surface at the end of the knickpoint retreat, while the blue and red colored dashed lines correspond to the elevation of the bedrock before knickpoint propagation. Light-blue and red areas represent the alluvium. A new knickpoint is generated only when the alluvium is removed from the profile. Note the abortion of knickpoint 3 after 3 min of retreat (see text for explanations). Vertical exaggeration is 1.375.

each drop to form a knickpoint (Fig. 4e and g). The face of a new knickpoint is irregular, i.e., its slope changes at the transition between the bedrock and the remaining bed sediments (Fig. 4g). In that case, the average period between knickpoints corresponds to the time between each base-level drop (e.g., 60 min for experiment 7 and 30 min for experiment 8; Table 1). In the case of $\Delta Z = 0.25 \text{ cm}$, the alluvium has to be removed before a new knickpoint can be generated and retreat (Fig. 4c and d). In this regime, the average period between knickpoints is therefore a function of the alluvium thickness to be eroded in the flume (Table 1). A detailed sequence is shown in Fig. 5 for experiment 3. Overall, the knickpoint period is about 70 min for most of this experiment (e.g., the time needed to produce a base-level fall equal to the alluvium thickness, 1.25 cm). However, the geometry of the bedrock surface is irregular and hence the sediment thickness too. Accordingly, the third knickpoint generated disappears upon reaching sediment deposits in the flume (Fig. 5). First, the alluvial layer is rapidly removed along the upper section of the knickpoint face. This produces a two-step knickpoint face that is progressively smoothed. This smoothing disturbs the flow: the hydraulic jump cannot be maintained and the knickpoint fades. As a consequence, thinner alluvium is left along the flume and the next (fourth) knickpoint starts after only 33 min (Fig. 5). This indicates that transient alluvial deposits can disturb the flow and temporarily prevent knickpoint formation or propagation.

3.2 Equilibrium slope and timescales

Figure 6 shows the overall evolution of experimental profiles as a function of base-level fall rate ($\Delta Z = 0.25 \text{ cm}$). These profiles correspond to the bed surface and not to the bedrock surface. Each experiment starts with a nearly flat profile whose slope increases (dashed lines; Fig. 6) until stabilization (plain lines). As base-level fall rate increases, profiles become steeper: Fig. 7a shows that profile slopes increase proportionally to the rate of base-level fall. Each ex-

periment reaches a quasi-equilibrium slope that is proportional to the rate of base-level fall applied. Knickpoint frequency also increases as a function of base-level fall rate and more knickpoints are captured along the profiles from Fig. 6a to e (see also Table 1). This configuration is enhanced for $U = 50 \text{ cm h}^{-1}$ (experiment 6), where several knickpoints can retreat simultaneously. In this configuration, and similar to experiments 7 and 8, knickpoints are propagating even though sediments are preserved along the profile. However, the downstream reach (first 10 cm of the flume) must be free of alluvium in order for a knickpoint to be generated.

Figure 7b shows the evolution of slope for experiments 7 and 8, which have base-level fall rate similar to experiments 1 and 2, respectively, but a ΔZ 10 times higher (e.g., 2.5 cm). Experiment 5 ($U = 0.5 \text{ cm h}^{-1}$; $\Delta Z = 0.25 \text{ cm}$) is shown for comparison. After 100 min, experiments 7 and 8 have a slope that is high but lower than experiments 1 and 2, respectively. Furthermore, the profiles of the former decrease and converge towards a low equilibrium slope, which is close to the equilibrium slope in experiment 5. In all these experiments (5, 7 and 8), a common characteristic is the low frequency of base-level drops and the conversely long period in between these drops ($\geq 30 \text{ min}$). This suggests that these experiments are more affected by smooth profile readjustment by diffusion during quiescent periods and less by knickpoint retreat.

An analysis of the stream slope according to lithology is shown in Fig. 7c. Lithology or substrate strength is represented as the kaolinite percentage within the substrate, f_k . For similar uplift rates, the experiment without kaolinite has a lower equilibrium slope than the experiment with 1 % kaolinite. However, the equilibrium slopes of experiments 1 and 10 (with respectively 1 and 2 % of kaolinite) are similar. Therefore, despite their different bedrock strengths, these two cases are at equilibrium with the alluvium and not the substrate. Indeed, shear stress calculated at the equilibrium slope for experiments 1, 2, 3, 5 and 6 goes as the base-level fall rate (Fig. 7d). A tentative exponential fit suggests that the shear stress for $U = 0 \text{ cm h}^{-1}$ (0.91 ± 0.5)

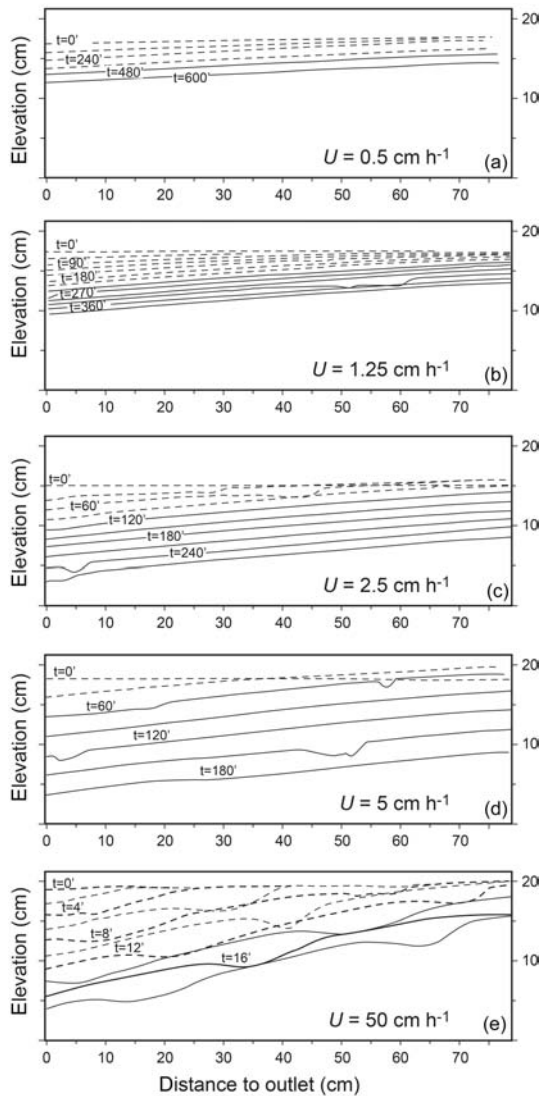


Figure 6. Evolution of the profile's bed surface elevation as a function of the base-level fall rate (see also Fig. 7a). The bed surface can be either the bedrock or the alluvium surface. Note that the amount of knickpoint increases with base-level fall rate.

would be above the shear stress of motion (i.e., ~ 0.13 Pa for $d_{50} = 0.1$ mm; Julien, 1998) and that the evolution of these slopes is controlled by alluvium removal. The comparison between Fig. 7a and c further suggests that the overall equilibrium slope varies more strongly with base-level fall rate than lithology. When $f_k = 5\%$, no equilibrium is attained and the quasi-equilibrium state has a strong sinusoidal shape (Fig. 7c): a maximum value is reached about every 100 min. Given a typical knickpoint velocity of about 0.7 cm min^{-1} (experiment 11; Table 1) and the flume experimental section length 75 cm, 100 min corresponds to the time required for a knickpoint to reach the upstream part of the flume. This indicates that low knickpoint velocity lengthens the readjust-

ment timescale of the overall profile as higher relief can be maintained until knickpoints pass through the system.

3.3 Controls on knickpoint characteristics

In Fig. 8, we investigate knickpoint properties in relation to U and f_k . Figure 8a to d show that the knickpoint face slope and plunge pool depth increase linearly as a function of f_k (Fig. 8e). These characteristics do not vary significantly as a function of the uplift rate: only a slight increase in knickpoint slope and plunge pool depth are suggested as functions of U (Fig. 8f). This shows that these knickpoint properties are primarily controlled by lithology. The same statement applies for knickpoint retreat velocity: while variations in U from 0.5 to 50 cm h^{-1} do not show a statistically significant increase in knickpoint velocity (Fig. 8h), an increase from 0 to 5 % kaolinite is responsible for a knickpoint velocity decrease from 17 to 0.7 cm h^{-1} (Fig. 8g). The effect of kaolinite fraction on knickpoint velocity can be fit by an equation of the form

$$V_{\text{kp}} = V_{\text{max}} e^{-\alpha \cdot f_k}, \quad (1)$$

where V_{max} is the maximum velocity attained over sand (e.g., $f_k = 0$) and α is a dimensionless fitting parameter. Less dramatically, the increase in ΔZ from 0.25 to 2.5 cm increases knickpoint retreat velocity by 20 % (i.e., comparison between experiments 1 and 7 and experiments 2 and 8 in Table 1). This indicates that knickpoint velocity may still be partially influenced by base-level fall velocity. Finally, while Bennett et al. (2000) showed that plunge pool depth increases with water discharge, our results suggest that this depth also goes with the kaolinite fraction (Fig. 8e):

$$H_p \sim f_k. \quad (2)$$

4 Discussion

4.1 Knickpoint self-organization

The experiments presented in this study were carried out in a small 1-D flume with very simple conditions compared to natural systems: constant discharge, constant lithology per experiment, no interfluvial processes (debris-flow, pedimentation, etc.) and no possibility for the channel to widen (although channel narrowing has been observed in experiment 11; see caption of Fig. 8). The first and most striking result of this study is that, even under these simple conditions, knickpoint dynamics remain surprisingly complex and exhibit strong autogenic (self-organized) variability mediated by alluvium dynamics and associated bed sheltering, and by the erosional threshold for the bedrock substrate. Indeed, the interaction between bed lithology and base-level fall style (i.e., overall rate and distribution of vertical offsets) provides a variety of configurations that strongly affects the evolution of river profiles.

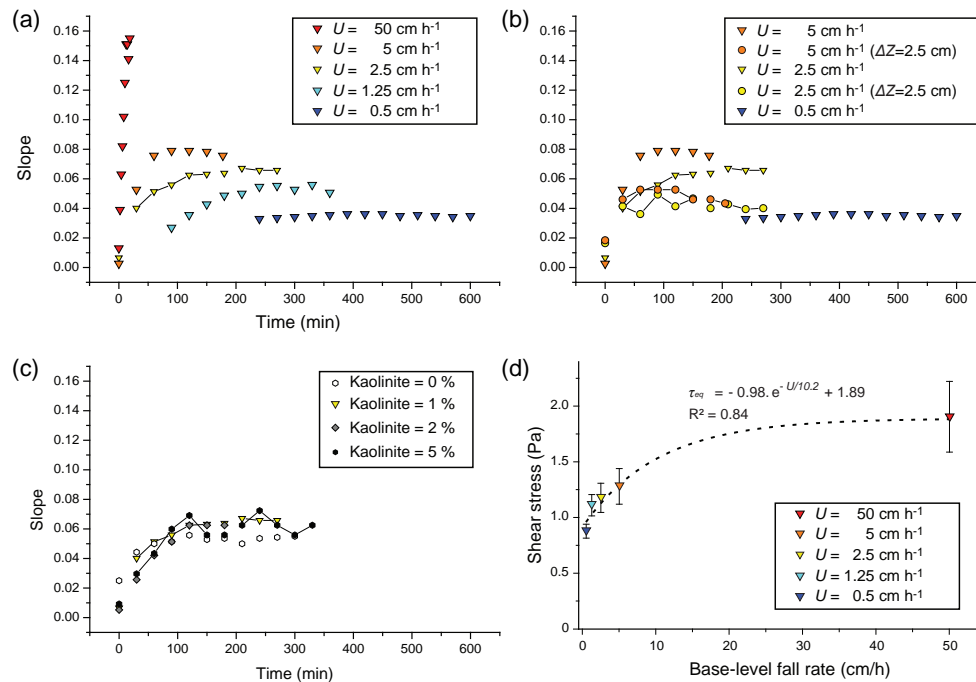


Figure 7. (a)–(c) Evolution of mean slope of the experiments with time for different sets of experiments. (a) Evolution with base-level fall rate. (b) Evolution with different base-level fall styles. For experiments 5, 7 and 8 (respectively represented by the blue triangles, yellow circles and orange circles), the minimum time between each base-level drop is 30 min. (d) Evolution of the equilibrium shear stress as a function of their base-level fall rate for experiments where $\Delta Z = 0.25$ cm. Exponential fit is shown with a dashed line.

As observed in other geomorphic physical experiments (Paola et al., 2009), the transient storage and release of sediments along the flume is responsible for self-organized dynamics that in the problem at hand delay knickpoint propagation in response to base-level fall (Figs. 4 and 5). This behavior is particularly observed when ΔZ is on the order of or lower than the flow depth (i.e., 0.25 cm; Table 1). As described for alluvial-bedrock rivers (Sklar and Dietrich, 2004), the alluvium acts as a shield for incision by knickpoint retreat and the river profile is characterized by overall diffusive removal of the sediments until it becomes too thin to shield the bedrock. However, when the incremental or cumulated base-level fall is large enough, i.e., larger than the sediment thickness, the effect of transient alluvium is less prominent, suggesting that high-magnitude external forcing is still likely to produce knickpoints (Fig. 4; Jerolmack and Paola, 2010). Hence, one directly testable outcome of this work is that offset can generate a knickpoint only when its magnitude exceeds the thickness of any alluvial layer present on the bed. The thickness of the alluvial layer sets an offset threshold for knickpoint generation. In an environment in which uplift is generated by earthquakes, we expect (1) knickpoint propagation in response to fault displacement if the offset exceeds the thickness of piedmont/alluvial deposits but (2) overall diffusion (no knickpoint) for offset is lower than the alluvial thickness. The latter therefore points to the ability of alluvial

covers to filter small-scale base-level variations that may not be recorded by knickpoint propagation.

While the rate of base-level fall (or uplift) primarily controls overall slope (Figs. 6, 7a and c; Bonnet and Crave, 2003), knickpoint characteristics are dominated by bedrock strength, which in the experiments increases with kaolinite content (Fig. 8). Earlier work has demonstrated that the critical shear stress of sand/clay mixtures increases with their clay content (Mitchener and Torfs, 1996). Hence, similar to field measurements (Cook et al., 2013), the velocity of knickpoint retreat is inversely proportional to substrate strength in our experiments. This militates against assuming that the retreat rate of knickpoints is constant over varying bedrock lithologies. Future studies investigating uplift history through inverse modeling should therefore integrate a lithological term (see Wilson et al., 2014) to simulate knickpoint or knickzone retreat rate.

Surprisingly, our 1-D experiments show that base-level variation, a key parameter studied in erosion /deposition systems, is not encoded by knickpoint height, i.e., H_p . Instead, H_p mostly goes with water discharge and bedrock strength (Bennett et al., 2000; this study). Specifically, our experiments show that, for base-level fall created by offsets, the sum of the offsets must reach a threshold ($>$ sediment thickness) to trigger a knickpoint. The experiments of Cantelli and Muto (2014) give insight into the complementary case:

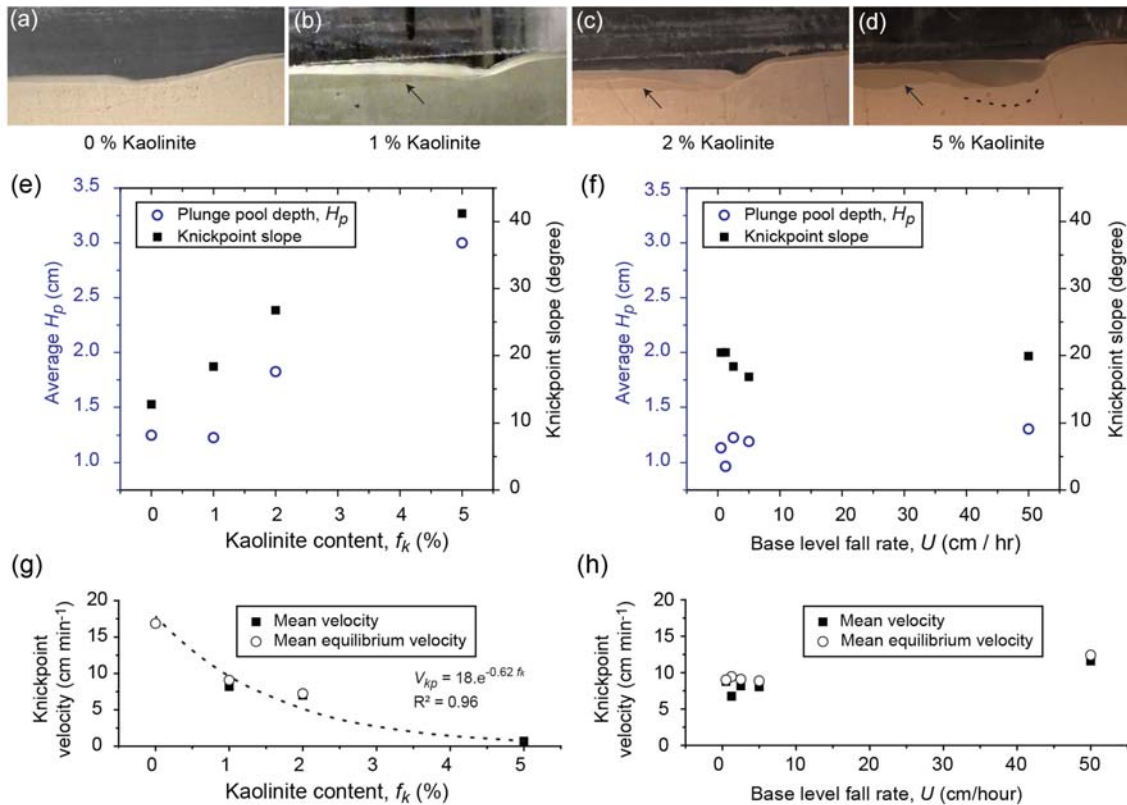


Figure 8. Knickpoint characteristics as a function of base-level fall rate and substrate. (a)–(d) Illustrations of the knickpoint shapes as a function of the kaolinite content (f_k) in the substrate. Note that the plunge pool depth could not be measured from photographs for experiment 11 ((d); $f_k = 5\%$): the substrate was so cohesive that it stuck on the walls and the bottom of the plunge pool was not accessible. H_p was, however, estimated to be ca. 3 cm on the flume during experiment 11. In this experiment, the geometry of the bed was more heterogeneous and the channel narrowed to incise the bedrock. The dashed line corresponds to the approximate bottom on the plunge pool. (e) Variations in knickpoint slope and plunge pool depth as a function of f_k . (f) Variations in knickpoint slope and plunge pool depth as a function of the base-level fall rate, U . (g) Mean knickpoint retreat velocity shown as a function of f_k . The exponential fit is represented with a dashed line. (h) Mean knickpoint retreat velocity shown as a function of U .

if the offset is too large, a series of knickpoints rather than just one is generated. Together, these findings suggest that, similar to drainage basins that tend to be regularly spaced in mountain belts (Hovius, 1996), knickpoints tend toward an optimal knickpoint shape – a kind of “unit knickpoint”. This unit knickpoint is a function of water discharge and lithology (Eq. 2), and presumably could be strongly influenced by, for example, layering in the substrate (e.g., Holland and Pickup, 1976), which is not present in our experiments and those of Cantelli and Muto. To summarize, there is no one-to-one correlation between knickpoints along river profiles and base-level events: one base-level drop can generate multiple knickpoints, but one knickpoint can also result from multiple events.

At this point, we are not able to predict theoretically the properties of unit knickpoints. Overall, plunge pool depth goes inversely with knickpoint velocity (Table 1), although there is more scatter when the lithology is constant and base-level fall rate varies (e.g., experiments 2, 3, 5 and 6). This

suggests that slow retreat of a knickpoint and associated plunge pool results in more vertical erosion of the bed by scouring and increases the plunge pool depth (see Stein and Julien, 1993). A second useful limit is the cyclic steps described by Parker (1996), which can be thought of as a train of linked unit knickpoints, and are what we observe in our experiments under rapid base-level fall (Fig. 6e). However, while Parker described these features as self-formed, the ones presented in this study are forced externally. The connection between individual knickpoints and trains of cyclic steps deserves further study; however, we note that in terms of local hydraulics and sediment motion, the knickpoints we generated function similarly to Parker’s steps, despite being solitary except in the limiting case of rapid base-level fall. Hence, the geometry of cyclic steps may provide a constraint on that of a unit knickpoint and hence a means of predicting the characteristics of knickpoints generated by specific scenarios of base-level fall. Another limit is that unit knickpoints may not be generated or preserved in the case of catas-

trophic base-level fall. This is suggested by the evolution of the Rhone Valley in response to the 1500 m drop associated with the salinity crisis in the Mediterranean Sea (Loget et al., 2006) and also in the case of a catastrophic drop simulated experimentally (A. Cantelli, personal communication, 2015).

4.2 Analysis of knickpoint distribution

The evolution of river bed and knickpoint retreat is commonly simulated numerically using a combined advection–diffusion equation (Howard and Kerby, 1983; Rosenbloom and Anderson, 1994; Whipple and Tucker, 1999; see Bressan et al., 2014). In this study, advection is observed through knickpoint generation every 3–120 min (Table 1). As a comparison, the diffusion response timescale T of the experiments can be approximated in the same way than alluvial systems, using the system (flume) length L and width W (m), the sediment discharge q_s ($\text{m}^3 \text{min}^{-1}$), and the overall equilibrium slope S (Métivier and Gaudemer, 1999; Allen, 2008).

$$T = \frac{L^2 W S}{q_s} \quad (3)$$

This timescale is 300–1400 min, i.e., longer than the period in between knickpoints. This indicates that most experiments presented in this study are dominated by knickpoint advection (except experiments 5, 7 and 8; Sect. 3.2): despite their relatively fast migration, knickpoints are generated too often to allow the stream to entirely relax by diffusion.

Erosion of the bed is usually modulated by a threshold that must be surpassed in order for the river to erode (van der Beek and Bishop, 2003; Snyder et al., 2003; Sklar and Dietrich, 2004). However, many simulations of knickpoint retreat assume that each base-level drop can generate a new knickpoint and that the initial geometry of knickpoints is offset by the base-level drop. As pointed out before, this is not reasonable if knickpoints tend to a unit form, independent of the magnitude of base-level fall. Our analysis has shown that unit knickpoints are generated when the alluvium is removed from the river bed, i.e., every time the base level reaches the bottom of the plunge pool, H_p (Figs. 4 and 5). The period between knickpoints, Δt , can then be simply approximated as a function of the base-level fall rate:

$$\Delta t = \frac{H_p}{U}. \quad (4)$$

This is supported by the comparison between knickpoint period measured from the experiments and estimated after Eq. (4) (e.g., for experiments 1, 2, 3, 5, 6, 9, 10 and 11; Fig. 9). Equation (4) can then be derived to estimate the spacing between knickpoints:

$$\Delta x = \Delta t V_{\text{kp}} = \frac{H_p}{U} V_{\text{kp}}. \quad (5)$$

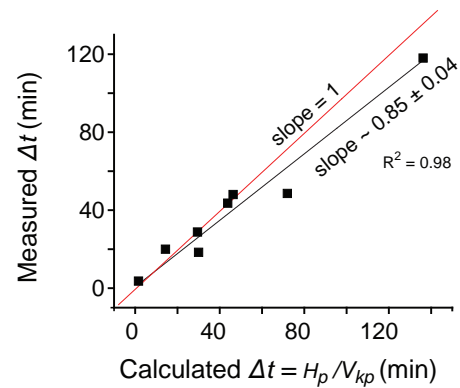


Figure 9. Comparison of the measured period between knickpoints (Δt) to the calculated period between knickpoints using Eq. (4). Linear fit of the data is shown in black.

and a dimensionless spacing is obtained when divided by the flow depth.

$$\Delta x^* = \frac{H_p}{U \cdot h} V_{\text{kp}} \quad (6)$$

These equations can be derived to simulate knickpoint generation and retreat using a rule-based model (Fig. 10). The upstream distance and elevation of the n th knickpoint, with migration velocity V_{kp} are then respectively

$$x_n = V_{\text{kp}} \cdot [t - (n - 1) \cdot \Delta t], \quad (7)$$

$$y_n = -H_p (n - 1) \cdot \Delta t. \quad (8)$$

In all simulations with a constant lithology, the upstream distance of the first knickpoint is similar, independent of the base-level fall rate (Fig. 10). Hence, rather than giving information about base-level fall rate, the position of this knickpoint allows assessment of the incipency of base-level fall within the model. In the field, this would correspond to when the base-level fall or uplift had first exceeded the thickness of alluvium within the channel.

Equation (6) and Fig. 10 also show that an increase in base-level fall rate leads to the creation of more knickpoints and that the spacing between knickpoints, Δx , is inversely proportional to base-level fall rate (e.g., Fig. 10; Eq. 4). Equation (6) therefore provides an alternative relationship for interpreting uplift or base-level fall rate from knickpoint distribution/spacing on the field. Knickpoint size (e.g., plunge pool depth) is the other critical parameter of this equation; it is strongly dependent on water discharge and substrate strength. In environments with poorly consolidated material, i.e., alluvial rivers, where substrate is strengthened only by a weak compaction or vegetation, base-level falls are quickly compensated for by the migration of close, shallow knickpoints (e.g., right side of Fig. 10). In the case of bedrock rivers (e.g., left side of Fig. 10), where the substrate is more resistant and more widely spaced, deeper knickpoints are observed indicating that the response timescale of the sediment

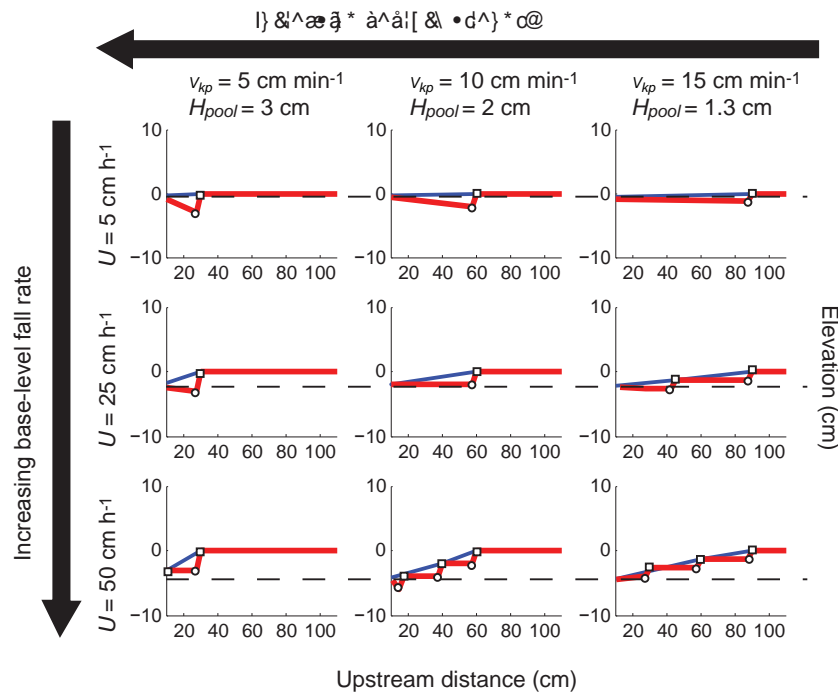


Figure 10. Snapshots of knickpoint migration calculated using Eqs. (4), (7) and (8). Each snapshot represents a simulation with a different set of parameters (U , V_{kp} , H_p) stopped after 6 min of runtime. The bedrock surface (red line) is simulated by tracking the positions of the knickpoint (white squares) and the bottom of their associated plunge pool (white circles). The alluvium surface (blue line) is shown for comparison with the experiments. The bedrock surface initial elevation is set to zero. The first knickpoint is assumed to retreat instantaneously at a velocity V_{kp} . The base-level falls at a rate U . A new knickpoint is generated each time the base level (shown by the black dashed line) reaches the depth of the plunge pool (H_p) associated with the previous retreating knickpoint. For the sake of simplicity, no diffusive processes are considered in the simulations. The water discharge and horizontal distance between knickpoints and their plunge pool bottom (2 cm) are assumed constant, while the velocity and height of unit knickpoints vary according to the main trend observed in the experiments (Table 1). The simulations are varying vertically as a function of base-level fall rate and horizontally as a function of substrate strength. This controls two parameters: when it is high, V_{kp} is low and H_p is deep, while when it is low, V_{kp} is high and H_p is shallower (Table 1).

routing system is increasingly longer. Interestingly, this behavior is the opposite of the one predicted by the analysis of Whipple (2001) that the advection response time (i.e., the time for a knickpoint to pass through a river system) is longer for alluvial (low-slope) rivers than for steeper bedrock rivers. To the extent that low-slope rivers are associated with weaker substrates, these strength variations act oppositely to the effect of slope on knickpoint propagation. At this point, without further information, the overall outcome of this competition cannot be determined.

Overall the experimental results suggest promising approaches for analyzing knickpoint dynamics as well as their spatial distribution in landscapes in relation to relative base-level fall. Figure 11 exemplifies how bedrock lithology affects knickpoint distribution on the field based on two neighboring watersheds of similar size ($25 \pm 2 \text{ km}^2$) near Duluth, Minnesota. In both watersheds, base-level history is controlled by the evolution of the level of Lake Superior during glaciation–deglaciation cycles (Wright, 1973). The major difference between the two watersheds is their bedrock lithology (Fig 11a; Fitzpatrick et al., 2006). While the stream

flowing above a loose sedimentary bedrock shows a small knickpoint located 10 km upstream (Fig. 11b), the stream flowing over a resistant gabbroic bedrock displays a big knickpoint located closer to the watershed outlet (4 km; Fig. 11c). These first-order observations are consistent with our experimental results that the increasing rock strength is favorable to the creation of bigger knickpoints whose upstream propagation is slower.

4.3 Knickpoints and waterfalls: erosion processes

Our experiments highlight the effects of sediment transport and lithology on knickpoint dynamics; a remaining challenge is to effectively link these laboratory observations to theoretical, empirical and field data. To achieve this, the mechanics and process of erosion in play must be understood and characterized. In our experiment, two erosion regimes can be observed: a background/“clear water” regime where erosion of the bed is triggered by sediment abrasion through saltation (e.g., erosion rate $\sim 0.2 \text{ mm min}^{-1}$; Sklar and Dietrich, 2004; Fig. 4c) and (ii) a waterfall regime where measured erosion

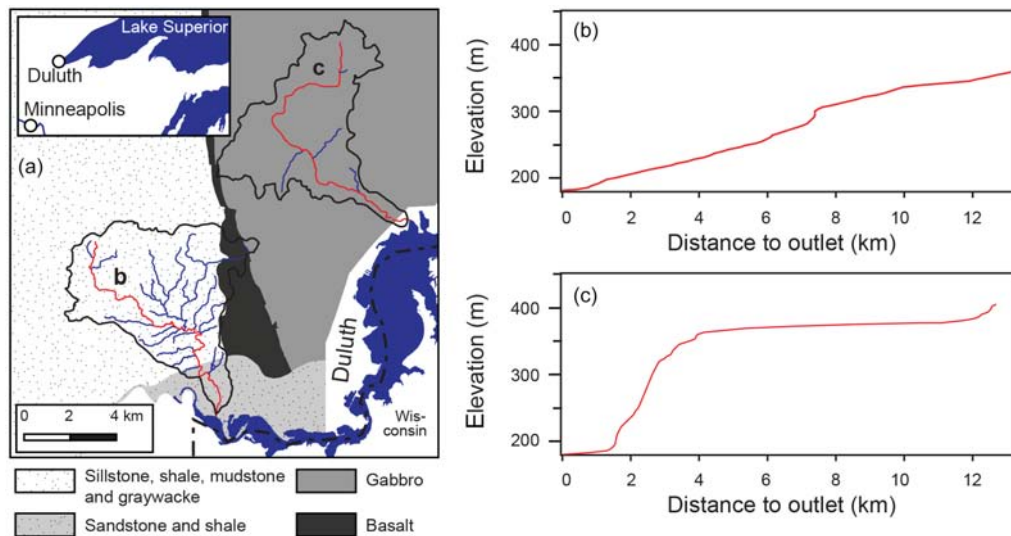


Figure 11. Morpho-geologic map showing two tributaries of the St. Louis River, close to Lake Superior shore, Duluth, Minnesota (a), and their associated long profiles: the Mission Creek (b) and Kingsbury Creek (c) rivers. Note that while the Kingsbury Creek watershed substrate is resistant gabbro, the substrate of the Mission Creek watershed is composed of loose sedimentary rocks (mainly sillstone, shale, mudstone and sandstone). The white area represents unmapped bedrock, the black line the watershed limit and the dashed line the Minnesota–Wisconsin border. Rivers are in blue. After Fitzpatrick et al. (2006). Vertical exaggeration is 20.

rate is 10 times higher ($\sim 1.5 \text{ mm min}^{-1}$; Fig. 4a and d). The turbidity observed within the plunge pool suggests that most sediments may be in suspension there, uncovering the bottom of the pool (Lamb et al., 2007) and perhaps providing abrasive tools for erosion. The steep knickpoint face is furthermore conducive to erosion rates higher than the background rate. A more accurate quantification of erosion through abrasion would, however, require detailed tracking of sediment and flow dynamics than we were able to do, particularly to identify what fraction of the sediment is transported in suspension as opposed to bedload. Our observations are indeed limited by the size of the experiment, but detailed study using advanced particle- and flow-tracking techniques such as laser holography (Toloui and Hong, 2015) in a larger facility would be a logical next step in this line of research.

Finally, we observe undercutting and collapse of the knickpoint face in the case of more resistant bedrock (2–5% kaolinite), similar to natural examples (Seidl et al., 1994; Lamb et al., 2007). In this case, we hypothesize that sediment-laden flows in the pool are able to erode backward compared to the overall flow sense due to vorticity in the pool and, potentially, the angle of incidence of the flow, which is set by the knickpoint slope. The conditions necessary for undercutting would be worth investigation in the future, for example combining physical experiments and high-resolution numerical simulations of flow and sediment transport.

5 Conclusion

Based on experimental study of the influence on knickpoint retreat of base-level fall, substrate strength and transient deposits along streams using a simple 1-D flume, we find the following:

1. Rather than being tied directly to the rate and rate distribution of base-level fall, knickpoint generation is strongly modulated by autogenic (self-organized) dynamics, consistent with other recent studies.
2. Under a constant rate of base-level fall, knickpoints of similar shape (unit knickpoints) are periodically generated. Temporary shielding of the bed by alluvium controls the spacing between these knickpoints. This shielding is, however, not efficient when base-level drops exceed alluvium thickness.
3. While the base-level fall rate controls the overall slope of experiments, it is not instrumental in dictating the major characteristics of unit knickpoints. Instead, knickpoint velocity, knickpoint face slope and associated plunge pool depth are all strongly influenced by lithology.
4. The period between knickpoints is controlled by both the alluvium thickness and the base-level fall rate that dictates how fast the alluvium is removed.

Author contributions. J.-L. Grimaud built the knickpoint flume and carried out the experiments under the supervision of C. Paola. J.-L. Grimaud developed the numerical modeling with advice from V. Voller. J.-L. Grimaud wrote the manuscript with input and corrections from C. Paola and V. Voller.

Acknowledgements. We thank Ben Erickson and Richard Christopher for their help during the flume building. We are also indebted to Alejandro Tejedor, Gary Parker, Leslie Hasbargen, Antoinette Abeyta, Aaron Buffe and Arvind Singh for fruitful discussions and suggestions, as well as to Jens Turowski and an anonymous reviewer for their input to the current version of the paper. The work was supported in part by the SAFL Industrial Consortium for Experimental Stratigraphy and the BanglaPIRE project, NSF Partnerships for International Research and Education grant IIA 09-68354.

Edited by: J. Braun

References

- Allen, P. A.: Time scales of tectonic landscapes and their sediment routing systems, in: *Earth's Dynamic Surface: Catastrophe and Continuity in Landscape Evolution*, edited by: Gallagher, K., Jones, S. J., and Wainwright, J., Special Publication Geological Society London, 7–28, 2008.
- Begin, Z. E. B., Meyer, D. F., and Schumm, S. A.: Development of longitudinal profiles of alluvial channels in response to base-level lowering, *Earth Surf. Proc. Land.*, 6, 49–68, 1981.
- Bennett, S. J., Alonso, C. V., Prasad, S. N., and Römken, M. J. M.: Experiments on headcut growth and migration in concentrated flows typical of upland areas, *Water Resour. Res.*, 36, 1911–1922, 2000.
- Bishop, P.: Long-term landscape evolution: linking tectonics and surface processes, *Earth Surf. Proc. Land.*, 32, 329–365, 2007.
- Bishop, P., Young, R. W., and McDougall, I.: Stream Profile Change and Longterm Landscape Evolution: Early Miocene and Modern Rivers of the East Australian Highland Crest, Central New South Wales, Australia, *J. Geol.*, 93, 455–474, 1985.
- Bishop, P., Hoey, T. B., Jansen, J. D., and Artza, I. L.: Knickpoint recession rate and catchment area: the case of uplifted rivers in Eastern Scotland, *Earth Surf. Proc. Land.*, 30, 767–778, 2005.
- Bonnet, S. and Crave, A.: Landscape response to climate change: Insights from experimental modeling and implications for tectonic versus climatic uplift of topography, *Geology*, 31, 123–126, doi:10.1130/0091-7613(2003)031<0123:lrtcci>2.0.co;2, 2003.
- Bressan, F., Papanicolaou, A. N., and Abban, B.: A model for knickpoint migration in first- and second-order streams, *Geophys. Res. Lett.*, 41, 4987–4996, doi:10.1002/2014GL060823, 2014.
- Brush, L. M. and Wolman, M. G.: Knickpoint behavior in noncohesive material: a laboratory study, *Geol. Soc. Am. Bull.*, 71, 59–74, doi:10.1130/0016-7606(1960)71[59:kbinma]2.0.co;2, 1960.
- Cantelli, A. and Muto, T.: Multiple knickpoints in an alluvial river generated by a single instantaneous drop in base level: experimental investigation, *Earth Surf. Dynam.*, 2, 271–278, 2014.
- Cook, K. L., Turowski, J. M., and Hovius, N.: A demonstration of the importance of bedload transport for fluvial bedrock erosion and knickpoint propagation, *Earth Surf. Proc. Land.*, 38, 683–695, 2013.
- Crosby, B. T. and Whipple, K. X.: Knickpoint initiation and distribution within fluvial networks: 236 waterfalls in the Waipaoa River, North Island, New Zealand, *Geomorphology*, 82, 16–38, doi:10.1016/j.geomorph.2005.08.023, 2006.
- Fitzpatrick, F. A., Pepler, M. C., DePhilip, M. M., and Lee, K. E.: *Geomorphic Characteristics and Classification of Duluth-Area Streams*, Minnesota, US Geological Survey Sci. Invest. Rep., available at: <http://pubs.usgs.gov/sir/2006/5029/> (last access: 21 December 2015), 5029, 62 pp., 2006.
- Frankel, K. L., Pazzaglia, F. J., and Vaughn, J. D.: Knickpoint evolution in a vertically bedded substrate, upstream-dipping terraces, and Atlantic slope bedrock channels, *Geol. Soc. Am. Bull.*, 119, 476–486, doi:10.1130/b25965.1, 2007.
- Gardner, T. W.: Experimental study of knickpoint and longitudinal profile evolution in cohesive, homogeneous material, *Geol. Soc. Am. Bull.*, 94, 664–672, doi:10.1130/0016-7606(1983)94<664:esokal>2.0.co;2, 1983.
- Gasparini, N. M., Bras, R. L., and Whipple, K. X.: Numerical modeling of non-steady-state river profile evolution using a sediment-flux-dependent incision model, in: *Tectonics, climate and landscape evolution*, edited by: Willett, S., Hovius, N., Brandon, M., and Fisher, D., GSA Special Paper, Geological Society of America, 127–141, 2006.
- Grimaud, J.-L., Chardon, D., and Beauvais, A.: Very long-term incision dynamics of big rivers, *Earth Planet. Sci. Lett.*, 405, 74–84, 2014.
- Hack, J. T.: Studies of longitudinal stream profiles in Virginia and Maryland, U.S. Geol. Surv., 294-B, 45–97, 1957.
- Hasbargen, L. E. and Paola, C.: Landscape instability in an experimental drainage basin, *Geology*, 28, 1067–1070, doi:10.1130/0091-7613(2000)28<1067:lialad>2.0.co;2, 2000.
- Holland, W. N. and Pickup, G.: Flume study of knickpoint development in stratified sediment, *Geol. Soc. Am. Bull.*, 87, 76–82, doi:10.1130/0016-7606(1976)87<76:fsokdi>2.0.co;2, 1976.
- Hovius, N.: Regular spacing of drainage outlets from linear mountain belts, *Basin Res.*, 8, 29–44, 1996.
- Howard, A. D. and Kerby, G.: Channel changes in badlands, *Geol. Soc. Am. Bull.*, 94, 739–752, doi:10.1130/0016-7606(1983)94<739:ccib>2.0.co;2, 1983.
- Jerolmack, D. J. and Paola, C.: Shredding of environmental signals by sediment transport, *Geophys. Res. Lett.*, 37, L19401, doi:10.1029/2010gl044638, 2010.
- Julien, P. Y.: *Erosion and Sedimentation*, Cambridge University Press, 280 pp., 1998.
- Ku, H. H.: Notes on the use of propagation of error formulas, *J. Res. Natl. Bur. Stand.*, 70C, 263–273, doi:10.6028/jres.070c.025, 1966.
- Lamb, M. P., Howard, A. D., Dietrich, W. E., and Perron, J. T.: Formation of amphitheater-headed valleys by waterfall erosion after large-scale slumping on Hawai'i, *Geol. Soc. Am. Bull.*, 119, 805–822, doi:10.1130/b25986.1, 2007.
- Loget, N., Davy, P., and Van Den Driessche, J. C. F.: Mesoscale fluvial erosion parameters deduced from modeling the Mediterranean sea level drop during the Messinian (late Miocene), *J. Geophys. Res.-Earth*, 111, F03005, doi:10.1029/2005JF000387, 2006.

- Métivier, F. and Gaudemer, Y.: Stability of output fluxes of large rivers in South and East Asia during the last 2 million years: implications on floodplain processes, *Basin Res.*, 11, 293–303, doi:10.1046/j.1365-2117.1999.00101.x, 1999.
- Miller, J. R.: The Influence of Bedrock Geology on Knickpoint Development and Channel-Bed Degradation along Downcutting Streams in South-Central Indiana, *J. Geol.*, 99, 591–605, 1991.
- Mitchener, H. and Torfs, H.: Erosion of mud/sand mixtures, *Coastal Eng.*, 29, 1–25, 1996.
- Paola, C., Straub, K., Mohrig, D., and Reinhardt, L.: The “unreasonable effectiveness” of stratigraphic and geomorphic experiments, *Earth-Sci. Rev.*, 97, 1–43, 2009.
- Parker, R. S.: Experimental Study of Drainage Basin Evolution and Its Hydrologic Implications, *Hydrology papers*, Colorado State University, Fort Collins, 85 pp., 1977.
- Parker, G.: Some speculations on the relation between channel morphology and channel-scale flow structures, in: *Coherent Flow in Open Channels*, edited by: Ashworth, P., Bennet, S., Best, J. L., and McLelland, S., John Wiley & Sons, New York, 429–432, 1996.
- Pederson, J. L. and Tressler, C.: Colorado River long-profile metrics, knickzones and their meaning, *Earth Planet. Sc. Lett.*, 345–348, 171–179, doi:10.1016/j.epsl.2012.06.047, 2012.
- Rosenbloom, N. A. and Anderson, R. S.: Hillslope and channel evolution in a marine terraced landscape, Santa Cruz, California, *J. Geophys. Res.-Sol. Ea.*, 99, 14013–14029, 1994.
- Seidl, M. A., Dietrich, W. E., and Kirchner, J. W.: Longitudinal Profile Development into Bedrock: An Analysis of Hawaiian Channels, *J. Geol.*, 102, 457–474, 1994.
- Sklar, L. S. and Dietrich, W. E.: Sediment and rock strength controls on river incision into bedrock, *Geology*, 29, 1087–1090, doi:10.1130/0091-7613(2001)029<1087:sarsco>2.0.co;2, 2001.
- Sklar, L. S. and Dietrich, W. E.: A mechanistic model for river incision into bedrock by saltating bed load, *Water Resour. Res.*, 40, W06301, doi:10.1029/2003WR002496, 2004.
- Snyder, N. P.: Channel response to tectonic forcing; field analysis of stream morphology and hydrology in the Mendocino triple junction region, Northern California, *Geomorphology*, 53, 97–127, 2003.
- Stein, O. and Julien, P.: Criterion Delineating the Mode of Headcut Migration, *J. Hydraul. Eng.*, 119, 37–50, doi:10.1061/(ASCE)0733-9429(1993)119:1(37), 1993.
- Toloui, M. and Hong, J.: High fidelity digital inline holographic method for 3D flow measurements, *Opt. Express*, 23, 27159–27173, 2015.
- van der Beek, P. and Bishop, P.: Cenozoic river profile development in the Upper Lachlan catchment (SE Australia) as a test of quantitative fluvial incision models, *J. Geophys. Res.*, 108, 2309, doi:10.1029/2002jb002125, 2003.
- Whipple, K. X. and Tucker, G. E.: Dynamics of the stream-power river incision model; implications for height limits of mountain ranges, landscape response timescales, and research needs, *J. Geophys. Res.*, 104, 17661–17674, 1999.
- Whipple, K. X.: Fluvial Landscape Response Time: How Plausible Is Steady-State Denudation?, *Am. J. Sci.*, 301, 313–325, doi:10.2475/ajs.301.4-5.313, 2001.
- Whipple, K. X.: Bedrock rivers and the geomorphology of active orogens, *Annu. Rev. Earth and Planet. Sci.*, 32, 151–185, 2004.
- Wilson, J. W. P., Roberts, G. G., Hoggard, M. J., and White, N. J.: Cenozoic epeirogeny of the Arabian Peninsula from drainage modeling, *Geochem., Geophys., Geosyst.*, 15, 3723–3761, 2014.
- Wright, H. E.: Tunnel Valleys, Glacial Surges, and Subglacial Hydrology of the Superior Lobe, Minnesota, *Geol. Soc. Am. Mem.*, 136, 251–276, doi:10.1130/MEM136-p251, 1973.

Cenozoic sediment budget of West Africa and the Niger delta

Jean-Louis Grimaud,*¹ Delphine Rouby,* Dominique Chardon*[†] and Anicet Beauvais[‡]

*Géosciences Environnement Toulouse, CNRS, IRD, UPS, CNES, Université de Toulouse, F-31400 Toulouse, France

[†]IRD and Département des Sciences de la Terre, Université Ouaga I Professeur Joseph Ki-Zerbo, 01 PB 182 Ougadougou 01, Burkina Faso, West Africa

[‡]Aix-Marseille Univ, CNRS, IRD, Coll France, CEREGE, BP 80, 13545 Aix-en-Provence, Cedex 4, France

ABSTRACT

Long-term (10^{6-7} yr) clastic sedimentary fluxes to the ocean provide first-order constraints on the response of continental surfaces to both tectonic and climatic forcing as well as the supply that builds the stratigraphic record. Here, we use the dated and regionally correlated relict lateritic landforms preserved over Sub-Saharan West Africa to map and quantify regional denudation as well as the export of main catchments for three time intervals (45–24, 24–11 and 11–0 Ma). At the scale of West Africa, denudation rates are low (*ca.* 7 m Myr⁻¹) and total clastic export rate represents 18.5×10^3 km³ Myr⁻¹. Export rate variations among the different drainage groups depend on the drainage area and, more importantly, rock uplift. Denuded volumes and offshore accumulations are of the same magnitude, with a noticeably balanced budget between the Niger River delta and its catchment. This supports the establishment of the modern Niger catchment before 29 Ma, which then provided sufficient clastic material to the Niger delta by mainly collecting the erosion products of the Hoggar hotspot swell. Accumulations on the remaining Equatorial Atlantic margin of Africa suggest an apparent export deficit but the sediment budget is complicated by the low resolution of the offshore data and potential lateral sediment supply from the Niger delta. Further distortion of the depositional record by intracontinental transient storage and lateral input or destabilization of sediments along the margin may be identified in several locations, prompting caution when deducing continental denudation rates from accumulation only.

INTRODUCTION

Clastic sediments fluxes represent the bulk terrigenous supply to oceanic basins derived from the dissection and erosion of continental surfaces (Fig. 1). They build the sedimentary record along continental margins over geological timescale (10^{5-7} yr) and, together with chemical fluxes, contribute to the global biogeochemical cycles. The stratigraphic record may allow retrieving paleoenvironmental information such as the climatic variations, landform evolution and vertical movements on the adjacent continental domains (Burbank, 1992; Molnar, 2004; Clift, 2010), documenting the long-term response of

landscapes to external forcing. Comprehensible clastic fluxes are therefore first-order data to geomorphologists, sedimentologists and geodynamicists to decipher sediment production, transfer and deposition in its ultimate basin sinks (Allen, 2008; Fig. 1).

Clastic fluxes are usually obtained from sedimentary basin accumulations (e.g. Rust & Summerfield, 1990; Métivier *et al.*, 1999; Guillocheau *et al.*, 2012). Stratigraphy alone, however, lacks information about catchment evolution (Bishop, 1995) and distribution of erosion within the source region. Furthermore, temporary storage and later erosion of sediments may delay or erase stratigraphic information (Sadler, 1981; Métivier & Gaudemer, 1999; Jerolmack & Paola, 2010). Sediment fluxes predicted from landscape evolution models are calibrated at macro- to mesoscale (m² to km²) and short term (10^{1-4} yr), and may not be representative of large continental surfaces ($>10^4$ km²) evolving at geological timescale (Simoes *et al.*, 2010). Sediment budgets comparing source and sink are therefore the most meaningful to

Correspondence: J.-L. Grimaud, Géosciences Environnement Toulouse, Université de Toulouse, CNRS, IRD, UPS, CNES, F-31400 Toulouse, France. E-mail: jean-louis.grimaud@mines-paristech.fr

¹Present address: MINES ParisTech, PSL Research University, Centre de Géosciences, 35 rue St Honoré, 77305 Fontainebleau Cedex, France

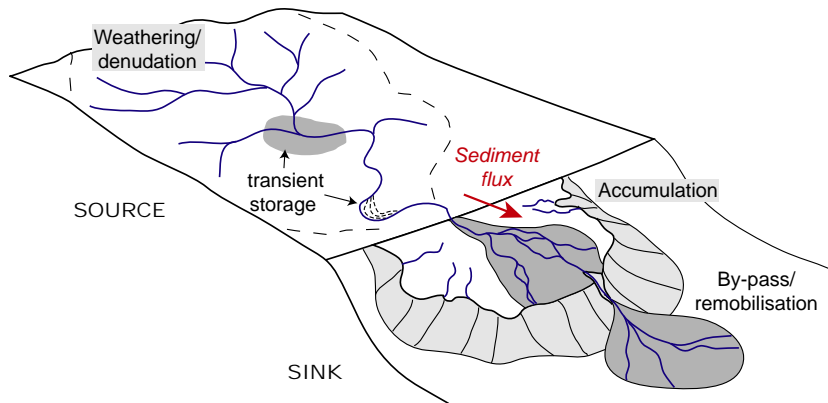


Fig. 1. Schematic representation of a source-to-sink system with the riverine transport of sediment from the continent to the ocean. The figure focuses on the clastic flux and does not represent the solute load.

understand relief dynamics at geological timescales but are limited by the lack of constraints on the source catchments and require making assumptions on their topographic and drainage evolution (e.g. Leturmy *et al.*, 2003; Campanile *et al.*, 2008; Rouby *et al.*, 2009; Macgregor, 2013). Better constraints on continent-scale surface evolution are required to calibrate long-term clastic fluxes and the associated sedimentary basin evolution.

Cratons represent low-lying, slowly eroding domains (Bishop, 2007; Beauvais & Chardon, 2013) but integrate large continental catchments (i.e. 10^6 km²; Fig. 2). Cratons are the source of major clastic accumulations over long-lasting segments of passive margins in Africa and worldwide, hosting extensive sediment archives as well as hydrocarbon resources (Bradley, 2008). The slow erosion rates of cratons result in the preservation of geomorphic markers as illustrated by the relicts of lateritic landscapes of tropical shields derived from Meso-Cenozoic intense weathering periods associated with warm climate (Tardy & Roquin, 1998; Zachos *et al.*, 2001; Beauvais & Chardon, 2013; Fig. 3). Quantifying erosion using these relict landforms has proven useful to apprehend the denudation rates and landform evolution of cratonic sediment routing systems (Beauvais & Chardon, 2013; Grimaud *et al.*, 2015).

This study presents a comparison between the volumes eroded and exported from the main catchments of Sub-Saharan West Africa and the sediments preserved in the adjoining continental margin basins of the Equatorial Atlantic Ocean during the Cenozoic. We use relict lateritic landforms and recently published paleodrainage maps (Chardon *et al.*, 2016) to constrain continental clastic exports, and a measure of offshore accumulations. We compare accumulation with erosion between the Niger delta and its catchment and between the remaining portion of the Equatorial Atlantic margin of Africa (i.e. without the Niger delta) and its sources. Accumulated and eroded volumes fall within the same range allowing discussion of the influence of rock uplift, catchment evolution and sediment transfers on sediment budgets.

GEOLOGICAL SETTING AND EARLIER WORK

The studied area comprises a 4×10^6 km² cratonic surface extending from the Senegal-Mauritania basin to the west and to the Hoggar and Adamaoua massifs to the northeast and southeast respectively (Fig. 2). Major river systems (the Niger, Senegal and Volta rivers) currently collect sediment supplied to the continental margin basins of this domain. The Niger catchment (2.3×10^6 km²) drains the main topographic massifs: the Guinean rise, the southern Hoggar massif and the Jos plateau and the Adamaoua massif bounding the Benue trough (Fig. 2). At the outlet, the Niger delta surface is 26×10^3 km² and its Cenozoic sediment thickness exceeds 9 km (Fig. 2). In contrast, the remaining portion of the Equatorial Atlantic of Africa (i.e. excluding the Niger delta; Fig. 2), fed by rivers such as the Volta, has a larger basin surface (750×10^3 km²) and a thinner Cenozoic sediment cover (<3 km; Helm, 2009).

The West African bedrock is composed of Archean and Paleoproterozoic basement bounded by mobile belts of Panafrican (*ca.* 800–450 Ma) and Variscan (*ca.* 360–250 Ma) ages (Villeneuve, 2005; Feybesse *et al.*, 2006). It is overlain by Neoproterozoic to Phanerozoic sedimentary series, the main depocenter of which is located in the Taoudeni basin (Villeneuve, 2005; Fig. 2). Cenozoic sedimentary series preserved onshore include Eocene carbonates found in the Senegal-Mauritania, Iullemeden and Togo-Benin basins overlain by Lutetian to Rupelian (49–29 Ma) continental deposits known as the Continental Terminal (Chardon *et al.*, 2016). Sub-Saharan West Africa is considered as tectonically stable since Late Cretaceous rifting in the Iullemeden, Chad and Benue basins, and has mostly undergone long-wavelength lithospheric deformation since (Ye *et al.*, 2017 and references therein). The Central Atlantic Ocean opened since the Late Triassic and the Equatorial Atlantic during the Late Early Cretaceous (Brownfield & Charpentier, 2006; Moulin *et al.*, 2010; Labails *et al.*, 2010; Ye *et al.*, 2017; Fig. 2). The offshore Cenozoic stratigraphic record in

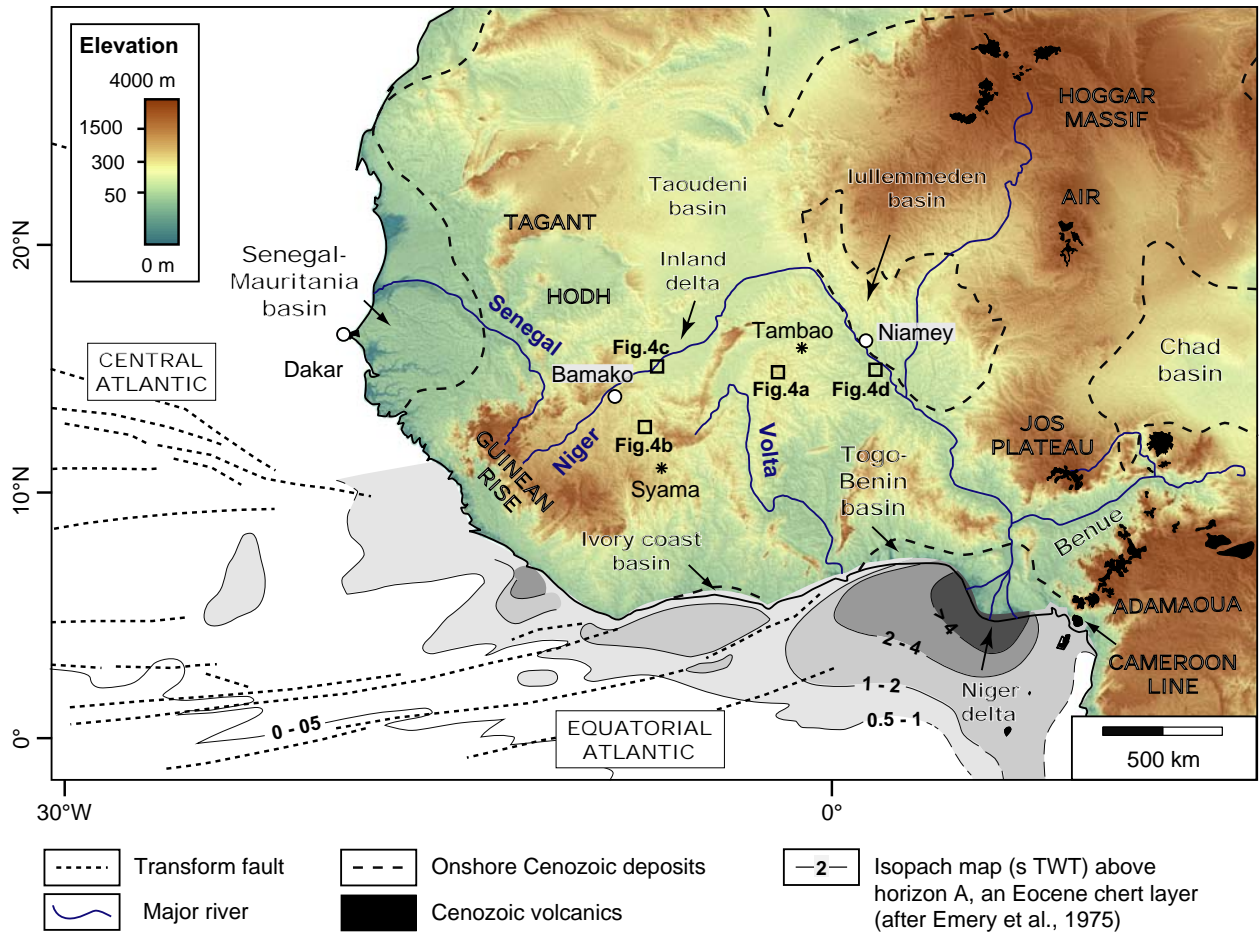


Fig. 2. Map showing the main geologic and morphologic features of Sub-Saharan West Africa modified after Grimaud *et al.* (2014). The offshore accumulation map of Emery *et al.* (1975) does not cover the Central Atlantic margin of Africa (i.e. offshore Senegal-Mauritania basin).

West Africa is characterized by a shift in sedimentation during the Oligocene. The Paleocene-Eocene was a period of relatively high sea level, intense inland weathering and preferential deposition of chemical sediments (i.e. carbonates and phosphates) in the intracratonic and marginal basins (Fig. 3) (Millot, 1970; Valetton, 1991). The Oligo-Miocene period marked the increase in clastic sedimentation in continental basins and adjacent passive margins (Séranne, 1999; Burke *et al.*, 2003). A paleo-Niger delta was likely established in the Benue during the Paleocene (Reijers, 2011), but the main delta progradation started at 34 Ma (Doust & Omatsola, 1990). In the literature, the Oligocene shift in sedimentation has been interpreted as resulting from either the effect of greenhouse to icehouse climatic transition (Séranne, 1999) or to the continental uplift of Africa contemporaneous with the development of its “basin-and-swell” topography driven by the growth of several hotspot swells such as the Hoggar, the Adamaoua or the Jos Plateau (Burke, 1976, 1996; Burke

et al., 2003; Fig. 2). Using the reconstructed geometries of dated paleolandscapes, Chardon *et al.* (2016) suggested the establishment of the modern Niger River watershed in, at least, the Late Oligocene (29 Ma) and possibly the Eocene-Oligocene boundary (34 Ma), that is, at the acceleration of the progradation of the Niger delta. The major drainage reorganization and the growth of the Hoggar hot spot swell would explain the increase in clastic fluxes towards the Niger delta (Chardon *et al.*, 2016). Post-Eocene clastic fluxes would also have been increased by uplift-related erosion along a marginal upwarp inherited from Mesozoic rifting that extended from the Jos Plateau to the Guinean rise (Beauvais & Chardon, 2013). The marginal upwarp is a 300–800 km wide strip of relief, running parallel to the coast. It is interpreted as initiating during the rifting and maintained by lithosphere flexure, erosional unloading and associated sediment loading on the adjoining margin (Gilschrist & Summerfield, 1990; Beaumont *et al.*, 2000).

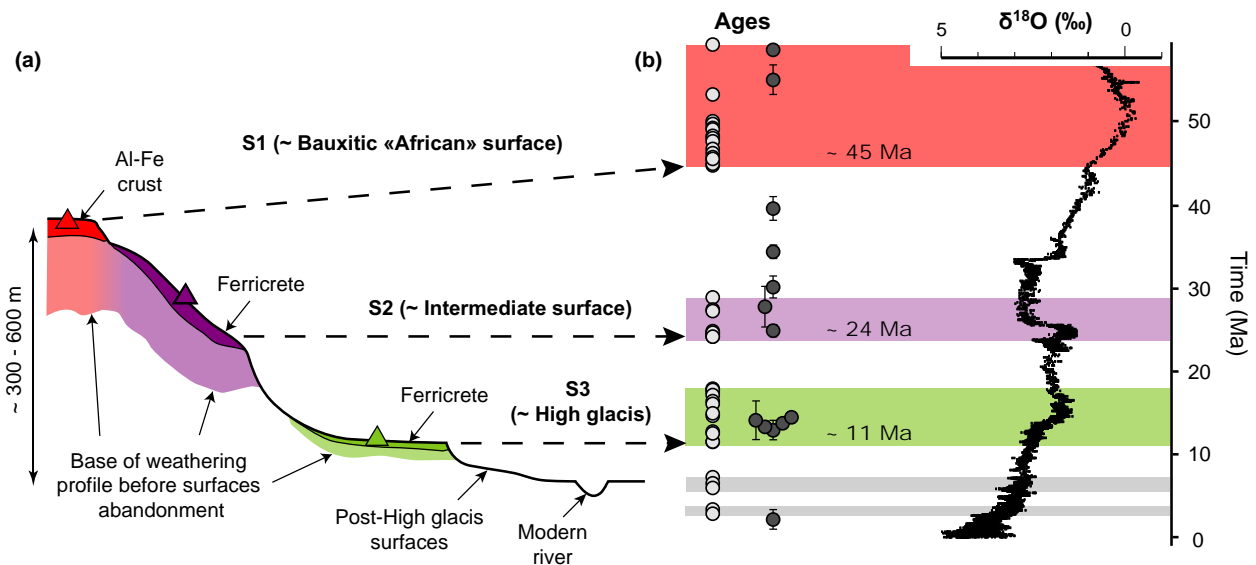


Fig. 3. Denudation chronology of Sub-Saharan West Africa during the Cenozoic. [a] Distribution of lateritic paleolandscapes and associated regoliths (weathering mantles and associated duricrusts) in the landscape. [b] Comparison of the ages acquired in the lateritic mantles of Tambaou and Syama, (Fig. 2) [after Beauvais *et al.* (2008) (light grey dots) and Vasconcelos *et al.* (1994a) (dark grey dots) respectively] to the oceanic $\delta^{18}\text{O}$ variation (‰) on benthic foraminifera tests recording global temperature variations (Zachos *et al.*, 2001). Only the ages with an uncertainty lower than 5 Myr have been reported in Syama (dark grey dots).

DENUATION CHRONOLOGY

Sub-Saharan West Africa was located within the tropical belt throughout the Cenozoic, allowing several generations of lateritic regoliths to be produced regionally. Rivers removed parts of these regoliths to form a unique geomorphic sequence of stepped paleolandscapes capped by duricrusts (Michel, 1973; Fig. 3a). These landscapes were not subcontinental flat planation surfaces as advocated by King (1962) but composite landscapes, the relief of which increased throughout the Cenozoic (Figs 4 and 5; Beauvais & Chardon, 2013; Grimaud, 2014; Grimaud *et al.*, 2015). Each member of the sequence has a specific morphology and type-regolith that reflect variation in weathering intensity and slope erosion processes (Boulangé *et al.*, 1973; Grandin, 1976; Tardy & Roquin, 1998). This allows for correlations of each type of paleolandscape remnant on a regional scale (e.g. Fig. 4; Beauvais & Chardon, 2013; Grimaud *et al.*, 2014). The regolith formed by lateritic weathering of the bedrock during long ($>10^6$ yr), warm and humid climatic periods (Fig. 3b). Weathering resulted in leaching of mobile elements and the accumulation of less mobile iron and/or aluminium in the shallow depths of the regolith profiles. Ultimately, the duricrusting of the upper horizons occurred when the weathering profiles became disconnected from the local base levels (i.e. following river incision and/or the return to drier climatic conditions). Hence, the terminal weathering age of a regolith profile capped by a duricrust is considered as marking the abandonment of the associated paleosurface (i.e. Fig. 3).

The first member of the West Africa geomorphic sequence (S1; Fig. 3) is a surface of continental scale, known as the “African Surface”, formed under a humid equatorial climate from the Late Cretaceous to the Eocene (Beauvais & Chardon, 2013; Chardon *et al.*, 2006). Weathering shaped a low-relief landscape and formed bauxites (i.e. Al-Fe crust; Figs 3 and 4). The S1 bauxite was abandoned to form an incised landscape during the development of the next member of the sequence, the so-called “Intermediate” surface (S2; Fig. 3), ultimately capped by a ferricrete. The S2 surface was dissected and abandoned during the development of the S3 erosion surface (“High glacis” in the French literature). S3 is a pediment, that is, a gently sloping concave-upward surface, formed under semi-arid to arid climate during which stable base level and high seasonality favour surface sheetwash during the monsoon (Hadley, 1967; Grandin, 1976). Ferricretes capping S3 formed under more contrasted humid conditions (Fig. 3b). S3 ferricrete often cements a detrital layer that contains clasts of S1 and S2 crusts (Boulangé *et al.*, 1973; Grandin, 1976; Grimaud *et al.*, 2015). Hence, S1, S2 and S3 remnants have first order distinctive landform–regolith associations that allow for regional correlation (Beauvais & Chardon, 2013; Grimaud *et al.*, 2014).

Ages of laterite formation were bracketed by ^{40}Ar – ^{39}Ar dating of supergene K-rich Mn oxides such as cryptomelane $[\text{K}_x(\text{Mn}^{3+})_x(\text{Mn}^{4+})_{8-x}\text{O}_{16}]$ in Tambaou, Burkina Faso (Beauvais *et al.*, 2008) and sulphates as alunite/jarosite in Syama, Mali (Vasconcelos *et al.*, 1994a; Fig. 3b). These minerals formed under weathering and oxidation

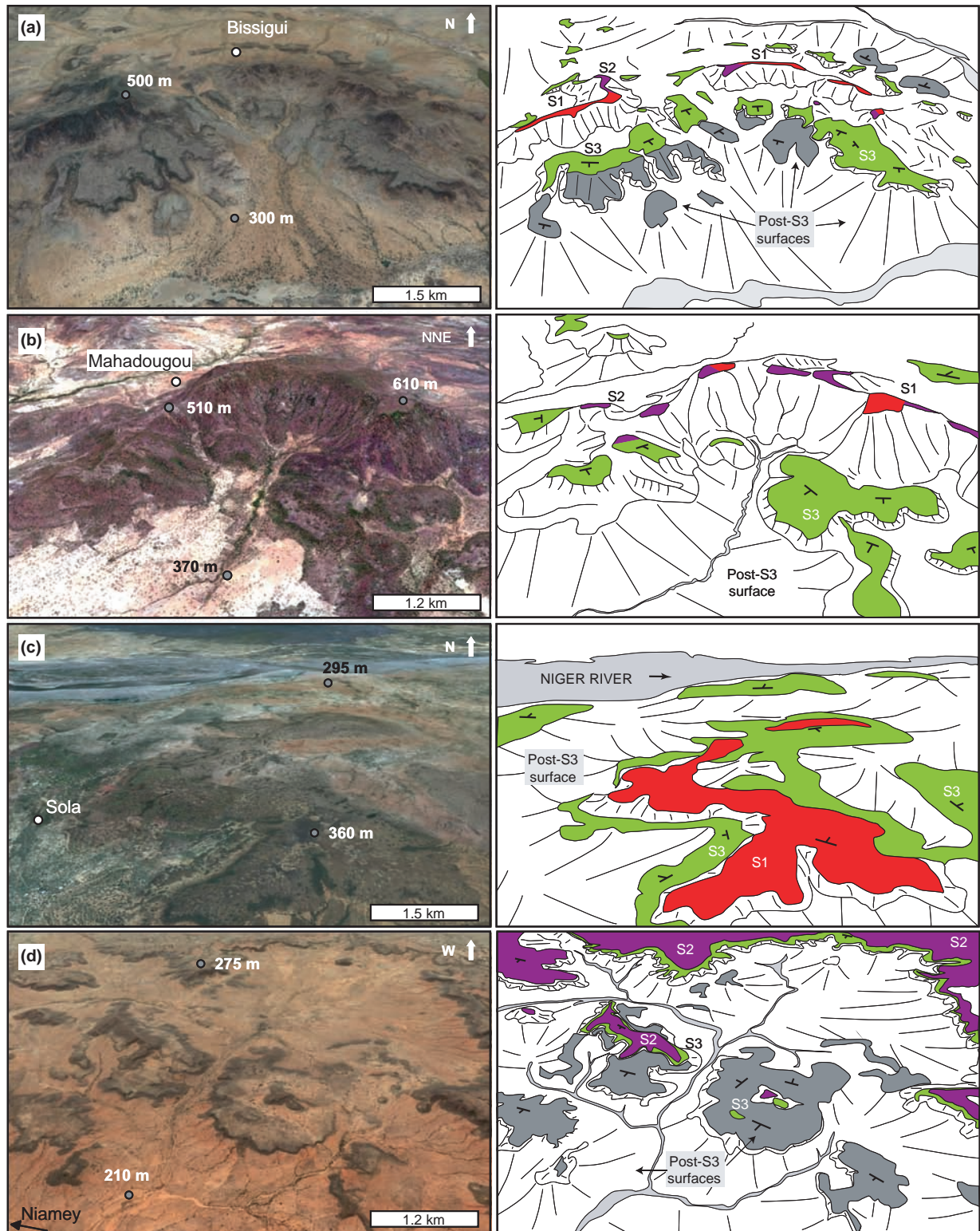
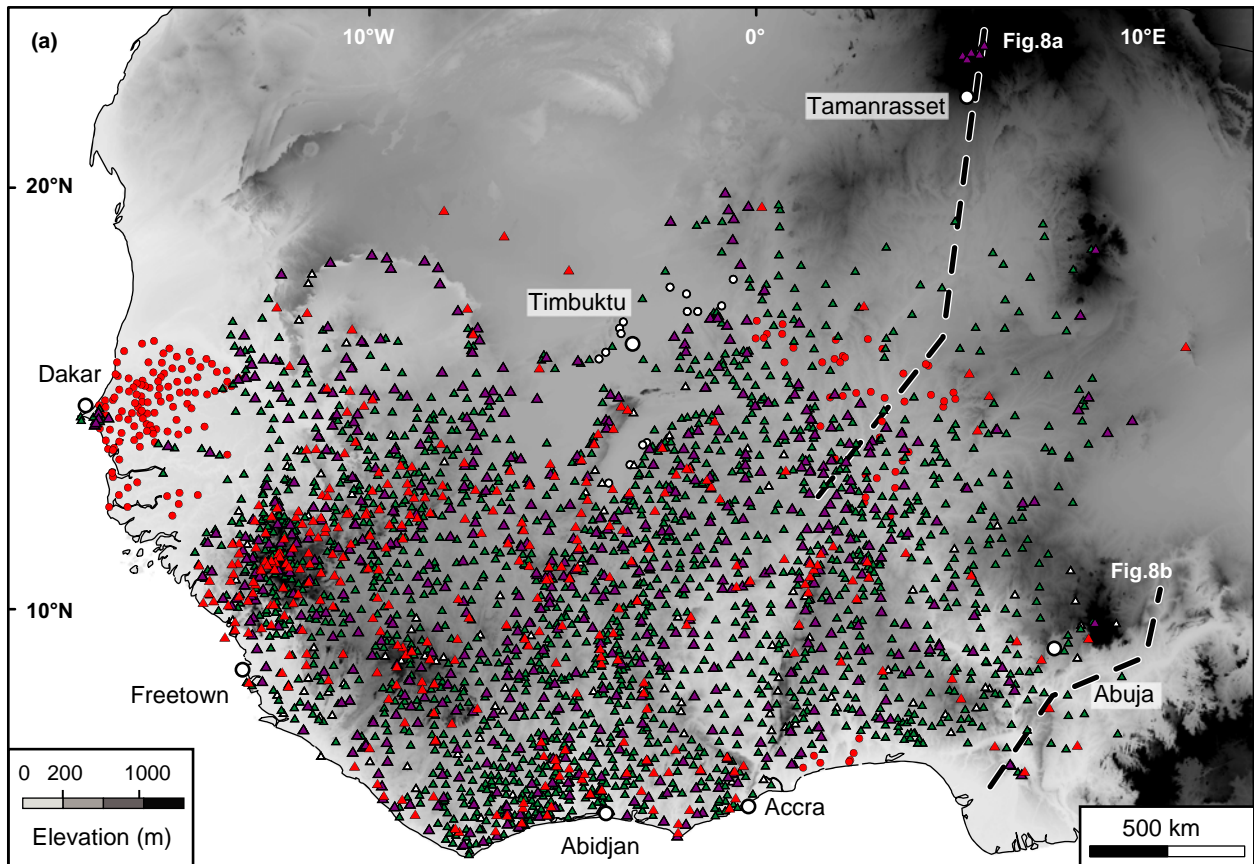
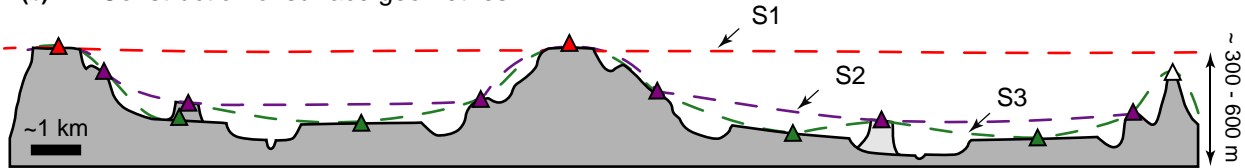


Fig. 4. Interpretation of paleolandsurface distribution after our field work in several type-locations in West Africa (see location on Fig. 2). Google-Earth view and interpretation of paleosurface distribution: [a] over the Precambrian basement, South of Tambaou (Burkina Faso); [b] over the Precambrian basement near the Manding Mountains (Mahadougou, Mali); [c] in the Niger inland delta, North of Bamako (Ségou, Mali) where bauxitic remnants are found 60 m above the Niger River; [d] in the Iullemmeden basin (North of Niamey, Niger) where the deposits of the “Continental Terminal”, capped with the Intermediate surface, have been incised by the Niger River system. The colour code of relict landforms interpretations is similar to Fig. 3.



(b) Construction of surface geometries



(c) Constraints in inland alluvial plains and sedimentary basins

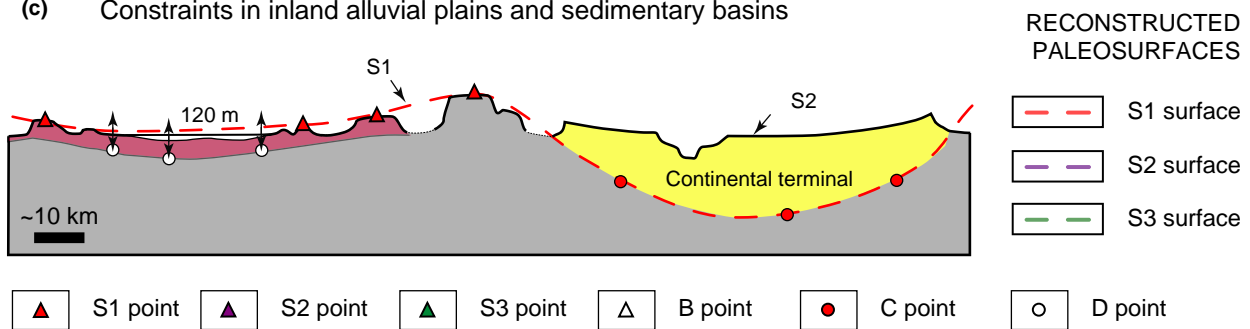


Fig. 5. [a] Map of the *ca.* 2900 data points used to build the 3D surfaces. [b] Schematic distribution of relict landforms and reconstructed surface geometries. [c] Schematic distribution of data points constraining the construction of surface geometries in alluvial plains and sedimentary basins. B points correspond to bedrock massifs summit (referred as “inselbergs”), C points to the top of Early-Mid Eocene carbonates and D points to S1 weathering profile remnants. B points inselbergs are often associated with eroded S1 weathering profiles. B points therefore constrain S1 minimum elevation. C points are time equivalents of S1 bauxite retrieved from well log in sedimentary basins. We used them as depth of S1 below the topography in these basins. D points constrain locally the elevation of S1 paleosurface, which have been eroded, on the basis that a bauxitic weathering profile cannot exceed the maximum depth of 120 m (Bardossy & Aleva, 1990).

conditions converting the bedrock into lateritic regolith and are therefore useful tracers of major weathering periods and associated formation of duricrusted surfaces. The S1 surface was abandoned after 45 Ma, S2 after 24 Ma and S3 after 11 Ma (Beauvais & Chardon, 2013; see also Grimaud *et al.*, 2015; Figs 3 and 4). The radiometric ages of the West African geomorphic sequence (Fig. 3b) are consistent with other time constraints. The weathering of the bauxitic paleoland surface is correlated with chemical marine sedimentation in Sub-Saharan West Africa during the Early-Mid Eocene interval (Millot, 1970), while the S2 ferricrete caps the weathering profiles developed upon Late Eocene-Oligocene “Continental Terminal” alluvial deposits (Chardon *et al.*, 2016).

MEASURE OF CONTINENTAL DENUDATION AND SEDIMENT EXPORT

Regional distribution and mapping of lateritic relict landforms

We referenced S1, S2 and S3 relicts over West Africa (Fig. 5) using a combination of fieldwork (in Benin, Burkina Faso, Mali, Niger, Guinea and Senegal), descriptions from existing literature (e.g. Newill & Dowling, 1968; Fölster, 1969; Eschenbrenner & Grandin, 1970; Boulangé & Eschenbrenner, 1971; Boulangé *et al.*, 1973; Michel, 1973, 1977a,b; Grandin & Hayward, 1975; Burke, 1976; Grandin, 1976; Fritsch, 1978; Thomas, 1980, 1994; Rognon *et al.*, 1983; Adegoké *et al.*, 1986; Bowden, 1987; Boulangé & Millot, 1988; Durotoye, 1989; Teeuw, 2002; Chardon *et al.*, 2006) (recent compilations in Beauvais & Chardon, 2013; Grimaud, 2014) and combined analyses of topography and satellite images. Field stations and the full compilation of the references can be found in the Appendix S1. We identified and reported the elevation of S1, S2 and S3 remnants based on their geomorphology and regolith type (see below). In order to further constrain the regional geometries of the surfaces, we also surveyed additional data such as topographic massifs summits (B points), Early-Mid Eocene carbonates (C points) and lower parts of S1 weathering profile remnants (D points) (Chardon *et al.*, 2016). Figure 5 illustrates how these data points were used to reconstruct surface geometries.

S1 relicts dominate West African landscapes in the form of bauxitic mesas capped by a flat duricrust of beige to pink colour reflecting the presence of aluminum (Figs 4a and 5b). In the Guinean rise and eastward (i.e. upwarp domain; Fig. 2), the S1 relicts are preserved 400–600 m above modern rivers (see Beauvais & Chardon, 2013). This local relief decreases towards the coast and the continental interiors, where S1 relicts are <60 m above the Niger River in the Inland Niger delta (Grimaud *et al.*, 2014; Figs 2 and 4c).

S2 ferricretes have red-purple colours on satellite images due to their high iron content and a morphological aspect different from S1 and S3 (Figs 4 and 5b). S2 relicts are usually distributed 50–200 m, and locally up to 400 m, vertically in the landscape below S1 remnants (Grandin, 1976; Beauvais & Chardon, 2013). They are either connected to bauxite relicts, forming convex-upwarp surfaces on the slopes of S1 mesas (Figs 3a and 4a, b), or occur stepped below S1 relicts. It has been shown that the elevation of S2 relicts decreases from the divides to the outlet of West African catchments, following the geometry of the main watersheds and implying that the S2 drainage was similar to the modern one (Beauvais & Chardon, 2013; Grimaud *et al.*, 2014; Chardon *et al.*, 2016; Fig. 4a, b, d).

S3 ferricretes can usually be identified in the field by their embedded conglomerate deposits and their brown to grey colour on satellite images. S3 relicts usually form gently dipping plateaus of several square kilometres in area with concave-up profiles (Figs 3a and 4). S3 plateaus are easily identified when radiating from the piedmont of S1 or S2 mesas (Fig. 4a, b). The downstream parts of S3 relicts are usually 10–100 m above modern rivers and well preserved throughout West Africa, suggesting modest post-11 Ma landscape dissection and denudation (Beauvais & Chardon, 2013; Grimaud *et al.*, 2015; Fig. 4).

Quantification of exported volumes and conversion into sediment fluxes

We estimated denudation volumes and the associated export to offshore basins using regional reconstructions of S1, S2 and S3 surface geometries, and the modern topography. S1, S2 and S3 geometries were reconstructed using the DSI method (Mallet, 1992) that allows building complex geologic surfaces (see Chardon *et al.*, 2016). By subtracting these surfaces, we obtained the S1–S2, S2–S3 and S3–modern elevation differences maps corresponding to incremental denudation maps for the 45–24, 24–11 and 11–0 Ma intervals (Fig. 6) as well as the total denudation map since 45 Ma (i.e. S1–modern map; Fig. 7). S1 and S2 surfaces geometries are those published by Chardon *et al.* (2016) and S3 surface is from this study.

The sediment volumes stored in continental sedimentary basins during the S1–S2 interval (blue colours on Fig. 6b) were subtracted to the eroded volumes to obtain the volumes exported to the continental margin (V_{ex}) (Table 1). These storage volumes were calculated between the S1 and S2 surface geometries. They are actually larger than the volumes currently preserved in the intracratonic sedimentary basins because of erosion after 24 Ma (see Fig. 8 for an illustration in the Iullemedden basin).

We developed an analysis of uncertainties on the exported volumes estimates. Overall, we found errors values around 10–30% (see Table 1 and Appendix S1). The first uncertainty was estimated for the construction of

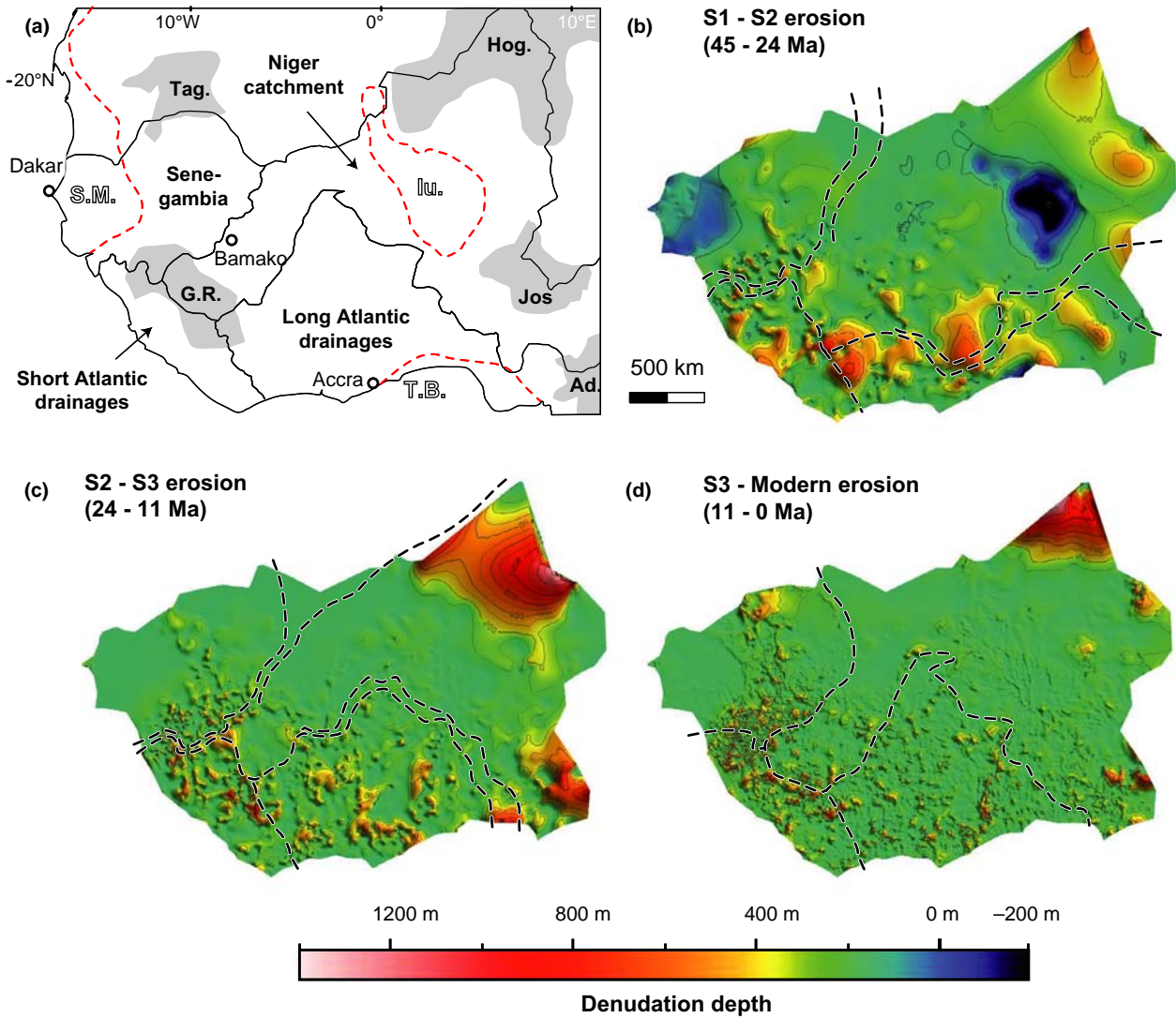


Fig. 6. [a] Simplified map of the four selected drainage groups (bounded by black lines): Senegambia drainage, Short Atlantic drainages, Long Atlantic drainages and the Niger catchment. The modern limits of the Cenozoic onshore sedimentary basins (Senegal-Mauritania [S.M.], Iullemedden [Iu.] and Togo-Benin [T.B] basins) (red dashed lines) and main topographic massifs (Tagant [Tag.], Hoggar [Hog.], Guinean Rise [G.R.] Jos plateau [Jos] and Adamaoua massif [Ad.]) (grey areas) are also shown. Denudations maps of the 45–24 Ma [b], 24–11 Ma [c] and 11–0 Ma intervals [d]. Successive divides (black dashed lines) are drawn after Chardon *et al.* (2016). Where the position of these divides was less constrained, the uncertainty area is represented between two dashed lines.

surface geometries. For that, we built replicates of the S2 and S3 surfaces, respectively, S'2 and S'3, to measure the variability in their geometries. S'2 and S'3 are less realistic and less elevated than S2 and S3 surfaces (Figs SI2 and SI3) because they were built using only S2 or S3 points, respectively, that is, they were not enforced at the location of the anterior surfaces or forced by the topography. The uncertainties on surface geometries were then measured by the elevation difference between S2 and S'2 and S3 and S'3 (Fig. SI3).

The second uncertainty related to the partitioning of erosion volumes of denudation maps, built at the scale of West Africa, between four drainage groups (Senegambia, Short Atlantic drainages, Long Atlantic drainages and the

Niger catchment; Fig. 6a). In this study, we used the paleodrainage maps of Chardon *et al.* (2016), where the drainage divide positions themselves are located within an area of uncertainty (i.e. Fig. 6b, c). We calculated the volume eroded within this uncertainty area to estimate the volume uncertainty associated with the divide location.

The last uncertainty was associated with the type of exported material. Lateritic regolith represents the type-material eroded from the West African continental domain during the Cenozoic (Beauvais & Chardon, 2013). The density and porosity of the eroded lateritic regolith is different from bedrock (e.g. Grimaud *et al.*, 2015). Exported volume (V_{ex}) was corrected for the lateritic regolith porosity, ϕ , which varies from 10 to 40%

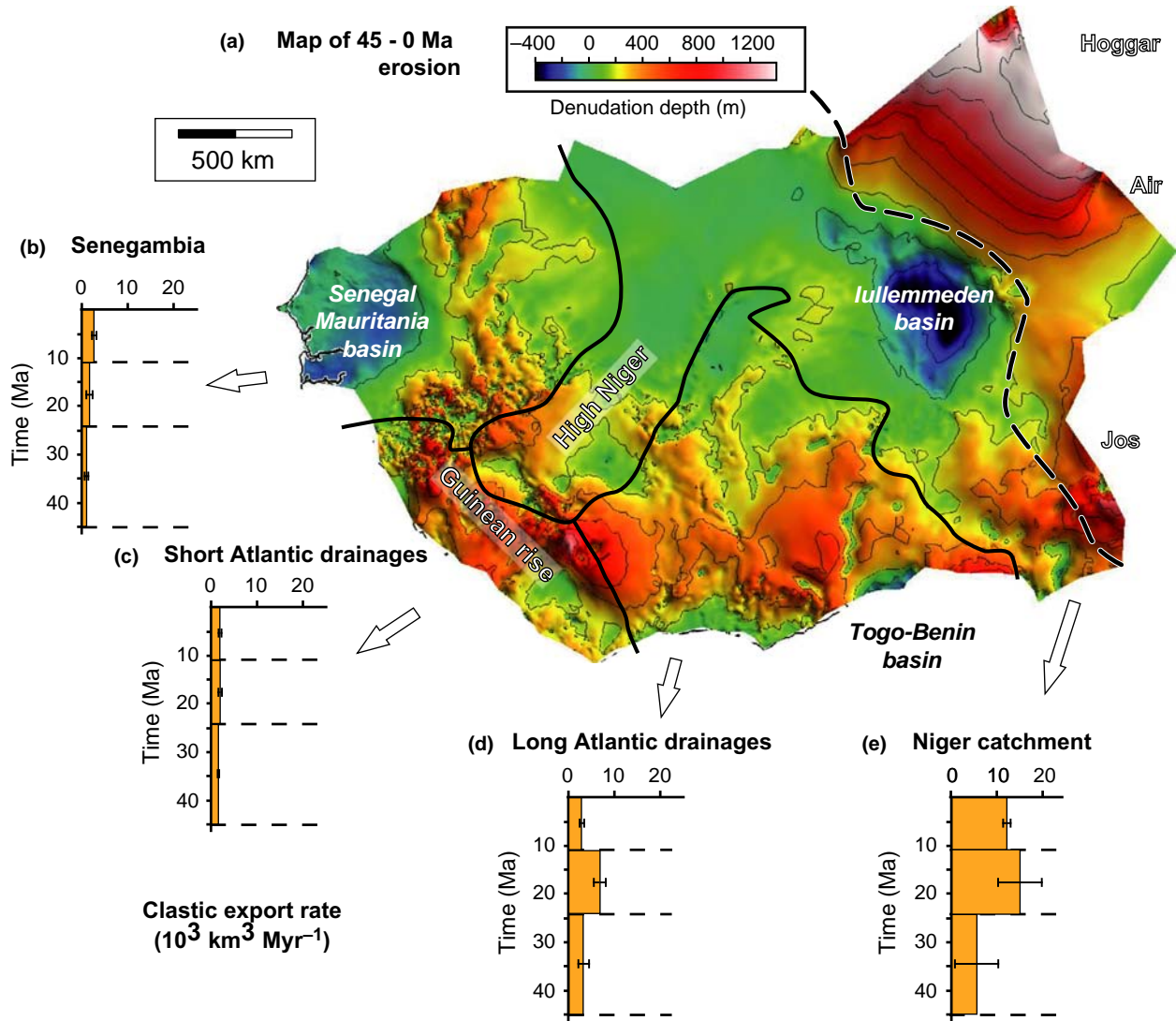


Fig. 7. Cenozoic denudation map and associated exported volumes. [a] Map of total denudation depth at the scale of Sub-Saharan West Africa since the abandonment of S1. Clastic export rates are shown by drainage groups (i.e. Senegambia drainage [b], Short Atlantic drainages [c], Long Atlantic drainages [d] and the Niger catchment [e]). The eastern swells are separated from the rest of the study area by the black dashed line.

(Boulangé, 1984; Valeton, 1991; Beauvais & Colin, 1993; Thomas, 1994). We thus estimated the clastic exported solid volume assuming a 25% mean porosity in the regolith (Table 1). Regolith bulk density is $2,000 \text{ kg m}^{-3}$ (Valeton, 1991), which corresponds to a grain density ρ of $2,650 \text{ kg m}^{-3}$. We estimate the clastic yields γ of each drainage group using:

$$\gamma = \frac{V_{\text{ex}} \cdot (1 - \phi) \cdot \rho}{100 \cdot A \cdot \Delta_t} \quad (1)$$

where A and Δ_t are the catchment area and the time interval, respectively, and γ has unit of mass per unit area per time ($\text{t km}^{-2} \text{ yr}^{-1}$). Calculations of clastic exported solid volumes and clastic yields, therefore, assumed that most eroded material was regolith. Because in West Africa

bedrock outcrops are rare, erosion rates are slow and regolith mantles are thick, the assumption seems reasonable (Grimaud *et al.*, 2015). This also implies that a sizeable portion of the denuded volume, which we did not quantify, was exported as solute load. However, in area with fast denudation rates, the eroded material may locally be only moderately weathered. In that case, the actual clastic export was higher than our estimate, which should therefore be considered as minimum.

OFFSHORE CLASTIC ACCUMULATION ON THE MARGIN(S)

Offshore accumulations were calculated in term of solid volumes (i.e. corrected for porosity and non-clastic

Table 1. Summary of Cenozoic erosion budgets of Sub-Saharan West Africa

Location	Interval	Eroded volume (10 ³ km ³)		Average equivalent denudation				Exported volume				Clastic export rate (10 ³ m ³ Myr ⁻¹)	Clastic yield (t km ⁻² yr ⁻¹)	
				Depth (m)		Rate (m Myr ⁻¹)		Total (<i>V_{ev}</i>) (10 ³ km ³)		Clastic (<i>V_c</i>)				
West Africa	45–0 Ma	1149		333		7.4		1112		834		18.5		13
Senegambia	45–24 Ma	39	5	74	3	3.5	0.1	30	5	22	4	1.1	0.2	4
	24–11 Ma	29	12	40	14	3.1	1.1	29	12	22	9	1.7	0.7	6
	11–0 Ma	40	5	59	8	5.3	0.7	40	5	30	4	2.7	0.4	11
Short Atlantic drainages	45–24 Ma	45	4	154	8	7.3	0.4	45	4	34	3	1.6	0.1	14
	24–11 Ma	37	7	119	19	9.2	1.4	37	7	27	5	2.1	0.4	19
	11–0 Ma	29	4	104	14	9.5	1.3	29	4	22	3	2.0	0.3	19
Long Atlantic drainages	45–24 Ma	99	41	197	17	9.4	0.8	97	40	73	30	3.5	1.4	17
	24–11 Ma	86	22	98	18	7.5	1.4	86	22	64	17	5.0	1.3	15
	11–0 Ma	44	7	53	8	4.8	0.8	44	7	33	5	3.0	0.5	9
Niger	45–24 Ma	196	178	138	31	6.6	1.5	153	136	115	102	5.5	4.8	7
	24–11 Ma	260	83	135	40	10.4	3.1	260	83	195	62	15.0	4.8	20
	11–0 Ma	177	11	86	5	7.8	0.5	177	11	133	8	12.1	0.7	15
Total	45–0 Ma	633	271	359	76	8.2	1.7	591	229	443	172	10.9	3.4	14
Niger														
Benue estimation	45–0 Ma					7.4				187				
Total Niger & Benue	45–0 Ma							630	172					

material such as volcanics and carbonates) following the method of Guillocheau *et al.* (2012), based on regional geological cross-sections (Fig. 9). The calculation technique, non-clastic material and remaining porosity corrections, and uncertainties estimations are presented in the Appendix S1.

In the Niger delta domain, we used the four sections published by Haack *et al.* (2000) that encompass most of the Cenozoic depocenters (Fig. 9a, b). Given the biostratigraphic age constraints available for the sediments, these sections allowed measuring accumulation at higher time resolution (10^{5–6} yr; Fig. 9d; Table 2) than the denudation maps. Hence, we recalculated accumulations for the 45–23, 23–11.6 and 11.6–0 Ma intervals to allow for comparison with the erosion chronology (Fig. 9e; Table 2). In the Equatorial Atlantic, we used six sections (after De Caprona, 1992; Macgregor *et al.*, 2003) that only encompass the proximal parts of the margins. We then used the extrapolation of these cross-sections to the abyssal plain proposed by Helm (2009) (Fig. 9c; Appendix S1) to include volume accumulated across the entire sedimentary wedge and to take into account erosion from, or by-pass of, the continental shelf (Fig. 9f). Volume for the 45–33.9 Ma interval was recalculated using the accumulation rate of the 55.8–33.9 Ma interval (Table 1).

RESULTS

Spatial and temporal denudation patterns

Incremental (45–24, 24–11 and 11–0 Ma) and total (45–0 Ma) denudations are heterogeneous at regional scale (i.e. Figs 6 and 7). Overall, denudation is greater in the eastern swells (i.e. massifs located to the east of the dashed line in Figs 6b, c, d) and along a 300–800 km wide strip running parallel to the coast (i.e. from the Jos Plateau to the Guinean rise and the Tagant) that we interpret as a marginal upwarp following Beauvais & Chardon (2013). Total denudation exceeds 1500 m in the Hoggar massif and ranges between 400 and 1000 m along the marginal upwarp (Figs 7 and 8a). Elsewhere, the total denudation is usually <400 m. Some onshore accumulation (i.e. negative erosion) is observed in the Togo-Benin, Senegal-Mauritania and Iullemeden basins, where up to 400 m were accumulated during the 45–24 Ma interval (Figs 6b and 8a). Post-24 Ma denudation is low in these basins (<100 m; Fig. 6c, d) with the noticeable exception of the northern Iullemeden basin where geological sections show that at least half of the “Continental Terminal” deposits were eroded (Fig. 8a).

From 45 Ma to the present, denudation was high in the Hoggar massif with a maximum during the 24–11 Ma interval (up to 1200 m; Fig. 6). During that period,

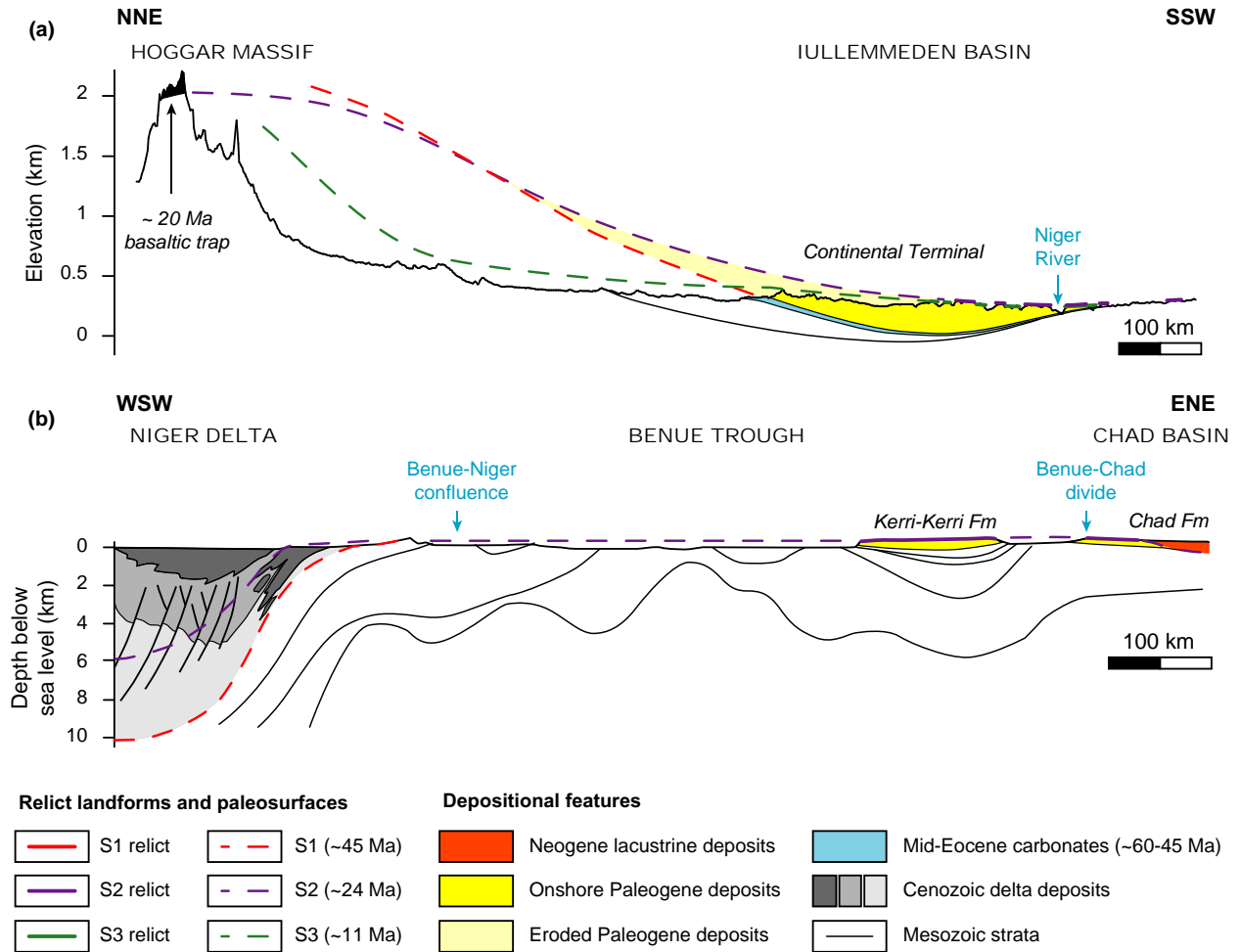


Fig. 8. Regional cross-sections of lateritic relict landforms distribution and contemporary sedimentary deposits (see Fig. 5 for location). [a] Cross section through the Hoggar massif and Iullemeden basin. [b] Cross section through the Benue trough and onshore Niger delta (geology after Benkhelil, 1989; volcanic accumulation in the Hoggar massif after Rognon *et al.*, 1983). The red, purple and green dashed lines represent large-scale interpolations of the S1, S2 and S3 surfaces respectively.

denudation was more broadly distributed (i.e. it extended towards the North Iullemeden basin; Fig. 8a) than during the 45–24 and 11–0 Ma intervals. Denudation was more homogeneously distributed on the marginal upwarp between 45 and 24 Ma than after 24 Ma. On the Guinean rise (i.e. mostly the Short Atlantic drainages group), relatively high denudation depths were maintained at all times (Fig. 6). Similarly, high denudation depths were recorded from 45 to 11 Ma by the Long Atlantic drainages group in an area that is currently lying low in comparison to the neighbouring Guinean rise (Fig. 2). In the Long Atlantic drainages and Niger catchment groups, denudation depths are overall lower during the 11–0 Ma interval (Fig. 6). In the Senegambia group, denudation increased after 11 Ma in both the Tagant massif and the north-western slope of the Guinean Rise (Beauvais & Chardon, 2013; Figs 2 and 6d). In the Benue trough, the tabular Paleocene Kerri-Kerri Formation is capped by a duricrust comparable to the Intermediate ferricrete

(Newell & Dowling, 1968; Adegoke *et al.*, 1986), which allows constraining the incision of these deposits after the abandonment of S2 surface (i.e. 24 Ma; Fig. 3). A geologic section suggests that Benue valley denudation did not exceed 200 m since 24 Ma, corresponding to a maximum denudation rate of 8.4 m Myr^{-1} (Fig. 8b).

These data show that denudation rates are overall low in West Africa since 45 Ma (mean denudation rate of 7.4 m Myr^{-1} ; Table 1). They are higher in the Hoggar massif (i.e. larger than 30 m Myr^{-1}) and the marginal upwarp (up to 10 m Myr^{-1}), where some temporal variations are also observed. Denudation rates remain lower than 5 m Myr^{-1} in the remainder of West Africa.

Export at the scale of major catchments

In total, the West African subcontinent exported $834 \times 10^3 \text{ km}^3$ of solid clastic sediments to the ocean (Table 1) since 45 Ma. These clastic volumes were

Table 2. Summary of Cenozoic clastic volumes accumulated in the Niger delta

	Interval (Ma)	Accumulated volume (10^3 km^3)
S3 – modern	1.8–0	46.8 ± 6.3
	5.3–1.8	142.3 ± 19.9
	11.6–5.3	127.7 ± 17.8
S2 – S3	16–11.5	85.4 ± 11.9
	23–11.5	61 ± 8.5
S1 – S2	33.9–23	69.8 ± 10.4
	45–33.9	44.4 ± 15.7
	55.8–33.9	87.6 ± 30.9
	Total 45–0	577.4 ± 90.5

distributed between the major drainage groups (Figs 6 and 7): $74 \times 10^3 \text{ km}^3$ from the Senegambia, $83 \times 10^3 \text{ km}^3$ from the Short Atlantic drainages, $170 \times 10^3 \text{ km}^3$ from the Long Atlantic drainages and $430 \times 10^3 \text{ km}^3$ from the Niger catchment (Table 1). At first order, exported solid volumes therefore increase with the size of the contributing area. Results also show that the export is modulated by onshore storage of sediments that we subtracted. Hence, 16% ($12 \times 10^3 \text{ km}^3$) of the total clastic export from Senegambia is stored onshore in the Senegal-Mauritania basin, whereas only 5% of the total clastic export from the Niger catchment is preserved in the Iullemmeden basin. In the Niger source-to-sink system, we did not measure denudation in the Benue trough and surrounding massifs (Figs 6 and 7) because the rare descriptions of regolith (Fritsch, 1978; Guillocheau *et al.*, 2015) would not allow to rigorously integrating them to the denudation chronology. However, we have estimated and added a Benue trough export to compare the clastic export from the Niger catchment to the accumulations in the Niger delta. We estimated that the Benue contributed a solid clastic volume of *ca.* $187 \times 10^3 \text{ km}^3$ assuming that the average West African denudation rate of 7.4 m Myr^{-1} applies to this area (*ca.* $0.77 \times 10^6 \text{ km}^2$; Table 1). This rate is compatible with observations in the Benue valley (see previous section). Denudation was potentially higher, enhanced by Neogene uplift, in the surrounding massifs (Burke, 1976). However, the preservation of Neogene volcanics and lateritic regoliths in the Jos Plateau and Adamaoua massifs (Boulangé & Eschenbrenner, 1971) suggests that denudation rates were probably much lower there than in the Hoggar area. In parallel, the neighbouring Chad basin has been constantly subsiding and trapping sediment since at least 24 Ma (Burke, 1976), suggesting that no sediment was diverted from the basin into the Benue trough (see Chardon *et al.*, 2016). Using a mean West Africa denudation rate seems therefore reasonable to estimate the erosion in the area of the Benue Trough. In line with these hypotheses, the resulting total clastic export of the Niger-

Benue catchment reaches $630 \pm 172 \times 10^3 \text{ km}^3$ since 45 Ma (Table 1). The Hoggar swell area has contributed *ca.* 66% of this volume.

Temporal variations in clastic export reflect the evolution of denudation rate and drainage. In most drainage groups, clastic export rates were lower during the 45–24 Ma interval than during the 24–11 Ma interval (Fig. 7b–e). Within the Senegambia drainage group, clastic export rate was slightly higher in the 11–0 Ma interval. In contrast, clastic export rate was steady for the Short Atlantic drainages group (Fig. 7b, c). In the Long Atlantic drainages group and the Niger catchment, export rates were lower during the 11–0 Ma interval than during the 24–11 Ma interval (Fig. 7d, e). The highest uncertainties on clastic export rates are estimated in the Long Atlantic drainages group and Niger catchment because of the major drainage reorganization between 45 and 24 Ma (Chardon *et al.*, 2016; Table 1; Appendix S1). Hence, the overall export trends among drainage groups appear regionally consistent in between the 45–24 and 24–11 Ma intervals and more contrasted in between the 24–11 and 11–0 Ma intervals.

Offshore accumulation

Offshore domains differ in their structural and sediment accumulation patterns (Fig. 9a). For the Niger delta, the sections used to estimate accumulation encompass the major part of the Cenozoic sedimentary wedge located along the margin (Fig. SI4). These sections show thick marginal clinofolds that have prograded over 150 km since the Oligocene and that are affected by faulting and folding (Figs 8b and 9b). Along the remaining part of the Equatorial Atlantic margin, 90% of the Cenozoic wedge is spread over the abyssal plain and extends over 300–600 km offshore (Fig. 9c).

Accumulation rates for the Niger delta can be estimated at higher resolution than denudation (Fig. 9d). These rates show a steady increase from *ca.* 5 to $10 \times 10^3 \text{ km}^3 \text{ Myr}^{-1}$ between 45 and 16 Ma. After 16 Ma, the accumulation rates increased to more than $20 \times 10^3 \text{ km}^3 \text{ Myr}^{-1}$. A peak in accumulation rate ($40 \times 10^3 \text{ km}^3 \text{ Myr}^{-1}$) is recorded between 5.3 and 1.8 Ma, followed by a relative decrease after 1.8 Ma (Jermannaud *et al.*, 2010). Solid accumulation rates, resampled for long-term intervals, are, respectively, *ca.* 5, 12 and $28 \times 10^3 \text{ km}^3 \text{ Myr}^{-1}$ during the 45–23, 23–11 and 11–0 Ma intervals. These data show that a larger volume of Neogene sediments is preserved in the delta compared to Paleogene sediments. The resulting total clastic accumulation since 45 Ma is about $580 \times 10^3 \text{ km}^3$ (Table 2). This number is remarkably consistent with – although slightly lower than – the calculated clastic volume exported by the Niger-Benue catchment since 45 Ma (*ca.* $630 \times 10^3 \text{ km}^3$; Table 1).

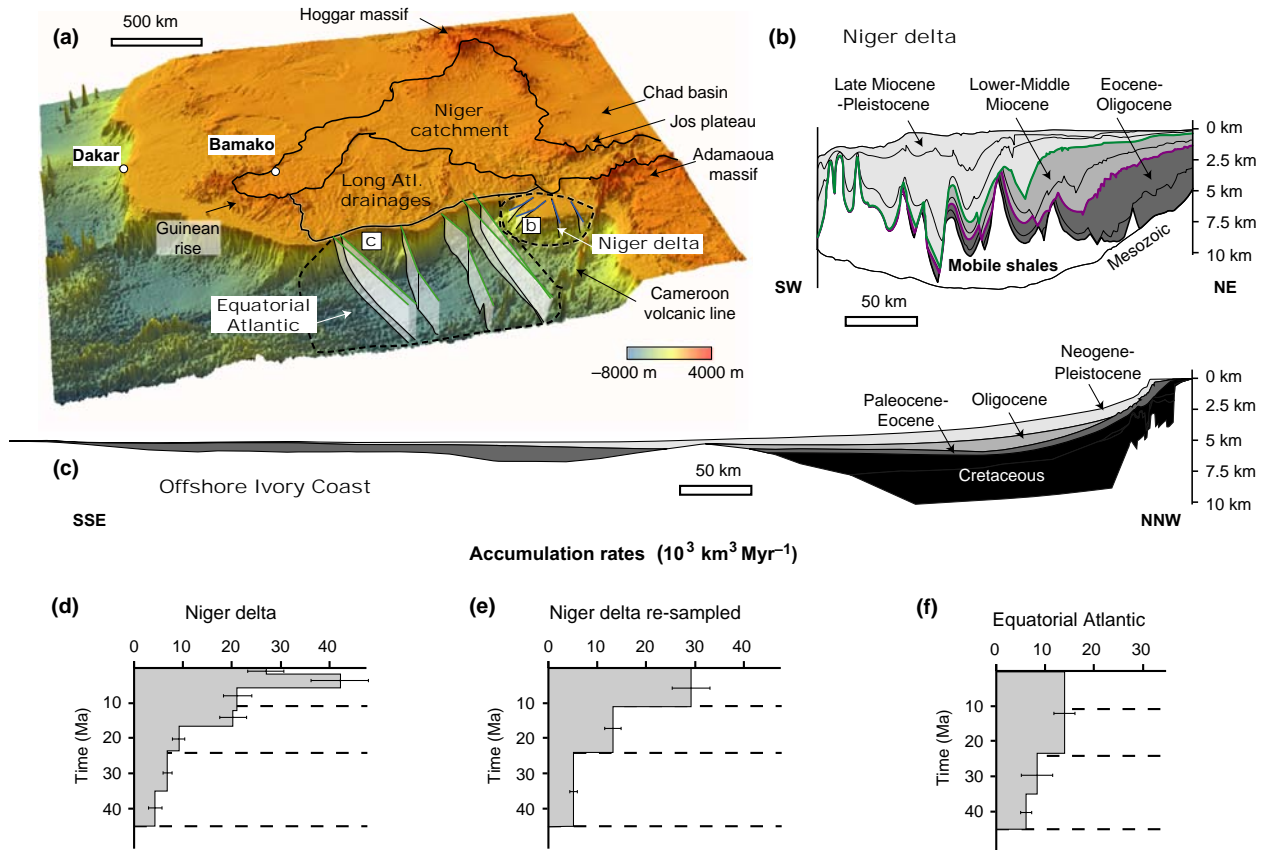


Fig. 9. Offshore accumulation histories. [a] 3D topography and bathymetry showing the location of the cross sections used in the study. [b] Example of cross section for the Niger delta (after Haack *et al.*, 2000). [c] Example of cross section for the sediment accumulation offshore Ivory Coast (after Helm, 2009; see Appendix S1). [d] Evolution of volumetric accumulation rates in the Niger delta (after Haack *et al.*, 2000 and Robin *et al.*, 2011). [e] Evolution of volumetric accumulation rates in the Niger delta after time re-sampling in order to compare to the continental denudation chronology (i.e. 45–23, 23–11.6 and 11.6–0 Ma; see Table 2). [f] Evolution of volumetric accumulation rates on the African margin of the Equatorial Atlantic (modified after Helm, 2009). See methods section and Appendix S1 for details. Error bars include a Monte Carlo estimation of uncertainties related to sections interpolation, as well as non-clastic material (i.e. carbonates and volcanics) and porosity corrections.

Along the rest of the margin, available data have a lower resolution than in the Niger delta, especially in the abyssal plain, and imply larger uncertainties (Fig. 9; see Helm, 2009). Accumulated volumes computed for the three time intervals suggest a long-term pattern of accumulation rate comparable to that of the Niger delta. The volumes are *ca.* 65, 85 and $300 \times 10^3 \text{ km}^3$ during the 45–33, 33–21 and 21–0 Ma intervals respectively (Fig. 9f). The total accumulated clastic volume since 45 Ma is $450 \pm 120 \times 10^3 \text{ km}^3$. This is 2–4 times higher than our estimate of exported clastic volumes ($151 \times 10^3 \text{ km}^3$) from the source area.

DISCUSSION

Cenozoic sediment budget

Surficial mass transfers from source to sink and the associated (un) loading of the crust are key aspects of the

topographic evolution and stratigraphic record of passive margins (Rouby *et al.*, 2013). Our study provides independent volumetric estimations of denudation at a sub-continental scale over the Cenozoic using relict paleolandforms and of accumulation using offshore regional sections. The main insight from our study is the fairly well-balanced sediment budget between the Niger delta and its source area. Such a finding supports the paleodrainage reconstruction of Chardon *et al.* (2016) who suggested the establishment of the modern Niger River watershed since at least the Late Oligocene (29 Ma). The modern-like Niger River catchment since at least 29 Ma collected sediments from a *ca.* $2 \times 10^6 \text{ km}^2$ catchment and transferred the large eroded volumes derived from the Hoggar hot spot swell to the ocean. The antiquity of the Niger catchment appears as a prerequisite to the large clastic accumulations in the Niger delta given the low denudation rates ($5\text{--}30 \text{ m Myr}^{-1}$) at the scale of West Africa.

Although our estimations fall within the same order of magnitude, we estimated a deficit on the volume of sediments exported by the Long Atlantic drainages group with respect to the accumulation along the Equatorial Atlantic margin they have fed (Fig. 9f; Table 1). Geometries of the offshore geological sections are, however, not well constrained and were deduced from low-resolution geophysical data with limited age constraints (Emery *et al.*, 1975). Thus, an uncertainty of merely 10 metres thickness on the distal geometry of a stratigraphic horizon may have significant repercussions on volume estimation in a basin as large as the Equatorial Atlantic, leading to under- or overestimation of accumulation. Clastic sediment budgets of the abyssal plains can further be affected by additional aeolian dust input from the Sahara (Windom, 1975), and more importantly by reworking by longitudinal bottom currents (Séranne & Nzé Abeigne, 1999; Anka *et al.*, 2009). Some sediments derived from the Niger catchment may also have by-passed the delta toe and have been deposited on these parts of the Equatorial Atlantic, further complicating the sediment budgets. This is supported by the westward extension of the Niger delta (Fig. 2) and consistent with the fact that, in our estimation, accumulation is slightly lower than denudation in the Niger source-to-sink budget. Future studies constraining westward sediment transfer in the western Niger delta would help to decipher the apparently low export of the Long Atlantic drainages group.

We measured a difference between the volumetric accumulation rate of the Niger delta (*ca.* $30 \times 10^3 \text{ km}^3 \text{ Myr}^{-1}$) and the export rate of the Niger catchment (*ca.* $12 \times 10^3 \text{ km}^3 \text{ Myr}^{-1}$) during the 11–0 Ma interval (i.e. Figs 7e and 9e). Assuming that the biostratigraphy used by Haack *et al.* (2000) is accurate, this difference could be explained by post-11 Ma erosion of sediments that were previously stored within the Niger sediment routing system, particularly on the shelf. As an analogy, the widespread erosion of Miocene sediments stored on the continent or the shelf has led to such reworking on the neighbouring South Atlantic margin (e.g. Lavier *et al.*, 2001; Walford & White, 2005; Linol *et al.*, 2014). In the study area, reworking of Cenozoic sediments is supported by the incision of large canyons in the Niger delta (Doust & Omatsola, 1990) and the removal of at least 50% of the former “Continental Terminal” after 24 Ma in the Lullemeden basin (see geological section in Fig. 8a). Overall, the discrepancy between accumulation and erosion is a point of caution when deducing denudation rates and paleosediment fluxes from the accumulation record only. Indeed, if the 11–0 Ma clastic deposits are partly composed of recycled material, their volume may overestimate continental denudation after 11 Ma, and underestimate denudation before that time.

Erosion dynamics in a non-orogenic domain

Our maps show that denudation is very heterogeneously distributed across West Africa as well as within each drainage group. Regional denudation patterns suggest an influence of long-wavelength rock uplift (>300 km) (Figs 7 and 8; Chardon *et al.*, 2016). Denudation focused on the Hoggar suggests a rock-uplift pattern with >700 km radius (Fig. 7a) related to mantle dynamics (Burke *et al.*, 2003; Chardon *et al.*, 2016). Recently published apatite (U–Th)/He thermochronological data indicate Cenozoic denudation in the Hoggar of 1–2 km between $78 \pm 22 \text{ Ma}$ and $13 \pm 3 \text{ Ma}$ (Rougier *et al.*, 2013), which is consistent with our estimation (*ca.* 1.5 km; Fig. 8a). Because we did not find the equivalent of S1 there, it is likely that we have even slightly underestimated the denudation of the Hoggar for the 45–24 Ma interval. Nevertheless, the eroded material derived from the Hoggar swell was instrumental in obtaining the volume accumulated in the Niger delta. As an illustration, applying the mean denudation rate of the other drainage groups (i.e. 6.6 m Myr^{-1}) over the Niger catchment for 45 Ma would have only resulted in only *ca.* $280 \times 10^3 \text{ km}^3$ clastic volume exported to the Niger delta instead of the *ca.* $450 \times 10^3 \text{ km}^3$ we estimated (Table 1). This simple calculation supports that forcing by mantle dynamics is a first-order process for enhancing the sediment export from the African continent (Burke *et al.*, 2003).

West of the dashed line in Fig. 7, maximum denudation depths within the upwarp domain suggest some rock uplift associated with flexure along the passive margin (Beauvais & Chardon, 2013; Grimaud *et al.*, 2014). In detail, denudation histories vary across the different segments along the margin, indicating a complex evolution. For example, erosion rates decreased along major valleys of the Long Atlantic drainages between the 24–11 and 11–0 Ma intervals during the progressive dissection of the upwarp, while they remained high in the Guinean Rise (i.e. Senegambia and Short Atlantic drainages; Fig. 6). These different erosion dynamics resulted in contrasted post-24 Ma evolution of clastic export rates in these drainage groups (Fig. 7b, c, d), resulting in source-to-sink systems that are not monotonous along the marginal upwarp. The variability in erosion rates may tentatively be related to uplift rate variations along the continental margin. Potentially, the stretching of a heterogeneous lithosphere or a non-cylindrical margin during the rifting stage generates potentially complex, laterally variable uplift patterns, which may be maintained long after rifting (Chardon *et al.*, 2013; Rouby *et al.*, 2013), leading to unevenly distributed erosion rates.

Our analysis shows that dated relict lateritic landforms are reliable markers of post-rift denudation of continental passive margins and adjacent cratonic domains with

sufficient spatial and temporal resolution. The variability in erosion histories along the margin shows (similarly to Pazzaglia & Gardner (1994) along the US Atlantic margin) that modern topography and paleodenudation rates do not necessarily correlate (Figs 2 and 7) and that independent geomorphic markers are more robust than present-day digital elevation models to constrain surface dynamics over geological timescales. West Africa is a non-orogenic domain where the erosion dynamics may be compared to the adjoining offshore record thanks to a spatially constrained onshore denudation chronology. In the future, new insights on the Cenozoic surface evolution of shields and their bounding margins (e.g. Australia, Brazil, India, South Africa) will arise from the mapping of relict landforms, whose lateritic cover has been dated using supergene minerals (e.g. Vasconcelos *et al.*, 1994a,b; Vasconcelos & Conroy, 2003; Bonnet *et al.*, 2014, 2016; Riffel *et al.*, 2015; Beauvais *et al.*, 2016).

CONCLUSIONS

We have quantified patterns and volumes of Cenozoic denudation and catchment export using dated and regionally correlated relict lateritic landforms of Sub-Saharan West Africa. Overall denudation rates are regionally low in this non-orogenic domain (*ca.* 7 m Myr⁻¹), but may increase significantly locally with rock uplift, whether driven by mantle dynamics or lithosphere deformation and flexure, as, for example, in the Hoggar hotspot swell and along a marginal upwarp. Comparisons with clastic volumes accumulated offshore show a fairly balanced sediment budget between the Niger catchment and its delta since 45 Ma. The Niger catchment was established since at least 29 Ma and allowed transporting sufficient clastic material to the delta; in particular, by collecting the erosion products of the growing Hoggar hotspot swell. Accumulations along the remaining Equatorial Atlantic margin of Africa suggest an apparent export deficit from its source but our estimation is poorly constrained by available offshore data, and complicated by potential sediment input from the Niger delta. Sediment reworking shredding the depositional record is also suggested in several locations, prompting caution when deducing continental denudation rates from accumulation only.

ACKNOWLEDGEMENT

This work was funded by WAXI, the CNRS and the ANR TopoAfrica (ANR-08-BLAN-572 0247-02) and supported by the gOcad consortium. We thank Michel Séranne and the SAFL sediment dynamics group for fruitful discussions and suggestions as well as Damien Huyghe and Stéphane Perrouty for support. The

manuscript also benefited from constructive reviews by Frank Pazzaglia, Luc Lavier and Peter van der Beek. We acknowledge AMIRA International and the industry sponsors, including AusAid and the ARC Linkage Project LP110100667, for their support of the WAXI project (P934A) as well as the Geological Surveys/Departments of Mines in West Africa as sponsors in kind of WAXI.

SUPPORTING INFORMATION

Additional Supporting Information may be found in the online version of this article:

Appendix S1. The method for building the 3D surfaces associated with the relict lateritic landforms, as well as the interpolation technique between offshore regional sections.

REFERENCES

- ADEGOKE, O.S., AGUMANU, A.E., BENKHELIL, M.J. & AJAYI, P.O. (1986) New stratigraphic, sedimentologic and structural data on the kerri-kerri formation, Bauchi and Borno States, Nigeria. *J. Afr. Earth Sci.*, **5**, 249–277.
- ALLEN, P.A. (2008) From landscapes into geological history. *Nature*, **451**, 274–276.
- ANKA, Z., SÉRANNE, M., LOPEZ, M., SCHECK-WENDEROTH, M. & SAVOYE, B. (2009) The long-term evolution of the Congo deep-sea fan: a basin-wide view of the interaction between a giant submarine fan and a mature passive margin (ZaiAngo project). *Tectonophysics*, **470**, 42–56.
- BÁRDOSY, G. & ALEVA, G.J.J. (1990) *Lateritic bauxites* (Vol. 27). Elsevier Science Ltd., Amsterdam, NY.
- BEAUMONT, C., KOOI, H. & WILLET, S. (2000) Coupled tectonic-surface process models with applications to rifted margins and collisional orogens. In: *Geomorphology and Global Tectonics* (Ed. by M.A. Summerfield), pp. 29–55. John Wiley & Sons, Chichester UK.
- BEAUVAIS, A. & CHARDON, D. (2013) Modes, tempo and spatial variability of Cenozoic cratonic denudation: the West African example. *Geochem. Geophys. Geosyst.*, **14**, 1590–1608.
- BEAUVAIS, A. & COLIN, F. (1993) Formation and transformation processes of iron duricrust systems in tropical humid environment. *Chem. Geol.*, **106**, 77–101.
- BEAUVAIS, A., RUFFET, G., HÉNOCQUE, O. & COLIN, F. (2008) Chemical and physical erosion rhythms of the West African Cenozoic morphogenesis: the 39Ar–40Ar dating of supergene K–Mn oxides. *J. Geophys. Res.*, **113**, F04007.
- BEAUVAIS, A., BONNET, N.J., CHARDON, D., ARNAUD, N. & JAYANANDA, M. (2016) Very long-term stability of passive margin escarpment constrained by ⁴⁰Ar/³⁹Ar dating of K–Mn oxides. *Geology*, **44**, 299–302.
- BENKHELIL, J. (1989) The origin and evolution of the Cretaceous Benue Trough (Nigeria). *J. Afr. Earth Sci.*, **8**, 251–282.







- BISHOP, P. (1995) Drainage rearrangement by river capture, beheading and diversion. *Prog. Phys. Geogr.*, **19**, 449–473.
- BISHOP, P. (2007) Long-term landscape evolution: linking tectonics and surface processes. *Earth Surf. Proc. Land.*, **32**, 329–365.
- BONNET, N.J., BEAUVAIS, A., ARNAUD, N., CHARDON, D. & JAYANANDA, M. (2014) First $^{40}\text{Ar}/^{39}\text{Ar}$ dating of intense late Palaeogene lateritic weathering in Peninsular India. *Earth Planet. Sci. Lett.*, **386**, 126–137.
- BONNET, N.J., BEAUVAIS, A., ARNAUD, N., CHARDON, D. & JAYANANDA, M. (2016) Cenozoic lateritic weathering and erosion history of Peninsular India from $^{40}\text{Ar}/^{39}\text{Ar}$ dating of supergene K–Mn oxides. *Chem. Geol.*, **446**, 33–53.
- BOULANGÉ, B. (1984) *Les Formations Bauxitiques Latéritiques de Côte D'Ivoire; les Faciès, Leur Transformation, Leur Distribution et L'évolution du Modelé*. ORSTOM, Bondy, France.
- BOULANGÉ, B. & ESCHENBRENNER, V. (1971) Note sur la présence de cuirasses témoins des niveaux bauxitiques et intermédiaires, plateau de Jos Nigéria. *Bull. Ass. Sénégal. Quatern. Ouest Afr.*, **31**, 83–92.
- BOULANGÉ, B. & MILLOT, G. (1988) La distribution des bauxites sur le craton ouest-africain. *Sci. Géol. Bull.*, **41**, 113–123.
- BOULANGÉ, B., SIGOLO, J.B. & DELVIGNE, J. (1973) Descriptions morphoscopiques, géochimiques et minéralogiques des faciès cuirassés des principaux niveaux géomorphologiques de Côte d'Ivoire. *Cah. ORSTOM, sér. Géol.*, **5**, 59–81.
- BOWDEN, D.J. (1987) On the composition and fabric of the foot-slop laterites (duricrusts) of the Sierra Leone, West Africa, and their geomorphological significance. *Z. Geomorphol. Suppl.*, **64**, 39–53.
- BRADLEY, D.C. (2008) Passive margins through earth history. *Earth-Sci. Rev.*, **91**, 1–26.
- BROWNFIELD, M.E. & CHARPENTIER, R.R. (2006) Geology and total petroleum systems of the Gulf of Guinea Province of West Africa. *U.S. Geol. Surv. Bulletin*, **2207-A**, 1–26.
- BURBANK, D.W. (1992) Causes of recent Himalayan uplift deduced from deposited patterns in the Ganges basin. *Nature*, **357**, 680–683.
- BURKE, K. (1976) The chad basin: an active intra-continental basin. *Tectonophysics*, **36**, 197–206.
- BURKE, K. (1996) The African Plate. *S. Afr. J. Geol.*, **99**, 339–409.
- BURKE, K., MACGREGOR, D.S. & CAMERON, N.R. (2003) Africa's petroleum systems; four tectonic 'aces' in the past 600 million years. In: *Petroleum Geology of Africa: New Themes and Developing Technologies* (Ed. by Arthur T.J., MacGregor D.S. & Cameron N.R.) *Geol. Soc. London. Spec. Publ.*, **207**, 21–60.
- CAMPANILE, D., NAMBIAR, C.G., BISHOP, P., WIDDOWSON, M. & BROWN, R. (2008) Sedimentation record in the Konkan-Kerala Basin: implications for the evolution of the Western Ghats and the Western Indian passive margin. *Basin Res.*, **20**, 3–22.
- CHARDON, D., CHEVILLOTTE, V., BEAUVAIS, A., GRANDIN, G. & BOULANGÉ, B. (2006) Planation, bauxites and epeirogeny: One or two paleosurfaces on the West African margin? *Geomorphology*, **82**, 273–282.
- CHARDON, D., ROUBY, D., ROBIN, C., CALVES, G., GRIMAUD, J.-L., GUILLOCHEAU, F., BEAUVAIS, A. & BRAUN, J. (2013) Source to sink study of non-cylindrical rifted passive margins: the case of the Gulf of Guinea. *Geophys. Res. Abstr.*, **15**, EGU2013–5223–1.
- CHARDON, D., GRIMAUD, J.-L., ROUBY, D., BEAUVAIS, A. & CHRISTOPHOUL, F. (2016) Stabilization of large drainage basins over geological time scales: Cenozoic West Africa, hot spot swell growth, and the Niger River. *Geochem. Geophys. Geosyst.*, **17**, 1164–1181.
- CLIFT, P.D. (2010) Enhanced global continental erosion and exhumation driven by Oligo-Miocene climate change. *Geophys. Res. Lett.*, **37**, L09402.
- DE CAPRONA, G.C. (1992) The continental margin of western Côte d'Ivoire: Structural framework inherited from intra-continental shearing. PhD Thesis. University of Gothenburg, Gothenburg, Sweden.
- DOUST, H. & OMATSOLA, E. (1990) Niger Delta. In: *Divergent/Passive Margin Basins* (Ed. by Edwards J.D. & Santogrossi P.A.) *AAPG Memoir*, **48**, 239–248.
- DUROTOYE, B. (1989) Quaternary sediments in Nigeria. In: *Geology of Nigeria*, 2nd edn (Ed. by C.A. Kogbe), pp. 431–444. Rock View International, Paris, France.
- EMERY, K.O., UCHUPI, E., PHILLIPS, J., BOWIN, C.O. & MASCLE, J. (1975) Continental margin of Western Africa: Angola to Sierra Leone. *Am. Assoc. Pet. Geol. Bull.*, **59**, 2209–2265.
- ESCHENBRENNER, R. & GRANDIN, G. (1970) La séquence de cuirasses et ses différenciations entre Agnibiléfrou et Diébougou (Haute-Volta). *Cah. ORSTOM. Sér. Géol.*, **2**, 205–246.
- FEYBESSE, J.-L., BILLA, M., GUERROT, C., DUGUEY, E., LESCUYER, J.-L., MILESI, J.-P. & BOUCHOT, V. (2006) The paleoproterozoic Ghanaian province: geodynamic model and ore controls, including regional stress modeling. *Precambrian Res.*, **149**, 149–196.
- FÖLSTER, H. (1969) Late Quaternary erosion phases in SW Nigeria. *Bull. Ass. Sénégal. Quatern. Ouest Afr.*, **21**, 29–35.
- FRITSCH, P. (1978) Chronologie relative des formations cuirassées et analyse géographique des facteurs de cuirassement au Cameroun. *Trav. Doc. CEGET*, **33**, 114–132.
- GILCHRIST, A.R. & SUMMERFIELD, M.A. (1990) Differential denudation and flexural isostasy in formation of rifted-margin upwarps. *Nature*, **346**, 739–742.
- GRANDIN, G. (1976) *Aplanissements Cuirassés et Enrichissement des Gisements de Manganèse Dans Quelques Régions D'Afrique de L'Ouest*. ORSTOM, Paris, France.
- GRANDIN, G. & HAYWARD, D.F. (1975) Aplanissements cuirassés de la péninsule de Freetown (Sierra-Léone). *Cah. ORSTOM, sér. Géol.*, **7**, 11–16.
- GRIMAUD, J.-L. (2014) Dynamique long-terme de l'érosion en contexte cratonique: l'Afrique de l'Ouest depuis l'Éocène. PhD Thesis, Toulouse University, Toulouse, France.
- GRIMAUD, J.-L., CHARDON, D. & BEAUVAIS, A. (2014) Very long-term incision dynamics of big rivers. *Earth Planet. Sci. Lett.*, **405**, 74–84.
- GRIMAUD, J.-L., CHARDON, D., METELKA, V., BEAUVAIS, A. & BAMBA, O. (2015) Neogene cratonic erosion fluxes and landform evolution processes from regional regolith mapping (Burkina Faso, West Africa). *Geomorphology*, **241**, 315–330.
- GUILLOCHEAU, F., ROUBY, D., ROBIN, C., HELM, C., ROLLAND, N., LE CARLIER DE VESLUD, C. & BRAUN, J. (2012) Quantification and causes of the terrigenous sediment budget at the

- scale of a continental margin: a new method applied to the Namibia–South Africa margin. *Basin Res.*, **24**, 3–30.
- GUILLOCHEAU, F., CHELALOU, R., LINOL, B., DAUTEUIL, O., ROBIN, C., MVONDO, F., CALLEC, Y. & COLIN, J.P. (2015) Cenozoic landscape evolution in and around the Congo Basin: constraints from sediments and planation surfaces. In: *Geology and Resource Potential of the Congo Basin* (Ed. by M.J. de Wit, F. Guillocheau & M.C.J. de Wit), Regional Geology Reviews, pp. 271–313. Springer Berlin Heidelberg, Berlin Germany.
- HAAK, R.C., SUNDARARAMAN, P., DIEDJOMAHOR, J.O., XIAO, H., GANT, N.J., MAY, E.D. & KELSCH, K. (2000) Niger Delta petroleum systems, Nigeria. In: *Petroleum Systems of South Atlantic Margins* (Ed. by Mello M.R. & Katz B.J.) *AAPG Mem.*, **48**, 213–231.
- HADLEY, R.F. (1967) Pediments and pediment-forming processes. *J. Geol. Educ.*, **15**, 83–89.
- HELM, C. (2009) Quantification des flux sédimentaires anciens à l'échelle d'un continent: le cas de l'Afrique au Méso-Cénozoïque. PhD Thesis. Rennes University, Rennes, France.
- JERMANNAUD, P., ROUBY, D., ROBIN, C., NALPAS, T., GUILLOCHEAU, F. & RAILLARD, S. (2010) Plio-Pleistocene sequence stratigraphic architecture of the eastern Niger Delta: a record of eustasy and aridification of Africa. *Mar. Pet. Geol.*, **27**, 810–821.
- JEROLMACK, D.J. & PAOLA, C. (2010) Shredding of environmental signals by sediment transport. *Geophys. Res. Lett.*, **37**, L19401.
- KING, L.C. (1962) *The Morphology of the Earth*. Oliver and Boyd, Edinburgh, UK.
- LABAILS, C., OLIVET, J.-L., ASLANIAN, D. & ROEST, W.R. (2010) An alternative early opening scenario for the Central Atlantic Ocean. *Earth Planet. Sci. Lett.*, **297**, 355–368.
- LAVIER, L.L., STECKLER, M.S. & BRIGAUD, F. (2001) Climatic and tectonic controls on the Cenozoic evolution of the West African margin. *Mar. Geol.*, **178**, 63–80.
- LETURMY, P., LUCAZEAU, F. & BRIGAUD, F. (2003) Dynamic interactions between the gulf of Guinea passive margin and the Congo River drainage basin: 1. Morphology and mass balance. *J. Geophys. Res. Solid Earth*, **108**, 2156–2202.
- LINOL, B., DE WIT, M.J., GUILLOCHEAU, F., DE WIT, M.C.J., ANKA, Z. & COLIN, J.-P. (2014) Formation and Collapse of the Kalahari Duricrust [‘African Surface’] Across the Congo Basin, with Implications for Changes in Rates of Cenozoic Off-Shore Sedimentation. In: *Geology and Resource Potential of the Congo Basin* (Ed. by M.J. de Wit, F. Guillocheau & M.C.J. de Wit), Regional Geology Reviews, pp. 193–210. Springer Berlin Heidelberg, Berlin Germany.
- MACGREGOR, D.S. (2013) Late Cretaceous–Cenozoic sediment and turbidite reservoir supply to South Atlantic margins. *Spec. Publ. Geol. Soc. London*, **369**, 109–128.
- MACGREGOR, D.S., ROBINSON, J. & SPEAR, G. (2003) Play fairways of the Gulf of Guinea transform margin. In: *Petroleum Geology of Africa: New Themes and Developing Technologies* (Ed. by Arthur T.J., MacGregor D.S. & Cameron N.R.) *Geol. Soc. London. Spec. Publ.*, **207**, 131–150.
- MALLET, J.L. (1992) Discrete smooth interpolation in geometric modelling. *Comput. Aided Des.*, **24**, 178–191.
- MÉTIVIER, F. & GAUDEMER, Y. (1999) Stability of output fluxes of large rivers in South and East Asia during the last 2 million years: implications on floodplain processes. *Basin Res.*, **11**, 293–303.
- MÉTIVIER, F., GAUDEMER, Y., TAPPONNIER, P. & KLEIN, M. (1999) Mass accumulation rates in Asia during the Cenozoic. *Geophys. J. Int.*, **137**, 280–318.
- MICHEL, P. (1973) *Les Bassins des Fleuves Sénégal et Gambie: Étude Géomorphologique*. ORSTOM, Paris, France.
- MICHEL, P. (1977a) Les modelés et dépôts du Sahara méridional et Sahel et du Sud-Ouest africain. *Rech. Géograph. Strasbourg*, **5**, 5–39.
- MICHEL, P. (1977b) Recherches sur le Quaternaire en Afrique occidentale. *Suppl. Bull. AFEQ*, **50**, 143–153.
- MILLOT, G. (1970) *Geology of Clays*. Springer Verlag, Berlin, Germany.
- MOLNAR, P. (2004) Late Cenozoic increase in accumulation rates of terrestrial sediment: how Might Climate Change Have Affected Erosion Rates? *Annu. Rev. Earth Planet. Sci.*, **32**, 67–89.
- MOULIN, M., ASLANIAN, D. & UNTERNEHR, P. (2010) A new starting point for the South and Equatorial Atlantic Ocean. *Earth-Sci. Rev.*, **98**, 1–37.
- NEWILL, D. & DOWLING, J.W.F. (1968) Laterites in West Malaysia and Northern Nigeria. *Int. Conf. SMFE, Spec. Sess. Eng. Properties of Lateritic Soils*, **2**, 133–150.
- PAZZAGLIA, F.J. & GARDNER, T.W. (1994) Late Cenozoic flexural deformation of the middle U.S. Atlantic passive margin. *J. Geophys. Res. Solid Earth*, **99**, 12143–12157.
- REIJERS, T. (2011) Stratigraphy and sedimentology of the Niger Delta. *Geologos*, **17**, 133–162.
- RIFFEL, S.B., VASCONCELOS, P.M., CARMO, I.O. & FARLEY, K.A. (2015) Combined ⁴⁰Ar/³⁹Ar and (U–Th)/He geochronological constraints on long-term landscape evolution of the Second Paraná Plateau and its ruiniform surface features, Paraná, Brazil. *Geomorphology*, **233**, 52–63.
- ROBIN, C., GUILLOCHEAU, F., JEANNE, S., PORCHER, F. & CALVÈS, G. (2011) Cenozoic siliciclastic fluxes evolution around Africa. *Geophys. Res. Abstr.*, **13**, EGU2011–EGU5659.
- ROGNON, P., GOURINARD, Y., BANDET, Y., KOENIGUER, J.C. & DELTEIL-DESNEUX, F. (1983) Précisions chronologiques sur l'évolution volcanotectonique et géomorphologique de l'Atakor (Hoggar); apports des données radiométriques (K/Ar) et paléobotaniques (bois fossiles). *Bull. Soc. Géol. Fr.*, **25**, 973–980.
- ROUBY, D., BONNET, S., GUILLOCHEAU, F., GALLAGHER, K., ROBIN, C., BIANCOTTO, F., DAUTEUIL, O. & BRAUN, J. (2009) Sediment supply to the Orange sedimentary system over the last 150 My: an evaluation from sedimentation/denudation balance. *Mar. Pet. Geol.*, **26**, 782–794.
- ROUBY, D., BRAUN, J., ROBIN, C., DAUTEUIL, O. & DESCHAMPS, F. (2013) Long-term stratigraphic evolution of Atlantic-type passive margins: a numerical approach of interactions between surface processes, flexural isostasy and 3D thermal subsidence. *Tectonophysics*, **604**, 83–103.
- ROUGIER, S., MISSENERD, Y., GAUTHERON, C., BARBARAND, J., ZEYEN, H., PINNA, R., LIÉGEOIS, J.-P., BONIN, B., OUBADI, A., DERDER, M.E.–M. & de LAMOTTE, D.F. (2013) Eocene

- exhumation of the Tuareg Shield (Sahara Desert, Africa). *Geology*, **41**, 615–618.
- RUST, D.J. & SUMMERFIELD, M.A. (1990) Isopach and borehole data as indicators of rifted margin evolution in southwestern Africa. *Mar. Pet. Geol.*, **7**, 277–287.
- SADLER, P.M. (1981) Sediment accumulation rates and the completeness of stratigraphic sections. *J. Geol.*, **89**, 569–584.
- SÉRANNE, M. (1999) Early Oligocene stratigraphic turnover on the west Africa continental margin: a signature of the Tertiary greenhouse-to-icehouse transition? *Terra Nova*, **11**, 135–140.
- SÉRANNE, M. & NZÉ ABEIGNE, C.-R. (1999) Oligocene to Holocene sediment drifts and bottom currents on the slope of Gabon continental margin (west Africa): consequences for sedimentation and southeast Atlantic upwelling. *Sed. Geol.*, **128**, 179–199.
- SIMÕES, M., BRAUN, J. & BONNET, S. (2010) Continental-scale erosion and transport laws: a new approach to quantitatively investigate macroscale landscapes and associated sediment fluxes over the geological past. *Geochem. Geophys. Geosyst.*, **11**, Q09001.
- TARDY, Y. & ROQUIN, C. (1998) *Dérive des Continents, Paléoclimats et Altérations Tropicales*. BRGM, Orléans, France.
- TEEUW, R.M. (2002) Regolith and diamond deposits around Tortiya, Ivory Coast, West Africa. *Catena*, **49**, 111–127.
- THOMAS, M.F. (1980) *Timescales of landform development on tropical shields; a study from Sierra Leone*. In: *Timescales in Geomorphology* (Ed. by R.A. Cullingford, D.A. Davidson, J. Lewin), pp. 333–354. John Wiley & Sons, Chichester, UK.
- THOMAS, M.F. (1994) *Geomorphology in the Tropics: A Study of Weathering and Denudation in Low Latitudes*. John Wiley & Sons, New York, NY.
- VALETON, I. (1991) Bauxites and associated terrestrial sediments in Nigeria and their position in the Bauxite belts of Africa. *J. Afr. Earth Sci.*, **12**, 297–310.
- VASCONCELOS, P.M. & CONROY, M. (2003) Geochronology of weathering and landscape evolution, Dugald River valley, NW Queensland, Australia. *Geochim. Cosmochim. Acta*, **67**, 2913–2930.
- VASCONCELOS, P.M., BRIMHALL, G.H., BECKER, T.A. & RENNE, P.R. (1994a) $^{40}\text{Ar}/^{39}\text{Ar}$ analysis of supergene jarosite and alunite: implications to the paleoweathering history of the western USA and West Africa. *Geochim. Cosmochim. Acta*, **58**, 401–420.
- VASCONCELOS, P.M., RENNE, P.R., BRIMHALL, G.H. & BECKER, T.A. (1994b) Direct dating of weathering phenomena by $^{40}\text{Ar}/^{39}\text{Ar}$ and K–Ar analysis of supergene K–Mn oxides. *Geochim. Cosmochim. Acta*, **58**, 1635–1665.
- VILLENEUVE, M. (2005) Paleozoic basins in West Africa and the Mauritanide thrust belt. *J. Afr. Earth Sci.*, **43**(1–3), 166–195.
- WALFORD, H.L. & WHITE, N.J. (2005) Constraining uplift and denudation of west African continental margin by inversion of stacking velocity data. *J. Geophys. Res.*, **110**, B04403.
- WINDOM, H.L. (1975) Eolian contributions to marine sediments. *J. Sediment. Res.*, **45**, 520–529.
- YÉ, J., CHARDON, D., ROUBY, D., GUILLOCHEAU, F., DALL’ASTA, M., FERRY, J.N. & BROUCKE, O. (2017) Paleogeographic and structural evolution of northwestern Africa and its Atlantic margins since the Early Mesozoic. *Geosphere*, **13**, 1–31.
- ZACHOS, J., PAGANI, M., SLOAN, L., THOMAS, E. & BILLUPS, K. (2001) Trends, rhythms, and aberrations in global climate 65 Ma to Present. *Science*, **292**, 686–693.

Manuscript received 25 November 2016; In revised form 24 April 2017; Manuscript accepted 11 June 2017.

Flexural deformation controls on Late Quaternary sediment dispersal in the Garo-Rajmahal Gap, NW Bengal Basin

Jean-Louis Grimaud^{1,2}  | Celine Grall³  | Steven Goodbred⁴  | Michael S. Steckler³ | Ryan Sincavage⁴  | Jennifer L. Pickering⁴  | Chris Paola^{1,2}  | Leonardo Seeber³ | Md. Saddam Hossain⁵

¹St Anthony Falls Laboratory, University of Minnesota, Minneapolis, MN, USA

²Department of Earth and Environmental Sciences, University of Minnesota, Minneapolis, MN, USA

³Lamont-Doherty Earth Observatory, Columbia University, Palisades, NY, USA

⁴Earth & Environmental Sciences Department, Vanderbilt University, Nashville, TN, USA

⁵Department of Geology, University of Dhaka, Dhaka, Bangladesh

Correspondence

Jean-Louis Grimaud, MINES ParisTech, Centre de Géosciences, PSL Research University, 35 rue St Honoré, 77305 Fontainebleau Cedex, France.
Email: jean-louis.grimaud@mines-paristech.fr

Present address

Jean-Louis Grimaud, MINES ParisTech, Centre de Géosciences, PSL Research University, 35 rue St Honoré, 77305, Fontainebleau Cedex, France

Ryan Sincavage, Department of Geology, Radford University, Radford, VA 24060, USA

Jennifer L. Pickering, Shell International Exploration and Production, Inc., Houston, TX 77082, USA

Funding information

SAFL Industrial consortium; National Science Foundation, Grant/Award Number: OISE 09-68354

Abstract

Subsurface deformation is a driver for river path selection when deformation rates become comparable to the autogenic mobility rate of rivers. Here we combine geomorphology, soil and sediment facies analyses, and geophysical data of the Late Quaternary sediments of the central Garo-Rajmahal Gap in Northwest Bengal to link subsurface deformation with surface processes. We show variable sedimentation characteristics, from slow rates (<0.8 mm/year) in the Tista megafan at the foot of the Himalaya to nondeposition at the exposed surface of the Barind Tract to the south, enabling the development of mature soils. Combined subsidence in the Tista fan and uplift of the Barind Tract are consistent with a N-S flexural response of the Indian plate to loading of the Himalaya Mountains given a low value of elastic thickness (15–25 km). Provenance analysis based on bulk strontium concentration suggests a dispersal of sediment consistent with this flexural deformation—in particular the abandonment of the Barind Tract by a Pleistocene Brahmaputra River and the current extents of the Tista megafan lobes. Overall, these results highlight the control by deeply rooted deformation patterns on the routing of sediment by large rivers in foreland settings.

KEYWORDS

geophysics, river, sediment routing, tectonics, weathering

The peer review history for this article is available at <https://publons.com/publon/10.1111/bre.12425>

1 | INTRODUCTION

Characterizing surface dynamics at the apex of deltas is key for understanding the behaviour of rivers as well as the large-scale distribution of their water and sediments, which in turn affects delta-surface evolution and stratigraphic architecture. The associated sediment heterogeneities affect ground permeability and are therefore studied as water/hydrocarbon reservoir analogues (e.g. Blum, Martin, Milliken, & Garvin, 2013; van Dijk et al., 2016). A classic method used to constrain sediment architecture is sequence stratigraphy (e.g. Catuneanu et al., 2010; Vail, Mitchum, & Thompson, 1977), which focuses on downstream (i.e. sea level) forcing that longitudinally displace the loci of depocentres. In the case of sea level fall, this displacement would be associated with the incision of a palaeovalley system bounded by wide interfluvies capped by palaeosols. The sequence stratigraphy method is under scrutiny, particularly for fluvial sections (e.g. Amorosi, Bruno, Cleveland, Morelli, & Hong, 2017; Pattison, 2018; Wright & Marriott, 1993). One reason sequence stratigraphy may not adequately model fluvial systems is that boundaries in the sedimentary record may also be triggered by lateral displacement of depositional lobes due to switching (avulsion) of river course (e.g. Slingerland & Smith, 2004).

The locations of recurring avulsions (i.e. avulsion nodes) control the distribution and size of sedimentary lobes within basins. This is the case in physical and numerical models, where lobe size and surface occupation dynamics are dominated by the location of the delta apex (e.g. Reitz, Jerolmack, & Swenson, 2010). But how can avulsion nodes persist at a single location in natural systems? Recent studies show that the backwater length influences avulsion node position in the coastal zone (e.g. Chatanantavet, Lamb, & Nittrouer, 2012; Ganti, Chadwick, Hassenruck-Gudipati, Fuller, & Lamb, 2016; Jerolmack, 2009). However, sea level influence on river hydrodynamics is reduced upstream when moving towards the piedmont and bedrock regions (Blum et al., 2013; Hartley, Weissmann, & Scuderi, 2016; Pickering et al., 2019).

At the piedmont of mountain ranges, tectonic deformation has a strong influence on river behaviour. Hence, these upstream areas represent targets for identifying external controls on delta evolution, as opposed to more commonly studied downstream forcing such as sea level. The growth of faults and fold structures has been shown to affect the path of rivers and associated sediment load through diversion, drainage reorganization or temporary sediment storage (Densmore, Sinha, Sinha, Tandon, & Jain, 2016; Gupta, 1997; Holbrook & Schumm, 1999; Humphrey & Konrad, 2000). However, directly linking river dynamics to substrate deformation in depositional environments over short timescales (10^2 – 10^5 year) is challenging because: (a) topographic and sediment thickness variations are often subtle and (b) processes related to millennial climatic variations or internal river dynamics may

Highlights

- Combined geomorphic–geophysical study of the Garo-Rajmahal Gap in Bangladesh.
- Sediment dispersal in the foreland basin is influenced by deep deformation pattern.
- N-S trends of uplift and subsidence suggest flexural response to Himalaya load.

overprint tectonic forcing (e.g. Amorosi et al., 2017; Hajek & Straub, 2017; Sincavage, Goodbred, & Pickering, 2018).

In this study, we combine analyses of sedimentological, geomorphic and geophysical data to constrain the Late Quaternary surface dynamics and stratigraphic architecture of the Garo-Rajmahal Gap in northwest Bengal (Figure 1). We show that river avulsion dynamics and sediment dispersal are influenced by a deeply rooted warping to the south and associated subsidence deep to the north, which are likely flexural features related to loading by the Himalaya.

2 | GEOLOGICAL SETTING

This study focused on the northwest margin of the Bengal basin and covers ca. 90×10^3 km² in northwest Bangladesh at the border with India (Figure 1). The Bengal basin has been active since the early Cretaceous rifting of India from Antarctica, and has been influenced by the convergence between the Indian– and Eurasian–Sunda plates since the Eocene (Steckler, Akhter, & Seeber, 2008). The margin is located north of the Hinge Zone (Figure 1), which marks the transition between the Indian craton to the northwest and thinned, rifted lithosphere to the southeast, where about 18–20 km of sediment accumulated since the Early Cretaceous (Alam, Alam, Curray, Chowdhury, & Gani, 2003; Mitra, Priestley, Kajaljyoti, & Gaur, 2018; Singh et al., 2016). The Hinge Zone today marks also the transition between the basin margin and the Ganges–Brahmaputra–Meghna (GBM) delta plain (Grall et al., 2018).

The Brahmaputra catchment originates in the Tibetan Plateau north of the main Himalayan divide where it collects sediments from erosion of trans-Himalayan batholiths and Tethys Himalaya (Figure 1). In contrast, the Ganges River drains a large portion of the Indian craton, although its sediment load derives primarily from the Himalaya (Singh, Santosh, & Krishnaswami, 2008). The Ganges and Brahmaputra Rivers each flow at the foot of the Himalayan orogen where they collect sediments from transverse sources varying from individual bedrock streams to mega-alluvial fans (Brammer, 2012). In the Bengal basin, the two rivers merge. The Tista River, located in northwest Bengal (Figures

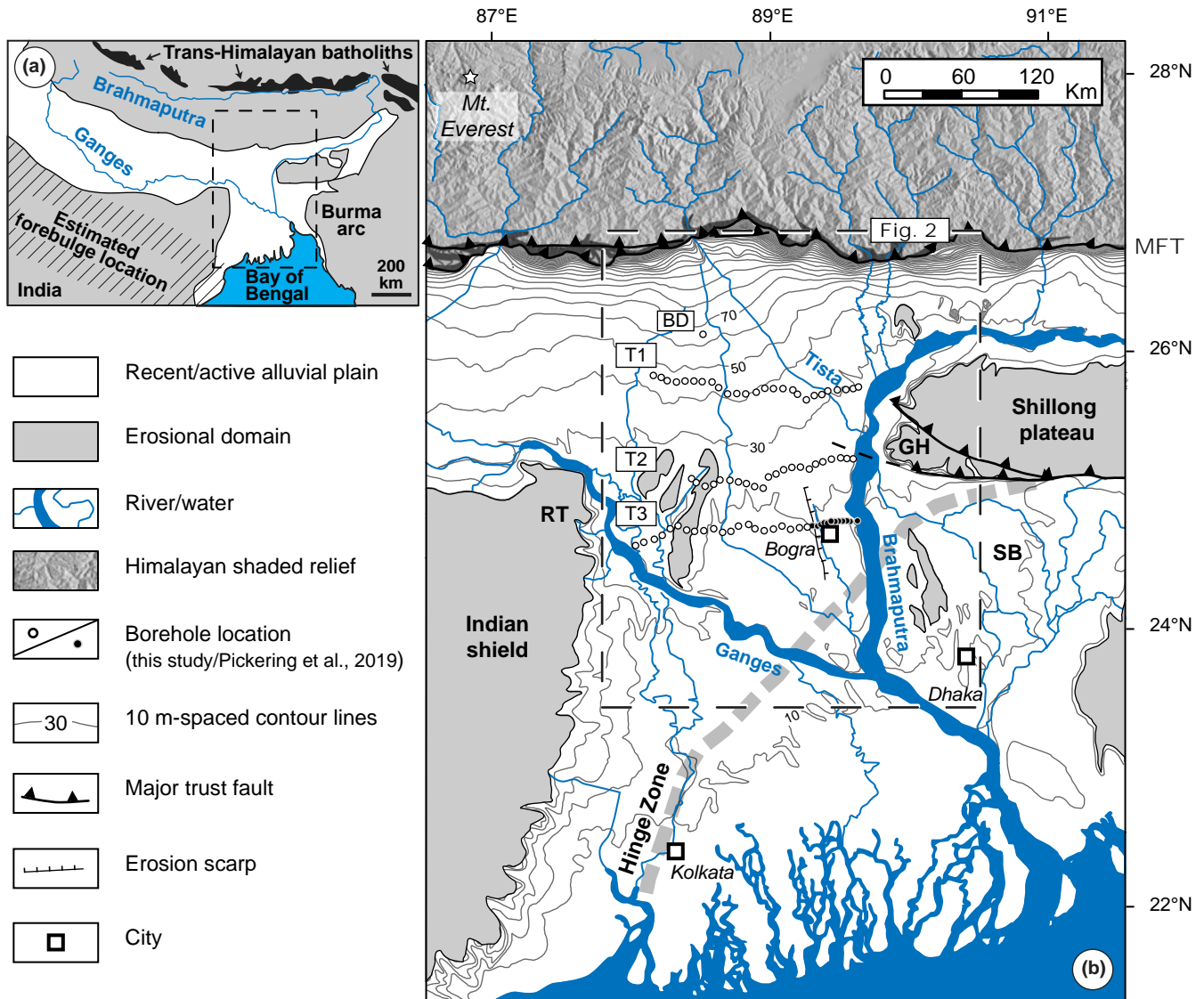


FIGURE 1 (a) Simplified regional map showing the Brahmaputra and Ganges rivers' main channel. The estimated location of the forebulge in the Indian craton is after DeCelles (2012). (b) Physiographic map of the Ganges–Brahmaputra–Meghna (GBM) delta. The study area is shown by the dashed rectangle. The grey dashed stripe corresponds to the hinge zone (after Goodbred et al., 2014). MFT stands for Main Frontal Thrust, GH for the Garo Hills of western Shillong Massif, SB for the Sylhet Basin, BD for the city of Boda (where borehole TXBD01 was drilled) and RT for the Rajmahal traps at the edge of the Indian craton

1 and 2), is one of the largest local sediment sources to the Bengal basin (ca. 5% of the total load transported by the Ganges–Brahmaputra). Over the Late Quaternary, total sediment delivery to the Bengal basin has varied an order of magnitude with orbital-scale climatic variations (Goodbred, 2003; Pickering et al., 2019; Wiedicke, Kudrass, & Hübscher, 1999), thus affecting the sediment-loading component of subsidence. Holocene sedimentation rates adjusted for subsidence range from 0.2 to 4.5 mm/year (Grall et al., 2018).

The Late Quaternary record of the Bengal basin is generally marked by well-developed Pleistocene palaeosols that are overlain by largely unweathered Holocene sediments (Hoque, McArthur, & Sikdar, 2014; McArthur, Nath, Banerjee, Purohit, & Grassineau, 2011; Morgan & McIntire,

1959; Pickering et al., 2014). Where buried by Holocene sediments, the Pleistocene boundary is often referred to as the 'LGM surface' after the Last Glacial Maximum when a ca. 130-m sea level fall triggered the development of large lowstand valleys and broad interfluvies were exposed to enhanced weathering (e.g. Goodbred & Kuehl, 2000). Such distinction between Pleistocene and Holocene sediments has been validated by over a hundred radiocarbon ages in the GBM delta (Figure 1; Pickering et al., 2014; Sincavage et al., 2018, 2019 and references therein). However, it is now increasingly recognized that the 'LGM' surface is really a composite surface of multiple Pleistocene episodes of deposition and incision (Pickering et al., 2014, 2019, 2017) in NW Bangladesh. River mobility is well constrained during

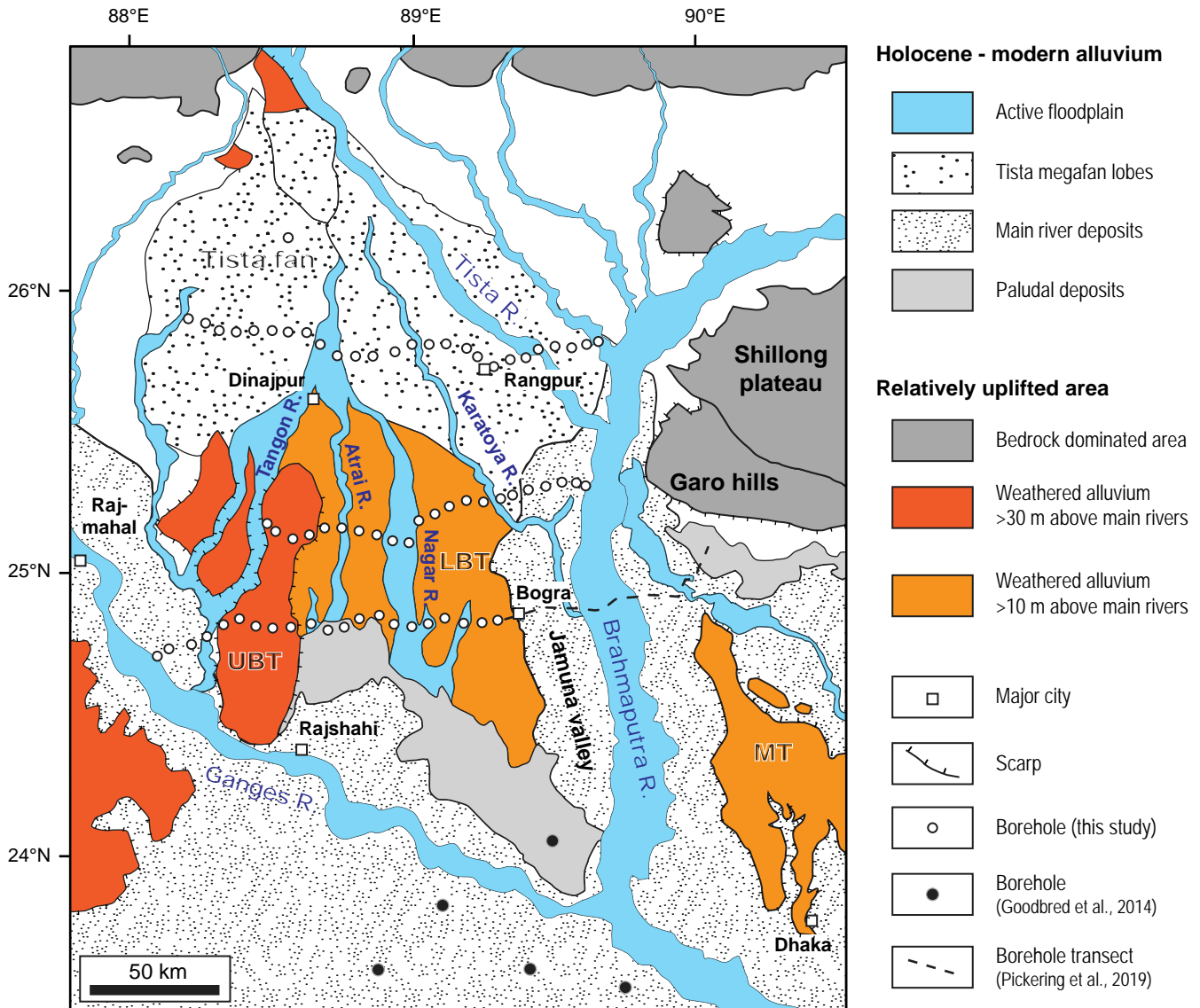


FIGURE 2 Mapping of present-day surface geomorphology in the study area based on our field observations as well as existing physical, geological and soil maps of the area (Alam et al., 1990; Brammer, 2012; Chakraborty & Gosh, 2010; McArthur et al., 2011; Morgan & McIntire, 1959; Pickering et al., 2014). Location is shown in Figure 1b

the Holocene for the Brahmaputra and Ganges Rivers; major avulsion periodicity is about 1,500–2,500 years (Goodbred et al., 2014; Pickering et al., 2014; Reitz et al., 2015; Sincavage et al., 2018). The course of the Tista River has also changed in past centuries, switching from the Atrai and Karatoa river channels to its present location along the eastern boundary of its fan (Chakraborty & Gosh, 2010; Figure 2). The evolution of the Tista megafan is, however, less constrained prior to historical times, although the degree of soil development suggests an abandonment of the western ‘old piedmont’ fan and the more recent occupation of the eastern active fan during the Holocene (Abramahi et al., 2018; Brammer, 2012; Chakraborty & Gosh, 2010).

South of the Tista megafan, the Barind Tract, a low-gradient topographic high divided into Lower (LBT) and Upper

(UBT) parts (Figure 2), is composed of Quaternary sediments currently located above the influence of sea level-related backwater effects (*sensu* Wilson & Goodbred, 2015). The nearby avulsion node between the Jamuna and the Old Brahmaputra valleys (Bristow, Smith, & Rogers, 1999; Sincavage et al., 2018) therefore lies beyond influence from sea level, at least since the mid-Holocene, and it is not directly influenced by bedrock due to Holocene alluvial cover (Ganti et al., 2016; Hartley et al., 2016); these circumstances suggest that there may be additional controls on avulsion dynamics, such as substrate deformation. Tectonic uplift has been invoked as controlling the Plio-Quaternary path of the Brahmaputra River, particular along the Shillong massif and its bounding Dauki fault (e.g. Govin et al., 2018; Najman, Bracciali, Parrish, Chisty, & Copley, 2016; Pickering et al.,

2014). In the Barind Tract, evidence for faulting is more speculative (Morgan & McIntire, 1959). In the following, we evaluate the hypothesis that, similar to the Mississippi River valley (Blum et al., 2013), flexural deformation explains rivers patterns and sediment routing in the Barind Tract and Tista fan.

3 | METHODS

3.1 | Geomorphic and subsurface data

Mapping of the present-day surface geomorphology (Figure 2) is based on field campaigns, topographic DEM analyses, as well as existing physical, geological and soil maps of the area (Alam, Hasan, Rahman Khan, & Whitney, 1990; Brammer, 2012; Chakraborty & Gosh, 2010; McArthur et al., 2011;

Morgan & McIntire, 1959; Pickering et al., 2014, 2019). In addition, sediment deposits were sampled along three east–west borehole transects (T1, T2 and T3 transects) in fall 2015 and an additional borehole (TXBD01) in spring 2016 (Figures 1 and 2). The unconsolidated sediments were percussion drilled through 5-cm diameter PVC tube sections by hand generating a reverse circulation flow (Figure 3a). During the drilling process, the sediments were incorporated into water in suspension and expelled with drilling fluids (water and sediment) that were collected at 1.5 m intervals, or finer with notice of lithological changes. The drilling method extended to 70 m below the surface (Figures 3 and 4). Because of the unconsolidated nature of the sediments, sedimentary structures were not preserved in the coarser samples; however, structure was preserved in cohesive mud intervals.

A fraction of sediment (ca. 200 g) was kept at each interval and analysed later. Dominant sediment grain sizes

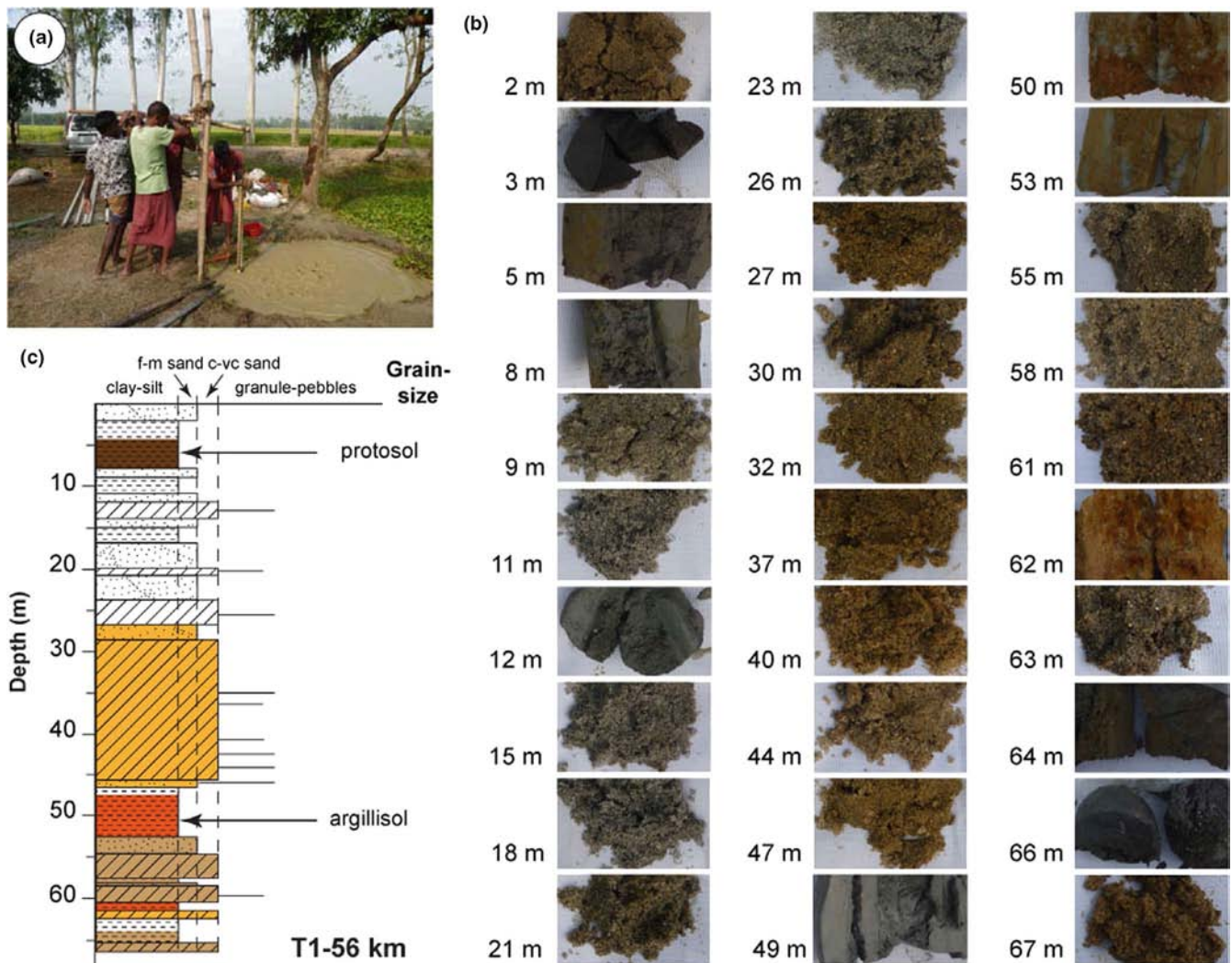


FIGURE 3 Description of the sample and description procedure for borehole data based on borehole T1-56 km (see Figure 2). (a) Picture showing the local drilling team at work, the driller is the person at the right holding the plastic tube (see Section 3 for details). (b) Picture of the sampled sediments showing variations of grain size, colouration related to oxidation/weathering and stiffness/cohesion. (c) Interpretation of the lithological succession from (b) based on grain size and weathering

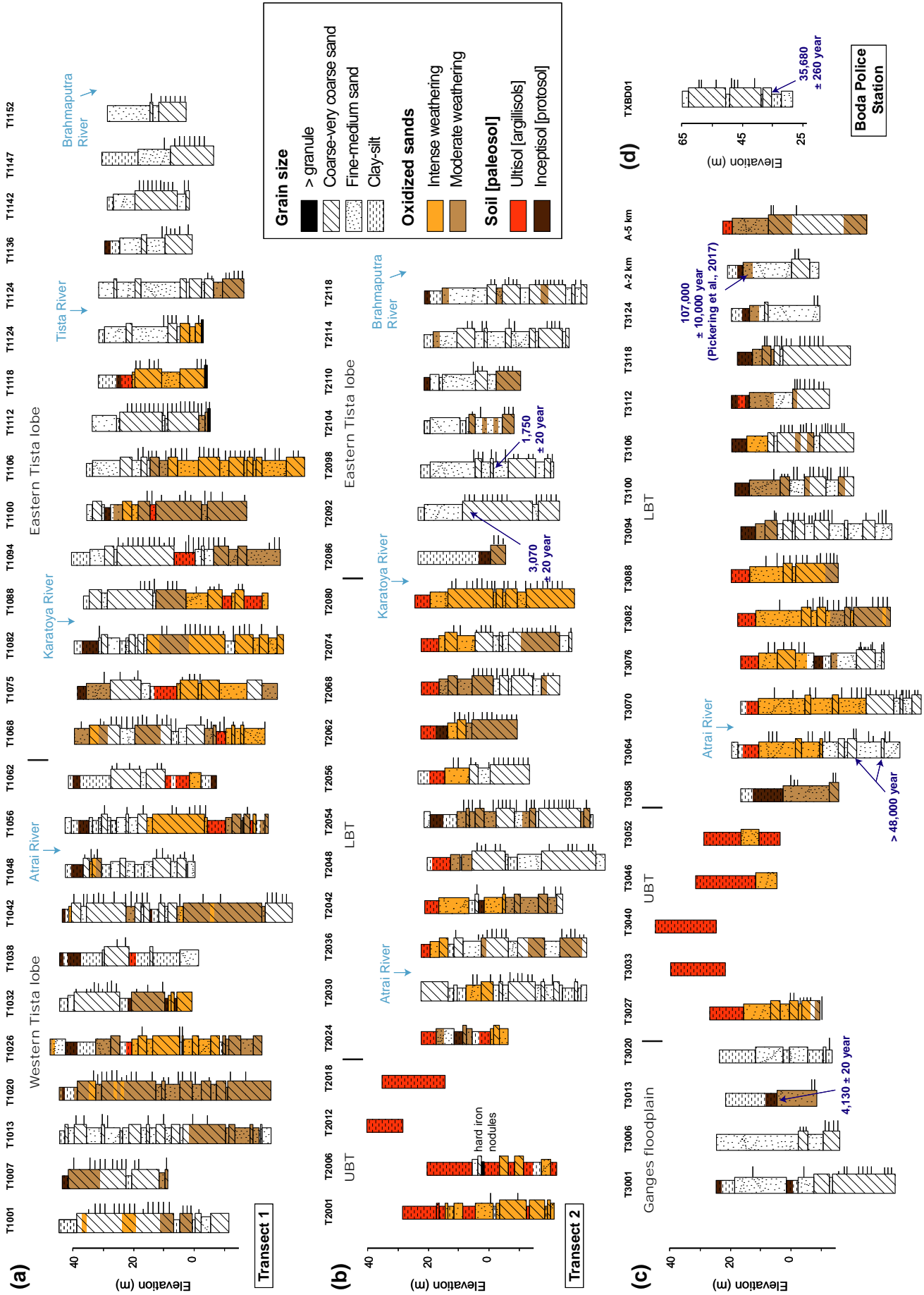


FIGURE 4 Borehole lithological successions along T1 (a), T2 (b), T3 (c) transects and TXBD01 borehole (d). Note that the last 3 digits of borehole names correspond to distance along transect in km. For borehole description method, see Figure 3. Borehole locations are shown in Figures 1 and 2. Boreholes A-2 and A-5, shown for comparison, are from Pickering et al. (2014, 2019)

TABLE 1 Description of main sedimentary facies in the vicinity of the Garo-Rajmahal Gap

Description						
Facies Name	Lithology	Thickness	Lateral continuity	Sr concentration	Locations	Interpretation
Large braidbelt deposits (LBf)	Well-sorted fine to medium sand alternating with coarse to very coarse sand; gravels often present; basal pebble layer may be found	Typically >50 m	>20–30 km	Typically > 120 ppm; locally 90–120 ppm	Jamuna valley and typically below 10 m in the Barind Tract	Alluvial deposits of the Brahmaputra River system; local mixing with Tista material
Small braidbelt deposits (SBf)	Moderately sorted coarse to very coarse sand alternating with fine to medium sand; gravels often present	Typically 10–40 m; locally up to 60 m	Typically > 10 km; up to 15 km	Typically 30–80 ppm; locally 90 ppm	Tista fan lobes and locally along the Atrai River	Alluvial deposits of the Tista megafan
Sinuuous stream deposits (SSf)	Intercalated sand deposits and clay–silt deposits	Typically < 10 m	<6 km	Typically 30–80 ppm; locally 90 ppm	Tista fan lobes and locally along the Atrai River	Alluvial deposits of the Tista megafan
Tista Overbank Muds (TOf)	Clay–silt layers, various degree of weathering observed	Typically 10–20 m	<6 km	Typically 30–80 ppm; locally 90 ppm	Tista fan lobes	Distal floodplain deposits of the Tista River system
Mixed Overbank Muds (MOF)		Typically 5–15 m; locally up to 40 m	>20–30 km	Variable (30–100 ppm)	Barind Tract	Distal floodplain deposits; Mixed provenance (Tista–Brahmaputra), interpretation complicated by weathering

and facies were described in the field (Figures 3 and 4; Appendix S1; Table 1). Seven wood and organic sediment samples were identified and collected for radiocarbon dating, performed at the National Ocean Sciences Accelerator Mass Spectrometry Facility (NOSAMS) and at Beta Analytic (Miami, FL; Figure 4; Appendix S2). Sediment weathering was described according to the palaeosols classification of Mack, James, and Monger (1993) combined with reference to the US soil order for the modern soil equivalent (Soil Survey Staff, 1999; Figures 3 and 4). In parallel, we also described the degree of sediment oxidation according to colouration (i.e. increasing from brown to red; Figures 3 and 4).

Sediment geochemistry and provenance were investigated by measuring Sr concentrations of the bulk sediments of selected borehole samples using a Niton XL3t X-Ray Fluorescence (XRF) handheld device mounted on a base (see results in Figure 5 and Appendix S2; Goodbred et al., 2014; Pickering et al., 2014). We performed analyses over 120 s with calibrations every 20 measurements. Sr concentration was specifically verified using NIST 2709a (239 ± 6 ppm Sr) and CCRMP Till-4 (109 ppm Sr) standards. We analysed 68 boreholes with a 6-km average horizontal spacing (Figure 5). Since UBT sediments were very intensely weathered (see below), we focus on the LBT and Tista fan.

Within the Ganges–Brahmaputra–Meghna river delta, Brahmaputra sediments have a distinctively higher Sr concentration due to the erosion of mafic minerals—mainly plagioclase where Sr substitutes for Ca—from the trans-Himalayan batholiths (Galy & France-Lanord, 2001; Garzanti et al., 2010; Goodbred et al., 2014; Figures 1, 5 and 6). In Holocene sediments, Sr concentrations of Brahmaputra sediment are typically >140 ppm, compared with 80–110 ppm for the Ganges. A lower limit of 120 ppm Sr may be used for Brahmaputra-derived sediment (Sincavage et al., 2018) when considering Pleistocene deposits with potential Sr leaching by weathering and mixing with other sources (i.e. Tista in the present case). In this study, an even lower limit of 100 ppm was considered for potential Brahmaputra-derived sediment, given that published Sr values for Tista river-bank samples are <95 ppm (Singh & France-Lanord, 2002; Figures 5 and 6).

3.2 | Geophysics data and modelling

We estimated the position of the peripheral bulge and the depression (foredeep) associated with the tectonic load of the Himalaya using continuous elastic plate models (e.g. Watts, Zhong, & Hunter, 2013; Figure 7), consistent with recent models for the Himalaya (Berthet et al., 2013; Hammer et al., 2013). We ran models using both the entire Himalaya as a load to produce the foredeep and flexural bulge and using

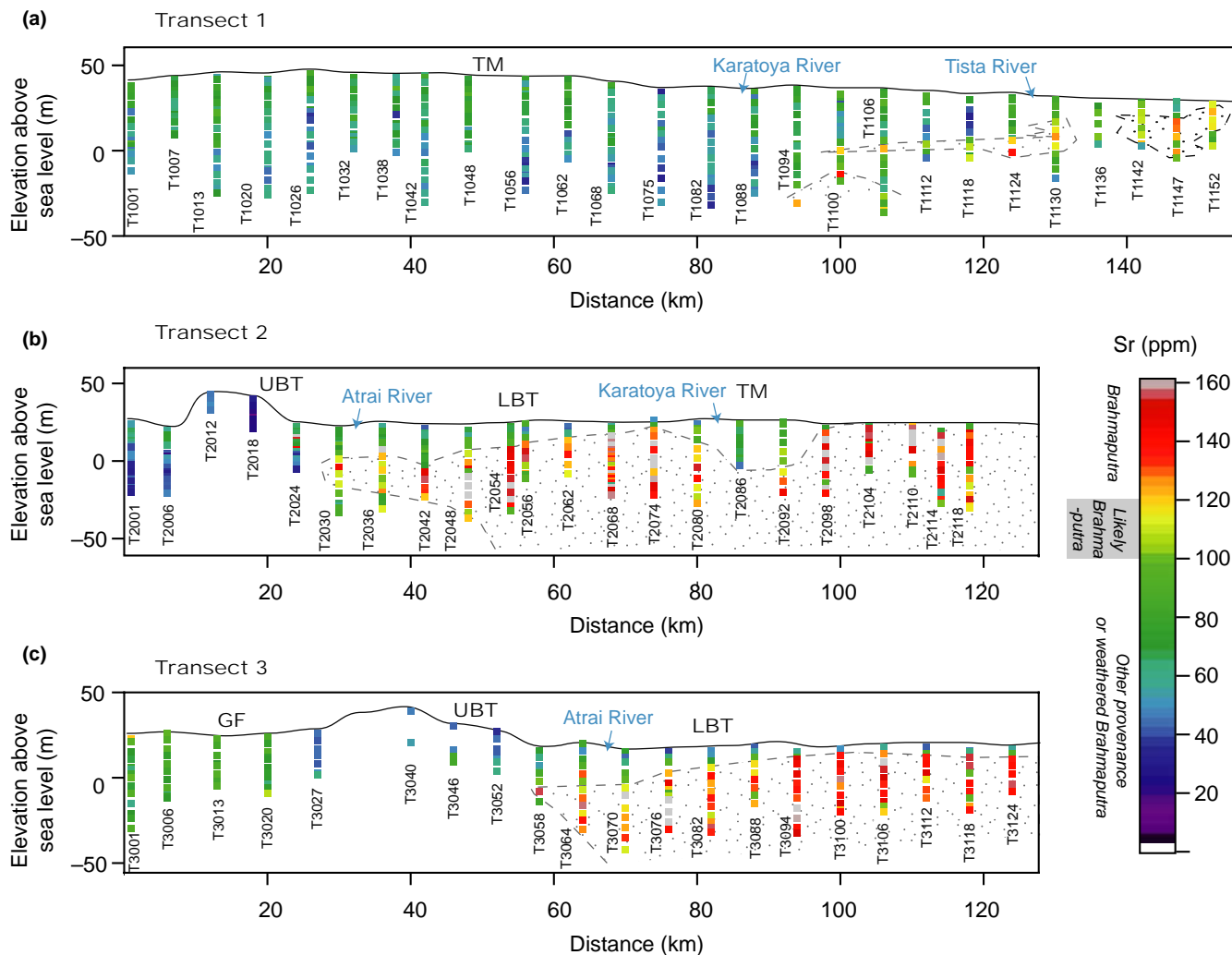


FIGURE 5 Variations of Strontium (Sr) of concentration (ppm) along transects T1 (a), T2 (b) and T3 (c). The dashed line draws an approximate boundary between Brahmaputra and Tista sediments. GF, Ganges Floodplain; LBT, Lower Barind Tract; TM, Tista Megafan; UBT, Upper Barind Tract

an advance rate of the Himalaya topography at 25 mm/year to estimate approximate rates of Holocene uplift.

For a 2D beam over a weak substratum, the flexural equation is

$$\frac{d^2}{dx^2} \left(D(x) \frac{d^2 \omega}{dx^2} \right) + \Delta \rho g \omega = V_0 \quad (1)$$

where x is distance, $D(x)$ is the flexural rigidity, ω is the deflection of the lithosphere, $\Delta \rho$ is density contrast between the mantle and the material infilling the deflection, g is the acceleration of gravity and V_0 is the weight of the load.

In the case of a line load on a 2D unbroken plate of constant flexural rigidity

$$\omega = \omega_0 \cdot e^{-x/\alpha} \cdot \left(\cos \frac{x}{\alpha} + \sin \frac{x}{\alpha} \right), \quad (2)$$

$$\text{with } \omega_0 = \frac{V_0 \cdot \alpha^3}{8D} \text{ and } \alpha = \left[\frac{4D}{\Delta \rho g} \right]^{1/4}$$

where α is the flexural parameter, ω_0 the maximum deflection at the loading location. D is a function of the effective elastic thickness Te with $D = ETe^3 / [12(1 - \sigma^2)]$, where E is Young's modulus and σ is Poisson's ratio. For this simple case, the forebulge starts where $\omega = 0$ at $x = (3\pi/4)\alpha$. The maximum height of the bulge is at $x = \pi\alpha$. For a distributed load, such as the Himalaya and Tibet, the deflection is the convolution of the line load with the response. For calculating the deflection for a spatially variable flexural rigidity, the flexure equation is solved numerically using finite differences.

The position of the forebulge is a function of the lithospheric elastic thickness. Te is high in the Indian craton (75–100 km; Jordan & Watts, 2005), although it decreases northward towards the Main Frontal Thrust (MFT) of the Himalaya due to thermal and flexural weakening (Berthet et al., 2013; Watts et al., 2013) and eastward towards the passive margin beneath the Bengal basin. In the study area, Te estimates are of 30 km across the Garo-Rajmahal Gap (Jordan & Watts, 2005), from 25 km to about 15 km towards the MFT beneath Sikkim and the Bhutan

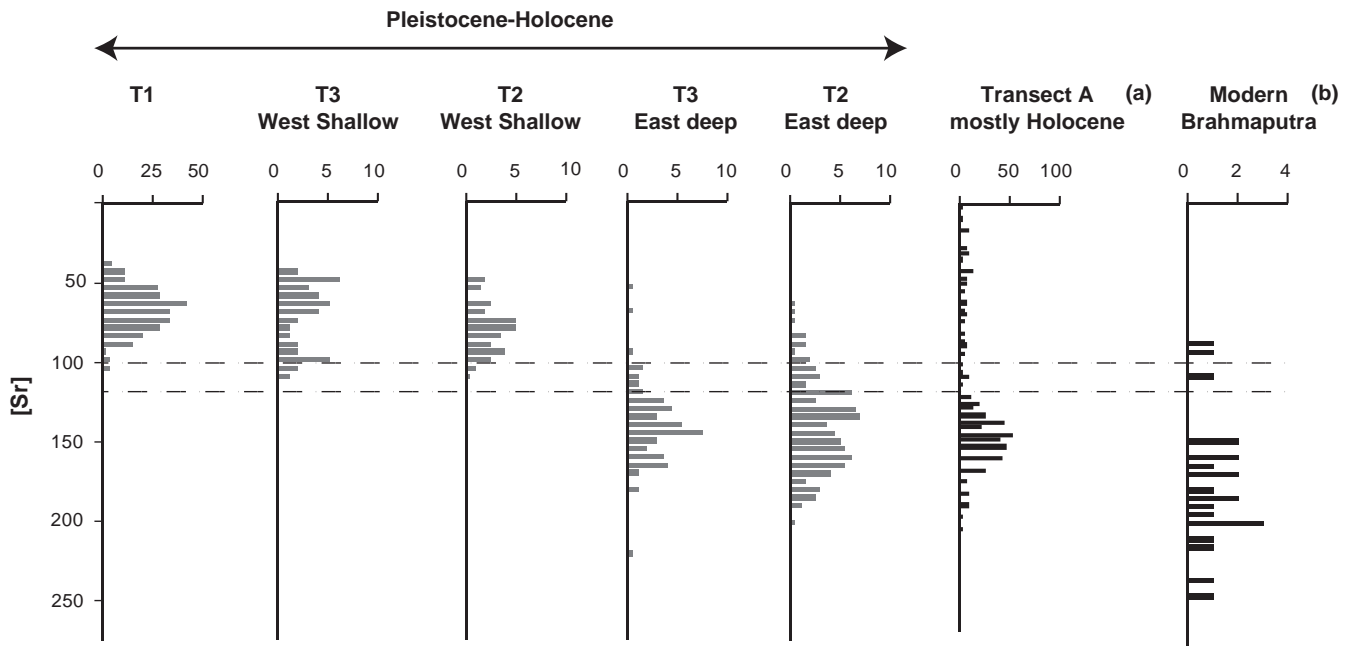


FIGURE 6 Distribution of Sr concentration showed for the different populations from Figure 5. Data in (a) and (b) are respectively from Pickering et al. (2014) and Singh and France-Lanord (2002)

Himalaya on either side of the Garo-Rajmahal Gap (Hammer et al., 2013) and of 5–20 km across the overthrust of the Shillong Massif (Mitra et al., 2018) over the Sylhet Basin (Figure 1). This suggests that the best estimate may be obtained for an intermediate (10–30 km) plate model. Thus we used a 15–25 km range (Figure 7; Appendix S2). For the infill density, we use 2,300 kg/m³ in the foreland and 2,700 kg/m³ beneath the Himalayas. The Bouguer gravity anomaly derived from satellite data (Bonvalot et al., 2012) is used as an independent constraint on the flexural models (Figure 8).

4 | RESULTS AND INTERPRETATIONS

4.1 | Sediment facies and weathering

4.1.1 | Lithofacies and soil type distribution

Five facies are found based on sediment lithology, thickness and lateral continuity (Table 1). Large braided deposits (LBf) consist of well-sorted fine to medium sand alternating with coarse to very coarse sand; gravels are often present. LBf are typically over 50-m thick and over 20–30 km wide. Small braided deposits (SBf) have roughly similar grain size and may be differentiated from LBf by lesser thickness and decreased lateral continuity (i.e. ca. 10–40 m and less than 10 km respectively). Sinuous stream deposits (SSf) are typically less than 10-m thick intercalated sand- and clay-silt deposits with limited (<6 km) lateral extent. Overbank

Mud facies (TOf and MOf) are clay-silts whose thickness (ca. 5–40 m) vary depending on the location. Tista overbank muds (TOf) may be distinguished from mixed provenance overbank muds (MOf) using Sr concentration (see Section 4.2). TOf and MOf facies were very often weathered. Two general soil types were observed (Figure 4): inceptisols and ultisols; together with their palaeosol equivalents: protosols and argillisols respectively. *Inceptisols* are slightly developed soils where many weatherable minerals are still retained. They are usually of brownish colour near the surface and grayish below the water table (1–4 m depth). *Ultisols* correspond to more intensely weathered soils. They contain more translocated clays, which increases their cohesiveness compared to inceptisols, and they may have a red colour that extends many metres deep due to the significant mobilization and oxidation of iron.

These facies and soil types can be found in specific locations across the study area (Figures 2 and 4) (Brammer, 2012). In the Tista megafan north of Dinajpur and Rangpur (T1 transect and borehole TXBD01; Figure 4a,d), deposits consist of SBf and TOf facies, with local SSf facies. Argillisols are observed from 20 to 60 m deep along T1 transect, except in borehole T1118 (10–15 m). All soils at the surface are inceptisols. They are abundant between boreholes T1007 and T1082, that is, the Western Tista lobe (Figure 4a). The UBT area (boreholes T2001 to T2018 and T3027 to T3052; Figure 4) is dominated by thick (ca. 20–40 m) MOf facies associated with ultisol at the surface. In UBT deeper layers, SBf and SSf facies are observed. The LBT area (i.e. boreholes T2024 to T2080, T3058 to T3124 and A-2 to A-5;

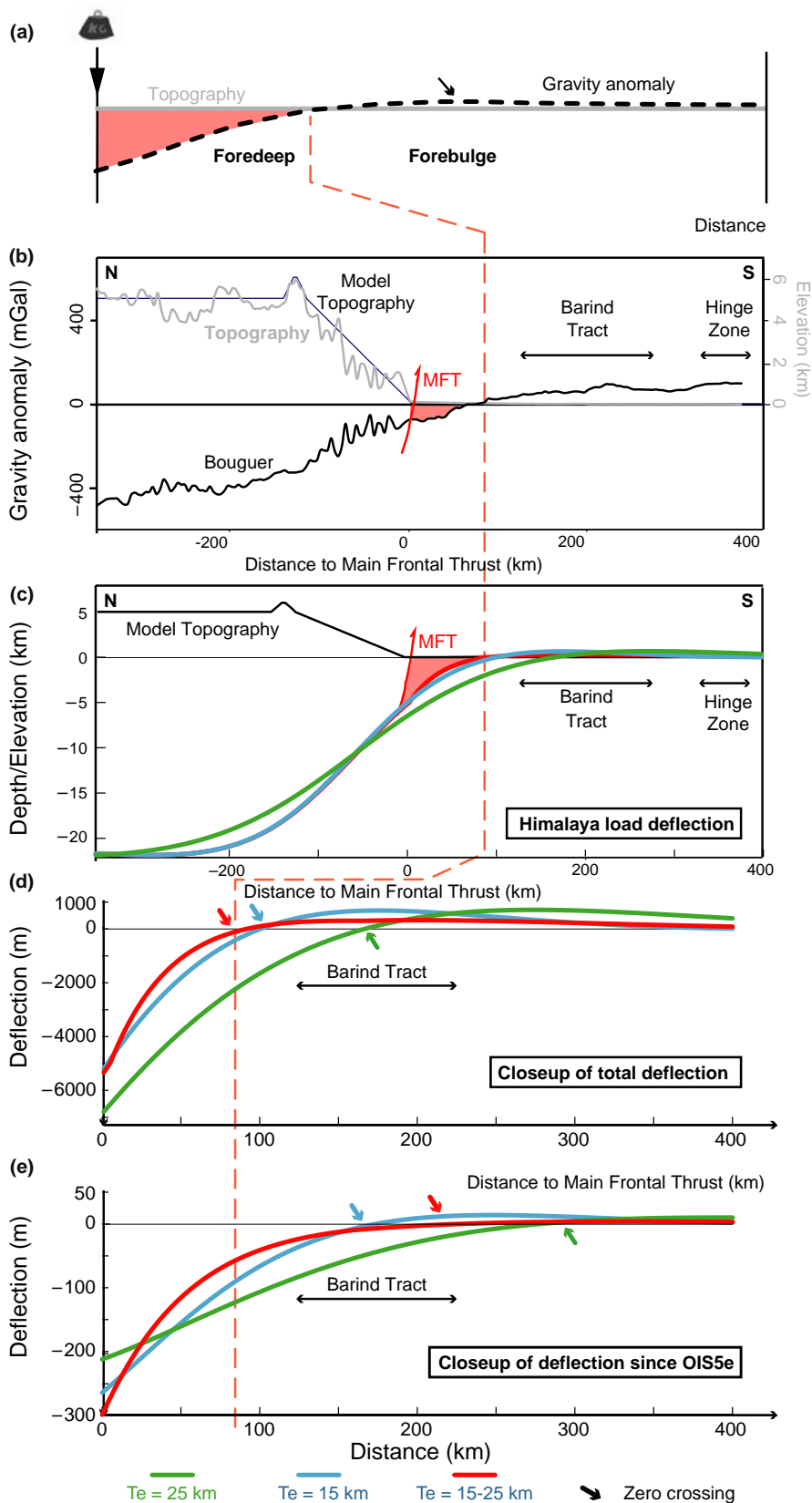


FIGURE 7 Prediction of forebulge position based on gravity data and various elastic models. (a) Sketch explaining the flexural deformation associated with a tectonic load. (b) Regional N-S gravity profile crossing the Himalaya, the Tista Fan and the Barind Tract (see Figure 7a for location). Note the 100-km width negative gravity anomaly observed at the Tista Fan in light red that is interpreted as a flexural depression and the positive anomalies observed at the Barind Tract. Topography and simplified topography used for modelling shown in grey and thin blue lines. (c) Predicted deflection under the Himalaya and Tibetan loads including the forebulge geometry for probable elastic thicknesses (Hammer et al., 2013). The variable elastic thickness model has a linear increase in elastic thicknesses from 15 km at the MFT to 25 km at 160 km farther south. (d) Closeup of the same models as in (c) showing the foreland basin and forebulge with deflection related to the total load by the Himalaya. (e) Closeup of the same models as in (c) with deflection related to an advancing Himalayan front at a rate of 25 mm/year since OIS5e. The red dashed line represents the transition from positive to negative Bouguer gravity anomaly and transition from foreland basin to forebulge

Figure 4b,c) is dominated by thin (ca. 5–15 m) MOF facies with varied degrees of weathering at the surface and LBF facies at depth. Ultisols are dominant at the surface of the LBT along T2 transect while they are restricted to the west

(i.e. from boreholes T3064 to T3088) along T3 transect. To the east, inceptisols are the most common (Figure 4c). Finally, along T2 and T3 transects, the Eastern Tista lobe (i.e. boreholes T2086 to T2118) and the Ganges floodplain

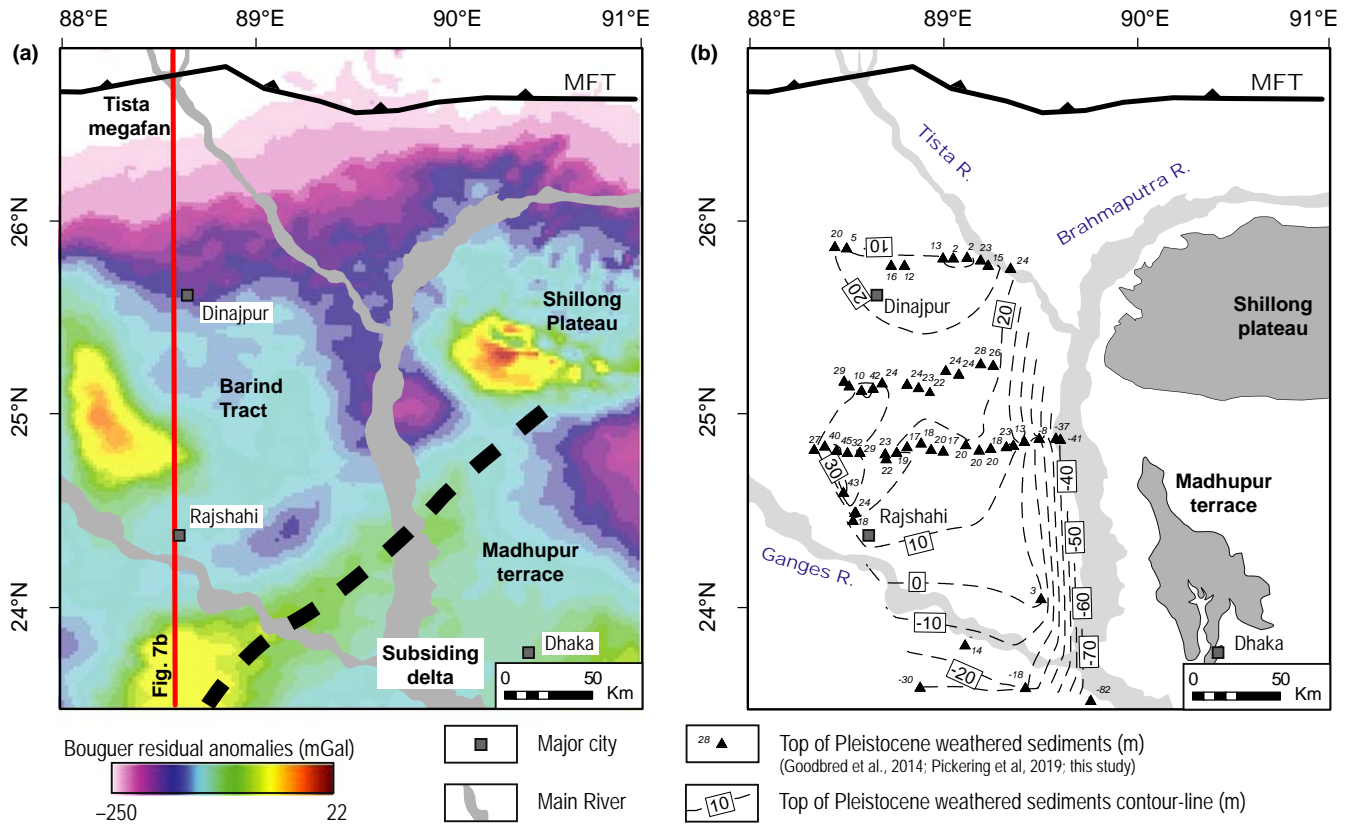


FIGURE 8 (a) Map of Bouguer residual anomalies. The black dashed stripe corresponds to the hinge zone (after Goodbred et al., 2014) that marks the northern boundary of the subsiding delta (Grall et al., 2018). (b) Map of the top of intensely weathered Pleistocene sediments (see Section 5.2). Such boundary has been identified on the field, and along boreholes (e.g. Figures 4 and 5). The interpolation is based on a simple natural neighbour's procedure using the ArcGis software

(i.e. boreholes T3001 to T3013) are both dominated by LBF facies with MOF at the limit with the Barind Tract (Figure 4b,c). Oxidation of these deposits is low as attested by the presence of only few inceptisols and protosols.

4.1.2 | Interpretation

The main difference between SBf and LBF is their lateral extent, which is typically <10 km for SBf (i.e. compared to 20–30 km for Brahmaputra deposits; Sincavage et al., 2018; Table 1). LBF is therefore similar to Brahmaputra River facies. In the Barind Tract, facies are dominantly LBF, supporting deposition by a large river near the scale of the Brahmaputra. In contrast, Tista deposited facies are dominantly SBf (Figure 4) with the occurrence of SSf that may be interpreted as low-energy streams (Chakraborty & Ghosh, 2010) and TOF corresponding to distal floodplain deposits and associated crevasse splays. These rapid lateral facies changes would be consistent with the deposition of smaller fan lobes associated with the Tista.

At the surface of the Barind Tract, palaeosols are widespread and laterally continuous with an overall eastward

decrease of weathering intensity, that is, from the UBT area to the Karatoya and Brahmaputra Rivers (Figure 4b,c). The high (30 m) elevation above main rivers and enhanced weathering of the UBT compared to the LBT suggests that this area has been abandoned for the longest period. The western Tista lobe associated with inceptisols at the surface roughly corresponds to the old, inactive piedmont fan described by Brammer (2012). Mature soils (argillisols), which are typical of Barind Tract and Madhupur terrace, are found below the surface of the Tista megafan.

4.2 | Geochemistry and age of the sediments

The distribution of Sr concentrations along boreholes is shown in Figure 5 (see Figure 4 for comparison with lithology). Along the T1 transect, the concentration of Sr is <100 ppm between boreholes T1001 and T1088 and 50–140 ppm between boreholes T1094 and T1152 (Figure 5a). Along the T2 and T3 transects, high and low Sr populations were delimited at a threshold of 100 ppm in the LBT. This limit is sharp and marks a boundary between overall low-strontium sediments in the western and shallow deposits (mostly MOF), and the

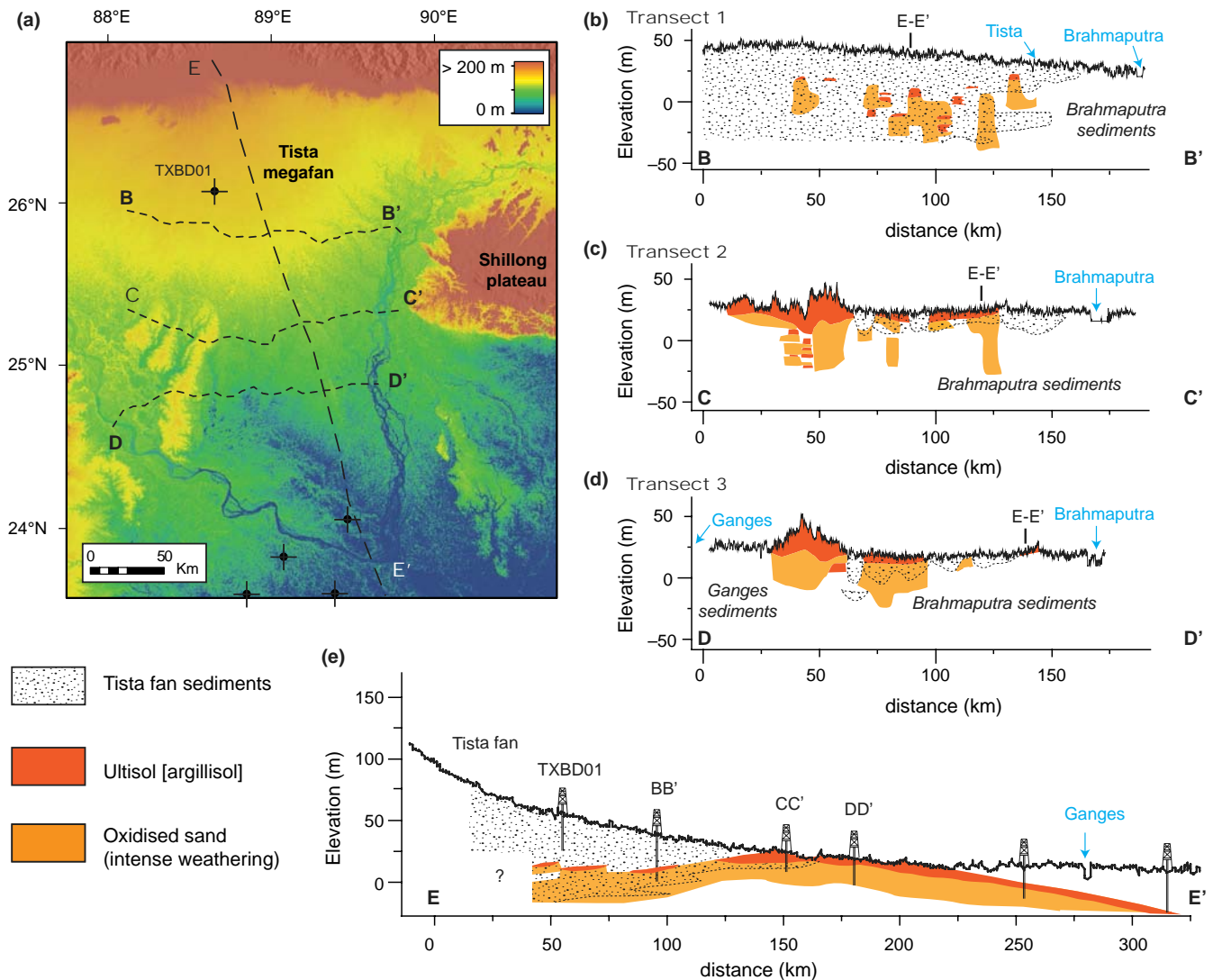


FIGURE 9 Interpretative sections of observations reported in Figures 2, 4 and 5. (a) Topographic map of the study area with location of the sections. Crossed circles correspond to boreholes described by Goodbred et al. (2014). (b, c, d) Interpretations of transects T1, T2 and T3 respectively. (e) Interpretation of a roughly N-S longitudinal profile across the Tista megafan and Barind Tract

high-strontium sediments in the deeper units and towards the east (Figure 5b,c).

Sr populations were considered in the light of published analyses (Pickering et al., 2014; Singh & France-Lanord, 2002) to evaluate the potential effects of weathering and mixing between sources on the measured Sr concentrations (Figure 6). The eastern, deeper sediments along transects T2 and T3 have a median Sr concentration of 135 ± 25 ppm (i.e. using standard deviation). These values are indicative of Brahmaputra provenance although they are lower than (a) that of Pickering et al. (2014) in Holocene sediments of Transect A (149 ± 44 ppm) and (b) that of Singh and France-Lanord (2002) along the bank or in monsoonal suspended sediment of the modern Brahmaputra channel (183 ± 41 ppm; Figure 6). Between T1001 and T1088, sediment of the Tista fan has a Sr concentrations median value of ca. 61 ± 13 ppm. This is lower than the ca. 90 ppm values

reported by Singh and France-Lanord (2002) for modern Tista sediment. T3001 to T3020 that lie in the Ganges floodplain yield Sr concentrations of 80–110 ppm, which is typical for unweathered Ganges sediments (Figure 5e; Goodbred et al., 2014; Lupker, France-Lanord, Galy, Lavé, & Kudrass, 2013). The western, shallow deposits along the T2 and T3 transects (excluding UBT and Ganges floodplain sediments) represent another definable set of samples that have Sr concentrations of 61 ± 17 ppm (Figures 5 and 6). This last set has a range comparable to that of Tista sediment but is not distributed normally, unlike T1. This suggests that the sediment here has not only a Tista provenance but incorporates other material such as reworked Brahmaputra sediment.

Corrected radiocarbon ages of sediments deposited in the vicinity of the Ganges are $4,130 \pm 20$ years BP at 15 m (Figure 4c). Between the Karatoya and Brahmaputra rivers, ages of shallow sediments are 1,750–4,000 years BP

FIGURE 10 Geological model explaining patterns of sediment provenance and weathering in the study area

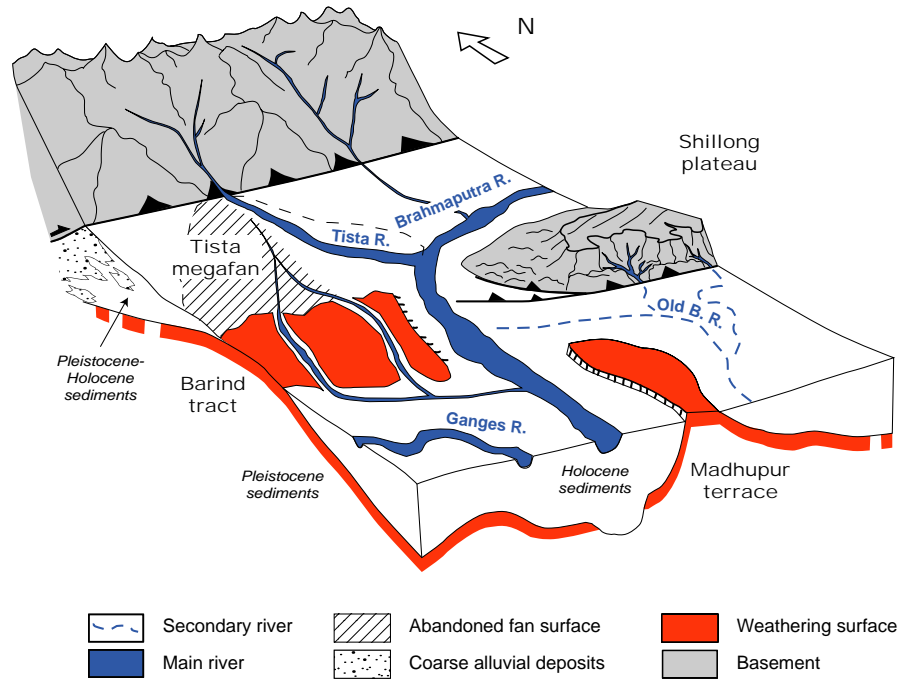


(Figure 4b). Along borehole T2092, the age at 20 m depth of 4,000 years BP is associated with changes of grain size (from coarse to medium sand) and Sr concentration (from 105 to 80 ppm). In the LBT, sediments are older than 48,000 years BP (the time limit of the radiocarbon technique) at 43–53 m deep (borehole T3064; Figure 4c). One Pleistocene age ($35,680 \pm 260$ years BP) is reported at 29 m deep in the Tista megafan (TXBD01 borehole; Figure 4d).

4.3 | Flexural deformation

In the study area, estimates of T_e suggest a decrease from 25 to 15 km towards the MFT (Hammer et al., 2013). We present models using these two values as well as a model in which the T_e decreases linearly from 25 (160 km from MFT) to 15 km (at MFT; Appendix S2). Results show that the MFT to zero crossing (i.e. the limit between subsiding foreland basin and uplifted flexural bulge) distance is between 90 and 170 km (Figure 7). The maximum elevation of the flexural bulge is found ca. 175, 200 and 275 km away from the MFT for the three models. These estimates yield a flexural bulge that fall within the Barind Tract area (Figures 7, 9 and 10). The fit could be improved if the lower rigidity close to the MFT was increased to 20 km or varying from 20 to 30 km yielding 130–135 km for MFT to zero crossing distance and 225–255 km from MFT to maximum elevation distance.

To estimate the rates of subsidence and uplift, we created a differential load by advancing the topography at 25 mm/year. This load is centred over the front face of the Himalaya. These models show a similar pattern to

the overall load, but the zero crossing and flexural bulge are farther from the MFT (Figure 7e). In fact, the node is close to the position of the maximum overall bulge. Thus, the differential loading indicates the southern part of the Barind tract is uplifting, while the northern part is subsiding to eventually be buried by the Tista Fan. The models yield maximum uplift rates from the Himalayan load of 0.03–0.11 m/kyr. This suggests 4–14 m of uplift since the OIS stage 5e highstand.

The wavelength of gravity anomalies derived from satellite data is consistent with the flexural deformation model (Figures 7 and 8). South of the MFT, a ca. 100–150 km wavelength negative anomaly is observed (Figure 8a), while even further south, the Bouguer anomalies become positive within the Barind Tract. The anomaly contrast between the Barind Tract and Tista megafan is around 200 mGal, that is, largely exceeding variability due to the density of sediment fill. Hence, the Bouguer anomalies observed are best explained by a deeper density contrast resulting from lithospheric warping below the Garo-Rajmahal Gap consistent with flexural deformation.

5 | DISCUSSION

5.1 | Distribution and timing of sediment accumulations

The present study contrasts surface dynamics and sediment infill between the Barind Tract and Tista megafan. Tista megafan stratigraphy is characterized by rapid lateral facies changes (ca. 10 km; Figure 4; Table 1). We interpret this as an

indication of deposition by fan lobes of limited lateral extent. The preservation of overbank muds further indicates that fine deposits were not completely reworked by the Tista River system. Radiocarbon dating of borehole TXBD01 (Figure 4) gives a sedimentation rate of 0.8 mm/year. Published sediment ages based on OSL and cosmogenic nuclide dating techniques at the surface of the Tista megafan (ca. 30 to 1 kyr BP) suggest sedimentation rates that may be even lower locally (Abrahami et al., 2018). Pleistocene to early Holocene ages were sampled in the western Tista lobe, which is capped by inceptisols (Figure 4). This supports previous interpretations that this lobe is older than the eastern one (Chakraborty & Gosh, 2010). Additionally, the ages indicate that the mature argillisols below the Tista megafan are older than 30 kyr BP and therefore formed prior to the LGM.

The Barind Tract—especially the LBT—preserves limited clay–silt deposits and soils at depth; rather, most fines are found at the surface (Figure 4). Apart from these shallow fine deposits, the stratigraphy of the LBT is sand dominated and characteristic of a big river able to efficiently rework fine deposits (Goodbred, Kuehl, Steckler, & Sarker, 2003). Strontium data indicate a Brahmaputra provenance for these sediments, in agreement with facies interpretations (Figure 6; Table 1). Recent OSL dating of the Bogra Terrace, the easternmost part of LBT, returned an age of 106 ± 10 kyr of the Brahmaputra sediments at 6 m deep (Pickering et al., 2017; Figure 4c). As also suggested by two radiocarbon ages along borehole T3064 (>48,000 years BP), LBT sediments are mostly Pleistocene and older than the LGM. This suggests that the Barind Tract remained exposed to weathering throughout the past 100,000 years as attested by the presence of mature soils at the surface (i.e. ultisols; Kraus, 1999). Hence, the Barind Tract was occupied by the Brahmaputra River system in the Late Pleistocene but has since been largely abandoned.

The UBT is capped by the thickest ultisol of the study area, with the local presence of iron nodules that resemble those of lateritic profiles on bedrock (Grimaud, Chardon, Metelka, Beauvais, & Bamba, 2015) and suggest very long-term exposure (10^{5-6} year; Targulian & Krasilnikov, 2007). The UBT is therefore likely the oldest landform of the Garo-Rajmahal Gap area. The UBT is separated from the Ganges River by a scarp, suggesting that the river is actively eroding the landform before entering the GBM delta (Figures 1, 2 and 9a). Similarly, rivers from the Tista system moderately incise the LBT surface. This is confirmed by field observations along the Atrai River (Figure 2), which locally flows over and loosely incises stiff ultisols in the LBT area. These observations suggest active uplift in the Barind Tract.

Sr concentrations show that T1 is dominated by low Sr, Tista sediment and that T2 and T3 are dominated to the east by high Sr, Brahmaputra sediment. Within a population, Sr concentration variability may be related to grain size differences, sediment reworking/mixing and chemical

weathering (Lupker et al., 2013; Sincavage et al., 2018). Overall, Quaternary Sr concentrations are 30% lower than modern Tista and Brahmaputra sediments (Figure 6). In the case of Tista, the fact that the source area is reduced—and that mixing with sediment from catchments other than the Tista would have essentially very similar lithology—supports the suggestion that this 30% reduction is mostly related to weathering and less so to sediment mixing. Sr depletion by weathering for Brahmaputra sediment is consistent with their age: the Pleistocene sediment of the Garo-Rajmahal Gap is more depleted than the Holocene sediment of the Jamuna valley (Pickering et al., 2014), which is more depleted than the modern sediment (Singh & France-Lanord, 2002; Figure 6). Singh and France-Lanord (2002) however, reported an increase in lower Sr sources in the modern Brahmaputra sediment towards Bangladesh. Hence the effects of sediments mixing and weathering may not always be isolated with certainty without further investigation using other tracers. The easternmost boreholes along T2 (T2098 to T2118; Figure 5b) have very high Sr concentrations and are not capped by palaeosols. Thus they are interpreted as part of the recent to modern Brahmaputra alluvial plain (Figure 2). The western shallow (MOF) deposits of the Barind Tract remain the most difficult to interpret (Figure 5). Because their transition with underlying Brahmaputra deposits is sharp, they may be interpreted as resulting from distal channels of the Tista that slightly rework underlying Brahmaputra sediments—that is, similarly to the modern Atrai River. This is consistent with a low Sr concentration valley visible below the Karatoya River (Figure 5b). Alternatively, Mof deposits may be related to extremely intense and long-lasting weathering that depleted Sr of Brahmaputra sediment by more than 30%. This further supports the suggestion that the Barind Tract remained exposed to reworking and weathering through the Late Quaternary.

The mature soils exposed at the surface of the Barind Tract and palaeosols buried in the Tista megafan are not dated with certainty. We do, however, know that they are older than 35 kyr BP, and potentially may be older than 100 kyr BP. This further supports the view that the ‘LGM’ surface is a composite surface of multiple Pleistocene episodes of deposition and incision (Pickering et al., 2019). Hence it cannot be simply used as a geologically instantaneous marker for sequence stratigraphy-based correlation, questioning how palaeovalleys may form in response to a single sea level fall event or incision (Pickering et al., 2019). In Figure 7b, the geometry of the top of this composite Pleistocene weathering surface is interpolated, using a basic GIS algorithm. A broad N-S upwarp is observed (see also Figure 9e). Further investigation on the associated weathering horizons and their ages would be promising for studying pre-Holocene climatic variations, and more generally, the stratigraphy of the GBM. This would require careful assessment of initial sediment

composition depending on provenance (Brammer, 2012; Garzanti et al., 2010; Pickering et al., 2017; this study).

5.2 | Regional deformation pattern

Gravity anomalies of the Garo-Rajmahal Gap are consistent with a lithosphere depressed towards the MFT (Figures 7 and 8). The geometry of the top of intensely weathered Pleistocene sediments also shows a deflection north of Dinajpur (Figure 8b). The Barind Tract has therefore remained a topographic (and basement) high since 100 ka while the Tista megafan has slowly subsided. The upward movement of the basement below the Barind Tract surface is referred to as the 'Rangpur saddle' in earlier geophysical studies (e.g. Alam, 1989; Mukhopadhyay & Dasgupta, 1988). Archaean rock of the Indian craton is found at about 500 m depth at Barakupuria in the Barind Tract (Norman, 1992). The tectonic activity in the Barind Tract could be explained by fault-related tectonics (e.g. Rashid, Sultan-Ul-Islam, & Islam, 2015), but there is little direct evidence for it. The uplifting Barind Tract has been considered as the western termination of the Shillong anticlinorium (e.g. Clark & Bilham, 2008) controlled by the continuation of the Dauki Fault, the Dapsi Fault, the proposed Dhubri-Chunghang Faults (Diehl et al., 2017) to the north, or unnamed fault to the south (Grall et al., 2018). However, the trend of seismicity and three crossings of the Dauki Fault by high-resolution seismic lines (Spiess et al., 2012) suggest that the boundary of the Shillong block bends to the NW (Diehl et al., 2017; Vernant et al., 2019) and does not underlie the Barind Tract. As we argue below, the broad deformation pattern in the Garo-Rajmahal Gap is more compatible with flexure.

Flexure in response to loading by the Himalaya can explain both the subsidence in the Tista fan and the uplift of the Barind Tract, that is, respectively, behaving as a foredeep and a forebulge (Figure 10), without the necessity of invoking additional faulting. The range of 2D estimates for bulge distances from the Himalayan front on a roughly N-S profile (90–275 km; Figure 7) supports a location in the Barind Tract given the estimates of elastic thicknesses in the area (15–30 km; Hammer et al., 2013; Jordan & Watts, 2005). The wavelength of the deformed Barind Pleistocene weathering surface (ca. 200–300 km; Figure 9e), which is broader than that of the fault-related Shillong topography along an N-S section (ca. 100 km), further supports deformation due to flexure in the Garo-Rajmahal Gap as the origin of the Barind Tract. In 3D, sedimentary loading of the GBM Delta and Shillong plateau, probably also contributes to the flexural pattern. This is a promising research direction, particularly because the Barind and Madhupur Tracts may be part of a single sinuous composite flexural bulge (Steckler et al.,

2018). Modelled forward motion of the Himalaya suggests 10–30 m elevation of the Barind Tract relative to the surrounding region over one to several hundred thousand years (Figure 8e,d). The total (i.e. at the scale of the Cenozoic sediments thickness) negative deflection observed at the MFT is ca. 5 km for $T_e = 15\text{--}25$ km (Figure 7c), that is, consistent with Himalayan foreland strata thickness at the same location (4–6 km; Burbank, 1992). At the MFT, estimates subsidence rates are thus ca. 1.5–2.5 mm/year for the Cenozoic and 0.4–1.4 mm/year for the Late Quaternary—consistent with the sediment accumulation rate in the Tista fan.

In Pakistan, Duroy, Farah, and Lillie (1989) also showed a bulge, located on the other side of the Indian craton, that they called the Sargoda ridge. Similar to the Rangpur saddle, the Sargoda ridge is narrow (i.e. 100–150 km) when compared to the forebulge interpreted from GRACE geoid data in the Indian craton (i.e. >500 km; see Bilham, Bendick, & Wallace, 2003; DeCelles, 2012; Figure 1a). Duroy et al. (1989) further suggested such a narrow bulge to be related to an elastic thickness that is lower in this area (ca. 30 km) than the rest of the Himalayan and Indian lithospheres. In the study area, shift of the Himalayan flexural bulge close to the MFT is consistent with the rigidity of the Indian plate decreasing eastward as it approaches the Hinge Zone and edge of the Indian craton (Hammer et al., 2013). In any case, it seems that lower plate rigidity at either end of the Indian craton supports the emergence of structural highs in the Himalayan foreland, whether related to faulting or flexure. With the forward migration of the mountain belt, the Garo-Rajmahal Gap forebulge is expected to propagate southward across India. The region north of the peak of the forebulge towards the Himalaya will undergo subsidence, while the frontside of the advancing forebulge undergoes uplift.

5.3 | Sediment dispersal by deep structure in foreland basins

Sediment routing related to tectonics is a key issue in foreland basins that have been extensively studied based on fieldwork, theory and experiments (e.g. DeCelles, 2012; Densmore et al., 2016; Grimaud, Paola, & Ellis, 2017; Gupta, 1997; Heller, Angevine, Winslow, & Paola, 1988; Humphrey & Konrad, 2000; Posamentier & Allen, 1993; Roddaz, Viers, Brusset, Baby, & Hérail, 2005). Rivers are sensitive to substrate deformation if their intrinsic mobility timescale is long compared to the tectonic deformation timescale. We estimated this intrinsic mobility for the Tista River based on existing theory (e.g. Grimaud et al., 2017; Reitz et al., 2015). The visitation timescale of an alluvial fan surface by a river (T_c) scales with the intrinsic timescale necessary to fill a unit depositional lobe (T_L) divided by the fan surface fraction f_A occupied by this lobe. T_L scales with the volume of the lobe (i.e. lobe

width B times fan radius r times channel depth h) divided by sedimentary flux Q_s .

$$T_c = \frac{T_L}{f_A} = \frac{hBr}{Q_s f_A} \quad (3)$$

Parameters of Equation (3) were estimated from this study and the literature. We used $h = 2$ m based on modern hydrologic surveys (Khan, 2001) and thickness of channel fills in the megafan (Chakraborty & Ghosh, 2010). Millennial denudation rates in the Tista catchment (1.31 mm/year; Abrahami, Beek, Huyghe, Hardwick, & Carcaillet, 2016) yielded 27 Mt/year for sediment flux at the apex of the fan. Sinha and Friend (1994), however, demonstrated that up to 90% of sediment is transferred to big rivers in the case of the Ganges, leaving only 10% to megafans (i.e. 2.7 Mt/year). We use $r = 150$ km and $B = 10$ km, based on LBf facies extent (Figure 4; Table 1), which returns $f_A \sim 0.08$. Using these parameters with 20%–40% porosity in deposits, we found $T_L \sim 2$ kyrs and $T_c \sim 25$ kyrs. The T_c estimate is roughly consistent with OSL ages up to 30 kyrs found at the surface of the Western Tista lobe (Abrahami et al., 2018).

In comparison, T_L is 550 years for the Brahmaputra River (Reitz et al., 2015). This indicates that the Brahmaputra River is intrinsically three to four times more laterally mobile than the Tista River. Therefore, the latter will be more sensitive to tectonic uplift (Bufe, Paola, & Burbank, 2016; Grimaud et al., 2017). This is in agreement with (a) the Tista River being steered to the east, (b) the Tista fan not extending further than the Barind Tract and (c) the Brahmaputra River cutting its way across the bulge. The Brahmaputra River system once flowed over the Barind Tract sometime in the Late Pleistocene, but has been confined to the Jamuna valley since then (Figures 4 and 8). Carving of the younger Jamuna valley is related to sea level drop during LGM times, augmented by Late Pleistocene and early Holocene megaflood outbursts (Pickering et al., 2019). In addition, our study demonstrates flexural rock uplift across the Barind Tract. This uplift reduces channel lateral mobility (Bufe et al., 2016) and likely contributed to the entrenchment of the Brahmaputra River in the Jamuna valley. We predict a similar fate for the Ganges River, which is currently confined in its valley flanked by the UBT to the east (Figures 1, 2 and 9). This flexural response of the lithosphere to loading also controls the downstream extent of depositional lobes of piedmont megafans. In accordance with the distribution of accommodation rates, it favours the entrenchment of big rivers that cross upwarps as well, which leads to long-lasting avulsion nodes. In conclusion, the Garo-Rajmahal example shows that deep structures are key features for sediment dispersal in foreland basins.

6 | CONCLUSION

Late Quaternary sediment dispersal was studied in the Garo-Rajmahal Gap by combining geomorphology, soils and sediment facies analyses, and geophysical data. We found that:

1. Surface dynamics vary from subsidence and sediment infilling (rate ca. 0.8–2 mm/year) in the Tista megafan, at the foot of the Himalaya, to uplift (rate ca. 0.03–0.11 mm/year) and prolonged weathering in the Barind Tract to the south.
2. Combined subsidence in the Tista fan and uplift of the Barind Tract are consistent with a N-S flexural response of the Indian plate to loading of the Himalaya Mountains, but with a flexural rigidity that is less than cratonic India farther west.
3. Provenance analysis shows a dispersal of sediment consistent with this flexural deformation, particularly the abandonment of the Barind Tract by the Pleistocene Brahmaputra River and the current extent of the Tista megafan lobes.

ACKNOWLEDGEMENTS

This work was supported by the SAFL Industrial Consortium for Experimental Stratigraphy and the BanglaPIRE project, NSF Partnerships for International Research and Education grant OISE 09-68354. We are grateful to Robert Hall, Neils Hovius and his colleagues at GFZ Postdam, and Christian France-Lanord for discussions and comments on this work. We thank the Bureau Gravimétrique International (BGI)/International Association of Geodesy for access to data. Lamont-Doherty Earth Observatory publication number 8371.

DATA AVAILABILITY STATEMENT

The data that support the findings of this study are provided in the supplementary material.

ORCID

Jean-Louis Grimaud  <https://orcid.org/0000-0001-8857-8269>

Celine Grall  <https://orcid.org/0000-0001-9377-845X>

Steven Goodbred  <https://orcid.org/0000-0001-7626-9864>

Ryan Sincavage  <https://orcid.org/0000-0003-2083-7345>

Jennifer L. Pickering  <http://orcid.org/0000-0003-3666-6907>

Chris Paola  <http://orcid.org/0000-0001-7398-6163>

REFERENCES

- Abrahami, R., Huyghe, P., van der Beek, P., Lowick, S., Carcaillet, J., & Chakraborty, T. (2018). Late Pleistocene–Holocene development of the tista megafan (West Bengal, India): ^{10}Be cosmogenic and IRSL age constraints. *Quaternary Science Reviews*, 185, 69–90. <https://doi.org/10.1016/j.quascirev.2018.02.001>
- Abrahami, R., van der Beek, P., Huyghe, P., Hardwick, E., & Carcaillet, J. (2016). Decoupling of long-term exhumation and short-term

- erosion rates in the Sikkim Himalaya. *Earth and Planetary Science Letters*, 433, 76–88. <https://doi.org/10.1016/j.epsl.2015.10.039>
- Alam, M. (1989). Geology and depositional history of Cenozoic sediments of the Bengal Basin of Bangladesh. *Palaeogeography, Palaeoclimatology, Palaeoecology*, 69, 125–139. [https://doi.org/10.1016/0031-0182\(89\)90159-4](https://doi.org/10.1016/0031-0182(89)90159-4)
- Alam, M., Alam, M. M., Curray, J. R., Chowdhury, M. L. R., & Gani, M. R. (2003). An overview of the sedimentary geology of the Bengal Basin in relation to the regional tectonic framework and basin-fill history. *Sedimentary Geology*, 155(3–4), 179–208. [https://doi.org/10.1016/S0037-0738\(02\)00180-X](https://doi.org/10.1016/S0037-0738(02)00180-X)
- Alam, M. K., Hasan, A. K. M. S., Rahman Khan, M., & Whitney, J. W. (1990). *Geological map of Bangladesh*. Bangladesh: Geological Survey of Bangladesh.
- Amorosi, A., Bruno, L., Cleveland, D. M., Morelli, A., & Hong, W. (2017). Paleosols and associated channel-belt sand bodies from a continuously subsiding late Quaternary system (Po Basin, Italy): New insights into continental sequence stratigraphy. *Geological Society of America Bulletin*, 129(3–4), 449–463. <https://doi.org/10.1130/B31575.1>
- Berthet, T., Hetényi, G., Cattin, R., Sapkota, S. N., Champollion, C., Kandel, T., ... Bonnin, M. (2013). Lateral uniformity of India Plate strength over central and eastern Nepal. *Geophysical Journal International*, 195(3), 1481–1493. <https://doi.org/10.1093/gji/ggt357>
- Bilham, R., Bendick, R., & Wallace, K. (2003). Flexure of the Indian plate and intraplate earthquakes. *Journal of Earth System Science*, 112(3), 315–329. <https://doi.org/10.1007/BF02709259>
- Blum, M., Martin, J., Milliken, K., & Garvin, M. (2013). Paleovalley systems: Insights from Quaternary analogs and experiments. *Earth-Science Reviews*, 116, 128–169. <https://doi.org/10.1016/j.earscirev.2012.09.003>
- Bonvalot, S., Balmino, G., Briais, A., Kuhn, M., & Peyrefitte, A., Vales, N., ... Sarrailh, M. (2012). World gravity map, 1: 50000000 map. Eds. BGI-CGMW-CNES-IRD, Paris.
- Brammer, H. (2012). *Physical geography of Bangladesh*. Dhaka, Bangladesh: The University Press Ltd.
- Bristow, C., Smith, N., & Rogers, J. (1999). Gradual avulsion, river metamorphosis and reworking by underfit streams: A modern example from the Brahmaputra River in Bangladesh and a possible ancient example in the Spanish Pyrenees. *Fluvial Sedimentology VI*, 28, 221e230.
- Bufe, A., Paola, C., & Burbank, D. W. (2016). Fluvial bevelling of topography controlled by lateral channel mobility and uplift rate. *Nature Geoscience*, 9(9), 706. <https://doi.org/10.1038/ngeo2773>
- Burbank, D. W. (1992). Causes of recent Himalayan uplift deduced from deposited patterns in the Ganges basin. *Nature*, 357, 680. <https://doi.org/10.1038/357680a0>
- Catuneanu, O., Bhattacharya, J. P., Blum, M. D., Dalrymple, R. W., Eriksson, P. G., Fielding, C. R., ... Tucker, M. E. (2010). Thematic Set: Sequence stratigraphy: Common ground after three decades of development. *First Break*, 28(1), 41–54. <https://doi.org/10.3997/1365-2397.2010002>
- Chakraborty, T., & Ghosh, P. (2010). The geomorphology and sedimentology of the Tista megafan, Darjeeling Himalaya: Implications for megafan building processes. *Geomorphology*, 115(3–4), 252–266. <https://doi.org/10.1016/j.geomorph.2009.06.035>
- Chatanantavet, P., Lamb, M. P., & Nittrouer, J. A. (2012). Backwater controls of avulsion location on deltas. *Geophysical Research Letters*, 39(1). <https://doi.org/10.1029/2011GL050197>
- Clark, M. K., & Bilham, R. (2008). Miocene rise of the Shillong Plateau and the beginning of the end for the Eastern Himalaya. *Earth and Planetary Science Letters*, 269(3–4), 337–351. <https://doi.org/10.1016/j.epsl.2008.01.045>
- DeCelles, P. G. (2012). Foreland basin systems revisited: Variations in response to tectonic settings, in C. Busby & A. Azor Pérez (Eds.), *Tectonics of sedimentary basins: Recent advances* (pp. 405–426). Chichester, UK: John Wiley & Sons.
- Densmore, A. L., Sinha, R., Sinha, S., Tandon, S., & Jain, V. (2016). Sediment storage and release from Himalayan piggyback basins and implications for downstream river morphology and evolution. *Basin Research*, 28(4), 446–461. <https://doi.org/10.1111/bre.12116>
- Diehl, T., Singer, J., Hetényi, G., Grujic, D., Clinton, J., Giardini, D., & Kissling, E. (2017). Seismotectonics of Bhutan: Evidence for segmentation of the Eastern Himalayas and link to foreland deformation. *Earth and Planetary Science Letters*, 471, 54–64. <https://doi.org/10.1016/j.epsl.2017.04.038>
- Duroy, Y., Farah, A., & Lillie, R. (1989). Sub-surface densities and lithospheric flexure of the Himalayan foreland in Pakistan, Tectonics of the Western Himalayas. *Special Papers – Geological Society of America*, 232, 217–236.
- Galy, A., & France-Lanord, C. (2001). Higher erosion rates in the Himalaya: Geochemical constraints on riverine fluxes. *Geology*, 29(1), 23–26. [https://doi.org/10.1130/0091-7613\(2001\)029<0023:HERITH>2.0.CO;2](https://doi.org/10.1130/0091-7613(2001)029<0023:HERITH>2.0.CO;2)
- Ganti, V., Chadwick, A. J., Hassenruck-Gudipati, H. J., Fuller, B. M., & Lamb, M. P. (2016). Experimental river delta size set by multiple floods and backwater hydrodynamics. *Science Advances*, 2(5), e1501768. <https://doi.org/10.1126/sciadv.1501768>
- Garzanti, E., Andò, S., France-Lanord, C., Vezzoli, G., Censi, P., Galy, V., & Najman, Y. (2010). Mineralogical and chemical variability of fluvial sediments: 1. Bedload sand (Ganga–Brahmaputra, Bangladesh). *Earth and Planetary Science Letters*, 299(3–4), 368–381. <https://doi.org/10.1016/j.epsl.2010.09.017>
- Goodbred, S. L. (2003). Response of the Ganges dispersal system to climate change: A source-to-sink view since the last interstade. *Sedimentary Geology*, 162, 83–104. [https://doi.org/10.1016/S0037-0738\(03\)00217-3](https://doi.org/10.1016/S0037-0738(03)00217-3)
- Goodbred, S. L., & Kuehl, S. A. (2000). The Significance of large sediment supply, active tectonism, and eustasy on margin sequence development: Late Quaternary stratigraphy and evolution of the Ganges-Brahmaputra delta. *Sedimentary Geology*, 133, 227–248. [https://doi.org/10.1016/S0037-0738\(00\)00041-5](https://doi.org/10.1016/S0037-0738(00)00041-5)
- Goodbred, S. L., Kuehl, S. A., Steckler, M. S., & Sarker, M. H. (2003). Controls on facies distribution and stratigraphic preservation in the Ganges-Brahmaputra delta sequence. *Sedimentary Geology*, 155(3–4), 301–316. [https://doi.org/10.1016/S0037-0738\(02\)00184-7](https://doi.org/10.1016/S0037-0738(02)00184-7)
- Goodbred, S. L., Paolo, P. M., Ullah, M. S., Pate, R. D., Khan, S. R., Kuehl, S. A., ... Rahaman, W. (2014). Piecing together the Ganges-Brahmaputra-Meghna River delta: Use of sediment provenance to reconstruct the history and interaction of multiple fluvial systems during Holocene delta evolution. *Geological Society of America Bulletin*, 126(11–12), 1495–1510. <https://doi.org/10.1130/B30965.1>
- Govin, G., Najman, Y., Copley, A., Millar, I., van der Beek, P., Huyghe, P., ... Davenport, J. (2018). Timing and mechanism of the rise of the Shillong Plateau in the Himalayan foreland. *Geology*, 46(3), 279–282. <https://doi.org/10.1130/G39864.1>
- Grall, C., Steckler, M. S., Goodbred, S. L., Pickering, J. L., Sincavage, R., Paola, C., ... Spiess, V. (2018). A base-level stratigraphic

- approach to determining Holocene subsidence of the Gange-Meghna-Brahmaputra Delta Plain. *Earth and Planetary Science Letter*, 499, 23–36.
- Grimaud, J.-L., Chardon, D., Metelka, V., Beauvais, A., & Bamba, O. (2015). Neogene cratonic erosion fluxes and landform evolution processes from regional regolith mapping (Burkina Faso, West Africa). *Geomorphology*, 241, 315–330. <https://doi.org/10.1016/j.geomorph.2015.04.006>
- Grimaud, J.-L., Paola, C., & Ellis, C. (2017). Competition between uplift and transverse sedimentation in an experimental delta. *Journal of Geophysical Research: Earth Surface*, 122(7), 1339–1354. <https://doi.org/10.1002/2017JF004239>
- Gupta, S. (1997). Himalayan drainage patterns and the origin of fluvial megafans in the Ganges foreland basin. *Geology*, 25(1), 11–14. [https://doi.org/10.1130/0091-7613\(1997\)025<0011:HDPAT O>2.3.CO;2](https://doi.org/10.1130/0091-7613(1997)025<0011:HDPAT O>2.3.CO;2)
- Hajek, E. A., & Straub, K. M. (2017). Autogenic sedimentation in clastic stratigraphy. *Annual Review of Earth and Planetary Sciences*, 45, 681–709. <https://doi.org/10.1146/annurev-earth-063016-015935>
- Hammer, P., Berthet, T., Hetényi, G., Cattin, R., Drukpa, D., Chopel, J., ... Doerflinger, E. (2013). Flexure of the India plate underneath the Bhutan Himalaya. *Geophysical Research Letters*, 40(16), 4225–4230. <https://doi.org/10.1002/grl.50793>
- Hartley, A. J., Weissmann, G. S., & Scuderi, L. (2016). Controls on the apex location of large deltas. *Journal of the Geological Society*, 174(1), 10–13. <https://doi.org/10.1144/jgs2015-154>
- Heller, P. L., Angevine, C. L., Winslow, N. S., & Paola, C. (1988). Two-phase stratigraphic model of foreland-basin sequences. *Geology*, 16(6), 501–504. [https://doi.org/10.1130/0091-7613\(1988\)016<0501:T-PSMOF>2.3.CO;2](https://doi.org/10.1130/0091-7613(1988)016<0501:T-PSMOF>2.3.CO;2)
- Holbrook, J. M., & Schumm, S. A. (1999). Geomorphic and sedimentary response of rivers to tectonic deformation: A brief review and critique of a tool for recognizing subtle epeirogenic deformation in modern and ancient settings. *Tectonophysics*, 305, 287–306. [https://doi.org/10.1016/S0040-1951\(99\)00011-6](https://doi.org/10.1016/S0040-1951(99)00011-6)
- Hoque, M. A., McArthur, J. M., & Sikdar, P. K. (2014). Sources of low-arsenic groundwater in the Bengal Basin: Investigating the influence of the last glacial maximum palaeosol using a 115-km traverse across Bangladesh. *Hydrogeology Journal*, 22, 1535–1547. <https://doi.org/10.1007/s10040-014-1139-8>
- Humphrey, N. F., & Konrad, S. K. (2000). River incision or diversion in response to bedrock uplift. *Geology*, 28(1), 43–46. [https://doi.org/10.1130/0091-7613\(2000\)028<0043:RIODIR>2.3.CO;2](https://doi.org/10.1130/0091-7613(2000)028<0043:RIODIR>2.3.CO;2)
- Jerolmack, D. J. (2009). Conceptual framework for assessing the response of delta channel networks to Holocene sea level rise. *Quaternary Science Reviews*, 28(17–18), 1786–1800. <https://doi.org/10.1016/j.quascirev.2009.02.015>
- Jordan, T. A., & Watts, A. B. (2005). Gravity anomalies, flexure and the elastic thickness structure of the India-Eurasia collisional system. *Earth and Planetary Science Letters*, 236(3), 732–750. <https://doi.org/10.1016/j.epsl.2005.05.036>
- Khan, A. S. (2001). Morphological changes due to construction of a barrage on the Teesta river. Master thesis. Bangladesh University of Engineering and Technology, Dhaka.
- Kraus, M. J. (1999). Paleosols in clastic sedimentary rocks: Their geologic applications. *Earth-Science Reviews*, 47(1–2), 41–70. [https://doi.org/10.1016/S0012-8252\(99\)00026-4](https://doi.org/10.1016/S0012-8252(99)00026-4)
- Lupker, M., France-Lanord, C., Galy, V., Lavé, J., & Kudrass, H. (2013). Increasing chemical weathering in the Himalayan system since the Last Glacial Maximum. *Earth and Planetary Science Letters*, 365, 243–252. <https://doi.org/10.1016/j.epsl.2013.01.038>
- Mack, G. H., James, W. C., & Monger, H. C. (1993). Classification of paleosols. *Geological Society of America Bulletin*, 105(2), 129–136. [https://doi.org/10.1130/0016-7606\(1993\)105<0129:COP>2.3.CO;2](https://doi.org/10.1130/0016-7606(1993)105<0129:COP>2.3.CO;2)
- McArthur, J. M., Nath, B., Banerjee, D. M., Purohit, R., & Grassineau, N. (2011). Palaeosol control on groundwater flow and pollutant distribution: The example of arsenic. *Environmental Science & Technology*, 45(4), 1376–1383. <https://doi.org/10.1021/es1032376>
- Mitra, S., Priestley, K., Kajaljyoti, B., & Gaur, V. (2018). Crustal structure and evolution of the eastern Himalayan plate boundary system. *Northeast India, Journal of Geophysical Research: Solid Earth*, 123(1), 621–640. <https://doi.org/10.1002/2017JB014714>
- Morgan, J. P., & McIntire, W. G. (1959). Quaternary geology of the Bengal basin, East Pakistan and India. *Geological Society of America Bulletin*, 70(3), 319–342. [https://doi.org/10.1130/0016-7606\(1959\)70\[319:QGOTBB\]2.0.CO;2](https://doi.org/10.1130/0016-7606(1959)70[319:QGOTBB]2.0.CO;2)
- Mukhopadhyay, M., & Dasgupta, S. (1988). Deep structure and tectonics of the Burmese arc: Constraints from earthquake and gravity data. *Tectonophysics*, 149(3–4), 299–322. [https://doi.org/10.1016/0040-1951\(88\)90180-1](https://doi.org/10.1016/0040-1951(88)90180-1)
- Najman, Y., Bracciali, L., Parrish, R. R., Chisty, E., & Copley, A. (2016). Evolving strain partitioning in the Eastern Himalaya: The growth of the Shillong Plateau. *Earth and Planetary Sciences Letters*, 433, 1–9. <https://doi.org/10.1016/j.epsl.2015.10.017>
- Norman, P. (1992). Evaluation of the Barapukuria coal deposit NW Bangladesh. *Geological Society, London, Special Publications*, 63(1), 107–120. <https://doi.org/10.1144/GSL.SP.1992.063.01.10>
- Pattison, S. A. J. (2018). Using classic outcrops to revise sequence stratigraphic models: Reevaluating the Campanian Desert Member (Blackhawk Formation) to lower Castlegate Sandstone interval, Book Cliffs, Utah and Colorado, USA. *Geology*, 47(1), 11–14. <https://doi.org/10.1130/G45592.1>
- Pickering, J. L., Diamond, M. S., Goodbred, S. L., Grall, C., Martin, J. M., Palamenghi, L., ... Spiess, V. (2019). Impact of glacial-lake paleofloods on valley development since glacial termination II: A conundrum of hydrology and scale for the lowstand Brahmaputra-Jamuna paleovalley system. *GSA Bulletin*, 131(1–2), 58–70. <https://doi.org/10.1130/B31941.1>
- Pickering, J. L., Goodbred, S. L., Beam, J. C., Ayers, J. C., Covey, A. K., Rajapara, H. M., & Singhvi, A. K. (2017). Terrace formation in the upper Bengal basin since the Middle Pleistocene: Brahmaputra fan delta construction during multiple highstands. *Basin Research*, 30(1), 550–567. <https://doi.org/10.1111/bre.12236>
- Pickering, J. L., Goodbred, S. L., Reitz, M. D., Hartzog, T. R., Mondal, D. R., & Hossain, M. S. (2014). Late Quaternary sedimentary record and Holocene channel avulsions of the Jamuna and Old Brahmaputra River valleys in the upper Bengal delta plain. *Geomorphology*, 227, 123–136. <https://doi.org/10.1016/j.geomorph.2013.09.021>
- Posamentier, H., & Allen, G. (1993). Siliciclastic sequence stratigraphic patterns in foreland, ramp-type basins. *Geology*, 21(5), 455–458. [https://doi.org/10.1130/0091-7613\(1993\)021<0455:SSSPI F>2.3.CO;2](https://doi.org/10.1130/0091-7613(1993)021<0455:SSSPI F>2.3.CO;2)
- Rashid, B., Sultan-Ul-Islam, M., & Islam, B. (2015). Evidences of neo-tectonic activities as reflected by drainage characteristics of the Mahananda river floodplain and its adjoining areas, Bangladesh. *American Journal of Earth Sciences*, 2(4), 61–70.

- Reitz, M. D., Jerolmack, D. J., & Swenson, J. B. (2010). Flooding and flow path selection on alluvial fans and deltas. *Geophysical Research Letters*, 37(6). <https://doi.org/10.1029/2009GL041985>
- Reitz, M. D., Pickering, J. L., Goodbred, S. L., Paola, C., Steckler, M. S., Seeber, L., & Akhter, S. H. (2015). Effects of tectonic deformation and sea level on river path selection: Theory and application to the Ganges-Brahmaputra-Meghna River Delta. *Journal of Geophysical Research: Earth Surface*, 120, 671–689. <https://doi.org/10.1002/2014JF003202>
- Roddaz, M., Viers, J., Brusset, S., Baby, P., & Hérail, G. (2005). Sediment provenances and drainage evolution of the Neogene Amazonian foreland basin. *Earth and Planetary Science Letters*, 239(1–2), 57–78. <https://doi.org/10.1016/j.epsl.2005.08.007>
- Steckler, M. S., Grall, C., Grimaud, J. L., Seeber, L., Betka, P. M., Akhter, S. H., ... Lavier, L. L. (2018, December). Sinuous track of the flexural bulge in the eastern Himalayas and Bengal Basin from multiple loads on a variable rigidity plate, an explanation for the Barind and Madhupur Pleistocene uplands. In AGU Fall Meeting Abstracts.
- Sincavage, R., Goodbred, S. L., & Pickering, J. L. (2018). Holocene Brahmaputra River path selection and variable sediment bypass as indicators of fluctuating hydrologic and climate conditions in Sylhet Basin, Bangladesh. *Basin Research*, 30(2), 302–320. <https://doi.org/10.1111/bre.12254>
- Sincavage, R. S., Paola, C., & Goodbred, S. L. (2019). Coupling mass extraction and downstream fining with fluvial facies changes across the Sylhet basin of the Ganges-Brahmaputra-Meghna Delta. *Journal of Geophysical Research: Earth Surface*, 124(2), 400–413. <https://doi.org/10.1029/2018JF004840>
- Singh, A., Bhushan, K., Singh, C., Steckler, M. S., Akhter, S. H., Seeber, L., ... Biswas, R. (2016). Crustal structure and tectonics of Bangladesh: New constraints from inversion of receiver functions. *Tectonophysics*, 680, 99–112. <https://doi.org/10.1016/j.tecto.2016.04.046>
- Singh, S. K., & France-Lanord, C. (2002). Tracing the distribution of erosion in the Brahmaputra watershed from isotopic compositions of stream sediments. *Earth and Planetary Science Letters*, 202(3–4), 645–662. [https://doi.org/10.1016/S0012-821X\(02\)00822-1](https://doi.org/10.1016/S0012-821X(02)00822-1)
- Singh, S. K., Santosh, K. R., & Krishnaswami, S. (2008). Sr and Nd isotopes in river sediments from the Ganga Basin: Sediment provenance and spatial variability in physical erosion. *Journal of Geophysical Research*, 113(F03006), 18. <https://doi.org/10.1029/2007JF000909>
- Sinha, R., & Friend, P. F. (1994). River systems and their sediment flux, Indo-Gangetic plains, Northern Bihar, India. *Sedimentology*, 41(4), 825–845. <https://doi.org/10.1111/j.1365-3091.1994.tb01426.x>
- Slingerland, R., & Smith, N. D. (2004). River avulsions and their deposits. *Annual Review of Earth and Planetary Sciences*, 32, 257–285.
- Soil Survey Staff. (1999). *Soil taxonomy: A basic system of soil classification for making and interpreting soil surveys* (869pp.). Washington, D.C.: US Department of Agriculture.
- Spieß, V., Schwenk, T., Palamenghi, L., Goodbred, S. L., Steckler, M. S., Seeber, L., ... Khan, S. R. (2012, December). Subsurface deformation in the Gangetic plain—first results from the BrahmaSeis multichannel seismic survey on Bangladesh Rivers. In AGU Fall Meeting Abstracts.
- Steckler, M. S., Akhter, S. H., & Seeber, L. (2008). Collision of the Ganges-Brahmaputra Delta with the Burma Arc: Implications for earthquake hazard. *Earth and Planetary Science Letters*, 273(3–4), 367–378. <https://doi.org/10.1016/j.epsl.2008.07.009>
- Targulian, V., & Krasilnikov, P. (2007). Soil system and pedogenic processes: Self-organization, time scales, and environmental significance. *Catena*, 71(3), 373–381. <https://doi.org/10.1016/j.catena.2007.03.007>
- Vail, P. R., Mitchum, R. Jr., & Thompson, S. III. (1977). Seismic stratigraphy and global changes of sea level: Part 3. Relative changes of sea level from Coastal Onlap: section 2. Application of seismic reflection Configuration to Stratigraphic Interpretation.
- van Dijk, W. M., Densmore, A. L., Singh, A., Gupta, S., Sinha, R., Mason, P. J., ... Rai, S. P. (2016). Linking the morphology of fluvial fan systems to aquifer stratigraphy in the Sutlej-Yamuna plain of northwest India. *Journal of Geophysical Research: Earth Surface*, 121(2), 201–222. <https://doi.org/10.1002/2015JF003720>
- Vernant, P., Bilham, R., Szeliga, W., Drupka, D., Kalita, S., Bhattacharyya, A. K., ... Berthet, T. (2014). Clockwise rotation of the Brahmaputra Valley relative to India: Tectonic convergence in the eastern Himalaya, Naga Hills, and Shillong Plateau. *Journal of Geophysical Research: Solid Earth*, 119(8), 6558–6571.
- Watts, A., Zhong, S., & Hunter, J. (2013). The behavior of the lithosphere on seismic to geologic timescales. *Annual Review of Earth and Planetary Sciences*, 41, 443–468. <https://doi.org/10.1146/annurev-earth-042711-105457>
- Wiedicke, M., Kudrass, H.-R., & Hübscher, C. (1999). Oolitic beach barriers of the last Glacial sea-level lowstand at the outer Bengal shelf. *Marine Geology*, 157(1–2), 7–18. [https://doi.org/10.1016/S0025-3227\(98\)00162-5](https://doi.org/10.1016/S0025-3227(98)00162-5)
- Wilson, C. A., & Goodbred, S. L. (2015). Construction and maintenance of the Ganges-Brahmaputra-Meghna delta: Linking process, morphology, and stratigraphy. *Annual Review of Marine Science*, 7, 67–88. <https://doi.org/10.1146/annurev-ev-marine-010213-135032>
- Wright, V. P., & Marriott, S. B. (1993). The sequence stratigraphy of fluvial depositional systems: The role of floodplain sediment storage. *Sedimentary Geology*, 86(3–4), 203–210. [https://doi.org/10.1016/0037-0738\(93\)90022-W](https://doi.org/10.1016/0037-0738(93)90022-W)

SUPPORTING INFORMATION

Additional supporting information may be found online in the Supporting Information section.

How to cite this article: Grimaud J-L, Grall C, Goodbred S, et al. Flexural deformation controls on Late Quaternary sediment dispersal in the Garo-Rajmahal Gap, NW Bengal Basin. *Basin Res.* 2020;32: 1242–1260. <https://doi.org/10.1111/bre.12425>

Preservation and Completeness of Fluvial Meandering Deposits Influenced by Channel Motions and Overbank Sedimentation

Jean-Louis Grimaud¹ , Fabien Ors¹ , Martin Lemay^{1,2}, Isabelle Cojan¹, and Jacques Rivoirard¹

¹MINES ParisTech, PSL University, Centre de Géosciences, Fontainebleau Cedex, France, ²Modis, Technopole HélioParc, Pau-Pyrénées, Bâtiment Newton, Pau, France

Key Points:

- Fluvial meandering simulations used to track topographic and facies changes to resolve the influence of stasis and reworking on completeness
- Timescale for visiting the floodplain corresponds to the transition from anti-persistent to persistent depositional regimes
- New simple formulation to assess average completeness

Supporting Information:

Supporting Information may be found in the online version of this article.

Correspondence to:

J.-L. Grimaud,
jean-louis.grimaud@mines-paristech.fr

Citation:

Grimaud, J.-L., Ors, F., Lemay, M., Cojan, I., & Rivoirard, J. (2022). Preservation and completeness of fluvial meandering deposits influenced by channel motions and overbank sedimentation. *Journal of Geophysical Research: Earth Surface*, 127, e2021JF006435. <https://doi.org/10.1029/2021JF006435>

Received 17 SEP 2021
Accepted 26 APR 2022

Author Contributions:

Conceptualization: Jean-Louis Grimaud, Fabien Ors, Isabelle Cojan
Data curation: Jean-Louis Grimaud
Formal analysis: Jean-Louis Grimaud, Jacques Rivoirard
Investigation: Martin Lemay, Isabelle Cojan, Jacques Rivoirard
Methodology: Jean-Louis Grimaud, Fabien Ors, Martin Lemay, Jacques Rivoirard
Software: Jean-Louis Grimaud, Fabien Ors, Martin Lemay
Supervision: Jean-Louis Grimaud
Validation: Jean-Louis Grimaud, Fabien Ors, Isabelle Cojan, Jacques Rivoirard
Writing – original draft: Jean-Louis Grimaud
Writing – review & editing: Fabien Ors, Martin Lemay, Isabelle Cojan, Jacques Rivoirard

Abstract Assessing the contribution of geomorphic processes to the (non-)preservation of sedimentary deposits is necessary to account for potential bias in measured accumulation rates in the stratigraphic record. In this study, a series of numerical simulations of fluvial meandering successions is performed using FLUMY, a model of channel motions and sedimentary facies deposition. We develop tools to measure non-deposition (stasis S) and reworking (R) of previously deposited sediment between iterations, which are both generators of hiatuses in the sedimentary record. We then compare S and R with measurements of accumulation rates and completeness (C). Results show that combining measurements of both topographic and facies changes allows for a better record of surface evolution than measuring topographies only. Accumulation rate dependence on measurement time span allows distinguishing between two regimes. The first one (anti-persistent) is characteristic of channel avulsion and compensational stacking until the whole domain is visited by overbank deposition, corresponding to the visitation timescale T_v . In the second regime (persistent), reworking by channel migration is the remaining active process until the whole system has aggraded one channel depth, corresponding to the compensation timescale T_c . Based on these results, we propose a new simple formulation based on stasis and reworking to estimate average completeness.

Plain Language Summary Sedimentary rocks contain a record of Earth's past environments and evolution, which has a lot of missing information. This is due to sedimentary processes dynamics. In the case of fluvial systems, deposition is limited to the area near rivers while the remaining landscape is “inactive.” With time, rivers move to other locations, which accumulate sediment whereas abandoned area do not anymore. In addition, river channels are erosive and can remove previously accumulated sediment: part of the record is then lost. The greater the recording time, the more information is missing. This study explores the factors that have an influence on time preservation in rocks in the case of meandering rivers deposits. To that purpose, we use a numerical model of a river-swept alluvial plain. We track changes of the depositional record with time using several indicators: the sediment deposition rates, the fraction of inactive surface and the fraction of erased record. Compared to previous studies, we measure changes of the sediment record between iterations in addition to measures of topographic change, which gives better results to assess time preservation. This leads us to propose a new formulation for estimating the average time preservation in sedimentary records.

1. Introduction

Preserved sedimentary accumulations record Earth's past geography, life and climate, as well as mass redistribution by surface processes. The probability of having continuous deposition and subsequent preservation in one location however is low (Ager, 1973). The question is then how meaningful is a measure of accumulation rate and how does it compare with other measured rates (Tipper, 1998; S. Trampush et al., 2017). Global compilations demonstrate that, in any depositional environment, sediment accumulation rates span orders of magnitude, and decrease when increasing the time-interval (time span) at which they are measured (Sadler, 1981). This “Sadler effect” is explained by the increasing incorporation with time of hiatuses in 1D sections (Plotnick, 1986) (Figure 1), a bias that can be lessened using 2D vertical sections and, in some cases, overcome when using large scale 3D data sets (Sadler & Jerolmack, 2015; Wheeler, 1958).

At the scale of outcrops, particularly in fluvial sections, hiatuses are nevertheless dominant: the stratigraphic record is incomplete. Current methods for assessing completeness based on strata geometry analysis are in their early stages (Holbrook & Miall, 2020; Tipper, 1998; S. Trampush et al., 2017; S. M. Trampush & Hajek, 2017)

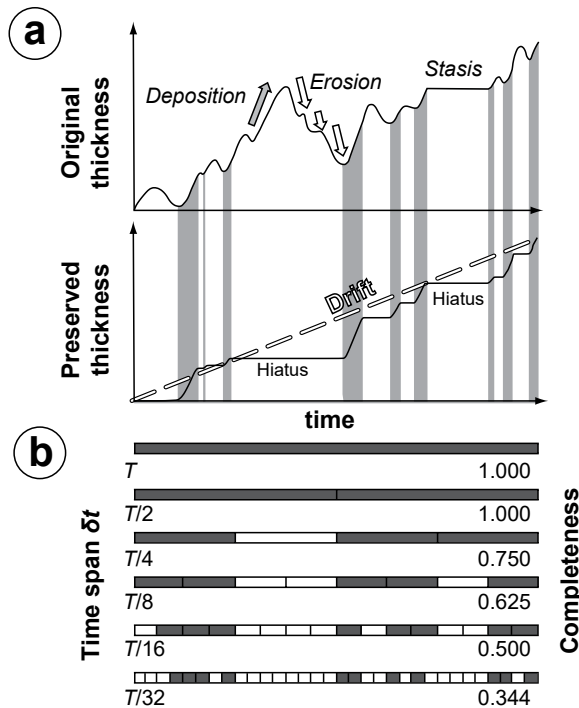


Figure 1. (a) Theoretical 1D evolution of the elevation at a 2D location in a depositional system. Erosion events induce differences between original thickness (top) and preserved thickness (bottom). Gray areas correspond to hiatus, which can arise from two processes: stasis (non-deposition) or erosion. U'_b is the velocity perturbation and E_0 is the erodibility coefficient at the bank (See Supporting Information S1 for a complete description). (b) Measure of completeness associated with the evolution in panel (a) based on the preserved sediment thickness at different time span. Dark gray areas correspond to intervals that have left a record. Completeness is the ratio of the sum of intervals that have left a record to the total number of intervals (after Sadler, 1981).

and will improve with knowledge on how morphodynamics impact stratigraphic completeness (Straub et al., 2020). The sources of hiatuses themselves are characteristic of geologic processes, that is, from erosion/transport to large-scale climatic and tectonic forcing (e.g., Holbrook & Miall, 2020; Paola et al., 2018; Reesink et al., 2015). Knowledge on hiatus formation is thus potentially additional information for reconstructing paleo-environments and sediment transfers (Figure 2a). Of particular importance are (a) sediment reworking (i.e., cannibalism), which is among the storage and release processes that buffer sediment transfers along large rivers (e.g., Jerolmack & Paola, 2010; Métivier & Gaudemer, 1999), and (b) stasis, which consists in pauses of the record in a depositional sense (Miall, 2015; Tipper, 2015) but that can be recorded for instance in alluvial systems with the development of paleosols (e.g., Abels et al., 2013; Grimaud et al., 2020; Retallack, 1984).

Theory on completeness has improved in the past decades through the development of 1D mathematical models and, more recently, the study of completeness on experimental fan deltas. Using numerical simulations, the dependence of accumulation rates on measurement interval (with power-law attributes) was investigated in relation with the distribution of hiatuses (Ganti et al., 2011; Schumer et al., 2011). Studies also focused on the saturation timescale, where the Sadler effect theoretically fades out (Jerolmack & Sadler, 2007). It was showed theoretically (Schumer & Jerolmack, 2009; Schumer et al., 2011) and experimentally (Straub & Esposito, 2013) that this timescale equaled the compensational timescale T_c , that is, the time necessary for sedimentation to fill the topographic roughness -usually the maximum channel depth.

Much of the many recent advances on completeness were thus theoretical and based on topographic analysis. In fluvial systems, a missing part is the irremediable replacement of facies by another (\sim facies replacement) that is not captured when using topographic clipping (i.e., difference between two topographies). It is exemplified by the replacement of overbank deposits by point bar as a fluvial channel migrates laterally (Figure 2b). In this study, we use FLUMY, a model that generates a fluvial meandering channel and associated deposits (point bars and overbank sedimentation), to track topographic and depositional changes and calculate completeness. Accumulation rates

measured at different time intervals in seven simulations, allow distinguishing between an anti-persistent and a persistent regime (see next section for definitions). We discuss in turn the specificities of these two regimes and how their characteristics can help quantify the mean completeness of fluvial deposits.

2. Background

2.1. Measured Accumulation Rates and Completeness of a Fluvial Meandering Section

Accumulation rates available in syntheses mostly consist of positive rates measured on 1D sections (\sim boreholes) using field observation, survey reoccupation or absolute radiometric dating (Sadler, 1981). They are not equivalent to measurements of accumulation over 2D domains (\sim maps), which also average area without deposition and are thus less biased (Sadler & Jerolmack, 2015). The vertical rates can nevertheless be recovered using the average of accumulation in a 2D domain D over the depositional area only (i.e., excluding inactivity or stasis S) (Figure 2a). For a given time span δt that divides a total duration T , the average 1D rate of accumulation is then:

$$A_{\delta t} = \frac{\sum_{j=1}^N (V_{\delta t j})}{TD(1 - S_{\delta t})} \quad (1)$$

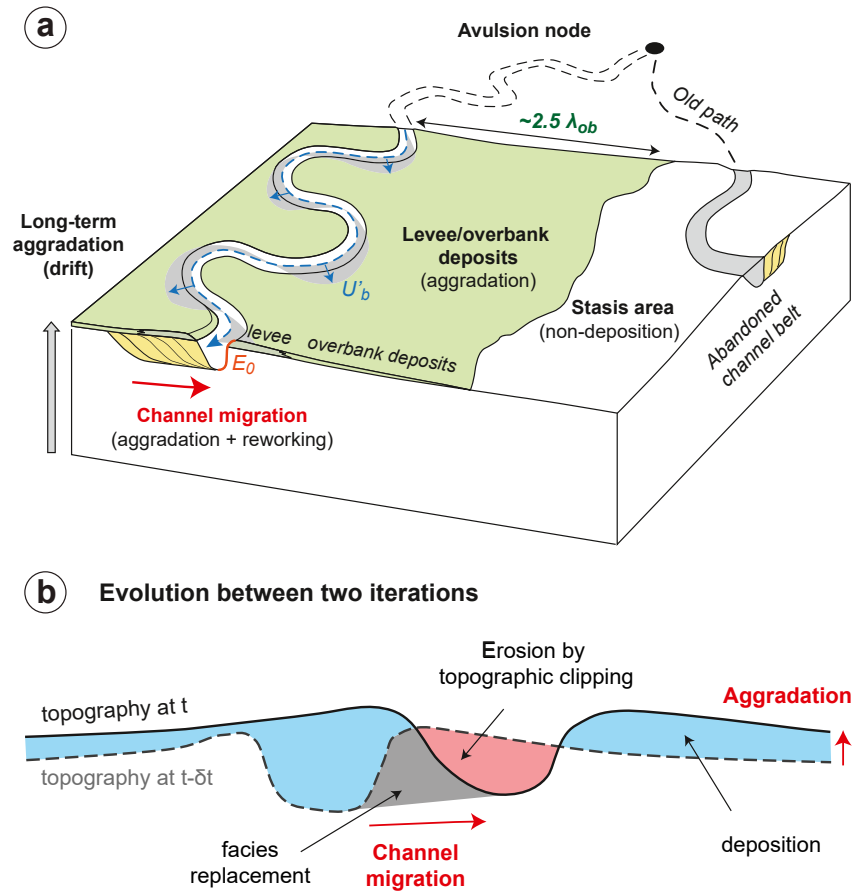


Figure 2. (a) Schematic 3D view of an alluvial meandering system showing the different processes at play: (a) continuous channel migration with associated point bar deposition in the inner bank and erosion at the outer bank, (b) levee/overbank sedimentation in the floodplain (as well as area of non-deposition or stasis), and (c) switch of depositional area following avulsion. (b) Detail of strata and topographic evolution (cross section) in between two iterations. Note that the gray area corresponding to facies replacement would not be captured by a simple clip between the two topographies.

where $V_{\delta t}$ is a measure of sediment volume accumulated during one interval, $N = T/\delta t$ the number of intervals, and $S_{\delta t}$ the average stasis fraction in the domain (see Supporting Information S1). There are several ways to measure $V_{\delta t}$ evolution with time from 2D data, for instance building synthetic stratigraphy using successive timed topographies of experiments (e.g., Straub & Foreman, 2018). Measure of $V_{\delta t}$ from topographic changes alone are however underestimated (see Figure 2b) and must be complemented with the record of deposit replacement (\sim facies replacement).

The completeness $C_{\delta t}$ of a stratigraphic section is the fraction of time intervals of duration δt that left a record (Sadler & Strauss, 1990) and is expressed as the number $n_{\delta t}$ of intervals leaving a record divided by the total number of intervals $N = T/\delta t$ (Figure 1).

$$C_{\delta t} = \frac{\delta t n_{\delta t}}{T} = \frac{n_{\delta t}}{N} \quad (2)$$

Sadler (1981) and Sadler and Strauss (1990) demonstrated that completeness increases as a function of (a) the duration of the section (difference between age of the bottom and top of a section), (b) the time span at which a record is discretized and (c) the long-term accumulation rate (referred to as the drift; Figure 1a); and decreases as a function of the unsteadiness of depositional processes. These authors summarized it as the ratio of the long-term accumulation rate A_T (measured over T) to the shorter-term accumulation rate $A_{\delta t}$ (measured with time span δt). Based on a compilation of thousands of accumulation rates, Sadler (1981) also expressed $C_{\delta t}$ as follow:

$$C_{\delta t} = \frac{A_T}{A_{\delta t}} \quad (3a)$$

Introducing $m = (d \ln A_T)/(d \ln T)$, a gradient or scaling exponent characteristic of each depositional environment, which varies between -1 and 0 , Equation 3a yields:

$$C_{\delta t} = \left(\frac{\delta t}{T} \right)^{-m} \quad (3b)$$

where $\delta t/T$ is the record precision. This scaling exponent m is thus that of the power law function relating measured accumulation rates with time span of measurement. For alluvial environments, m is comprised between -0.5 and -1 (Paola et al., 2018; Sadler & Jerolmack, 2015).

Finally, surface fluctuations driving the Sadler effect can be described as a Brownian fractional motion with positive jumps representing deposition, negative jumps representing erosion and the Hurst exponent h - the correlation structure between negative and positive jumps (see references in Paola et al., 2018). Under this assumption, Schumer et al. (2011) demonstrated that h can be related to the scaling exponent defined by Sadler (1981) ($m = h - 1$). When h is 0.5 , fluctuations mimic a pure random walk and no correlation can be found between positive and negative jumps. If $h > 0.5$, the motion is persistent and an either decreasing or increasing trend may be observed while if $h < 0.5$ the motion is anti-persistent and jumps are negatively correlated (positive jumps most often follow negative jumps and vice versa).

Most studies have stressed the importance of stasis S and reworking R in setting completeness. R can be defined as the ratio of the sediment lost (eroded) to the sediment gained (deposited) while S is the areal fraction without deposition over the considered domain. Both are measured at a time resolution δt . A simple mathematical expression of their relationship with completeness is the following proposition:

$$C_{\delta t} = (1 - S_{\delta t})(1 - R_{\delta t}) \quad (4)$$

This formulation can be thought of as the “glimpse of a glimpse” preserved in stratigraphy (Holbrook & Miall, 2020). The first term $(1 - S)$ would represent the area not in stasis (i.e., deposition) while the second $(1 - R)$ would represent the sediment that does not get reworked (i.e., preservation). This new formulation for quantifying completeness will be tested against synthetic data generated with FLUMY.

3. Methods

Alluvial deposits of meandering rivers were generated using the FLUMY software. The deposits were analyzed using Python scripts to measure completeness, stasis, accumulation rates and reworking (Figures 2–9). Results were compared with existing formulations of completeness (see previous section).

3.1. Alluvial Deposits Simulations

The FLUMY model combines a pseudo-1D description of channel lateral migration together with parametric generation of associated fluvial processes (e.g., aggradation and avulsion). A detail description of FLUMY can be found in Supporting Information S1. The channel is discretized in a series of nodes representing the centerline. Channel migration rate is calculated at each node of the centerline based on the pioneer bank instability model of Ikeda et al. (1981), adapted by Johannesson and Parker (1989), and many others (e.g., Eke et al., 2014; A. D. Howard, 1996; Imran et al., 1999; Parker et al., 2011; Seminara, 2006; Sun et al., 1996) -including Lopez (2003) in the case of FLUMY (Figure 2a). The conservation of channel bankfull mean aspect ratio $2 B/H$ was assumed based on existing literature compilations (Held, 2011; Lemay et al., 2020; Leopold & Wolman, 1960; Richards, 1982; Williams, 1984, 1986). Fluvial mean bankfull channel depth H , maximum bankfull channel depth H_{\max} and mean bankfull channel width W were related using:

$$W = 2B = 15H = 10 H_{\max} \quad (5)$$

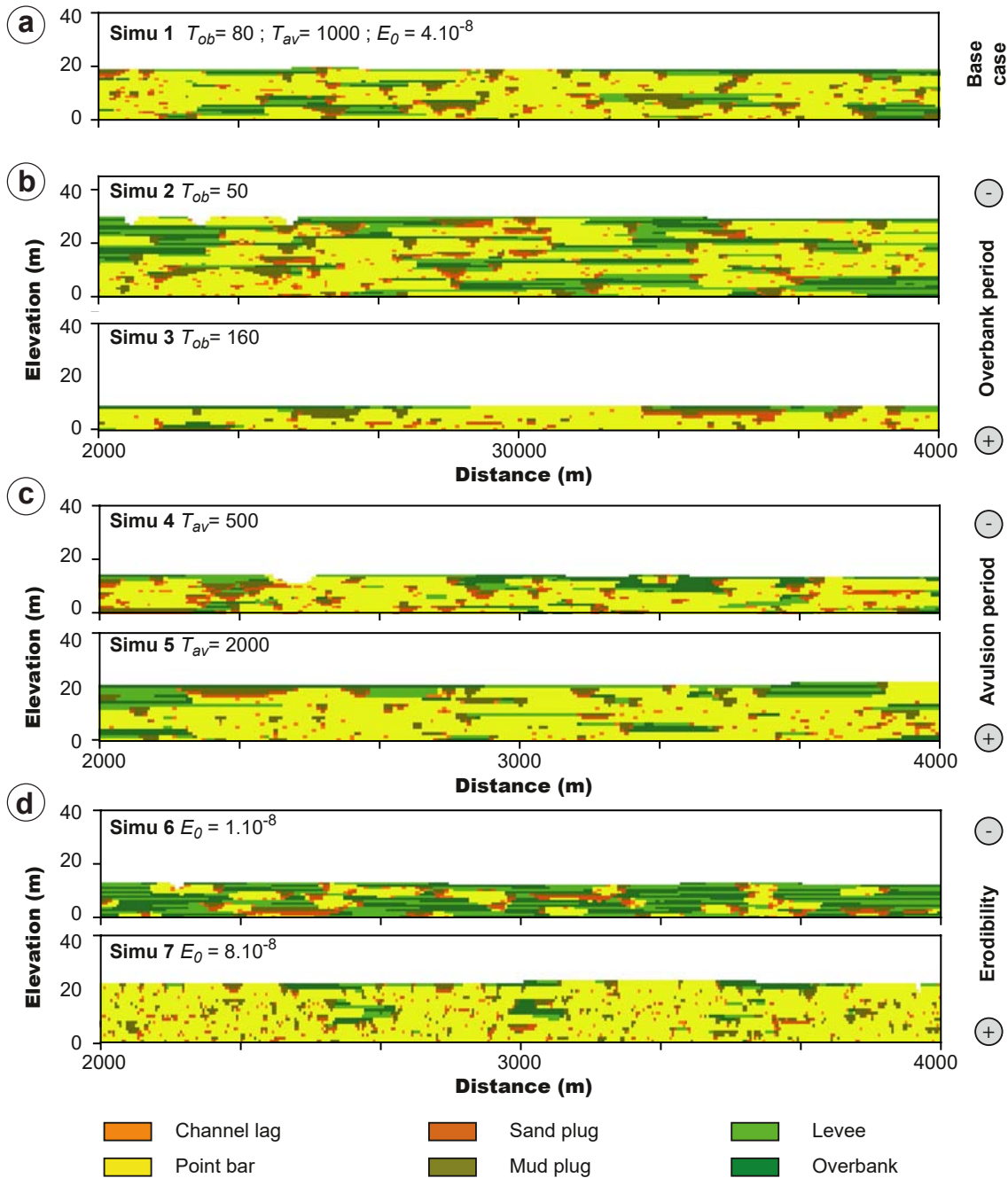


Figure 3. Cross-sectional view (xz at $y = 75$) of facies distribution resulting from the different scenarios tested in this study: (a) base case, (b) varying aggradation rate, (c) varying avulsion period, and (d) varying bank erodibility. See Table 2 for parameters. T_{ob} is the time-span between successive levee/overbank deposition events, and T_{av} between successive avulsion events.

These average relationships were chosen for their simplicity, keeping in mind that (a) they may be more diverse in nature depending on climate or vegetation (Lemay et al., 2020; after; Held, 2011) and that (b) they may be modified by the user in FLUMY.

In FLUMY, deposits are stored according to lithofacies (Table 1) in the domain, a regular 2D pillar grid. To avoid numerical edge effects related to channel migration on the sides, the simulated domain is larger than the domain where facies are saved. *Point Bar* facies (Table 1) are deposited along the inner bank of the channel during lateral migration and allow the adjustment of channel width to erosion on the opposite bank (Figure 2a). Overbank

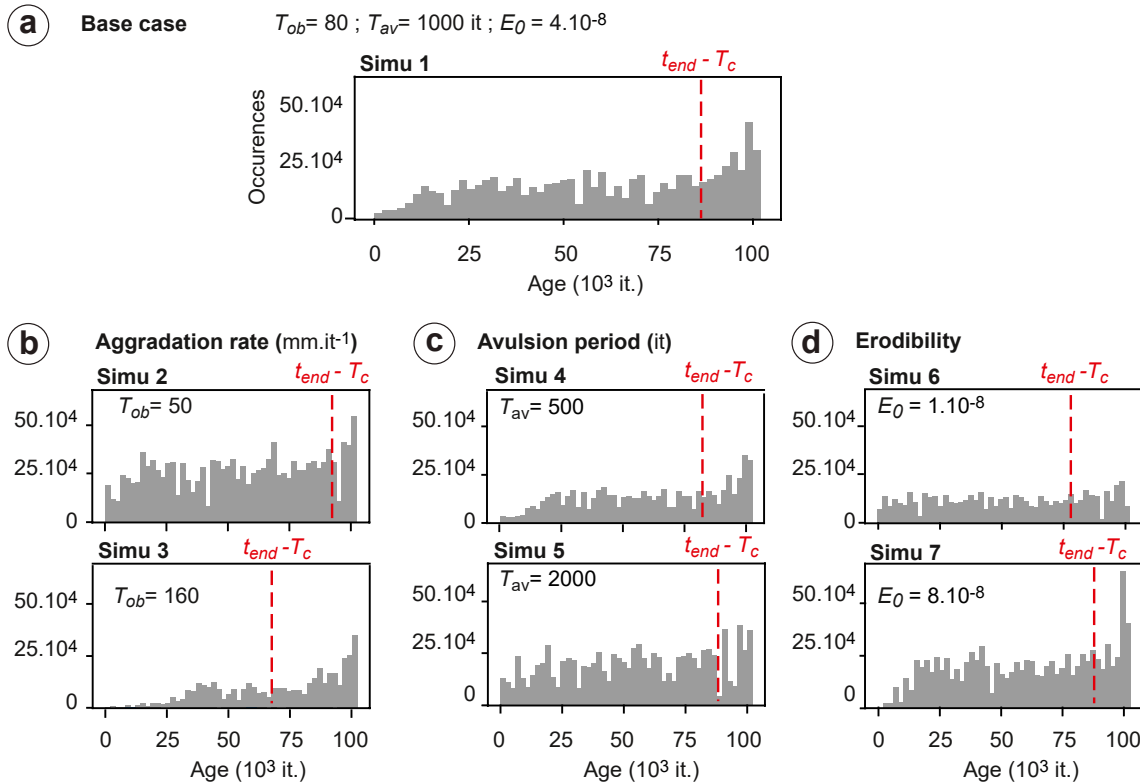


Figure 4. Age distribution of deposits along the cross-sections shown in Figure 3. The red dashed line represents the time limit beyond which older deposits are no longer subject to reworking.

flood geometry is simulated using an exponential thickness decrease away from the channel (Lopez, 2003; Pizzuto, 1987) set by the following input parameters: (a) an initial maximum thickness of overbank deposits i_{ob} and (b) a lateral extension-decrease length of overbank deposits λ_{ob} (Figure 2a) (Supporting Information S1). Overflow events occur following an overbank period T_{ob} , which is also set by the user. *Levee* deposits are generated from the channel to a distance set by the user where they transition to *Overbank* deposits. Note that since FLUMY does not explicitly models flow spilling from the channel, there is no flood-induced erosion on the floodplain. *Channel Lag* is deposited at the bottom of the channel, with a thickness equal to the imposed aggradation thickness to maintain channel depth constant. A regional avulsion process is generated (following an imposed period T_{av} between avulsion events) by changing the entire path of the river on the deposition domain (Supporting Information S1). The old channel path is filled by channel fill deposits (*Sand Plug* and *Mud Plug*) in one iteration, which is an oversimplification as it prevents reoccupation.

Table 2 summarizes parameters that varied in the 7 simulated scenarios. Total duration T of simulation was 102,400 iterations. This duration was chosen to avoid artifacts when discretizing into time spans. With a recurrence of flood (i.e., one iteration in the model) considered as 1.5 years from observations of modern fluvial systems (Lopez, 2003), all simulations may be considered as about 150 kyr long.

A 3 m maximum channel depth (Table 2) was used, resulting in channel width of 30 m (Equation 5). For simplicity, we used a strictly periodic generation for aggradation and avulsion processes. A default scenario (base case; $T_{ob} = 80$ it., $T_{av} = 1,000$ it., $E_0 = 4.10^{-8}$) was defined for comparison with other simulations. In the latter, parameters were changed in turn: (a) T_{ob} to 50 and 160 iterations (Simus 2–3), (b) T_{av} between 500 and 2,000 iterations (Simus 4–5) and (c) E_0 to 1.10^{-8} and 8.10^{-8} (Simus 6–7) (Table 2). For each scenario, a compensation timescale T_c was calculated (Table 2) by dividing the maximum channel depth by the long-term accumulation rate A_T .

During a simulation, depositional information is temporary stored in deposition units of various thicknesses (minimum 1 cm thick) and stacked in vertical pillars. The information can be saved regularly in 3D grids. In the present study, xyz grid were $600 \times 150 \times 200$ with a $10 \times 10 \times 0.2$ m discretization (resulting block was thus

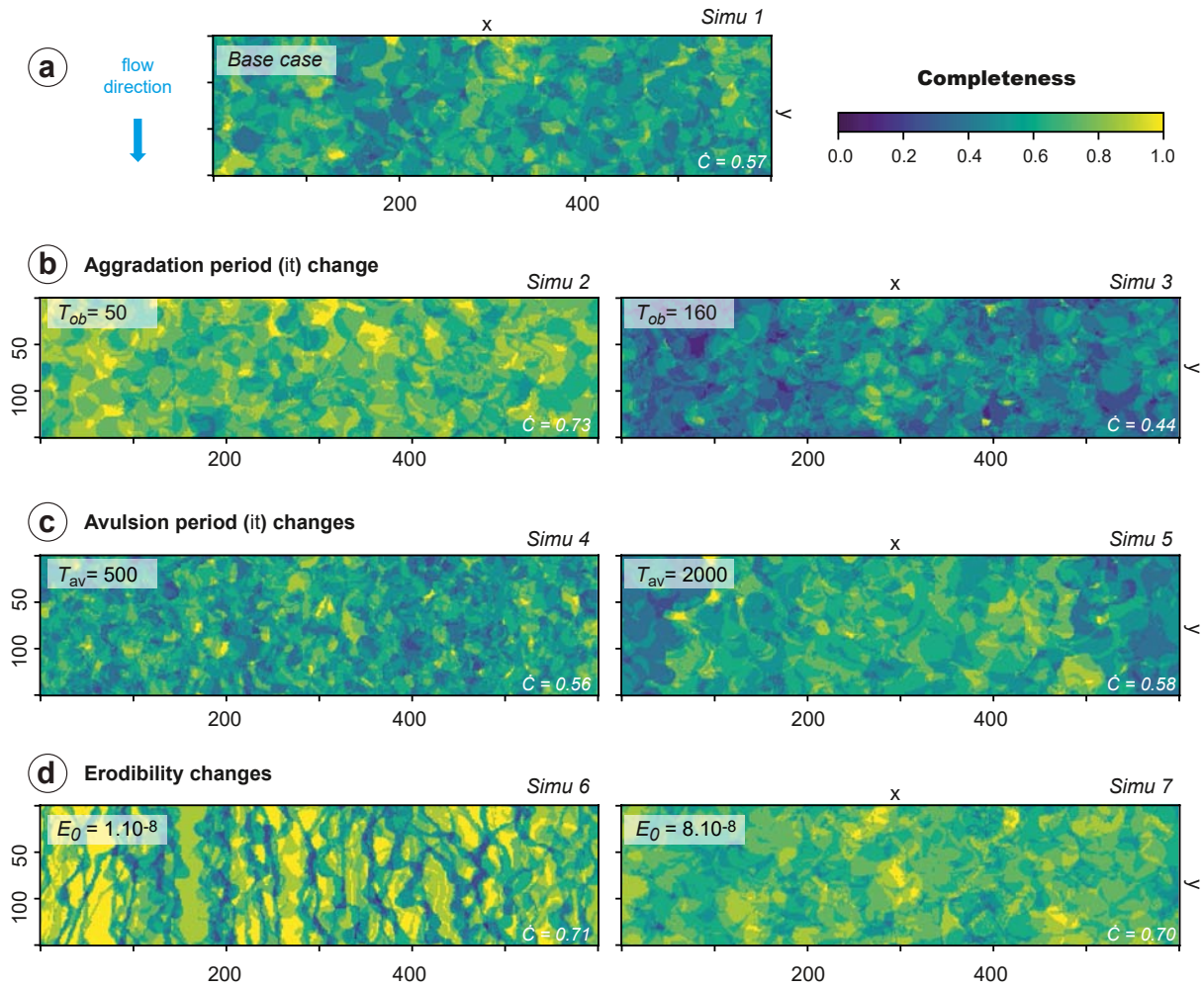


Figure 5. Map (x,y) view of computed completeness values measured at $\delta t = 6,400$ iterations for the (a) base case, (b) varying aggradation rate, (c) varying avulsion period, and (d) varying bank erodibility scenarios. Average completeness over the domain \bar{C} is indicated.

6,000 m perpendicularly to flow direction, 1,500 m in the flow direction and 40 m thick). Overbank parameters i_{ob} and λ_{ob} were set at 0.1 ± 0.03 m (normal distribution used in this study, although it can be set to be uniform or log-normal by user) and 450 m, respectively. The resulting levee-overbank extension was thus 1,125 m at maximum (Figure 2a, thickness = 1 cm for $2.5 \lambda_{ob}$). The simulation domain was then larger than the floodplain, which would correspond to the distal part of large alluvial fans to the proximal part of deltaic systems. Note that

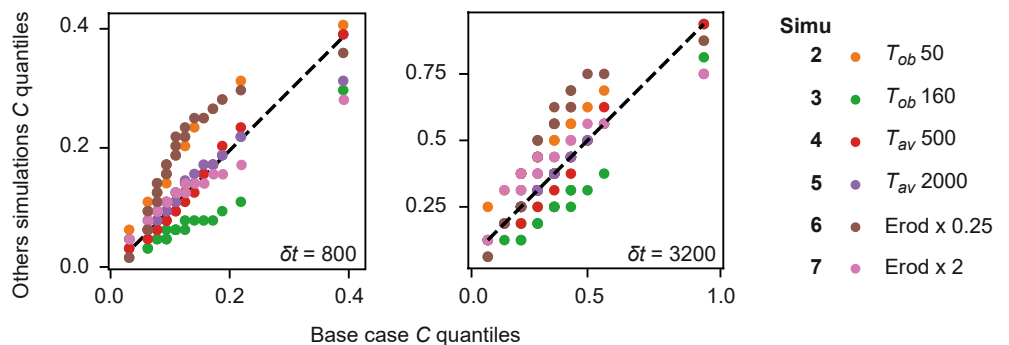


Figure 6. Q-Q plots of completeness values comparing scenarios with the base case ($\delta t = 800$ and $3,200$ iterations). See Table 2 for parameters.

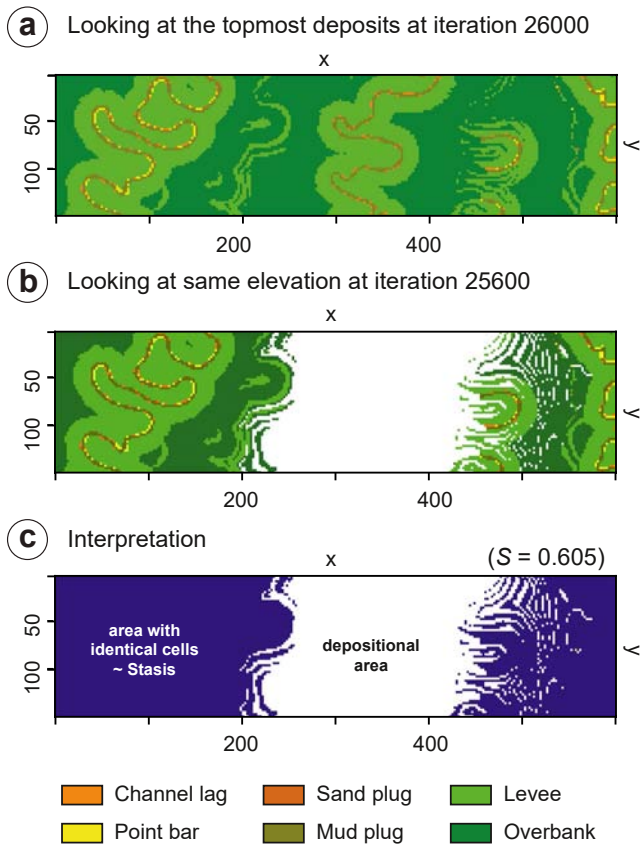


Figure 7. Map (x,y) view showing steps in measuring stasis: a comparison is made between the deposit at the topmost cell of a given 3D grid (a) and the same elevation some δt iterations before panel (b). Stasis corresponds to the number of cells that did not change between the two grids (c) divided by the total amount of cells (x,y). See methods for details.

3D grid (at t ; Figure 7a). Second, the corresponding cells were compared with that of the oldest 3D grid (at $t - \delta t$; Figure 7b). Stasis corresponded to the proportion at the surface of the map where t and $t - \delta t$ cells were identical (Figure 7c), that is, no change was observed. Because the system is aggrading at the timescale of 3D grids extraction, there is no configuration where pure facies replacement occurs—that is, without deposition above—and that could be confused with stasis (Figure 8). It is exemplified in Figure 2b: there is always levee deposits observed above point bar deposits.

3.2.3. Accumulation and Reworking

Changes in facies were measured similarly to stasis, that is, by comparing the cells of the 3D grids between t and $t - \delta t$. Apart from the cells that did not change between iterations (see above), three cases were considered: (a) going from nothing to a deposit was counted as deposition (*depo*), (b) going from a deposit to nothing was counted as erosion (*erod*) and (c) changing the deposit type was counted as facies replacement (*fr*) (Figure 2b). It was possible from these measurements to visualize how changes in the depositional record evolved as a function of δt . It is illustrated in Figure 9, where *fr* and *erod* in Simu 2 are plotted as a fraction of deposition (*depo* + *fr*); the remaining part corresponding to preservation.

R was measured as the sum of cells with erosion and facies replacement divided by the sum of cells with facies replacement and deposition (summed on all pairs with spacing δt):

for a default value of 30 m for channel width (Equation 5), the 2D (map) grid resolution was $0.34 W$; that is, finer than the value of $0.4 W$, above which unexpected threshold effects related to grid resolution occur (Limaye & Lamb, 2013).

3.2. Measurements and Comparison With Theory

Alluvial deposit evolution was monitored by saving a 3D grid of the evolving facies every 200 iterations, a period longer than T_{ob} . Deposit type (Table 1) was saved in each grid while the “age” (i.e., iteration of deposition) of preserved deposits was also saved in the final grid (i.e., iteration 102,400). Figure 3 shows the final arrangement of the deposits for all scenarios along the cross-section (xz) located at the 75th y -node of the grid while Figure 4 shows the age distribution of the preserved deposits along the same section. Computation of completeness, stasis, reworking and accumulation rates (Figures 5–11) were made in the interval between 25,600 (to generate a deposition substrate of thickness nearly equivalent to one channel depth) and 76,800 iterations (to exclude the last deposits, less affected by erosion (see Figure 4)).

3.2.1. Completeness

Ages of deposits at the final (102,400th) iteration were used to calculate stratigraphic completeness based on Equation 2 for each time span (200; 400; 800; 1,600; 3,200; 6,400; 12,800; 25,600 and 51,200). $C(x,y)$ maps were computed for the different forcing scenarios (see Figure 5 for $\delta t = 6,400$). C values distribution were compared using Q-Q plots on 900 values by sub-sampling the grids every 10 nodes (Figure 6).

3.2.2. Stasis

S was calculated by comparing pairs of 3D grids with spacing δt (i.e., computing on all possible pairs and returning the average). First, the elevations and facies type of the topmost deposits were identified for the youngest

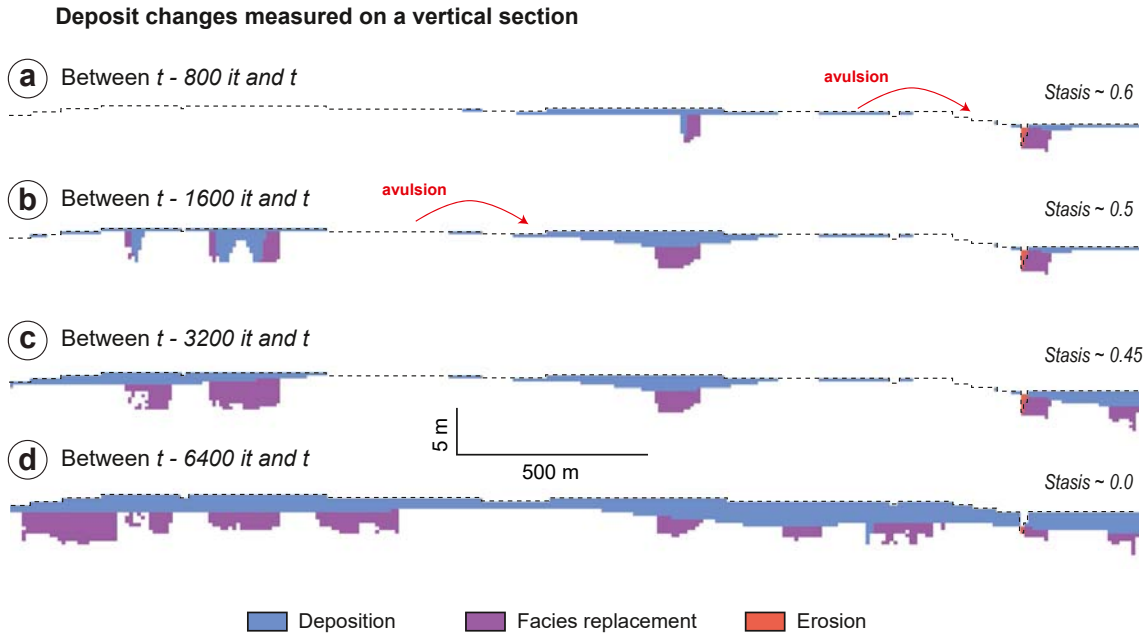


Figure 8. Cross-sectional view (xz at $y = 75$) of deposits changes between 3D grids measured in Simu 2 for increasing δt (from 800 to 6,400 it.). The 3D grid was saved at 25,600 it (iteration t). Comparisons between (a) $t-800$ and t , (b) $t-1,600$ and t , (c) $t-3,200$ and t , and (d) $t-6,400$ and t illustrate the spatial distribution of facies replacement, deposition and erosion. See methods for details.

$$R_{\delta t} = \frac{\sum_{j=1}^N (erod_{\delta t j} + fr_{\delta t j})}{\sum_{j=1}^N (fr_{\delta t j} + depo_{\delta t j})} \quad (6)$$

Resulting values of R were plotted, together with C and S as a function of δt (Figure 10).

Finally, the short-term accumulation rate was computed using Equation 1 in two different ways: one that measured topographic changes alone ($A_{\delta t}$) and one that also included facies replacement ($A_{\delta t}^*$) (Figure 11).

$$A_{\delta t} = \frac{\sum_{j=1}^N (depo_{\delta t j} - erod_{\delta t j})}{TD(1 - S_{\delta t})} \quad (7)$$

$$A_{\delta t}^* = \frac{\sum_{j=1}^N (depo_{\delta t j} - erod_{\delta t j} + fr_{\delta t j})}{TD(1 - S_{\delta t})} \quad (8)$$

$A_{\delta t}$ included deposition ($depo$) less erosion ($erod$) while $A_{\delta t}^*$ included deposition less erosion and facies replacement (fr). D denotes the area of the 2D domain considered (see Supporting Information S1 for a detailed description).

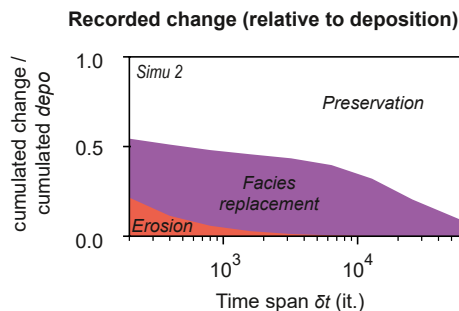


Figure 9. Record of facies change measured as a function of δt expressed relative to deposition: example of Simu 2. Note that erosion becomes negligible when measured over 3,000 iterations.

3.2.4. Comparison With Existing Theory

Boxplots of completeness calculated from all simulations were plotted against their theoretical predictions in Figure 12. These included Equation 3a using either $A_{\delta t}$ or $A_{\delta t}^*$ (Figure 10d), Equation 3b using either $m = (d \ln A_T) / (d \ln T)$ —which returned values of -0.8 ± 0.05 - (Figure 10c) or $m = -0.5$ (Figure 10b), and Equation 4 (Figure 10e). T_c , that is, the limit where the Sadler effect saturates, was used instead of T to calculate precision. Finally, theoretical predictions for C using Equation 3a with $A_{\delta t}^*$ and Equation 4 were plotted against each other for comparison.

Table 1
Deposit Types Used in the Simulations and Associated Processes

Location	Deposit facies	Associated process
Overbank flooding area	Overbank	Fine (silt-clay) deposition mostly by decantation after flood
	Levees	Rapid settling of suspended sediments flooding out of the channel as a result of decreasing turbulence
Channelized deposits	Mud Plug	Fine-grained fraction of abandoned channel fill
	Sand Plug	Coarse-grained fraction of abandoned channel fill
	Point Bar	Fining-up, usually sandy deposits accumulating in the inner bend of channel as it migrates
	Channel Lag	Coarse deposits associated with high transport capacity at the bottom of channel

4. Results and Interpretations

4.1. Deposit Architecture and Age Distribution

The seven simulations tested in this study showed contrasted sedimentary architectures in response to parameter changes (Lopez et al., 2009) (Figure 3). Increasing aggradation rate (by reducing T_{ob}) leads to higher final elevations (Table 2) and increase in proportion of overbank deposits compared to channelized deposits (Figure 3b). Decreasing avulsion period leads to increased channel abandonments and associated channel-fill deposits, but also to narrowed point bar due to abandonment occurring before the establishment of high sinuosity channels (Figure 3c). On the contrary, increasing bank erodibility favored lateral migration of channels, which increased the proportion of point bar deposits (Figure 3d).

Age distributions of the preserved deposits varied depending on the simulated scenarios, although some similarities were observed (Figure 4). In all scenarios, the time interval that has a maximum time preservation was found at the end of simulations, between $(t_{end}-T_c)$ and t_{end} . It is best exemplified in simulations with either low accumulation rate (Simu 3), high avulsion rate (Simu 4) or high erodibility (Simu 7). Before $t_{end}-T_c$, age distribution was also heterogeneous in most scenarios with large fluctuations (Figure 4). It was sometimes observed that these fluctuations scaled with T_c such as in Simu 1 where about six fluctuations were identified (Figure 4a), or in Simu 5 where about seven fluctuations were observed (Figure 4c). Age distributions in all simulations were thus consistent with theory on compensation timescale and further validated the choice not to include the youngest deposits in estimating C , R and S , as these “younger” deposits were better preserved than the other ones.

4.2. Distribution and Evolution of Completeness

Completeness maps showed heterogeneous distribution in space, as illustrated on Figure 5 by the maps at $\delta t = 6,400$. C values were more spatially variable in cases with low erodibility (Simu 6) or short overbank flow

Table 2
Parameters Varied in the Simulations and Resulting Series Characteristics (Z_{end} , A_T and T_c)

Simu	Overbank flood period T_{ob} (it.)	Regional avulsion period T_{av} (it.)	Erodibility coefficient E_0	Section age t_{end} (it.)	Mean final elevation Z_{end} (m)	Acc. Rate (m/it.) $A_T = Z_{end}/t_{end}$	Compensation timescale (it.) $T_c = H_{max}/A_T$
1-Base case	80	1000	$4.00 \cdot 10^{-8}$	102,400	18.73	$1.83 \cdot 10^{-4}$	16,400
2-Aggrad50	50	1000	$4.00 \cdot 10^{-8}$	102,400	29.45	$2.88 \cdot 10^{-4}$	10,432
3-Aggrad160	160	1000	$4.00 \cdot 10^{-8}$	102,400	8.78	$8.57 \cdot 10^{-5}$	34,990
4-Avuls500	80	500	$4.00 \cdot 10^{-8}$	102,400	14.33	$1.40 \cdot 10^{-4}$	21,434
5-Avuls2000	80	2000	$4.00 \cdot 10^{-8}$	102,400	21.82	$2.13 \cdot 10^{-4}$	14,080
6-Ero0.25	80	1000	$1.00 \cdot 10^{-8}$	102,400	12.34	$1.20 \cdot 10^{-4}$	24,898
7-Ero2	80	1000	$8.00 \cdot 10^{-8}$	102,400	21.84	$2.22 \cdot 10^{-4}$	13,488

Note. 3D grids were saved every 200 iterations.

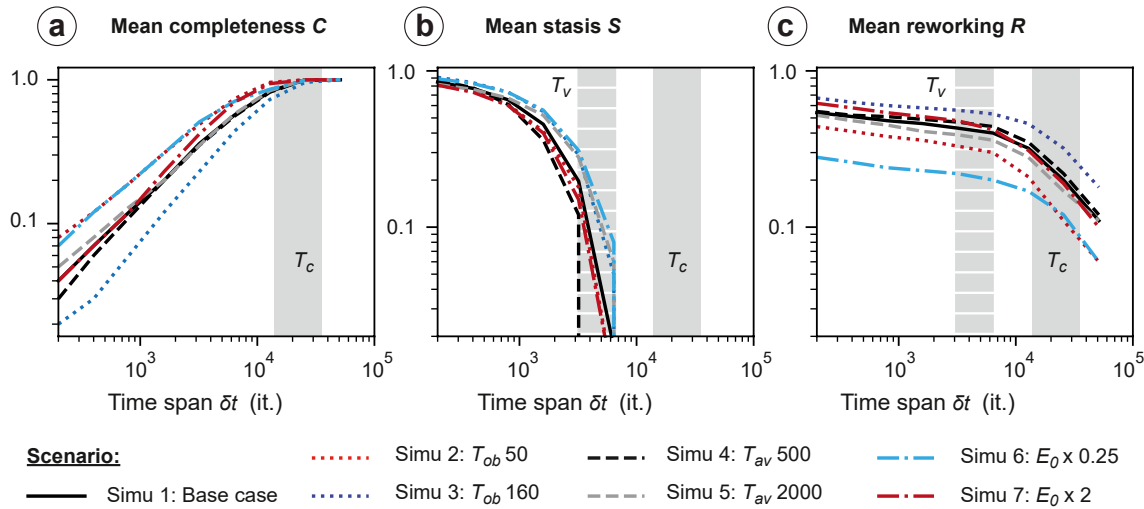


Figure 10. (a) Mean completeness, (b) stasis, and (c) reworking shown for all simulations as a function of δt . T_c and T_v correspond to compensational and visitation timescales, respectively.

period (Simu 2) (Figures 5 and 6). In the case with low bank erodibility (Figure 5d; Simu 6), the sinuous channel shapes correspond to low values of C , separated by high values of C of preserved overbank deposits in areas that had not been swept by the channel thanks to the limited migration.

Comparisons of C distributions with the base case showed that simulations with high aggradation rate or low erodibility (Simus 2 and 6) typically had a higher dispersion and median value, compared to simulations with low aggradation rate or high erodibility (Simus 3 and 7) (Figure 6). Simu 7 crossed the $y = x$ line, likely because of a bimodal distribution of values. Simulations with changing avulsion period had C distributions comparable with that of the base case. C median values overall increased with δt without significantly altering this trend (Figure 6).

All curves of mean completeness as a function of δt had similar shapes (Figure 10a). Mean completeness started at ~ 0.1 for $\delta t = 200$ and increased with δt and equal one when measured for $\delta t > T_c$ (Figure 10a). On average, Simu 3 (low accumulation rate) had the lowest completeness while Simu 2 (high accumulation rate) had the highest completeness. For δt values higher than 200, C increased rapidly for Simu 7 to reach values like that observed in Simu 2.

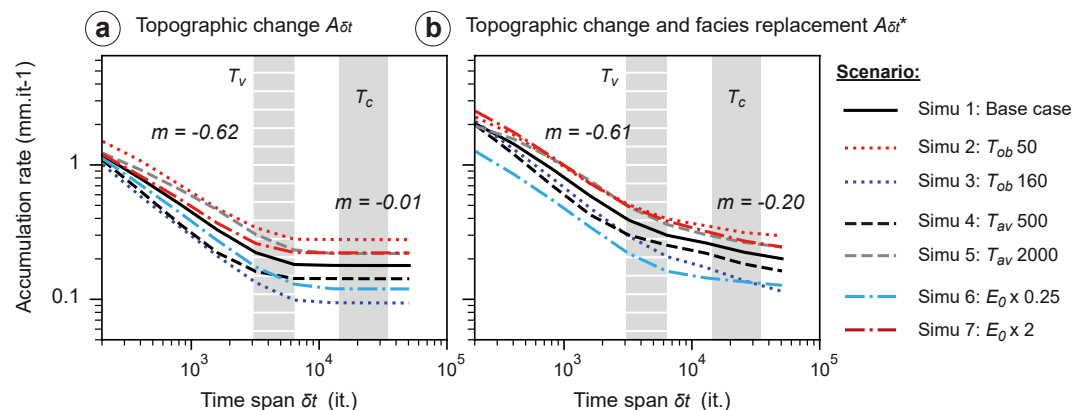


Figure 11. Short-term accumulation rates $A_{\delta t}$ and $A_{\delta t}^*$ for each simulation as a function of δt . T_c and T_v correspond to compensational and visitation timescales, respectively.

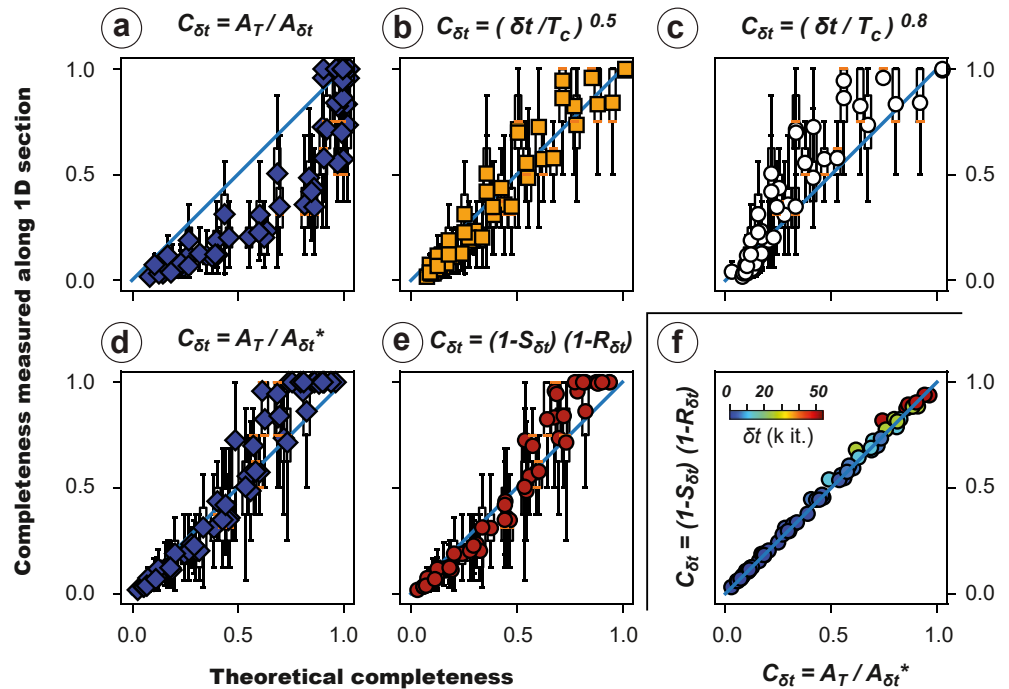


Figure 12. Comparison between the distributions of completeness values (boxplot) measured from simulations and estimates from theory. (a–d) are from Sadler (1981) (e) from this study while panel (f) is a cross plot between the theoretical predictors in panels (d and e).

4.3. Surface Evolution Related to Channel Motion

The stasis fraction started around 0.8 for $\delta t = 200$ and decreased as a function of δt (Figure 10b). Around $\delta t = 1,000$ —which corresponded to T_{av} in most simulations except Simu 4 and 5— the decrease of S was faster. This likely illustrated the start of avulsion that greatly enhanced visitation of the floodplain by new channel path and associated overbank deposits. S went down to zero for δt above 3,000–17,000 iterations depending on simulations. We defined this threshold, which roughly corresponded to 6–10 avulsions depending on the scenario, as the timescale T_v of visitation of the entire domain by overbank sedimentation (Figure 8). Overall, S did not vary by more than 25% between simulations. A high stasis fraction was observed for simulations with long T_{av} (Simu 5), low erodibility (Simu 6), or long T_{ob} (Simu 3). Finally, Figure 10 shows that completeness C and stasis fraction S had opposite trends, suggesting an inverse coupling between the two parameters (i.e., Tipper, 2015).

Figure 8 shows that facies replacement and erosion were mostly measured in the lowest part of sections - corresponding to the migration of the active channel incising the floodplain and depositing point bars - while deposition was located at the top, corresponding mainly to levee and overbank deposition. Erosion was small as it corresponded to the channel volume and kept a fairly constant value through time (albeit depending on channel sinuosity) (Figure 8). Facies replacement increased with δt but much slowly than deposition. With increasing δt , the fraction of erosion and facies replacement that could be recorded relative to deposition thus decreased (Figure 9), and R also mechanically decreased (Figure 10c).

Figure 9 shows that for Simu 2 at $\delta t = 200$, about 20% of $erod$ and 40% of fr relative to $depo$ could be measured, that is, an equivalent R of 0.4 (Figure 10c). The ability (proportion) to measure erosion (channel volume) vanished exponentially with δt so that it was close to zero when measured using δt over 4,000 it (Figure 9). After that timescale, the ability to measure reworking was available through facies replacement only. Overall, R slowly decreased with increasing δt until a break is observed around 5,000–15,000 it. and the decrease was faster (Figures 9 and 10c). The break corresponded to T_v , that is, stasis was then zero (Table 2). This behavior was observed in all simulations although the mean value of R varied by a factor of 2–3 between simulations. R values were low for low erodibility coefficient (Simu 6) and low overbank period (Simu 2), and high for large overbank period (Simu 3) (Figure 10c).

Measured short-term accumulation rates $A_{\delta t}$ and $A_{\delta t}^*$ decreased with increasing δt and looked very similar between the different simulations (Figure 11). Simu 7 (with high erodibility) had an accumulation rate similar to that of Simu 2 (i.e., low T_{ob}). The value of $A_{\delta t}$ was lower than $A_{\delta t}^*$. Both $A_{\delta t}$ and $A_{\delta t}^*$ curves show a break around T_v (Figure 11). They both converge toward a similar value, which corresponds to A_p , although it is attained much more rapidly (at T_v) in the case of $A_{\delta t}$. In the case of $A_{\delta t}$, power law fits of the two segments of the curve in the 200–3,200 and 6,400–51,200 intervals returned exponents of -0.62 and -0.01 respectively while a fit in the 200–51,200 interval returned -0.44 (Figure 11a). In the case of $A_{\delta t}^*$, power law fits of the two segments of the curve in the 200–3,200 and 6,400–51,200 intervals returned exponent of -0.61 and -0.20 respectively while a fit in the 200–51,200 interval returned -0.44 (Figure 11b).

4.4. Predicted vs Measured Completeness

A comparison was made between the results of this study and existing theory on completeness (Figure 12). The first striking result was that C was better estimated when using Equation 3b of Sadler (1981) with $A_{\delta t}^*$ (Figure 12d) than topographic change only $A_{\delta t}$ (Figure 12a). In detail, the former was an especially good predictor for value of C lower than 0.5 and more variable for values of C above 0.5. For estimations using the precision $\delta t/T$, a better agreement was observed when using $m = -0.5$ (Figure 12b) instead of $m = -0.8$ (Figure 12c), suggesting that m is close to -0.5 . In the latter, the theory seemed to underpredict measurements from the simulation (Figure 12c). The new Equation 4 relating mean completeness to mean deposition area ($1 - S$) and the mean preserved deposits ($1 - R$) was in good agreement with measurements (Figure 12e). Finally, a cross plot between the theoretical estimates in Figures 12d and 12e, which were rather good predictors, was presented in Figure 12f. It showed that the two formulations have very similar outcomes, although some slight variability was observed for the values of C above 0.5.

5. Discussion

In this study, it was possible to track both topographic and sediment changes associated with fluvial meandering dynamics, that is, complementing works that mainly tracked topographic changes in physical experiments (Straub & Esposito, 2013; Straub & Foreman, 2018) or numerical simulations (e.g., Durkin et al., 2017; Wang et al., 2021; Yan et al., 2021). Results show that this combination of topographic and facies replacement measurement allows for a better prediction of completeness than topographic data alone (comparison between Figures 12a and 12d).

5.1. Anti-Persistent and Persistent Regimes

In the present study, several thresholds are identified. For instance, the avulsion timescale corresponds to an accelerated decrease of S . Another threshold is perhaps reached when the ability to track erosion is low (Figure 9). The compensation timescale T_c corresponds to the transition where C equals one (Figure 10a). T_v (i.e., the timescale from which $S = 0$) corresponds to breaks in short-term accumulation rate (Figure 11) and R (Figure 10c) decreases as a function of δt .

Similarly to previous studies, a decrease of accumulation rates $A_{\delta t}$ with the time span δt is shown. A power-law fit of $A_{\delta t}^*$ versus δt (Figure 11) over the whole δt range returned an exponent m close to -0.5 (i.e., -0.44 with $R^2 = 0.85$). Using $m = -0.5$ rather than the empirical one found by Sadler (1981) (ca. -0.8 for fluvial data) allowed a rather good prediction of mean observed C (Figures 12b and 12c). According to Schumer et al. (2011), this suggests that the surface evolution in the model could be described as a Fractional Brownian motion ($h = 0.5$). This means that topographic fluctuations building the stratigraphy worked as if positive and negative jumps were uncorrelated, which would correspond to a random walk. Such result is surprising as the parameters used in the model were set so that stochasticity was limited. Overall, this can tentatively be explained by the variety of (fluvial) processes at play in the model.

In detail, the changes in the rate of $A_{\delta t}^*$ decrease with δt allows distinguishing between a non-persistent (when $\delta t < T_v$) and a persistent regime (when $\delta t > T_v$). Before T_v , m is -0.62 , which mean that h is between 0 and 0.5 (Schumer et al., 2011). This indicates that the jumps are negatively correlated, suggesting a regime typically

dominated by compensational stacking (Straub & Esposito, 2013; Straub et al., 2009). In this regime, channel motion—i.e., by avulsion—is influenced by levee topography (Figures 2 and 8). Sedimentation is then more likely to occur in topographic lows where sediment has not deposited yet (Pelletier & Turcotte, 1997). Thus $A_{\delta t}^*$ decreases very fast with δt . When measured beyond T_v , $A_{\delta t}^*$ keeps decreasing, although much slowly. The power-law exponent m is -0.2 ; therefore h is between 0.5 and 1, which reveals persistence phenomenon (Jerolmack & Sadler, 2007). In this regime, a positive correlation between elevation jumps is found, which supposes that an area receiving sediment is more likely to receive sediment at the next step. This is consistent with stasis being zero and accumulation being recorded everywhere in the domain at such timescale (Figure 8d). Only after T_v can then accumulation be considered as a drift in the sense of ubiquitous deposition. Reworking related to channel migration is then the unsteady surface process. $A_{\delta t}^*$ then converges toward A_T .

5.2. Stasis Dynamics

Simulations showed that stasis strongly impacted the value of completeness as pointed out by many authors (Paola et al., 2018 and references therein). Indeed, as shown above, the timescale T_v beyond which S equals zero corresponds to a major change in accumulation dynamics (Figure 11). This is further attested by an (inverse) similarity of the shapes of C and S curves (i.e., Figures 10a and 10b). The strong (anti) correlation between C and S is perhaps best shown by Equation 4 (Figure 10d). Recently, following Tipper (2015), Straub and Foreman (2018) have illustrated the importance of stasis in the value of C , although no direct relation has been proposed yet. The present study allows for a quantification of the importance of this phenomenon.

The timescale T_v used in this study for overbank visitation of the entire domain is similar to the channel timescale necessary to occupy a substantial fraction (e.g., >90%–95%) of a sedimentary basin (Cazanacli et al., 2002; Kim et al., 2010). The latter was defined for experimental fluvial system datasets by cumulating overlapping wetted areas of a basin. In these experimental simulations, floodplain aggradation was proportional to channel aggradation. Topography changed by the migration of bedload-rich systems that occasionally spill out during flooding stages, which occurred autogenically (e.g., Scheidt et al., 2016). Apart from the determinism of flooding occurrence and shapes of overbank deposits, the dynamics in FLUMY and tank experiments are however not fundamentally different, and the existing theory developed for channel timescale may well be adapted to assess T_v .

In the simulations, performed over a given domain, stasis is inversely proportional to levee/overbank deposition length, which was roughly constant ($\sim 1,125$ m). Considering the width of the domain (6,000 m) and overlaps between overbank deposits, about 6–10 avulsions are necessary to occupy the domain, in agreement with observations (Figure 10b). Consistently, values of T_v are respectively lower and higher in cases with shorter and longer avulsion periods (Figure 10b). Some variability is however observed depending on how well channels can sweep across the floodplain between avulsions (i.e., comparison between Simus 6 and 7).

5.3. Reworking Dynamics

Reworking is a process measured at all timescales (Figure 10c). With a lateral migration rate of bends in the order of $0.5\text{--}1\text{ m.it}^{-1}$ in average in the simulations, the channel migrate about 100–200 m (i.e., 3.5–7 channel widths) in between extractions of 3D grids. It is a much more efficient reworking than avulsion, which erodes only one channel width at best every 500 iterations. Observed reworked fraction varied between simulations (Figure 10c). It was typically 40%–70% when measured over short time span (i.e., 200 it.), except for Simu 6 (25%) for which erodibility was low. These values thus quantify at centennial scale the potential for storage and release of sediments on floodplains (Métivier & Gaudemer, 1999). They suggest that fluvial sediments have about a 50% chance to be reworked after their deposition in relation with the continuous migration of a channel. This probability remains high (40%) until δt reaches the T_v value when R decreases faster (Figure 10c). Sustained high R values until T_v likely illustrate enhanced reworking by avulsion, which works by carving new channel paths, until the whole domain is occupied—a counterweight for increased overbank sedimentation in FLUMY. Figure 8 indeed shows that before T_v , each avulsion induces erosion of previous deposits by one channel depth. After T_v , measured reworking decrease rapidly but is still observable. A fraction of migrating channel (point bars) located below the levees at the beginning of measurement is indeed always counted as reworking (Figures 7 and 8). It is inherent to

the incisional nature of avulsions in FLUMY, who carve the floodplain and are not aggradational, as sometimes observed in natural systems (Mohrig et al., 2000).

In this study, morphologies (channel, levee/overbank deposits) sizes were kept constant. In nature, these morphologies vary with time. One may thus expect that C would be lowered if channel depth was increased—for instance associated with climate change - as deposits would be reworked more deeply. In that case however, both overbank deposit size and avulsion frequency will likely increase, which would tend to increase C . Testing the impact of channel size change, particularly during transience (e.g., Chen et al., 2018), on strata preservation would require further investigation.

5.4. Completeness Related to Channelized and Non-Channelized Processes

Overall, the anti-persistent and persistent regimes respectively result from non-channelized and channelized processes actions on alluvial plains. C maps are indeed often organized into clusters of high and low C (Figure 5). In cases of short T_{ob} (Simu 2), low erodibility or short avulsion period, the contrast between the values of C in these two domains is further enhanced. Areas of higher C define surviving areas (see Durkin et al., 2017) that have not been reworked by channel sweep. These surviving areas are well developed in the case of low bank erodibility (Simu 6; Figure 5d), isolated but significantly large in the case of short T_{ob} (Simu 2; Figure 5b) or high bank erodibility (Simu 7; Figure 5d). They correspond to floodplain deposits, which were minimally eroded and are separated by areas of lower C swept by channel migration. These patterns are consistent with the preferential preservation of lower-order (here levee/overbank deposits) relative to higher-order (here point bars and channel fill deposits) hierarchical forms (Ganti et al., 2020). In Simu 6 (Figure 5d), the wide range of C values – also observed in the associated Q-Q plot (Figure 6)– is due to limited channel migration that favored a ribbon geometry elongated along the main slope. For the other simulations (2 and 7), the contrasts are lower and no specific shape of the high C remnants is observed.

The duality between erosive (channelized) and depositional (mainly non-channelized) processes is also present in Equation 4. It is suggested that this formulation is very similar to Equation 3a of Sadler (1981) by the cross plot in Figure 12f, which can also be demonstrated theoretically, especially for values of $\delta t > 1,000$ iterations (See Supporting Information S1). A current limitation is that $erod$ is very small compared to fr and $depo$ and its impact on the formulations is difficult to assess (See Supporting Information S1). Nevertheless, Equation 4 appears appropriate to assess how well a signal is recorded on average along fluvial stratigraphic sections. This formulation could well be tested on the field as follow.

First, S could be assessed by measuring the ratio of depositional (~basin) width to overbank deposits width at a given time step. Such estimation is feasible using interpretations of levee-overbank geometry extent on seismic data. Alternatively, depositional width could be estimated using existing models of the decrease in overbank deposit thickness with distance from the levees (i.e., Gross & Small, 1998; A. D. Howard 1996; A. H. Howard, 1992; Lopez, 2003; Pizzuto, 1987). Second, R could be assessed from field data using proxies such as bar preservation based on their geometry and facies (e.g., Chamberlin & Hajek, 2019). An alternative way would be to use Equation 6 with point bar deposits area as fr , floodplain deposits area as $depo$, and $erod$ neglected (e.g., Figures 8 and 9).

The seemingly chaotic stratigraphic architecture observed in the model fades away when considering the scaling (and thus process) break at T_v in the dependence of accumulation rates to measurement time span (Figure 9). In other word doing a regression fit of accumulation over the whole range of measurement time spans, which returns m close to -0.5 , is surely an oversimplification. Nevertheless, it remains striking that completeness measured in the synthetic stratigraphy can be approximated assuming a chaotic construction (Figure 12b). The example of such “chaos arising from order” (Chris Paola, personal communication 2020) highlights that breaks in scale related to geological process may be found, which would allow retrieving information on depositional systems dynamics. For instance, the fact that m is -0.585 for alluvial data (Paola et al., 2018; Sadler & Jerolmack, 2015) implies dominance of compensational stacking. In fluvial systems however, and it may not be incompatible, other breaks in scaling including for instance external forcings such angular unconformities driven by tectonic deformation or change of river mobility or size driven by climate may exist. Using different parameterization in FLUMY, for example, allowing local avulsions to occur within the depositional domain or forcing topographic

deformation by tectonic processes, could potentially have changed the shape of the dependence of accumulation rate to measurement time span.

5.5. Limitations of the Approach

Although consistent with the general theory, the present results particularly apply to meandering systems, which are less represented than distributive fluvial systems in nature (Weissmann et al., 2015). Results could however be tested in other contexts, for instance in aggrading turbidite environments where similarities to fluvial systems can be observed (Lemay et al., 2020). Of interest will be how T_v and T_c encompass changes in accumulation dynamics there. In fluvial system, avulsion period scales with the time for aggradation to elevate the channel above the levees by one channel depth (Jerolmack & Mohrig, 2007). Aggradation and formation of channel plugs can however occur rapidly (tens of years) (e.g., Szewczyk et al., 2022) and force avulsion with limited overbank deposition at the scale of the floodplain. Such dynamics of rapid switches compared to aggradation may explain how reworking can be well expressed in alluvial systems (Figure 7c). On the contrary, the reworking might be limited due to important levee aggradation (and thus superelevation) before avulsion in submarine channel belts (Jobe et al., 2020). In that case, the evolution of R with measurement time span would look different than in alluvial systems, which should enhance completeness.

Another limitation is that the size of the domain is relatively small compared to the deposition area, hence hiatus duration is short in the present study. There is therefore a bias toward short hiatus, which is enhanced as simulations run for hundreds of thousands of years compared to tens of millions of years in nature. On the other hand, we chose to extract grid data every 200 iteration, which corresponds to ca. 300 years in nature, so that this study has a limited resolution on lower architectural hierarchies (accretion packages) compared to a recent study by Yan et al. (2021). We do include a comparable degree of complexity at the scale of channel belt, since FLUMY also includes changes of direction of migration and bend cut-offs (Lemay, 2018).

Finally, the fact that no reoccupation is allowed is an oversimplification of the model compared to nature and experiments (e.g., Ashworth et al., 2007; Aslan et al., 1999; Morozova & Smith, 2000). In natural systems, after a rapid disconnection stage associated to sand plug formation (e.g., Szewczyk et al., 2020) abandoned channels are slowly filled (10^{2-3} yrs). This is propitious to reoccupation as old channels remain topographic lows. In the simulations, the stratigraphy was thus built by compensational stacking mainly (Sahoo et al., 2020). If reoccupations were allowed, they would decrease reworking compared to the simulations of this study where a new channel path systematically erodes sediments. On the other hand, it would lengthen the time that some areas remain in stasis, that is, away from reoccupied channel paths. Hence, C values should be affected by allowing reoccupations, but because R and S will be affected too, and it should still be possible to predict C using Equation 4.

6. Conclusion

In this study, the evolution of fluvial meandering river deposits was tracked on a series of numerical simulations by combining measurement of topographic and facies evolution. We found that:

1. Accumulation rate dependence on measurement time span allows distinguishing between an anti-persistent and a persistent regime.
2. The former is characteristic of channel avulsion and compensational stacking until the whole domain is visited by overbank deposition, which corresponds to the timescale T_v when stasis $S = 0$.
3. The latter is related to surface fluctuations by channel continuous migration and the associated erosion of formerly deposited alluvium. As persistence in accumulation is attained, reworking R is the remaining active process until the whole system has aggraded one channel depth (i.e., compensation timescale T_c).
4. Based on these results, the mean completeness C can be approximated using $C_{\delta t} = (1 - S_{\delta t})(1 - R_{\delta t})$.

Data Availability Statement

Data are reproducible using this version with the batch files available in Supporting Information S1. Flumy (2019) version 5.906 was used in this study. The FLUMY software can be found here: <https://flumy.minesparis.psl.eu/> and activated using an activation number provided by the FLUMY team.

Acknowledgments

We would like to thank the partners that supported this research: ENI, Engie, Exxon, Petrobras, and Shell. This work was motivated by discussions with Chris Paola and David Morhig. We thank Kyle Straub and two anonymous reviewers, as well as Mikael Attal and associate editor for detailed comments that greatly improved the manuscript.

References

- Abels, H. A., Kraus, M. J., & Gingerich, P. D. (2013). Precession-scale cyclicity in the fluvial lower Eocene Willwood Formation of the Bighorn Basin, Wyoming (USA). *Sedimentology*, *60*(6), 1467–1483. <https://doi.org/10.1111/sed.12039>
- Ager, D. V. (1973). *The nature of the stratigraphical record*. The MacMillan Press.
- Ashworth, P. J., Best, J. L., & Jones, M. A. (2007). The relationship between channel avulsion, flow occupancy and aggradation in braided rivers: Insights from an experimental model. *Sedimentology*, *54*(3), 497–513. <https://doi.org/10.1111/j.1365-3091.2006.00845.x>
- Aslan, A., Blum, M., Smith, N., & Rogers, J. (1999). Contrasting styles of Holocene avulsion, Texas Gulf coastal plain, USA. *Fluvial sedimentology VI*, *28*, 193–209.
- Cazanacchi, D., Paola, C., & Parker, G. (2002). Experimental steep, braided flow: Application to flooding risk on fans. *Journal of Hydraulic Engineering*, *128*(3), 322–330. [https://doi.org/10.1061/\(asce\)0733-9429\(2002\)128:3\(322\)](https://doi.org/10.1061/(asce)0733-9429(2002)128:3(322))
- Chamberlin, E. P., & Hajek, E. A. (2019). Using bar preservation to constrain reworking in channel-dominated fluvial stratigraphy. *Geology*, *47*(6), 531–534. <https://doi.org/10.1130/g46046.1>
- Chen, C., Guerit, L., Foreman, B. Z., Hassenruck-Gudipati, H. J., Adatte, T., Honegger, L., et al. (2018). Estimating regional flood discharge during Palaeocene-Eocene global warming. *Scientific Reports*, *8*(1), 13391. <https://doi.org/10.1038/s41598-018-31076-3>
- Durkin, P. R., Hubbard, S. M., Holbrook, J., & Boyd, R. (2017). Evolution of fluvial meander-belt deposits and implications for the completeness of the stratigraphic record. *GSA Bulletin*, *130*(5–6), 721–739. <https://doi.org/10.1130/b31699.1>
- Eke, E., Parker, G., & Shimizu, Y. (2014). Numerical modeling of erosional and depositional bank processes in migrating river bends with self-formed width: Morphodynamics of bar push and bank pull. *Journal of Geophysical Research: Earth Surface*, *119*(7), 1455–1483. <https://doi.org/10.1002/2013jf003020>
- Flumy (2019). Process-based channelized reservoir models [dataset]. Retrieved from <https://flumy.minesparis.psl.eu/download>
- Ganti, V., Hajek, E. A., Leary, K., Straub, K. M., & Paola, C. (2020). Morphodynamic hierarchy and the fabric of the sedimentary record. *Geophysical Research Letters*, *47*(14), e2020GL087921. <https://doi.org/10.1029/2020gl087921>
- Ganti, V., Straub, K. M., Fofoula-Georgiou, E., & Paola, C. (2011). Space-time dynamics of depositional systems: Experimental evidence and theoretical modeling of heavy-tailed statistics. *Journal of Geophysical Research*, *116*(F2), F02011. <https://doi.org/10.1029/2010jf001893>
- Grimaud, J. L., Grall, C., Goodbred, S., Steckler, M. S., Sincavage, R., Pickering, J. L., et al. (2020). Flexural deformation controls on Late Quaternary sediment dispersal in the Garo-Rajmahal Gap, NW Bengal Basin. *Basin Research*, *32*(5), 1252–1270. <https://doi.org/10.1111/bre.12425>
- Gross, L. J., & Small, M. J. (1998). River and floodplain process simulation for subsurface characterization. *Water Resources Research*, *34*(9), 2365–2376. <https://doi.org/10.1029/98wr00777>
- Held, A. E. (2011). *Apport de la paléohydrologie dans la quantification des rôles respectifs du climat et de la tectonique des systèmes fluviaux méandriques fossiles: Application à des systèmes oligo-miocènes d'Europe occidentale*. ENMP.
- Holbrook, J., & Miall, A. D. (2020). Time in the Rock: A field guide to interpreting past events and processes from a fragmentary siliciclastic archive. *Earth-Science Reviews*, *203*, 103121. <https://doi.org/10.1016/j.earscirev.2020.103121>
- Howard, A. D. (1996). *Modeling channel evolution and floodplain morphology* (pp. 15–62).
- Howard, A. H. (1992). Modeling channel migration and floodplain sedimentation in meandering streams. In *Lowland floodplain rivers. Geomorphological perspectives* (pp. 1–41). John Wiley.
- Ikeda, S., Parker, G., & Sawai, K. (1981). Bend theory of river meanders. Part 1. Linear development. *Journal of Fluid Mechanics*, *112*, 363–377. <https://doi.org/10.1017/s0022112081000451>
- Imran, J., Parker, G., & Pirmez, C. (1999). A nonlinear model of flow in meandering submarine and subaerial channels. *Journal of Fluid Mechanics*, *400*, 295–331. <https://doi.org/10.1017/s0022112099006515>
- Jerolmack, D. J., & Morhig, D. (2007). Conditions for branching in depositional rivers. *Geology*, *35*(5), 463–466. <https://doi.org/10.1130/g23308a.1>
- Jerolmack, D. J., & Paola, C. (2010). Shredding of environmental signals by sediment transport. *Geophysical Research Letters*, *37*(19), L19401. <https://doi.org/10.1029/2010gl044638>
- Jerolmack, D. J., & Sadler, P. (2007). Transience and persistence in the depositional record of continental margins. *Journal of Geophysical Research*, *112*(F3), F03S13. <https://doi.org/10.1029/2006jf000555>
- Jobe, Z. R., Howes, N. C., Straub, K. M., Cai, D., Deng, H., Laugier, F. J., et al. (2020). Comparing aggradation, superelevation, and avulsion frequency of submarine and fluvial channels. *Frontiers of Earth Science*, *8*, 53. <https://doi.org/10.3389/feart.2020.00053>
- Johannesson, H., & Parker, G. (1989). Velocity redistribution in meandering rivers. *Journal of Hydraulic Engineering*, *115*(8), 1019–1039. [https://doi.org/10.1061/\(asce\)0733-9429\(1989\)115:8\(1019\)](https://doi.org/10.1061/(asce)0733-9429(1989)115:8(1019))
- Kim, W., Sheets, B. A., & Paola, C. (2010). Steering of experimental channels by lateral basin tilting. *Basin Research*, *22*(3), 286–301. <https://doi.org/10.1111/j.1365-2117.2009.00419.x>
- Lemay, M. (2018). *Transposition à l'environnement turbiditique chenalisé d'un modèle de systèmes fluviaux méandriques pour la modélisation de réservoirs* (p. 145). Paris Sciences et Lettres.
- Lemay, M., Grimaud, J.-L., Cojan, I., Rivoirard, J., & Ors, F. (2020). Geomorphic variability of submarine channelized systems along continental margins: Comparison with fluvial meandering channels. *Marine and Petroleum Geology*, *115*, 104295. <https://doi.org/10.1016/j.marpetgeo.2020.104295>
- Leopold, L. B., & Wolman, M. G. (1960). River meanders. *GSA Bulletin*, *71*(6), 769–793. [https://doi.org/10.1130/0016-7606\(1960\)71\[769:rm\]2.0.co;2](https://doi.org/10.1130/0016-7606(1960)71[769:rm]2.0.co;2)
- Limaye, A. B. S., & Lamb, M. P. (2013). A vector-based method for bank-material tracking in coupled models of meandering and landscape evolution. *Journal of Geophysical Research: Earth Surface*, *118*(4), 2421–2437. <https://doi.org/10.1002/2013jf002854>
- Lopez, S. (2003). *Modélisation de réservoirs chenalisés méandriques: Une approche génétique et stochastique*.
- Lopez, S., Cojan, I., Rivoirard, J., & Galli, A. (2009). Process-based stochastic modelling: Meandering channelized reservoirs. In *Analogue and numerical Modelling of sedimentary systems: From Understanding to prediction* (pp. 139–144). Wiley.
- Métivier, F., Gaudemer, Y., Tapponnier, P., & Klein, M. (1999). Mass accumulation rates in Asia during the Cenozoic. *Geophysical Journal International*, *137*(2), 280–318. <https://doi.org/10.1046/j.1365-246x.1999.00802.x>
- Miall, A. D. (2015). Updating uniformitarianism: Stratigraphy as just a set of 'frozen accidents'. *Geological Society, London, Special Publications*, *404*(1), 11–36. <https://doi.org/10.1144/sp404.4>
- Morhig, D., Heller, P. L., Paola, C., & Lyons, W. J. (2000). Interpreting avulsion process from ancient alluvial sequences: Guadalope-Matarranya system (northern Spain) and Wasatch Formation (western Colorado). *The Geological Society of America Bulletin*, *112*(12), 1787–1803. [https://doi.org/10.1130/0016-7606\(2000\)112<1787:iapfaa>2.0.co;2](https://doi.org/10.1130/0016-7606(2000)112<1787:iapfaa>2.0.co;2)

- Morozova, G. S., & Smith, N. D. (2000). Holocene avulsion styles and sedimentation patterns of the Saskatchewan River, Cumberland Marshes, Canada. *Sedimentary Geology*, *130*(1–2), 81–105. [https://doi.org/10.1016/S0037-0738\(99\)00106-2](https://doi.org/10.1016/S0037-0738(99)00106-2)
- Paola, C., Ganti, V., Mohrig, D., Runkel, A. C., & Straub, K. M. (2018). Time not our time: Physical controls on the preservation and measurement of geologic time. *Annual Review of Earth and Planetary Sciences*, *46*(1), 409–438. <https://doi.org/10.1146/annurev-earth-082517-010129>
- Parker, G., Shimizu, Y., Wilkerson, G. V., Eke, E. C., Abad, J. D., Lauer, J. W., et al. (2011). A new framework for modeling the migration of meandering rivers. *Earth Surface Processes and Landforms*, *36*(1), 70–86. <https://doi.org/10.1002/esp.2113>
- Pelletier, J. D., & Turcotte, D. L. (1997). Synthetic stratigraphy with a stochastic diffusion model of fluvial sedimentation. *Journal of Sedimentary Research*, *67*(6), 1060–1067.
- Pizzuto, J. E. (1987). Sediment diffusion during overbank flows. *Sedimentology*, *34*(2), 301–317. <https://doi.org/10.1111/j.1365-3091.1987.tb00779.x>
- Plotnick, R. E. (1986). A fractal model for the distribution of stratigraphic hiatuses. *The Journal of Geology*, *94*(6), 885–890. <https://doi.org/10.1086/629094>
- Reesink, A., Van den Berg, J., Parsons, D. R., Amsler, M. L., Best, J. L., Hardy, R. J., et al. (2015). Extremes in dune preservation: Controls on the completeness of fluvial deposits. *Earth-Science Reviews*, *150*, 652–665. <https://doi.org/10.1016/j.earscirev.2015.09.008>
- Retallack, G. (1984). Completeness of the rock and fossil record: Some estimates using fossil soils. *Paleobiology*, *10*(1), 59–78. <https://doi.org/10.1017/s0094837300008022>
- Richards, K. S. (1982). *Rivers: Form and process in alluvial channels*. Methuen.
- Sadler, P. M. (1981). Sediment accumulation rates and the completeness of stratigraphic sections. *The Journal of Geology*, *89*(5), 569–584. <https://doi.org/10.1086/628623>
- Sadler, P. M., & Jerolmack, D. J. (2015). Scaling laws for aggradation, denudation and progradation rates: The case for time-scale invariance at sediment sources and sinks. *Geological Society, London, Special Publications*, *404*(1), 69–88. <https://doi.org/10.1144/sp404.7>
- Sadler, P. M., & Strauss, D. J. (1990). Estimation of completeness of stratigraphical sections using empirical data and theoretical models. *Journal of the Geological Society*, *147*(3), 471–485. <https://doi.org/10.1144/gsjgs.147.3.0471>
- Sahoo, H., Gani, M. R., Gani, N. D., Hampson, G. J., Howell, J. A., Storms, J. E. A., et al. (2020). Predictable patterns in stacking and distribution of channelized fluvial sand bodies linked to channel mobility and avulsion processes. *Geology*, *48*(9), 903–907. <https://doi.org/10.1130/g47236.1>
- Scheidt, C., Fernandes, A. M., Paola, C., & Caers, J. (2016). Quantifying natural delta variability using a multiple-point geostatistics prior uncertainty model. *Journal of Geophysical Research: Earth Surface*, *121*(10), 1800–1818. <https://doi.org/10.1002/2016jef003922>
- Schumer, R., Jerolmack, D., & McElroy, B. (2011). The stratigraphic filter and bias in measurement of geologic rates. *Geophysical Research Letters*, *38*(11), L11405. <https://doi.org/10.1029/2011gl047118>
- Schumer, R., & Jerolmack, D. J. (2009). Real and apparent changes in sediment deposition rates through time. *Journal of Geophysical Research*, *114*(F3), F00A06. <https://doi.org/10.1029/2009jef001266>
- Seminara, G. (2006). Meanders. *Journal of Fluid Mechanics*, *554*, 271–297. <https://doi.org/10.1017/s0022112006008925>
- Straub, K. M., Duller, R. A., Foreman, B. Z., & Hajek, E. A. (2020). Buffered, incomplete, and shredded: The challenges of reading an imperfect stratigraphic record. *Journal of Geophysical Research: Earth Surface*, *125*(3), e2019JF005079. <https://doi.org/10.1029/2019jef005079>
- Straub, K. M., & Esposito, C. R. (2013). Influence of water and sediment supply on the stratigraphic record of alluvial fans and deltas: Process controls on stratigraphic completeness. *Journal of Geophysical Research: Earth Surface*, *118*(2), 625–637. <https://doi.org/10.1002/jgrf.20061>
- Straub, K. M., & Foreman, B. Z. (2018). Geomorphic stasis and spatiotemporal scales of stratigraphic completeness. *Geology*, *46*(4), 311–314. <https://doi.org/10.1130/g40045.1>
- Straub, K. M., Paola, C., Mohrig, D., Wolinsky, M. A., & George, T. (2009). Compensational stacking of channelized sedimentary deposits. *Journal of Sedimentary Research*, *79*(9), 673–688. <https://doi.org/10.2110/jsr.2009.070>
- Sun, T., Meakin, P., Jøssang, T., & Schwarz, K. (1996). A simulation model for meandering rivers. *Water Resources Research*, *32*(9), 2937–2954. <https://doi.org/10.1029/96wr00998>
- Szewczyk, L., Grimaud, J. L., & Cojan, I. (2020). Experimental evidence for bifurcation angles control on abandoned channel fill geometry. *Earth Surface Dynamics*, *8*(2), 275–288. <https://doi.org/10.5194/esurf-8-275-2020>
- Szewczyk, L., Grimaud, J.-L., Cojan, I., & Piégay, H. (2022). Bedload infilling and depositional patterns in chute cutoffs channels of a gravel-bed river: The Ain River, France. *Earth Surface Processes and Landforms*, *47*(2), 459–476. <https://doi.org/10.1002/esp.5260>
- Tipper, J. C. (1998). The influence of field sampling area on estimates of stratigraphic completeness. *The Journal of Geology*, *106*(6), 727–740. <https://doi.org/10.1086/516056>
- Tipper, J. C. (2015). The importance of doing nothing: Stasis in sedimentation systems and its stratigraphic effects. *Geological Society, London, Special Publications*, *404*(1), 105–122. <https://doi.org/10.1144/sp404.6>
- Trampush, S., Hajek, E., Straub, K., & Chamberlin, E. (2017). Identifying autogenic sedimentation in fluvial-deltaic stratigraphy: Evaluating the effect of outcrop-quality data on the compensation statistic. *Journal of Geophysical Research: Earth Surface*, *122*(1), 91–113. <https://doi.org/10.1002/2016jef004067>
- Trampush, S. M., & Hajek, E. A. (2017). Preserving proxy records in dynamic landscapes: Modeling and examples from the Paleocene-Eocene Thermal Maximum. *Geology*, *45*(11), 967–970. <https://doi.org/10.1130/g39367.1>
- Wang, Y., Storms, J. E., Martinius, A. W., Karssenberg, D., & Abels, H. A. (2021). Evaluating alluvial stratigraphic response to cyclic and non-cyclic upstream forcing through process-based alluvial architecture modelling. *Basin Research*, *33*(1), 48–65. <https://doi.org/10.1111/bre.12454>
- Weissmann, G., Hartley, A. J., Scuderi, L., Nichols, G., Owen, A., Wright, S., et al. (2015). Fluvial geomorphic elements in modern sedimentary basins and their potential preservation in the rock record: A review. *Geomorphology*, *250*, 187–219. <https://doi.org/10.1016/j.geomorph.2015.09.005>
- Wheeler, H. E. (1958). Time-stratigraphy. *AAPG Bulletin*, *42*(5), 1047–1063. <https://doi.org/10.1306/0BDA5AF2-16BD-11D7-8645000102C1865D>
- Williams, G. P. (1984). Paleohydrologic equations for rivers. In F. P. J., Costa (ed.), *Developments and applications of geomorphology*. Springer.
- Williams, G. P. (1986). River meanders and channel size. *Journal of Hydrology*, *88*(1), 147–164. [https://doi.org/10.1016/0022-1694\(86\)90202-7](https://doi.org/10.1016/0022-1694(86)90202-7)
- Yan, N., Colombera, L., & Mountney, N. P. (2021). Evaluation of morphodynamic controls on the preservation of fluvial meander-belt deposits. *Geophysical Research Letters*, *48*(16), e2021GL094622. <https://doi.org/10.1029/2021gl094622>